Doctoral theses at NTNU, 2022:373

Erlend Andreas Basso

Nonlinear and Hybrid Feedback Control of Marine Vehicles and Multirotors

Doctoral thesis

NTNU
Norwegian University of Science and Technology
Thesis for the Degree of
Philosophiae Doctor
Faculty of Information Technology and Electrical Engineering
Department of Engineering Cybernetics

NTNU
Norwegian University of
Science and Technology

Erlend Andreas Basso

Nonlinear and Hybrid Feedback Control of Marine Vehicles and Multirotors

Thesis for the Degree of Philosophiae Doctor

Trondheim, November 2022

Norwegian University of Science and Technology
Faculty of Information Technology and Electrical Engineering
Department of Engineering Cybernetics

NTNU
Norwegian University of
Science and Technology

NTNU
Norwegian University of Science and Technology

Thesis for the Degree of Philosophiae Doctor

Faculty of Information Technology and Electrical Engineering
Department of Engineering Cybernetics

ISBN 978-82-326-5429-1 (printed ver.)
ISBN 978-82-326-6967-7 (electronic ver.)
ISSN 1503-8181 (printed ver.)
ISSN 2703-8084 (online ver.)

Doctoral theses at NTNU, 2022:373

Printed by NTNU Grafisk senter

Summary

This thesis presents new results and solutions for prioritized control of robotic systems and hybrid feedback control of marine and aerial vehicles. We introduce a novel task-priority framework for redundant robotic systems based on a hierarchy of control Lyapunov function (CLF) and control barrier function (CBF) based quadratic programs. The proposed method guarantees strict priority among different groups of tasks such as safety-related, operational and optimization tasks. Subsequently, we present a prioritized control scheme for safety-critical control of autonomous surface vehicles in the presence of unknown ocean currents. The stabilization objective is formulated as a maneuvering problem and integral action is introduced in the CLFs to counteract the effect of unknown irrotational ocean currents. Moreover, ocean current estimates are constructed for robust control barrier function design, and analytic conditions under which the estimates guarantee safety are derived.

The use of hybrid feedback is motivated by its ability to employ logic variables together with a properly defined switching mechanism to overcome inherent topological obstructions to global asymptotic stability. These topological obstructions are associated with the rotational degrees of freedom of marine and aerial vehicles. We introduce a hybrid proportional-derivative (PD) control law with a hysteretic switching mechanism for left-invariant systems whose configuration space can be identified with a matrix Lie group. This baseline hybrid PD control law has global asymptotic stability properties when the model parameters are known. Although full state measurements are usually assumed throughout the thesis, we develop an output-feedback variant of the baseline PD control law which only requires measurements of the configuration. Moreover, we augment the PD control law with integral action to obtain two slightly different hybrid proportional-integral-derivative (PID) control laws that both achieve global asymptotic tracking in the presence of unknown and constant disturbances.

The aforementioned hybrid control laws are designed using the notion of a synergistic function, also known as a synergistic potential function. Synergistic Lyapunov function and feedback (SLFF) pairs generalize the notion of a synergistic function. We propose a generalization of SLFF pairs, which allows the logic variable in traditional synergistic control, denoted the synergy variable, to change during flows. Moreover, we introduce synergy gaps relative to components of product sets, enabling us to define jump conditions in the form of synergy gaps for different components of the synergy variable. We demonstrate how the proposed generalization can be employed for synergistic maneuvering control of a marine surface vehicle

with discrete path dynamics.

In the subsequent chapter, we introduce hysteretic control Lyapunov functions (HCLFs). A family of HCLFs consists of local control Lyapunov functions defined on open domains, and include finite collections of open and closed sets that cover the state-space, implicitly defining a hysteresis-based switching mechanism. We have highlighted the connection between HCLFs and synergistic Lyapunov functions and feedbacks. Specifically, we have shown that HCLFs generalize the concept of synergistic control Lyapunov functions (SCLFs), and that an SCLF family together with a collection of continuous control laws synthesized from the SCLF family constitute an SLFF pair. Furthermore, given an HCLF family, we derive sufficient conditions for the existence of globally asymptotically stabilizing control laws. Moreover, we provide a constructive design procedure for synthesis of optimization-based feedback laws under mild conditions on the objective functions.

Then, we design a sliding-surface type adaptive hybrid control law for marine vehicles for global asymptotic tracking in the presence of parametric modeling errors. This control law is derived from a set of potential functions and a hysteretic switching mechanism. The assumptions on the potential functions and the hysteretic switching mechanism are less restrictive than the conditions for synergistic control. In contrast to e.g. backstepping-based control approaches, the switching mechanism remains independent of the vehicle velocities in this approach, which enables estimation of the inertial parameters. Moreover, we experimentally validate the proposed control scheme for surface and underwater vehicles.

Finally, we synthesize a tuning function-based adaptive hybrid control law which achieves global asymptotic position and heading tracking for multirotors in the presence of unknown and constant disturbances in both the translational and rotational dynamics. The use of tuning functions results in a minimal number of parameter estimates, and ensures global convergence of the disturbance estimates to their true values.

Sammendrag

Denne avhandlingen presenterer nye resultater og løsninger for prioritert bevegelsesstyring av robotsystemer samt bevegelsesstyring av marine og flyvende farkoster ved hjelp av hybrid reguleringsteknikk. Vi introduserer et nytt rammeverk for oppgavebasert regulering av redundante robotsystemer. Dette rammeverket er basert på et hierarki av kontroll-Ljapunov-funksjon- (CLF) og kontrollbarrierefunksjonbaserte kvadratiske programmer. Metoden garanterer streng prioritet mellom forskjellige grupper av reguleringsoppgaver, som for eksempel sikkerhetsrelaterte, operasjonelle og optimaliseringsoppgaver. Deretter presenteres en metode for sikkerhetskritisk bevegelsesstyring av marine overflatefartøy som opererer i farvann med ukjente havstrømmer. Stabiliseringsoppgaven er formulert som et manøvreringsproblem og integralvirkning er introdusert i CLF-ene for å motvirke effekten av de ukjente havstrømmene. Videre genererer vi havstrømsestimater for design av robuste kontrollbarrierefunksjoner, og vi utleder analytiske betingelser som garanterer at de sikkerhetsrelaterte oppgavene er oppfylt når havstrømestimatene benyttes.

Bruken av hybrid reguleringsteknikk er motivert av dens evne til å benytte logiske variable sammen med en veldefinert svitsjemekanisme for å overkomme iboende topologiske obstruksjoner til global asymptotisk stabilitet. Disse topologiske obstruksjonene er assosiert med rotasjonsfrihetsgradene til marine og flyvende farkoster. Vi utvikler en hybrid proposjonal-derivat-regulator (PD-regulator) med en hysteretisk svitsjemekanisme for venstreinvariante systemer beskrevet på matrise Lie-grupper. Denne regulatoren har globale og asymptotiske stabilitetsegenskaper og er utgangspunktet for resten av regulatordesignene i dette kapittelet. Selv om vi som regel antar at hele tilstanden er målbar i denne avhandlingen, så utvikler vi en utgangstilbakekoblet variant av den hybride PD-regulatoren som bare benytter konfigurasjonsmålinger. Videre utvider vi PD-regulatoren med integralvirkning på to forskjellige måter, noe som resulterer i to litt forskjellige proposjonal-integral-derivat-regulatorer (PID-regulator) som begge oppnår global asymptotisk stabilitet selv når systemdynamikken er utvidet med en konstant og ukjent forstyrrelse.

De tidligere nevnte hybride regulatorene er designet ved å benytte såkalte synergistiske funksjoner, også kjent som synergistiske potensialfunksjoner. Synergistiske Ljapunov-funksjon og tilbakekoblings (SLFF) par generaliserer synergistiske potensialfunksjoner. Vi forslår en generalisering av SLFF par som tillater den logiske variabelen i tradisjonell synergistisk regulering, som vi betegner synergivariabelen, å være vektorevaluert og ha kontinuerlig dynamikk definert av en gitt differensialligning, i tillegg til diskret dynamikk. Videre introduserer vi synergigap relativt

til komponenter av produktmengder, som følge av dette kan vi definere hoppbetingelser i form av synergigap for forskjellige komponenter av synergivariabelen. Vi demonstrerer hvordan den foreslåtte generaliseringen kan benyttes til å forene synergistisk regulering med manøvreringsproblemet gjennom en casestudie av et marint overflatefartøy. Her augmenterer vi i tillegg banedynamikken med diskret hoppdynamikk, noe som ikke er mulig i den originale manøvreringsteorien som begrenser seg til kontinuerlige dynamiske systemer beskrevet av differensialligninger.

Deretter introduserer vi hysteretiske kontroll-Ljapunov-funksjoner (HCLF-er). En samling av HCLF-er består av lokale CLF-er definert på åpne definisjonsmengder, og inkluderer endelige samlinger av åpne og lukkede mengder som overdekker tilstandsrommet. Disse overdekningene definerer implisitt en hysteresebasert svitsjemekanisme. Vi har fremhevet sammenhengen mellom HCLF-er og SLFF-er ved å vise at HCLF-er generaliserer konseptet av synergistiske kontroll-Ljapunov-funksjoner (SCLF-er). Spesifikt, så har vi vist at en samling av SCLF-er sammen med en samling av kontinuerlige regulatorer avledet av en samling av SCLF-er utgjør et SLFF par. Dessuten utleder vi tilstrekkelige betingelser for eksistensen av en samling kontinuerlige regulatorer som garanterer global asymptotisk stabilitet av systemet i lukket-sløyfe, gitt en samling av HCLF-er. Vi presenterer også en konstruktiv prosedyre for konstruere optimaliseringsbaserte regulatorer under milde antagelser på objektfunksjonene.

Senere foreslår vi en adaptiv hybrid regulator for marine farkoster som sørger for global asymptotisk følging av et hybrid referansesystem for marine farkoster hvor modellstrukturen er kjent, men modellparameterne er ukjente. Regulatoren er utledet fra en mengde av potensialfunksjoner og en hysteretisk svitsjemekanisme. Bemerk at antagelsene på potensialfunksjonene og svitsjemekanismen er svakere enn ved bruk av synergistiske regulatorer. I motsetning til f.eks. backsteppingbaserte regulatorer, så forblir svitsjemekanismen uavhengig av hastighetene til farkosten ved bruk av denne metoden, noe som muliggjør estimering av treghetsparametrene. Videre utleder vi potensialfunksjoner og svitsjemekanismer for marine overflatefartøy og undervannsfarkoster, og validerer regulatorene eksperimentelt for en skalamodell av et slepefartøy og en fjernstyrt undervannsfarkost.

Avslutningsvis betrakter vi problemet med global asymptotisk posisjon- og kursfølging for multirotorer. Vi antar her at modelleringsfeil og eksterne forstyrrelser kan slås sammen og modelleres som konstante og ukjente forstyrrelser i translasjons- og rotasjonsdynamikken. For å løse dette problemet utvikler vi en adaptiv hybrid regulator basert på tuningfunksjoner som garanterer global asymptotisk posisjon- og kursfølging av en begrenset referansetrajektorie, selv med ukjente forstyrrelser i translasjons- og rotasjonsdynamikken. Bruken av tuningfunksjoner resulterer i et minimalt antall parameterestimater, og gir global konvergens av parameterne til deres sanne verdier.

Contents

List of Symbols

$\mathbb{R}$	The set or real numbers.
$\mathbb{R}_{\geq 0}$	The set of nonnegative real numbers.
$\mathbb{C}$	The set of complex numbers.
$\mathbb{Z}_{\geq 0}$	Set of nonnegative integers.
$\mathbb{R}^n$	n-dimensional Euclidean space.
$\mathbb{C}^n$	n-dimensional space of complex numbers.
$\mathbb{R}^{n\times n}$	Space of $n \times n$ matrices with real entries.
$\mathbb{C}^{n\times n}$	Space of $n \times n$ matrices with complex entries.
$r\mathbb{B}^n$	The closed ball of radius r in $\mathbb{R}^n$.
$\mathbb{S}^n$	The unit n-sphere embedded in $\mathbb{R}^{n+1}$.
$\subset$	The (strict or nonstrict) subset symbol.
$\overline{S}$	The closure of the set S.
S°	The interior of the set S.
∂S	The boundary of the set S.
$S_1 \setminus S_2$	The relative complement of S_2 in S_1 .
$\pi_i(S)$	The projection of $S \subset X = X_1 \times X_2 \times \cdots \times X_n$ onto the set $X_i, 1 \leq i \leq n$.
(x, y)	Equivalent notation for the vector $\begin{pmatrix} x^\mathsf{T} & y^\mathsf{T} \end{pmatrix}^\mathsf{T}$.
$\langle x, y\rangle$	The Euclidean inner product of two vectors $x, y \in \mathbb{R}^n$.
$\lvert x\rvert$	The Euclidean norm of a vector $x \in \mathbb{R}^n$.
$\langle\langle a, b\rangle\rangle$	The Frobenius inner product $\operatorname{tr}(a^\mathsf{T} b)$ of two matrices $a, b \in \mathbb{R}^{n\times n}$.
$\lvert x\rvert_{\mathcal{A}}$	The distance from a point $x \in \mathbb{R}^n$ to a set $\mathcal{A} \subset \mathbb{R}^n$, which is given by $\inf_{y\in\mathcal{A}} \lvert x - y\rvert$.
$\nabla V(x_0)$	The gradient of a function $V : \mathbb{R}^n \to \mathbb{R}$ at $x_0 \in \mathbb{R}^n$.
$\nabla_i V(x_1, \ldots, x_n)$	The gradient of a function $V : \mathbb{R}^{n_1} \times \mathbb{R}^{n_2} \times \cdots \times \mathbb{R}^{n_N} \to \mathbb{R}$ with respect to $x_i, 1 \leq i \leq n$ at $x = (x_1, \ldots, x_n) \in \mathbb{R}^{n_1} \times \cdots \times \mathbb{R}^{n_N}$.
∇^M	The bilinear map $\nabla^M : \mathbb{R}^k \times \mathbb{R}^k \to \mathbb{R}^k$ induced by a left-invariant metric $M \in \mathbb{R}^{k\times k}$.
$\nabla f(x_0)$	The Jacobian of $f : \mathbb{R}^m \to \mathbb{R}^n$ at $x_0 \in \mathbb{R}^m$.
$\mathrm{D}V(x_0)$	The derivative of $V : \mathbb{R}^m \times \mathbb{R}^m \to \mathbb{R}$ at $x_0 \in \mathbb{R}^m \times \mathbb{R}^m$.

$\mathrm{d}V(g_0)$	The trivialized derivative of $V : \mathcal{G} \to \mathbb{R}$ at $g_0 \in \mathcal{G}$, where $\mathcal{G}$ is a matrix Lie group.
$f'(x_0)$	The derivative of a function $f : \mathbb{R} \to \mathbb{R}^n$ at $x_0 \in \mathbb{R}$.
e	The identity element on a matrix Lie group .
$(e_1, e_2, \ldots, e_n)$	The standard basis for $\mathbb{R}^n$.
$f : \mathbb{R}^m \to \mathbb{R}^n$	A single-valued mapping from $\mathbb{R}^m$ to $\mathbb{R}^n$.
$F : \mathbb{R}^m \rightrightarrows \mathbb{R}^n$	A set-valued mapping from $\mathbb{R}^m$ to $\mathbb{R}^n$.
$\operatorname{rge} f$	The range (or equivalently, the image) of a mapping $f : \mathbb{R}^m \to \mathbb{R}^n$.
$\operatorname{gph} f$	The graph of the map f .
C^r	r-times continuously differentiable.
$\mathcal{K}$	The class of functions from $\mathbb{R}_{\geq 0}$ to $\mathbb{R}_{\geq 0}$ that are continuous, zero at zero, and strictly increasing.
$\mathcal{K}_\infty$	The class of functions from $\mathbb{R}_{\geq 0}$ to $\mathbb{R}_{\geq 0}$ that are continuous, zero at zero, strictly increasing and unbounded.
$\mathcal{PD}$	The class of positive definite functions.
$\mathcal{G}$	A matrix Lie group.
$\mathfrak{g}$	Lie algebra of a Lie group $\mathcal{G}$.
$\mathcal{S}_\mathcal{H}$	The set of all maximal solutions ϕ to the hybrid system $\mathcal{H}$.
$\mathcal{S}_\mathcal{H}(S)$	The set of all maximal solutions ϕ to $\mathcal{H}$ with $\phi(0,0) \in S$.
$\mathrm{SO}(n)$	The special orthogonal group of dimension n.
$\mathrm{SE}(n)$	The special Euclidean group of dimension n.
$\widetilde{\mathrm{SE}}(3)$	The universal covering group of SE(3).
$\mathrm{SU}(2)$	The special unitary group of dimension 2. Isomorphic to the group of unit quaternions.
$\mathfrak{so}(n)$	Vector space of skew-symmetric $n \times n$ matrices, and the Lie algebra of $\mathrm{SO}(n)$.
$\mathfrak{se}(n)$	Lie algebra of $\mathrm{SE}(n)$.
$\mathfrak{su}(2)$	Lie algebra of SU(2). Isomorphic to $\mathfrak{so}(3)$.
$(\cdot)^\wedge$	Isomorphism between $\mathbb{R}^m$ and $\mathfrak{g}$ for an m-dimensional Lie group $\mathcal{G}$.
$(\cdot)^\vee$	Inverse of $(\cdot)^\wedge$.
$T_\Sigma(\eta)$	The tangent cone to the set $\Sigma \subset \mathbb{R}^n$ at $\eta \in \overline{\Sigma}$.
$\operatorname{tr} A$	The trace of a matrix $A \in \mathbb{R}^{n \times n}$.

Preface

This thesis is submitted in partial fulfillment of the requirements for the degree of philosophiae doctor (PhD) at the Norwegian University of Science and Technology (NTNU), Trondheim. The work presented in this thesis has been carried out from August 2019 to August 2022 at the Centre for Autonomous Marine Operations and Systems (NTNU AMOS) and the Department of Engineering Cybernetics under the supervision of Professor Kristin Y. Pettersen (Dept. Engineering Cybernetics, NTNU) and co-supervision of Professor Asgeir J. Sørensen (Dept. Marine Technology, NTNU) and Professor Jan Tommy Gravdahl (Dept. Engineering Cybernetics, NTNU). The work was supported by the Research Council of Norway (grant number 223254 - NTNU AMOS).

Acknowledgments

I am deeply grateful to my supervisor Professor Kristin Ytterstad Pettersen for giving me the opportunity to pursue a PhD at the Department of Engineering Cybernetics. She has provided me with excellent academic advice and has let me discover, explore and pursue my own research interests over the course of my PhD. Her insightful feedback and positive attitude has made the supervision meetings a joy to attend. My co-supervisor Professor Asgeir J. Sørensen has been an exceptional motivator and has given me a lot of valuable insight from an industry perspective. It was a particularly great experience to be a part of a research cruise aboard R/V Gunnerus. I also thank my other co-supervisor Professor Jan Tommy Gravdahl for his valuable insights and comments.

I would like to thank Professor Roger Skjetne at the Department of Marine Technology for the opportunity to contribute in modernizing the dynamic positioning lab in his course TMR4243 - Marine Control Systems II and for his advice on our joint publications and academic life in general.

I would also like to offer my special thanks to Assistant Professor Ole Kristian Fossum at UiT - The Arctic University of Norway for his inspiring mathematics lectures during my year-long preparatory course for engineering studies in Tromsø. His mathematical rigor and focus on understanding rather than memorization has helped me immensely in my studies ever since.

I have had the privilege to work with a large number of highly intelligent people over the course of my PhD. First and foremost, I want to thank Henrik Schmidt-Didlaukies for being a great friend and collaborator during the past two and a half years. This thesis would have been very different if we had never met. I would also

like to thank my fellow PhD students Trym Tengesdal, Mathias Marley and Emil Thyri and for their friendship and our fruitful collaborations.

Finally, I would like to thank my mother for her unconditional support over the years.

Erlend Andreas Basso
Trondheim, August 2022

Publications

The results presented in this thesis are based on the following conference and journal papers:

Journal Papers

1. E. A. Basso[#], H. M. Schmidt-Didlaukies[#] and K. Y. Pettersen, "Global Asymptotic Position and Heading Tracking for Multirotors using Tuning Function-based Adaptive Hybrid Feedback", *IEEE Control Systems Letters*, 2022
2. E. A. Basso[#], H. M. Schmidt-Didlaukies[#], K. Y. Pettersen and A. J. Sørensen, "Global Asymptotic Tracking for Marine Vehicles using Adaptive Hybrid Feedback", *IEEE Transactions on Automatic Control*, 2022.

Conference Papers

1. E. A. Basso[#], H. M. Schmidt-Didlaukies[#], K. Y. Pettersen and J. T. Gravdahl, "Synergistic PID and Output Feedback Control on Matrix Lie Groups ", *Proc. 12th IFAC Symposium on Nonlinear Control Systems*, Canberra, Australia, Jan. 4-6, 2023.
2. H. M. Schmidt-Didlaukies[#], E. A. Basso[#], A. J. Sørensen and K. Y. Pettersen, "A Generalization of Synergistic Hybrid Feedback Control with Application to Maneuvering Control of Ships", *Proc. 61st Conference on Decision and Control (CDC)*, Cancún, Mexico, Dec. 6-9, 2022.
3. E. A. Basso[#], H. M. Schmidt-Didlaukies[#], K. Y. Pettersen and A. J. Sørensen, "Global Asymptotic Tracking for Marine Surface Vehicles using Hybrid Feedback in the Presence of Parametric Uncertainties," *Proc. 2021 American Control Conference (ACC)*, Online/New Orleans, LA, USA, May 25-28, 2021.
4. E. A. Basso[#], H. M. Schmidt-Didlaukies[#] and K. Y. Pettersen, "Hysteretic Control Lyapunov Functions with Application to Global Asymptotic Tracking for Underwater Vehicles," *Proc. 59th Conference on Decision and Control (CDC)*, Online/Jeju island, Republic of Korea, Dec. 8-11, 2020.
5. E. A. Basso, E. H. Thyri, K. Y. Pettersen, M. Breivik and R. Skjetne, "Safety-critical control of autonomous surface vehicles in the presence of ocean cur-

[#]E. A. Basso and H. M. Schmidt-Didlaukies contributed equally to these articles and should be considered co-first authors.

rents", Proc. 4th IEEE Conference on Control Technology and Applications (CCTA) Online/Montréal, Canada, August 24-26, 2020.
6. E. A. Basso and K. Y. Pettersen, "Task-priority control of redundant robotic systems using control Lyapunov and control barrier function based quadratic programs," *Proc. 21st IFAC World Congress*, Online/Berlin, Germany, July 12-17, 2020.

Other publications

The following publications were written during the PhD, but are not included in this thesis.

Journal Papers

1. H. M. Schmidt-Didlaukies, E. A. Basso, A. J. Sørensen and K. Y. Pettersen, "Symmetry Considerations for Underwater Vehicles", *Submitted to the IEEE Journal of Oceanic Engineering*, 2022.
2. T. Tengesdal, S. V. Rothmund, E. A. Basso, T. A. Johansen and H. M. Schmidt-Didlaukies, "Obstacle Intention Awareness in Automatic Collision Avoidance: Full Scale Experiments in Confined Waters", *Submitted to Field Robotics*, 2022.

Conference Papers

1. M. Marley, R. Skjetne, E. A. Basso and A. R. Teel, "Maneuvering with safety guarantees using control barrier functions", *Proc. 13th IFAC Conference on Control Applications in Marine Systems, Robotics, and Vehicles (CAMS)*, Online/Oldenburg, Germany, 22-24 September, 2021.
2. J. Matouš, E. A. Basso, E. H. Thyri and K. Y. Pettersen, "Unifying Reactive Collision Avoidance and Control Allocation for Multi-Vehicle Systems", *Proc. 5th IEEE Conference on Control Technology and Applications (CCTA)*, Online/San Diego, CA, USA, August 8-11, 2021.
3. E. H. Thyri, E. A. Basso, M. Breivik, K. Y. Pettersen, R. Skjetne and A. M. Lekkas, "Reactive collision avoidance for ASVs based on control barrier functions", *Proc. 4th IEEE Conference on Control Technology and Applications (CCTA)*, Online/Montréal, Canada, August 24-26, 2020.
4. E. A. Basso and K. Y. Pettersen, "MIMO Feedback Linearization of Redundant Robotic Systems using Task-Priority Operational Space Control", *Proc. 21st IFAC World Congress*, Online/Berlin, Germany, July 12-17, 2020.

Chapter 1

Introduction

The intent of this thesis is to present new results and solutions for prioritized control of robotic systems and hybrid feedback control of marine and aerial vehicles. Since these two topics are somewhat disjoint, this thesis is divided into two parts. The first part considers task-priority control of redundant robotic systems and task-priority control for safety-critical control of fully actuated marine surface vehicles. A robotic system is kinematically redundant when it has more degrees of freedom (DOFs) than those strictly required to execute a given task. Tasks are often divided into groups according to their priority, such as safety-related tasks, operational tasks and optimization tasks. Safety-related tasks are typically set-based, that is, control objectives with a range of valid values. Since a robotic system is typically initialized in such a way that the safety-related tasks are satisfied, safety can often be recast as a forward invariance property of the so-called safe set, that is, the set in which the safety-related task is satisfied. Operational tasks are usually equality-based, which is to say that they should be controlled to some desired value, while optimization tasks could be either set-based or equality-based. For instance, a manipulability index task is inherently set-based, while a desired robot pose as determined by a set of desired joint angles, is equality-based.

Kinematic redundancy enables additional tasks to be executed simultaneously by utilizing the redundant DOFs of the system. However, care must be taken when resolving kinematic redundancy. In particular, if compatibility between two or more tasks cannot be guaranteed at all time, then lower-priority tasks may prevent convergence of higher-priority tasks. Since tasks at the lowest-priority level are often added to ensure joint-space stability of a robotic system, they are inherently incompatible with mission-related tasks such as end-effector control. Moreover, high-priority safety-related tasks such as collision avoidance are always incompatible with positioning tasks when the position reference is not collision free. Consequently, redundancy should be resolved by ensuring strict-priority between tasks, i.e. that lower-priority tasks have no effect on the execution of higher-priority tasks.

The second part of this thesis marks the departure from the world of classical control theory where the closed-loop system is of a continuous-time nature. Instead, by designing feedback control laws for continuous-time systems which combine both continuous- and discrete-time behavior, the closed-loop system becomes a hybrid

dynamical system. In contrast to continuous-time feedback control laws, hybrid feedback control laws enable the use of logic variables, timers and memory states in the control law [1]. Logic variables can be employed to overcome topological obstructions preventing any continuous-time control law from robustly and globally asymptotically stabilizing a continuous-time nonlinear system to an equilibrium point or to a set of equilibrium points. Logic variables can also be used to synthesize hybrid control laws that switch between different locally stabilizing control laws. This may in turn, improve transient performance.

1.1 Task-Priority Control

Kinematic task-priority control is a redundancy resolution method introduced in [2], developed in [3] and generalized to any number of priority levels in [4]. This control approach decouples the controller into a kinematic and dynamic controller, and has been successfully implemented on a number of robotic systems. The framework was extended to support tasks described by sets or inequalities in [5], [6] and [7]. These kinematic control approaches all resolve redundancy at the velocity level by generating velocity references for some dynamic controller to follow. An immediate drawback is that acceleration references cannot be included, resulting in worse tracking performance.

Operational space control [8] is a holistic approach that assigns joint torques directly by transforming the equations of motion from joint space into the operational space (also known as task space). Although it was mainly introduced for non-redundant systems, a dynamically consistent null space operator was defined in [8], that allowed two operational space tasks to be defined and controlled simultaneously. In [9], the scheme was extended to a task-priority framework with an arbitrary number of tasks by generalizing the dynamically consistent null space operator from [8] to an arbitrary number of priority levels. These null space operators ensure that torques generated by lower-priority tasks do not generate accelerations that affect the task dynamics of higher-priority tasks. The operational space framework was extended to include set-based tasks, i.e. control objectives with a range of valid values in [10]; however, this approach does not scale well for systems with a high number of DOFs.

Control Lyapunov functions (CLFs) extend Lyapunov theory to systems with inputs and have become an essential part of nonlinear control design after the pioneering work in [11–13]. The CLF concept was extended to rapidly exponentially stabilizing control Lyapunov functions (RES-CLFs) in [14], which achieve exponential convergence at a controllable rate. Through CLFs or RES-CLFs, the control designer is free to chose among an infinite number of controllers. An important example is the point-wise minimum norm controller [15, 16], which selects the control value of minimum norm from all control values rendering the time derivative of the CLF negative definite. The point-wise minimum norm controller has a closed-form solution since it is the solution to a quadratic program (QP) with only one inequality constraint. This QP can be augmented with control input saturation limits and other control input constraints, at the expense of a closed-form solution [17]. For redundant robotic systems, two control tasks can be satisfied simultane-

ously by defining CLFs for each task and finding a control input that minimizes some quadratic objective function while ensuring that the time derivatives of the CLFs are negative definite [18]. However, strict priority between tasks cannot be ensured.

Barrier functions have been used extensively in constrained optimization [19, 20], and have motivated the concept of barrier certificates for safety-critical control. Barrier certificates were introduced as a tool for proving forward invariance of sets [21, 22]. Since these sets often encode safety-related objectives, proving invariance of a safe set implies that the system will remain safe, as long as you start safe. These barrier certificates tend to infinity as the state tends to the boundary of the safe set, and in order to obtain safety guarantees beyond the boundary of the safe set, various Lyapunov-like approaches have been proposed such as [23], where a positive definite barrier certificate is employed as a barrier Lyapunov function. However, these conditions are overly conservative since the positive definiteness property enforces the invariance of every level set, and not just the safe set of the set-based task in question. The notion of barrier functions in [24] do not require the barrier functions to tend to infinity as the state tends to the boundary of the safe set. Moreover, the sufficient conditions ensuring forward invariance of the safe set must only be verified in a neighborhood of the boundary of the safe set.

Barrier certificates were extended to systems with inputs by introducing the first notion of a control barrier function (CBF) in [25]. These control barrier functions were combined with control Lyapunov functions in [26], and further improved in [27] to establish conditions for so-called control Lyapunov-barrier functions, which jointly guarantee safety and stability. However, these conditions were shown to be too restrictive, and subsequently relaxed in [28, 29], which extended control barrier functions to the entire safe set, and thus enabling controller synthesis through optimization-based methods [30]. In particular, the CLF-based QPs in [18] and [17] could be augmented with CBFs to ensure stability and safety [28, 29]. CBFs were generalized to exponential control barrier functions (ECBFs) in [31], which enforce forward invariance of set-based tasks with a higher relative degree.

It is clear that velocity level kinematic task-priority control has been extensively studied in the literature, and successfully extended to account for set-based tasks. However, as highlighted by the previous paragraphs, there only exists one framework for set-based task-priority control at the dynamic level [10], which does not scale well for systems with a high number of DOFs. Furthermore, kinematic task-priority control may be undesirable for a number of reasons. In particular, the mathematical stability proofs for velocity-level kinematic control schemes assume that the velocity references are perfectly tracked by some dynamic controller, which typically requires significant bandwidth separation between the kinematic and dynamic controllers. Moreover, task-space acceleration references cannot be included by velocity-level kinematic task-priority control frameworks. Finally, the inherent redundancy of the system cannot be used to optimize the desired velocity references calculated by the kinematic task-priority control law with respect to physically realizable actuator control inputs.

1.2 Hybrid Feedback Control

It is well known that continuous-time systems whose state-space can be identified with a vector bundle on a compact manifold have no point that can be globally asymptotically stabilized by continuous-time state feedback [32]. This is referred to as a topological obstruction to global asymptotic stability and follows from the fact that no compact manifold is contractible.

Topological obstructions to global asymptotic stability can be overcome by employing hybrid feedback with a properly defined switching logic [33]. Examples include hybrid feedback derived from patchy CLFs [34] and synergistic control. Synergistic control is a hybrid feedback control methodology that selects the state-feedback control action based on the value of multiple Lyapunov-like functions [1, 35, 36]. A hybrid synergistic control law solves the tracking problem robustly and globally on noncontractible manifolds, which is unattainable using conventional continuous or discontinuous control laws [32, 37].

The synergistic control paradigm is applied to orientation tracking control for rigid bodies utilizing quaternions in [37], where a globally asymptotically stabilizing PD-controller is derived. The paper also introduces an output-feedback version of this control law. The aforementioned approach is utilized for trajectory tracking of translation-underactuated rigid vehicles in [38]. Synergistic potential functions are utilized to derive PD-controllers for global asymptotic tracking control for rigid body orientation on SO(3) in [39]. A smoothing approach for the devised controller is presented, which ensures continuity of the control signal provided that desired acceleration is continuous. The work also presents a procedure to construct synergistic functions from modified trace functions, which were first employed for control of orientation in [40]. A synergistic approach that does not utilize velocity measurements is presented in [41]. Moreover, [41] also provides a systematic procedure to construct synergistic functions by angular warping, an idea first introduced in [42]. Synergistic potential functions are generalized to synergistic Lyapunov functions and feedback pairs in [36], while an extension of the synergistic functions in [39] to a case where the logic variable is allowed to flow, is introduced in [43]. Synergistic control of rigid body planar and spherical orientation is presented in [44] and [45], respectively, while synergistic control barrier functions are introduced in [46].

While employing hybrid feedback to overcome topological obstructions on compact manifolds has been extensively studied through simulations in the idealized case where the model structure and the model parameters are assumed to be known, little attention has been paid to the more practical case involving parametric modeling uncertainties. In [47], a global exponential tracking controller with integral action is derived for the orientation control of a spatial rigid body subject to a matched and constant disturbance. However, the switching mechanism depends explicitly on the value of the integral state. Hybrid feedback using synergistic potential functions was extended to the case where the original control system is subject to matched uncertainties in [48]. However, when applying this approach to mechanical systems, the switching mechanism is not independent of the system velocities. Moreover, the approach does not permit estimation of the inertia matrix parameters.

1.3 Outline and Contributions

This thesis is organized into two parts and nine chapters. Chapter 2 introduces the mathematical notation and background theory relevant to the rest of this thesis. In the following, we summarize the topic and contributions of each chapter in this thesis.

1.3.1 Part I: Task-Priority Control

Task-Priority Control of Redundant Robotic Systems (Chapter 3)

Chapter 3 presents a novel task-priority control framework for redundant robotic systems based on a hierarchy of control Lyapunov function (CLF) and control barrier function (CBF) based quadratic programs (QPs). The proposed method guarantees strict priority among different groups of tasks such as safety-related, operational and optimization tasks. Moreover, a soft priority measure in the form of penalty parameters can be employed to prioritize tasks at the same priority level. As opposed to kinematic control schemes, the proposed framework is a holistic approach for control of redundant robotic systems, which solves the redundancy resolution, dynamic control and control allocation problems simultaneously. Numerical simulations of a hyper-redundant articulated intervention autonomous underwater vehicle (AIAUV) is presented to validate the proposed framework.

The main contribution of this chapter is a novel dynamic task-priority framework for an arbitrary number of equality- and set-based control tasks encoded by CLFs and CBFs, where equality and set-based tasks are control objectives that should be driven to a desired value and kept within a desired set, respectively. The framework builds on the CLF-based QP proposed for two equality tasks in [18] by extending it to an arbitrary number of equality tasks, unifying CLFs with CBFs via QPs to support set-based tasks as done in [28, 29], and establishing any number of priority levels through a hierarchy of QPs. An important feature of this approach is that it yields strict priority between tasks at different priority levels, in the sense that tasks at lower-priority levels have no effect on the execution of tasks at higher-priority levels. The inclusion of set-based tasks at the dynamic level is a key novelty within task-priority control, which has to the best of our knowledge only been accounted for in [10].

This chapter is based on the following publication:

[49] E. A. Basso and K. Y. Pettersen, "Task-priority control of redundant robotic systems using control Lyapunov and control barrier function based quadratic programs," *Proc. 21st IFAC World Congress*, Online/Berlin, Germany, July 12-17 2020.

Safety-Critical Control of Autonomous Surface Vehicles (Chapter 4)

Autonomous surface vehicles (ASVs) are safety-critical systems that must provide strict safety guarantees such as collision avoidance to enable fully autonomous operations. Chapter 4 is motivated by Chapter 3 and presents a unified framework for safety-critical control of ASVs for maneuvering, dynamic positioning, and con-

trol allocation with safety guarantees in the presence of unknown ocean currents. The framework utilizes control Lyapunov function (CLF)- and control barrier function (CBF)-based quadratic programs (QPs), and is applicable to a general class of nonlinear affine control systems. The stabilization objective is formulated as a maneuvering problem and integral action is introduced in the CLFs to counteract the effect of unknown irrotational ocean currents. Furthermore, ocean current estimates are constructed for robust CBF design, and analytic conditions under which the estimates guarantee safety are derived. Subsequently, robust CBFs are designed to achieve collision avoidance of static obstacles. The chapter concludes by verifying the framework through simulations of a double-ended passenger ferry.

The contributions of this chapter are threefold. Firstly, we provide conditions under which an arbitrary number of nonlinear mappings estimating some unknown system nonlinearity and a CBF guarantee safety. Moreover, we show how this result can be employed to synthesize safe optimization-based control laws. Secondly, we employ this result in combination with CLFs endowed with integral action to synthesize an optimization-based and collision-free maneuvering control law for ASVs in the presence of unknown ocean currents. Finally, by utilizing an optimization-based control law,the control problem is formulated in terms of the actuator control inputs, and thereby unifying the control problem with the control allocation problem. This unification handles control input saturations more effectively than a decoupled approach and is less likely to lead to instability [17], which is especially relevant during emergency collision avoidance maneuvers.

This chapter is based on the following publication:

[50] E. A. Basso, E. H. Thyri, K. Y. Pettersen, M. Breivik and R. Skjetne, "Safety-critical control of autonomous surface vehicles in the presence of ocean currents", *Proc. 4th IEEE Conference on Control Technology and Applications (CCTA)*, Online/Montréal, Canada, August 24-26, 2020.

1.3.2 Part II: Hybrid Feedback Control of Marine and Aerial Vehicles

Synergistic PID and Output Feedback Control on Matrix Lie Groups (Chapter 5)

In this chapter, we develop multiple synergistic hybrid feedback control laws for mechanical systems on matrix Lie groups with left-invariant metrics. With the goal of globally asymptotically tracking a desired reference trajectory, we propose a hybrid proportional-derivative (PD) type control law and an output feedback version which only utilizes configuration measurements. Moreover, to ensure global asymptotic tracking in the presence of a constant and unknown disturbance in the system dynamics, we introduce two novel proportional-integral-derivative (PID) type control laws with slightly different properties in terms of gain selection and integral action. The theoretical developments are validated through numerical simulation of an underwater vehicle.

The contributions of this chapter are threefold. First, we propose a baseline synergistic PD control law ensuring global asymptotic tracking for mechanical systems on matrix Lie groups with a left-invariant Riemannian metric. The second

contribution is a generalization of the synergistic output-feedback control law proposed for orientation control in [37] to any system whose configuration space can be identified with a matrix Lie group. Finally, we present two novel synergistic PID type control laws, both of which ensure global asymptotic tracking in the presence of unknown constant disturbances.

This chapter is based on the following publication:

[51] E. A. Basso[#], H. M. Schmidt-Didlaukies[#], K. Y. Pettersen and J. T. Gravdahl, "Synergistic PID and Output Feedback Control on Matrix Lie Groups ", *Proc. 12th IFAC Symposium on Nonlinear Control Systems*, Canberra, Australia, Jan. 4-6, 2023.

Synergistic Lyapunov Functions and Feedback Triples (Chapter 6)

Chapter 6 generalizes results on synergistic hybrid feedback control. Specifically, we propose a generalized definition of synergistic Lyapunov functions and feedbacks which allows the logic variable in traditional synergistic control, denoted the synergy variable, to be vector-valued and change during flows. Moreover, we introduce synergy gaps relative to components of product sets, which enables us to define jump conditions in the form of synergy gaps for different components of the synergy variable. In particular, this enables us to formulate existing hybrid output feedback control schemes within the synergistic control framework. Furthermore, we show that our generalized definition is amenable to backstepping. Finally, we give an example of how traditional synergistic control can be combined with ship maneuvering control with discrete path dynamics.

The main contribution of this chapter is the extension of the SLFF definition from [36]. The proposed generalization allows the logic variable, now referred to as the synergy variable, to be vector-valued and possess flow dynamics. Moreover, since the synergy variable is vector-valued, we define synergy gaps relative to components of product sets. These synergy gaps enable us to define flow and jump sets and jump conditions in the form of synergy gaps for different components of the synergy variable. As a result, we can show that the output feedback control method for rigid-body scheme outlined in [37] is synergistic. The proposed generalization encompasses the results for SO(3) and SE(3) in [43], in which the scalar logic variable is also allowed to change during flows. However, our proposed framework also includes path-following control scenarios in which the path variable exhibits jump dynamics, such as instantaneously moving the desired state closer to the actual state. As a result, ship maneuvering control as outlined in [52] and [53] can be augmented with discrete path dynamics and combined with a traditional synergistic control approach such as [44] to ensure global asymptotic stability within the proposed framework.

This chapter is based on the following publication:

[54] H. M. Schmidt-Didlaukies[#], E. A. Basso[#], A. J. Sørensen and K. Y. Pettersen, "A Generalization of Synergistic Hybrid Feedback Control with Application to Maneuvering Control of Ships", *Proc. 61st Conference on Decision and Control (CDC)*, Cancún, Mexico, Dec. 6-9, 2022.

Hysteretic Control Lyapunov Functions (Chapter 7)

This chapter introduces hysteretic control Lyapunov functions (HCLFs) for hybrid feedback control of a class of continuous-time systems. A family of HCLFs consists of local control Lyapunov functions defined on open domains, and include finite collections of open and closed sets that cover the state-space, implicitly defining a hysteresis-based switching mechanism.

The main contribution of this chapter is the concept of a hysteretic control Lyapunov function and its application to hybrid feedback control with global asymptotic stability properties for nonlinear continuous-time systems. Specifically, we show that the existence of a family of HCLFs satisfying the small control property implies global stabilizability of a compact set. Moreover, we prove that optimization-based hybrid feedback laws can be constructed under minor assumptions on the objective functions. The collection of optimization-based feedback laws are continuous along flows, implying that the hybrid basic conditions hold such that the stability is robust in the sense of [55].

As a case study, we construct an HCLF family for tracking control of an underwater vehicle through a backstepping approach. The HCLF family is subsequently employed to synthesize a hybrid control law ensuring global asymptotic trajectory tracking. In contrast to traditional backstepping, we find the control input that pointwise minimizes a strictly convex objective function from the set-valued map of stabilizing control inputs defined by the HCLFs. The HCLF construction is reminiscent of the backstepping-based synergistic Lyapunov functions constructed for set-point regulation in [56]. However, we extend the work in [56] to the tracking problem in terms of HCLFs, and exploit inherent stabilizing nonlinear terms through online optimization.

This chapter is based on the following publication:

[57] E. A. Basso[#], H. M. Schmidt-Didlaukies[#] and K. Y. Pettersen, "Hysteretic Control Lyapunov Functions with Application to Global Asymptotic Tracking for Underwater Vehicles," *Proc. 59th Conference on Decision and Control (CDC)*, Online/Jeju island, Republic of Korea, Dec. 8-11, 2020.

Global Asymptotic Tracking for Marine Vehicles (Chapter 8)

Chapter 8 presents an adaptive hybrid feedback control law for global asymptotic tracking of a hybrid reference system for marine vehicles in the presence of parametric modeling errors. The reference system is constructed from a parametrized loop and a speed assignment specifying the motion along the path, which decouples the geometry of the path from the motion along the path. During flows, the hybrid feedback consists of a proportional-derivative action and an adaptive feedforward term, while a hysteretic switching mechanism that is independent of the vehicle velocities determines jumps. The effectiveness of the proposed control law is demonstrated through experiments.

The main contribution of this chapter is the development of an adaptive hybrid feedback controller for global asymptotic tracking of a hybrid reference system for marine vehicles subject to parametric uncertainties. In contrast to backstepping-based hybrid adaptive control [48], the proposed approach permits estimation of

the inertia matrix, and the switching mechanism is independent of the system velocities. As our approach is based on traditional Euler-Lagrange system models, the adaptive hybrid control law is applicable to other mechanical systems as well. In particular, it can easily be extended to robot manipulators or, more generally, vehicle-manipulator systems. The hybrid reference system is constructed from a parametrized loop and a speed assignment for the motion along the loop. The main benefit of this formulation is that it decouples the design of the path from the motion along the path, allowing us to globally asymptotically track a given parametrized loop at a desired and time-varying speed. The proposed reference system can be considered an adaptation of the maneuvering problem [52, 53] to a hybrid dynamical systems setting. Preliminary results were presented in [58], and in this chapter we extend the hybrid feedback control law from surface vehicles to a more general class of Euler-Lagrange systems on SE(2) or SE(3) satisfying a set of general conditions on the switching mechanism and the potential functions. Moreover, we show that the potential functions and switching mechanisms introduced in [58] and [37] satisfy these conditions, and these potential functions and switching mechanisms are subsequently employed to design hybrid adaptive control laws for surface and underwater vehicles, respectively. Finally, we validate the theoretical developments for surface and underwater vehicle applications through experiments.

This chapter is based on the following publications:

[59] E. A. Basso#, H. M. Schmidt-Didlaukies#, K. Y. Pettersen and A. J. Sørensen, "Global Asymptotic Tracking for Marine Vehicles using Adaptive Hybrid Feedback", *IEEE Transactions on Automatic Control*, 2022.

[58] E. A. Basso#, H. M. Schmidt-Didlaukies#, K. Y. Pettersen and A. J. Sørensen, "Global Asymptotic Tracking for Marine Surface Vehicles using Hybrid Feedback in the Presence of Parametric Uncertainties," *Proc. 2021 American Control Conference (ACC)*, Online/New Orleans, LA, USA, May 25-28, 2021.

Global Asymptotic Position and Heading Tracking for Multirotors (Chapter 9)

Chapter 9 considers the problem of global asymptotic position and heading tracking for multirotors. We propose a hybrid adaptive feedback control law that globally asymptotically tracks a position and heading reference in the presence of unknown constant disturbances in both the translational and rotational dynamics. By employing a tuning function-based backstepping approach, the number of parameter estimates are minimized. Moreover, using ideas from Chapter 8, we propose a novel bounded control law for the translational subsystem, which leads to a simpler virtual control law when backstepping. Global asymptotic heading tracking is achieved through a novel construction of the desired rotation matrix. The theory is verified through experiments on a quadrotor.

The goal of this chapter is to achieve uniform global asymptotic tracking of both the position and heading of a multirotor in the presence of unknown constant disturbances in both the translational and rotational dynamics. To this end, we build on the work in [38], which we extend as follows. First, we propose a novel bounded

adaptive control law for the translational subsystem, which leads to a simpler virtual control law when backstepping. Second, we propose a novel construction for the desired rotation matrix, which avoids the use of intermediary Euler angles, and is crucial in ensuring global asymptotic tracking of the desired heading reference. Third, we augment the rotational dynamics with a constant disturbance, and by employing tuning functions [60], the number of parameter estimates becomes equal to the number of unknown parameters. As a consequence, we can show that the disturbance estimates in both the translational and rotational dynamics converge to their true values.

This chapter is based on the following publication:

[61] E. A. Basso[#], H. M. Schmidt-Didlaukies[#] and K. Y. Pettersen, "Global Asymptotic Position and Heading Tracking for Multirotors using Tuning Function-based Adaptive Hybrid Feedback", *IEEE Control Systems Letters*, 2022.

Chapter 2

Mathematical Preliminaries

This chapter introduces mathematical preliminaries and notation relevant to the rest of this thesis.

2.1 Regularity

Definition 2.1 (Proper function)**.** *Let $X \subset \mathbb{R}^n$. A continuous function $V : X \to \mathbb{R}_{\geq 0}$ is proper if the sublevel set $\{x \in X : V(x) \leq c\}$ is compact for every $c \in \mathbb{R}_{\geq 0}$.*

Definition 2.2 (Passive functions)**.** *A function $\varphi : \mathbb{R}^n \to \mathbb{R}^n$ is passive if it is continuous and satisfies $\varphi(x)^\mathsf{T} x \geq 0$ for all $x \in \mathbb{R}^n$.*

Definition 2.3 (Strongly passive functions)**.** *A function $\varphi : \mathbb{R}^n \to \mathbb{R}^n$ is strongly passive if it is continuous and satisfies $\varphi(x)^\mathsf{T} x > 0$ for all $x \in \mathbb{R}^n \setminus \{0\}$.*

Definition 2.4 (Class-$\mathcal{K}$ functions)**.** *A function $\alpha : \mathbb{R}_{\geq 0} \to \mathbb{R}_{\geq 0}$ is a class-$\mathcal{K}$ function, also written $\alpha \in \mathcal{K}$, if α is zero at zero, continuous, and strictly increasing.*

Definition 2.5 (Class-$\mathcal{K}_\infty$ functions)**.** *A function $\alpha : \mathbb{R}_{\geq 0} \to \mathbb{R}_{\geq 0}$ is a class-$\mathcal{K}_\infty$ function, also written $\alpha \in \mathcal{K}_\infty$, if α is zero at zero, continuous, strictly increasing, and unbounded; i.e., $\alpha \in \mathcal{K}$ and unbounded.*

Definition 2.6 (Extended class-$\mathcal{K}_\infty$ functions)**.** *A function $\alpha : \mathbb{R} \to \mathbb{R}$ is an extended class-$\mathcal{K}_\infty$ function, if α is zero at zero, continuous, strictly increasing, and unbounded.*

Definition 2.7 (Class-$\mathcal{KL}$ functions)**.** *A function $\beta : \mathbb{R}_{\geq 0} \times \mathbb{R}_{\geq 0} \to \mathbb{R}_{\geq 0}$ is a class-$\mathcal{KL}$ function, also written $\beta \in \mathcal{KL}$, if it is nondecreasing in its first argument, nonincreasing in its second argument, $\lim_{r \searrow 0} \beta(r, s) = 0$ for each $s \in \mathbb{R}_{\geq 0}$, and $\lim_{s \to \infty} \beta(r, s) = 0$ for each $r \in \mathbb{R}_{\geq 0}$.*

Definition 2.8 (Monotonicity)**.** *Let $f : \mathbb{R}^m \to \mathbb{R}^m$ and $A \in \mathbb{R}^{m \times m}$. The mapping f is A-monotone if*

$$\langle f(x) - f(y), x - y \rangle \geq \langle A(x - y), x - y \rangle, \tag{2.1}$$

for all $(x, y) \in \mathbb{R}^m \times \mathbb{R}^m$. Moreover, f is monotone if it is 0-monotone.

Lemma 2.1. *Let $A \in \mathbb{R}^{m\times m}$ and $f : \mathbb{R}^m \to \mathbb{R}^m$ be continuously differentiable. Then f is A-monotone if and only if the matrix $\nabla f(x) - A$ is positive semidefinite for all $x \in \mathbb{R}^m$.*

Proof. Apply [62, Prop. 12.3] to $f(x) - Ax$. □

2.2 Set-Valued Analysis

This section provides a brief introduction to certain basic aspects from set-valued analysis. See the excellent book [62] by Rockafellar and Wets for more details.

A set-valued mapping is denoted as $M : \mathbb{R}^n \rightrightarrows \mathbb{R}^m$. We define the domain, range and graph of a set-valued mapping M by

$$\operatorname{dom} M := \{x \in \mathbb{R}^n : M(x) \neq \emptyset\}, \tag{2.2}$$

$$\operatorname{rge} M := \{y \in \mathbb{R}^m : \exists x \in \mathbb{R}^n \text{ such that } y \in M(x)\}, \tag{2.3}$$

$$\operatorname{gph} M := \{(x, y) \in \mathbb{R}^n \times \mathbb{R}^m : y \in M(x)\}. \tag{2.4}$$

The inverse mapping of M, $M^{-1} : \mathbb{R}^m \rightrightarrows \mathbb{R}^n$, is defined by

$$M^{-1}(y) := \{x \in \mathbb{R}^n : y \in M(x)\}. \tag{2.5}$$

Moreover, we define the image of a set S under M and the inverse image of a set R under M, respectively, by

$$M(S) := \left\{y \in \mathbb{R}^m : M^{-1}(y) \cap S \neq \emptyset\right\}, \tag{2.6}$$

$$M^{-1}(R) := \left\{x \in \mathbb{R}^n : M(x) \cap R \neq \emptyset\right\}. \tag{2.7}$$

Definition 2.9. *Let $M : \mathbb{R}^n \rightrightarrows \mathbb{R}^m$ be a set-valued mapping.*

1. *M is inner semicontinuous (isc) relative to S at $x \in \mathbb{R}^n$ if for every $y \in M(x)$ and every neighborhood Y of y there exists a neighborhood X of x such that $S \cap X \subset M^{-1}(Y)$.*
2. *M is outer semicontinuous (osc) relative to S at $x \in \mathbb{R}^n$ if for every $y \notin M(x)$ there are neighborhoods X of x and Y of y such that $S \cap X \cap M^{-1}(Y) = \emptyset$.*

M is isc relative to S if it is isc relative to S at every $x \in \mathbb{R}^n$. Similar terminology is used for the osc case. Finally, M is continuous relative to S if it is both isc relative to S and osc relative to S.

Lemma 2.2 (Osc and closed graph)**.** *A set-valued mapping $M : \mathbb{R}^n \rightrightarrows \mathbb{R}^m$ is outer semicontinuous if and only if* gph M *is closed. More generally, given a set $S \subset \mathbb{R}^n$, a set-valued mapping $M : \mathbb{R}^n \rightrightarrows \mathbb{R}^m$ is outer semicontinuous relative to S if and only if the set $\{(x, y) \in \mathbb{R}^n \times \mathbb{R}^m : x \in S, y \in M(x)\}$ is relatively closed in $S \times \mathbb{R}^m$.*

We also require a notion of local boundedness for set-valued mappings.

Definition 2.10. *Let $M : \mathbb{R}^n \rightrightarrows \mathbb{R}^m$ be a set-valued mapping. M is locally bounded at $x \in \mathbb{R}^n$ if there exists a neighborhood X of x such that $M(X)$ is bounded. M is locally bounded if it is locally bounded at every $x \in \mathbb{R}^n$, and M is locally bounded relative to a set $S \subset \mathbb{R}^n$ if the restriction of M to S is locally bounded at every $x \in S$.*

Note that every continuous single-valued mapping is locally bounded.

Inner semicontinuity is also known as lower semicontinuity in the literature, e.g. in the seminal work [63]. Another widely used notion in the literature of set-valued mappings is upper semicontinuity of a set-valued mapping. Outer semicontinuity and upper semicontinuity are related through the following result [1, Lemma A.35]

Lemma 2.3 (Osc vs upper semicontinuous set-valued mappings)**.** *Let $M : \mathbb{R}^n \rightrightarrows \mathbb{R}^m$ be a set-valued mapping. Let $x \in \mathbb{R}^n$ be such that $M(x)$ is closed. If M is upper semicontinuous at x, then M is is outer semicontinuous at x. If M is locally bounded at x, then the reverse implication is true.*

Definition 2.11 (Tangent cone)**.** *The tangent cone to a set $S \subset \mathbb{R}^n$ at a point $x \in \mathbb{R}^n$, denoted $T_S(x)$, is the set of all vectors $w \in \mathbb{R}^n$ for which there exist $x_i \in S, \tau_i > 0$ with $x_i \to x, \tau_i \searrow 0$, and*

$$w = \lim_{i \to \infty} \frac{x_i - x}{\tau_i}. \tag{2.8}$$

2.3 Hybrid Systems

In this section, we introduce the notion of a hybrid dynamical system. This introduction is by no means complete, and the reader is referred to [55] and [1] for more details.

A hybrid dynamical system, or simply a hybrid system, allows for both continuous-time and discrete-time evolution of the state. In this thesis, we employ the hybrid systems framework of [1, 55]. In those works, a hybrid system $\mathcal{H}$ is defined by four objects (C, F, D, G) known as the data of the hybrid system and represented by

$$\mathcal{H} : \begin{cases} \dot{x} \in F(x), & x \in C \\ x^+ \in G(x), & x \in D \end{cases} \tag{2.9}$$

where $x \in \mathbb{R}^n$ is the state of the system, the set-valued mapping $F : \mathbb{R}^n \rightrightarrows \mathbb{R}^n$ is called the flow map, $G : \mathbb{R}^n \rightrightarrows \mathbb{R}^n$ is called the jump map and $C \subset \mathbb{R}^n$ and $D \subset \mathbb{R}^n$ are called the flow and jump sets, respectively.

A solution ϕ to (2.9) is called a hybrid arc and is parametrized by the elapsed time $t \in \mathbb{R}_{\geq 0}$ and the number of jumps $j \in \mathbb{Z}_{\geq 0}$ that have occurred. To formally define a hybrid arc, we require the notion of a hybrid time domain [55, Definition 2.3]

Definition 2.12 (Hybrid time domains)**.** *A subset $E \subset \mathbb{R}_{\geq 0} \times \mathbb{Z}_{\geq 0}$ is a compact hybrid time domain if*

$$E = \bigcup_{j=0}^{J-1} ([t_j, t_{j+1}], j) \tag{2.10}$$

for some finite sequence of times $0 = t_0 \leq t_1 \leq \cdots \leq t_J$. It is a hybrid time domain if for all $(T, J) \in E, E \cap ([0, T] \times \{0, 1, \ldots, J\})$ is a compact hybrid domain.

The notion of a hybrid arc is introduced in the following definition [55, Definition 2.4].

Definition 2.13 (Hybrid arc)**.** *A function $\phi : E \to \mathbb{R}^n$ is a hybrid arc if E is a hybrid time domain and if for each $j \in \mathbb{Z}_{\geq 0}$, the function $t \mapsto \phi(t, j)$ is locally absolutely continuous on the interval $I^j = \{t : (t, j) \in E\}$.*

The notation $\operatorname{dom} \phi$ represents the domain of a hybrid arc, which is a hybrid time domain.

Definition 2.14 (Solution to a hybrid system)**.** *A hybrid arc ϕ is a solution to the hybrid system $\mathcal{H}$ if $\phi(0, 0) \in \overline{C} \cup D$, and*

(S1) *for all $j \in \mathbb{Z}_{\geq 0}$ such that $I^j := \{t : (t, j) \in \operatorname{dom} \phi\}$ has nonempty interior*

$$\begin{aligned} \phi(t, j) &\in C && \text{for all} \quad t \in \operatorname{int} I^j, \\ \frac{\mathrm{d}}{\mathrm{d}t}\phi(t, j) &\in F(\phi(t, j)) && \text{for almost all} \quad t \in I^j; \end{aligned} \tag{2.11}$$

(S2) *for all $(t, j) \in \operatorname{dom} \phi$ such that $(t, j + 1) \in \operatorname{dom} \phi$,*

$$\phi(t, j) \in D, \phi(t, j + 1) \quad \in G(\phi(t, j)). \tag{2.12}$$

A solution ϕ to $\mathcal{H}$ is said to be complete if $\operatorname{dom} \phi$ is unbounded and maximal if ϕ is not the truncation of another solution. The set of all maximal solutions ϕ to $\mathcal{H}$ is denoted $\mathcal{S}_{\mathcal{H}}$. Similarly, $\mathcal{S}_{\mathcal{H}}(S)$ denotes the set of all maximal solutions ϕ to $\mathcal{H}$ with $\phi(0, 0) \in S$.

Definition 2.15 (Uniform global pre-asymptotic stability (UGpAS))**.** *A closed set $\mathcal{A} \subset \mathbb{R}^n$ is said to be*

- *uniformly globally stable for $\mathcal{H}$ if there exists a class $\mathcal{K}_\infty$ function α such that any solution ϕ to $\mathcal{H}$ satisfies $|\phi(t, j)|_{\mathcal{A}} \leq \alpha(\phi(0, 0))$ for all $(t, j) \in \operatorname{dom} \phi$;*
- *uniformly globally pre-attractive for $\mathcal{H}$ if for each $\epsilon > 0$ and $r > 0$ there exists $T > 0$ such that, for any solution ϕ to $\mathcal{H}$ with $\phi(0, 0) \leq r$, $(t, j) \in \operatorname{dom} \phi$ and $t + j \geq T$ implies $|\phi(t, j)|_{\mathcal{A}} \leq \epsilon$;*
- *uniformly globally pre-asymptotically stable for $\mathcal{H}$ if it is both uniformly globally stable and uniformly globally pre-attractive.*

The prefix *pre* is employed to emphasize the fact that maximal solutions are not required to be complete. An equivalent characterization of uniform global pre-asymptotic stability which utilizes class-$\mathcal{KL}$ functions is now introduced.

Theorem 2.16. *A closed set $\mathcal{A} \subset \mathbb{R}^n$ is uniformly globally pre-asymptotically stable for $\mathcal{H}$ if and only if there exists a $\mathcal{KL}$ function β such that any solution ϕ to $\mathcal{H}$ satisfies*

$$|\phi(t, j)|_{\mathcal{A}} \leq \beta(|\phi(0, 0)|_{\mathcal{A}}, t + j), \tag{2.13}$$

for all $(t, j) \in \operatorname{dom} \phi$.

We typically assume that the data (C, F, D, G) of the hybrid system $\mathcal{H}$ satisfies the following three basic assumptions [55, Assumption 6.5]

Assumption 2.17 (Hybrid basic conditions)**.**

(A1) *C and D are closed subsets of $\mathbb{R}^n$;*
(A2) *$F : \mathbb{R}^n \rightrightarrows \mathbb{R}^n$ is outer semicontinuous and locally bounded relative to C, $C \subset \operatorname{dom} F$, and $F(x)$ is convex for every $x \in C$;*
(A3) *$G : \mathbb{R}^n \rightrightarrows \mathbb{R}^n$ is outer semicontinuous and locally bounded relative to D, and $D \subset \operatorname{dom} G$.*

It should be emphasized that when F is a single-valued and continuous mapping, the differential equation $\dot{z} = F(z)$ corresponds to a hybrid system satisfying the hybrid basic conditions.

When the set to be stabilized is compact and our system satisfies the hybrid basic conditions, global pre-asymptotic stability is equivalent to uniform global pre-asymptotic stability, and we typically write GpAS instead of UGpAS.

Definition 2.18 (Stability of compact sets)**.** *A compact set $\mathcal{A} \subset \mathbb{R}^n$ is said to be*

- *stable for $\mathcal{H}$ if for every $\epsilon > 0$ there exists $\delta > 0$ such that every solution ϕ to $\mathcal{H}$ with $|\phi(0,0)|_{\mathcal{A}} \leq \delta$ satisfies $|\phi(t,j)|_{\mathcal{A}} \leq \epsilon$ for all $(t,j) \in \operatorname{dom} \phi$;*
- *globally pre-attractive for $\mathcal{H}$ if every solution ϕ to $\mathcal{H}$ is bounded and, if ϕ is complete, then also $\lim_{t+j\to\infty} |\phi(t,j)|_{\mathcal{A}} = 0$;*
- *globally pre-asymptotically stable for $\mathcal{H}$ if it is both stable and globally pre-attractive.*

Proposition 2.19 (Basic existence of solutions)**.** *Let the hybrid system $\mathcal{H}$ satisfy Assumption 2.17. Take an arbitrary $\xi \in C \cup D$. If $\xi \in D$ or*

(VC) *there exists a neighborhood U of ξ such that for every $x \in U \cap C$,*

$$F(x) \cap T_C(x) \neq \emptyset, \tag{2.14}$$

then there exists a nontrivial solution ϕ to $\mathcal{H}$ with $\phi(0,0) = \xi$. If (VC) holds for every $\xi \in C \backslash D$, then there exists a nontrivial solution to $\mathcal{H}$ from every initial point in $C \cup D$, and every $\phi \in \mathcal{S}_{\mathcal{H}}$ satisfies exactly one of the following conditions:

(a) *ϕ is complete;*
(b) *$\operatorname{dom} \phi$ is bounded and the interval I^J, where $J = \sup_j \operatorname{dom} \phi$, has nonempty interior and $t \mapsto \phi(t, J)$ is a maximal solution to $\dot{z} \in F(z)$, in fact $\lim_{t\to T} |\phi(t,J)| = \infty$, where $T = \sup_t \operatorname{dom} \phi$;*
(c) *$\phi(t, J) \notin C \cup D$, where $(T, J) = \sup \operatorname{dom} \phi$.*

Furthermore, if $G(D) \subset C \cup D$, then (c) above does not occur.

Definition 2.20 (Forward invariance)**.** *A nonempty set $K \subset \mathbb{R}^n$ is said to be*

1. *forward pre-invariant for $\mathcal{H}$ if each $\phi \in \mathcal{S}_{\mathcal{H}}(K)$ satisfies $\phi(t,j) \in K$ for all $(t,j) \in \operatorname{dom} \phi$;*
2. *forward invariant for $\mathcal{H}$ if it is forward pre-invariant and each $\phi \in \mathcal{S}_{\mathcal{H}}(K)$ is complete.*

2.4 Control Lyapunov and Control Barrier Functions

Consider the nonlinear control affine system

$$\dot{x} = f(x) + g(x)u, \quad (x, u) \in \mathbb{R}^n \times U \tag{2.15}$$

where the mappings $f\colon \mathbb{R}^n \to \mathbb{R}^d$ and $g\colon \mathbb{R}^n \to \mathbb{R}^{n\times p}$ are continuous and the input space $U \subset \mathbb{R}^p$ is nonempty, closed and convex.

CLFs are continuously differentiable and positive definite functions whose time derivatives can be made negative definite by appropriate selection of the control input. Exponentially stabilizing CLFs achieve convergence rates within explicitly given bounds, and provides an inherent robustness property to disturbances, in terms of input-to-state stability.

Definition 2.21 (Definition 1. [14])**.** *For the system (2.15), a continuously differentiable function $V : \mathbb{R}^n \to \mathbb{R}$ is an exponentially stabilizing control Lyapunov function (ES-CLF) if there exists positive constants $c_1, c_2, c_3 > 0$ such that*

$$c_1\|x\|^2 \leq V(x) \leq c_2\|x\|^2, \tag{2.16}$$

$$\inf_{u\in U} \left[\nabla V(x)^\mathsf{T} f(x,t) + \nabla V(x)^\mathsf{T} g(x)u + c_3 V(x)\right] \leq 0, \tag{2.17}$$

for all $x \in \mathbb{R}^n$.

Safety-related objectives are often described by inequalities or sets. Control barrier functions are continuously differentiable functions $h : \mathbb{R}^n \to \mathbb{R}$ for which the superzero level set

$$K \coloneqq \{x \in \mathbb{R}^n : h(x) \geq 0\}, \tag{2.18}$$

can be rendered forward invariant (or forward pre-invariant) by appropriate selection of the control input. The following definition is given in [46]

Definition 2.22. *Let $h : \mathbb{R}^n \to \mathbb{R}$ be a continuously differentiable function that defines the set (2.18). Then, h is a CBF for (2.15) if there exists an extended class $\mathcal{K}_\infty$ function σ and an open set X with $K \subset X$ such that*

$$\sup_{u\in U} \left[\nabla h(x)^\mathsf{T}(f(x) + g(x)u)\right] \geq -\sigma(h(x)), \quad \forall x \in X. \tag{2.19}$$

The following theorem can be found in [46] and provides conditions guaranteeing safety of (2.15) with the input constrained to the admissible set-valued input set $U_h : \mathbb{R}^n \rightrightarrows \mathbb{R}^p$ defined by

$$U_h(x) \coloneqq \{u \in U : \nabla h(x)^\mathsf{T}(f(x) + g(x)u) \geq -\sigma(h(x))\}. \tag{2.20}$$

Theorem 2.23. *If h is a CBF on $\mathbb{R}^n$ defining K, then K is forward pre-invariant for the system*

$$\dot{x} \in \{f(x) + g(x)u : u \in U_h(x)\}, \quad x \in \mathbb{R}^n. \tag{2.21}$$

A direct consequence of Equation (2.20) is that a continuous selection from U_h guarantees safety of (2.15).

Corollary 2.24. *If h is a CBF on $\mathbb{R}^n$ defining K and $\kappa : \mathbb{R}^n \to U$ is continuous and satisfies $\kappa(x) \in U_h(x)$ for all $x \in X$, then K is forward pre-invariant for the system*

$$\dot{x} = f(x) + g(x)\kappa(x), \quad x \in \mathbb{R}^n. \tag{2.22}$$

2.5 Manifolds in Euclidean Space

Definition 2.25. *A set $\mathcal{M} \subset \mathbb{R}^n$ is a k-manifold, where $0 \leq k \leq n$, if the following equivalent conditions hold:*

1. *For each $x \in \mathcal{M}$, there exists an open set $U \subset \mathbb{R}^n$ containing x, an open set $W \subset \mathbb{R}^k$, and a smooth injective immersion $\chi : W \to \mathbb{R}^n$ such that $\chi(W) = \mathcal{M} \cap U$.*
2. *For each $x \in \mathcal{M}$, there exists an open set $U \subset \mathbb{R}^n$ containing x and a smooth submersion $\vartheta : U \to \mathbb{R}^{n-k}$ such that $\{x \in U : \vartheta(x) = 0\} = \mathcal{M} \cap U$.*

Definition 2.25 presents two equivalent characterizations of a k-manifold in $\mathbb{R}^n$. In particular, item 1 characterizes the manifold in terms of local parametrizations, and item 2 in terms of local defining mappings.

Definition 2.26. *Let $\mathcal{M} \subset \mathbb{R}^n$ be a k-manifold. The tangent cone to $\mathcal{M}$ at x is a linear subspace of $\mathbb{R}^n$, and referred to as the tangent space to $\mathcal{M}$ at x. The following characterizations are equivalent:*

1. *For $x \in \mathcal{M}$ and (U, χ) as in item 1 in Definition 2.25,*

$$T_{\mathcal{M}}(x) = \{v \in \mathbb{R}^n : w \in \mathbb{R}^k, v = \nabla\chi \circ \chi^{-1}(x)w\}$$

   for all $x \in \mathcal{M} \cap U$.
2. *For $x \in \mathcal{M}$ and (U, ϑ) as in item 2 in Definition 2.25,*

$$T_{\mathcal{M}}(x) = \{v \in \mathbb{R}^n : \nabla\vartheta(x)v = 0\}.$$

   for all $x \in \mathcal{M} \cap U$.

With an abuse of notation, we write $T_{\mathcal{M}} \subset \mathcal{M} \times \mathbb{R}^n$. This set is defined such that $(x, v) \in T_{\mathcal{M}}$ if $x \in \mathcal{M}$ and $v \in T_{\mathcal{M}}(x)$.

2.6 Matrix Lie Groups

Matrix Lie groups are manifolds that are also matrix groups.

Definition 2.27. *A matrix Lie group $\mathcal{G}$ is a k-manifold in $\mathbb{R}^{n\times n}$ satisfying*

1. *if $g \in \mathcal{G}$, then $g^{-1} \in \mathcal{G}$;*
2. *if $g, h \in \mathcal{G}$, then $gh \in \mathcal{G}$.*

A matrix Lie group $\mathcal{G}$ is a closed subgroup of the general linear group $\mathrm{GL}(n) = \{g \in \mathbb{R}^{n\times n} : \det g \neq 0\}$. The identity element is denoted $e \in \mathcal{G}$. In what follows, we define the matrix commutator $[\![\cdot, \cdot]\!] : \mathbb{R}^{n\times n} \times \mathbb{R}^{n\times n} \to \mathbb{R}^{n\times n}$ by $[\![A, B]\!] \coloneqq AB - BA$. With every matrix Lie group, one can associate a particular algebra, known as the Lie algebra of the matrix Lie group.

Definition 2.28. *Let $\mathcal{G} \subset \mathbb{R}^{n\times n}$ be a matrix Lie group. The Lie algebra $\mathfrak{g}$ of $\mathcal{G}$ is the tangent space to $\mathcal{G}$ at the identity equipped with the matrix commuator, $\mathfrak{g} \coloneqq (T_{\mathcal{G}}(e), [\![\cdot, \cdot]\!])$.*

The Lie algebra $\mathfrak{g}$ is a real vector space with dimension equal to the dimension of $\mathcal{G}$ as a manifold. In the robotics literature, it has become commonplace to work in $\mathbb{R}^k$ instead of $\mathfrak{g}$. This is accomplished by choosing a basis $(X_i)_{i\in\{1,\dots,k\}}$ for $\mathfrak{g}$ and defining the vector space isomorphism $(\cdot)^\wedge : \mathbb{R}^k \to \mathfrak{g}$ and the commutator on $\mathbb{R}^k$, $[\cdot, \cdot] : \mathbb{R}^k \times \mathbb{R}^k \to \mathbb{R}^k$ as

$$\begin{aligned} \xi^\wedge &\coloneqq \sum_{i=1}^{k} X_i \xi^i \\ [\xi, \zeta] &\coloneqq [\![\xi^\wedge, \zeta^\wedge]\!]^\vee \end{aligned} \tag{2.23}$$

where $(\cdot)^\vee : \mathfrak{g} \to \mathbb{R}^k$ is the inverse mapping of $(\cdot)^\wedge$. Hence, $\mathfrak{g} \simeq (\mathbb{R}^k, [\cdot, \cdot])$. For each $g \in \mathcal{G}$ and $y \in \mathbb{R}^6$, we define the adjoint mappings $\mathrm{Ad}_g : \mathbb{R}^k \to \mathbb{R}^k$ and $\mathrm{ad}_\xi : \mathbb{R}^k \to \mathbb{R}^k$,

$$\begin{aligned} \mathrm{Ad}_g \zeta &\coloneqq (g\zeta^\wedge g^{-1})^\vee, \\ \mathrm{ad}_\xi \zeta &\coloneqq [\xi, \zeta]. \end{aligned} \tag{2.24}$$

It can be shown that for each $g \in \mathcal{G}$, there exists an open set $W \subset \mathbb{R}^k$ such that the mapping $\chi_g : W \to \mathbb{R}^{n\times n}$ defined by $\chi_g(\xi) \coloneqq g \exp(\xi^\wedge)$ is a local parametrization of a neighborhood of g, as utilized in item 1 of Definition 2.25.

For each $\xi \in \mathbb{R}^k$, we define a left-invariant vector field $X_\xi(g) = g\xi^\wedge$ on $\mathcal{G}$ with $g \in \mathcal{G}$. The Lie derivative of a continuously differentiable function $V : \mathcal{G} \to \mathbb{R}$ along the vector field X_ξ can be written as $\langle\!\langle \mathrm{D}V(g), X_\xi(g) \rangle\!\rangle$, where $\langle\!\langle a, b \rangle\!\rangle \coloneqq \mathrm{tr}(a^\mathsf{T} b)$ is the Frobenius inner product and

$$\mathrm{D}V(g) = \begin{pmatrix} \frac{\partial V}{\partial g_{11}} & \cdots & \frac{\partial V}{\partial g_{1j}} \\ \vdots & \ddots & \vdots \\ \frac{\partial V}{\partial g_{i1}} & \cdots & \frac{\partial V}{\partial g_{ij}} \end{pmatrix} (g).$$

The Lie derivative can be rewritten using the Euclidean inner product by defining the mapping $\mathrm{d}V : \mathcal{G} \to \mathbb{R}^k$ by

$$\langle \mathrm{d}V(g), \xi \rangle \coloneqq \langle\!\langle \mathrm{D}V(g), X_\xi(g) \rangle\!\rangle. \tag{2.25}$$

Finally, the bilinear map $\nabla^M : \mathbb{R}^k \times \mathbb{R}^k \to \mathbb{R}^k$ induced by the inertia matrix M is defined by [64]

$$\nabla^M_\nu \eta \coloneqq \tfrac{1}{2} \mathrm{ad}_\nu \eta - \tfrac{1}{2} M^{-1} [\mathrm{ad}^\mathsf{T}_\nu M\eta + \mathrm{ad}^\mathsf{T}_\eta M\nu]. \tag{2.26}$$

Observe that $M\nabla^M_\nu \nu = -\mathrm{ad}^\mathsf{T}_\nu M\nu$.

Lemma 2.4. *For every $\xi \in \mathbb{R}^m$, it holds that*

$$\langle \xi, M\nabla^M_\zeta \xi \rangle = 0, \tag{2.27}$$

for all $\zeta \in \mathbb{R}^m$.

Proof. From the identities $\langle \eta, \operatorname{ad}_\xi \zeta \rangle = \langle \operatorname{ad}^\mathsf{T}_\xi \eta, \zeta \rangle$ and $\operatorname{ad}_\xi \xi = 0$, it holds that

$$\begin{aligned} 2\langle \xi, M\nabla^M_\zeta \xi \rangle &= \langle \xi, M \operatorname{ad}_\zeta \xi - \operatorname{ad}^\mathsf{T}_\xi M\zeta - \operatorname{ad}^\mathsf{T}_\zeta M\xi \rangle \\ &= \langle \xi, M \operatorname{ad}_\zeta \xi - \operatorname{ad}^\mathsf{T}_\zeta M\xi \rangle. \end{aligned} \tag{2.28}$$

By rewriting the last term in (2.28) as

$$\langle \xi, -\operatorname{ad}^\mathsf{T}_\zeta M\xi \rangle = -\langle \operatorname{ad}_\zeta \xi, M\xi \rangle, \tag{2.29}$$

symmetry of M implies that $\langle \xi, M \operatorname{ad}_\zeta \xi \rangle = \langle M\xi, \operatorname{ad}_\zeta \xi \rangle$ and the result follows from linearity of the inner product. □

Part I

Task-Priority Control

Chapter 3

Task-Priority Control of Redundant Robotic Systems using Control Lyapunov and Control Barrier Function based Quadratic Programs

This chapter presents a novel dynamic task-priority framework for an arbitrary number of equality- and set-based control tasks encoded by CLFs and CBFs, where equality and set-based tasks are control objectives that should be driven to a desired value and kept within a desired set, respectively. The framework builds on the CLF-based QP proposed for two equality tasks in [18] by extending it to an arbitrary number of equality tasks, unifying CLFs with CBFs via QPs to support set-based tasks as done in [28, 29], and establishing any number of priority levels through a hierarchy of QPs. An important feature of this approach is that it yields strict priority between tasks at different priority levels, in the sense that tasks at lower-priority levels have no effect on the execution of tasks at higher-priority levels. The inclusion of set-based tasks at the dynamic level is a key novelty within task-priority control, which has to the best of our knowledge only been accounted for in [10].

The proposed scheme represents a holistic control approach since the QPs can be formulated in terms of the actuator inputs, instead of the commanded forces and torques. Consequently, the proposed framework also solves the control allocation problem. For task-priority control of robotic systems where computation of the actuator inputs from the commanded forces and torques is non-trivial, the unification of redundancy resolution and control allocation is a key advantage because strict priority between tasks can be ensured at all times. In contrast, redundancy resolution schemes that decouple dynamic control and control allocation, such as kinematic or operational space control, provide no a priori guarantee that the commanded forces and torques computed by the dynamic controller can be exactly allocated, since the commanded forces and torques are typically computed with no regard to physical actuator limits, rate constraints, or singularities of the actuator configuration matrix. If the commanded forces and torques cannot be exactly allo-

cated, the forces and torques are usually allocated to actuator inputs by minimizing the allocation error [65], which is performed independently of the redundancy resolution algorithm. As a result, strict priority is lost and tasks become coupled whenever exact allocation is infeasible.

The material in this chapter is based on [49].

3.1 Introduction

This section presents the necessary background material for this particular chapter. For compactness, we will slightly abuse notation and denote

$$L_g h(x) = \frac{\partial \vartheta(x)}{\partial x} g(x), \tag{3.1}$$

whenever ϑ is a scalar or vector-valued function, and g is a vector field or a matrix. Note that (3.1) is only equal to the Lie derivative of ϑ along g when ϑ is a multivariable scalar function and g a vector field.

3.1.1 Model

Consider the nonlinear affine control system

$$\dot{x} = f(x) + g(x)u, \tag{3.2}$$

where f and g are locally Lipschitz, $x \in \mathbb{R}^l$ and $u \in U \subset \mathbb{R}^p$ is the set admissible control inputs. Let $y = \vartheta(x) = \sigma(x) - \sigma_d$ describe the error coordinates of some locally Lipschitz equality task $\sigma : \mathbb{R}^l \to \mathbb{R}^m$ with desired value $\sigma_d \in \mathbb{R}^m$. Under the assumption that

$$L_g L_f^k \vartheta(x) = 0, \quad 0 \leq k \leq \rho - 2 \tag{3.3}$$

$$L_g L_f^{\rho-1} \vartheta(x) \neq 0, \tag{3.4}$$

for all $x \in \mathbb{R}^l$, the input-output dynamics becomes

$$y^{(\rho)} = \underbrace{L_f^\rho \vartheta(x)}_{b(x)} + \underbrace{L_g L_f^{\rho-1} \vartheta(x)}_{A(x)} u. \tag{3.5}$$

The system (3.2) can be decomposed into transverse dynamics states

$$\eta = \left(y, \dot{y}, \ldots, y^{(\rho-1)} \right) \in X \subset \mathbb{R}^{\rho m}$$

and internal dynamics states $z \in Z \subset \mathbb{R}^{l-\rho m}$ as follows

$$\dot{\eta} = \bar{f}(\eta, z) + \bar{g}(\eta, z)u, \tag{3.6a}$$

$$\dot{z} = f_z(\eta, z), \tag{3.6b}$$

with $\bar{f}(\eta, z) = \Lambda\eta + \Gamma b(x)$ and $\bar{g}(\eta, z) = \Gamma A(x)$ where

$$\Lambda = \begin{pmatrix} 0 & I & 0 & \cdots & 0 \\ 0 & 0 & I & \cdots & 0 \\ \vdots & \ddots & \ddots & \ddots & \vdots \\ 0 & 0 & 0 & \cdots & I \\ 0 & 0 & 0 & 0 & 0 \end{pmatrix}, \quad \Gamma = \begin{pmatrix} 0 \\ 0 \\ 0 \\ \vdots \\ I \end{pmatrix}, \tag{3.7}$$

where 0 is the $m \times m$ matrix of zeros and I is the $m \times m$ identity matrix.

3.1.2 Control Lyapunov Functions

A control Lyapunov function is a candidate Lyapunov function whose derivative can be made pointwise negative by appropriate selection of the control input [15]. In order to explicitly control the rate of exponential convergence, a specific type of CLF is defined in [14] as follows:

Definition 3.1. *A continuously differentiable and positive definite function $V_\epsilon : X \to \mathbb{R}$ is said to be a rapidly exponentially stabilizing control Lyapunov function (RES-CLF) for the system (3.6) if there exists constants $c_1, c_2, c_3 > 0$ such that for all $0 < \epsilon < 1$ and for all states $(\eta, z) \in X \times Z$ it holds that*

$$c_1\|\eta\|^2 \leq V_\epsilon(\eta) \leq \frac{c_2}{\epsilon^2}\|\eta\|^2, \tag{3.8}$$

$$\inf_{u \in U}\left[L_{\bar{f}}V_\epsilon(\eta, z) + L_{\bar{g}}V_\epsilon(\eta, z)u + \frac{c_3}{\epsilon}V_\epsilon(\eta)\right] \leq 0. \tag{3.9}$$

Such a function can be constructed by solving the continuous time algebraic Riccati equation

$$\Lambda^\mathsf{T}P + P\Lambda - P\Gamma\Gamma^\mathsf{T}P + Q = 0, \tag{3.10}$$

for $P = P^\mathsf{T} > 0$, where Q is any positive definite matrix. In order to stabilize the transverse dynamics at a rate ϵ define

$$V_\epsilon(\eta) = \eta^\mathsf{T}\begin{pmatrix} \frac{1}{\epsilon}I & 0 \\ 0 & I \end{pmatrix} P \begin{pmatrix} \frac{1}{\epsilon}I & 0 \\ 0 & I \end{pmatrix}\eta := \eta^\mathsf{T}P_\epsilon\eta. \tag{3.11}$$

When $A(x)$ has linearly independent rows for all $x \in \mathbb{R}^l$, it can be shown that the time derivative of (3.11) satisfies [14]

$$\inf_{u \in U}\left[L_{\bar{f}}V_\epsilon(\eta, z) + L_{\bar{g}}V_\epsilon(\eta, z)u\right] \leq -\frac{\gamma}{\epsilon}V_\epsilon(\eta), \tag{3.12}$$

where $\gamma := \frac{\lambda_{\min}(Q)}{\lambda_{\max}(P)} > 0$ and

$$L_{\bar{f}}V_\epsilon(\eta, z) = \eta^\mathsf{T}\left(\Lambda^\mathsf{T}P_\epsilon + P_\epsilon\Lambda\right)\eta + 2\eta^\mathsf{T}P\Gamma b(x), \tag{3.13}$$

$$L_{\bar{g}}V_\epsilon(\eta, z) = 2\eta^\mathsf{T}P_\epsilon\Gamma A(x). \tag{3.14}$$

3.1.3 Exponential Control Barrier Functions

Control objectives described by inequalities or sets can be enforced by rendering the superzero level set

$$K = \left\{ x \in \mathbb{R}^l : h(x) \geq 0 \right\}, \tag{3.15}$$

of some continuously differentiable function $h : D \to \mathbb{R}$ forward pre-invariant [30].

Definition 2.22 assumes that the relative degree of h is equal to one. However, safety-related tasks for robotic systems are often a function of the configuration variables only, meaning that they have a higher relative degree. Introduced in [31] and refined in [30], exponential control barrier functions generalizes CBFs to functions h with arbitrary relative degree $r \geq 1$. To this end, we define $\eta_b(x) \coloneqq \begin{pmatrix} h(x), L_f h(x), L_f^2 h(x), \ldots, L_f^{r-1} h(x) \end{pmatrix}$ and consider the following definition.

Definition 3.2. *Given a set $K \subset D \subset \mathbb{R}^l$ defined as the superzero level set of an r-times continuously differentiable function $h : D \to \mathbb{R}$, then h is an exponential control barrier function (ECBF) for the control system (3.2) if there exists a row vector $K_\alpha \in \mathbb{R}^r$ and an open set X with $K \subset X$ such that*

$$\sup_{u \in U} \left[L_f^r h(x) + L_g L_f^{r-1} h(x) u \right] \geq -K_\alpha \eta_b(x), \quad \forall x \in X. \tag{3.16}$$

3.1.4 Combining CLFs and ECBFs

The RES-CLF and ECBF conditions in (3.9) and (3.16) are both affine in the control input u, which means that the control problem can be formulated as a convex optimization problem, enabling the incorporation of control input saturation limits and rate constraints [17]. By employing RES-CLFs, the CLF-ECBF-based QP from [29, 30] becomes:

$$\begin{aligned} &\underset{u \in \mathbb{R}^m, \delta \in \mathbb{R}}{\text{minimize}} \quad \frac{1}{2} u^\mathsf{T} H(x) u + c(x)^\mathsf{T} u + w\delta^2 \\ &\text{subject to} \\ &L_{\bar{f}} V_\epsilon(\eta, z) + L_{\bar{g}} V_\epsilon(\eta, z) u \leq -\frac{\gamma}{\epsilon} V_\epsilon(\eta) + \delta, \\ &L_f^r h(x) + L_g L_f^{r-1} h(x) u \geq -K_\alpha \eta_b(x), \end{aligned} \tag{3.17}$$

where $H(x)$ is positive semi-definite for all $x \in \mathbb{R}^l$, $c : D \to \mathbb{R}^m$, and $\delta \in \mathbb{R}$ is a slack variable penalized by $w > 0$, ensuring the feasibility of the QP in case of conflicting set-based and equality-based control objectives.

The remainder of this chapter is organized as follows. Section 3.2 introduces the main contribution of this chapter, namely, a task-priority framework for equality- and set-based tasks. Section 3.3 presents simulation results of the framework implemented on an articulated intervention autonomous underwater vehicle (AIAUV), while conclusions and future work can be found in Section 3.4.

3.2 Quadratic Programs for N Equality- and M Set-Based Control Tasks

This section extends the CLF-ECBF QP controller in (3.17) to an arbitrary number of equality- and set-based control tasks distributed to an arbitrary number of priority levels.

3.2.1 CLF Penalty Parameters as a Priority Measure

Inspired by [18], the QP in (3.17) can be extended to N equality-based control objectives by deriving the input-output dynamics for each control objective, i.e.

$$y_i^{(\rho_i)} = \underbrace{L_f^{\rho_i}\vartheta_i(x)}_{b_i(x)} + \underbrace{L_g L_f^{\rho_i-1}\vartheta_i(x)}_{A_i(x)}\, u, \tag{3.18}$$

for each $i = 1, \dots, N$. Transverse dynamics states $\eta_i = \left(y_i, \dot{y}_i, \dots, y_i^{(\rho_i-1)}\right)$ and RES-CLFs $V_{\epsilon,i}$ can then be defined analogously to (3.6a), (3.7) and (3.11). Moreover, M set-based tasks described by the superzero level set K_j of some r_j times continuously differentiable function h_j can be included at the highest priority level (which is implied by no slack variables). The control input can then be obtained from the QP:

$$\begin{aligned}
&\underset{(u,\delta)\in\mathbb{R}^{m+N}}{\text{minimize}} \quad u^\mathsf{T} H(x) u + c^\mathsf{T}(x) u + \delta^\mathsf{T} W \delta \\
&\text{subject to} \\
&L_{\bar{f}_i} V_{\epsilon,i} + L_{\bar{g}_i} V_{\epsilon,i} u \leq -\frac{\gamma_i}{\epsilon} V_{\epsilon,i} + \delta_i, \qquad i = 1, \dots, N, \\
&L_f^{r_k} h_k + L_g L_f^{r_k-1} h_k u \geq -K_{\alpha,k} \eta_{b,k}, \quad k = 1, \dots, M,
\end{aligned} \tag{3.19}$$

where $\eta_{b,k} = \left(h_k(x), L_f h_k(x), \dots, L_f^{r-1} h_k(x)\right)$, $W \in \mathbb{R}^{N\times N}$ is a diagonal matrix of penalty parameters and

$$L_{\bar{f}_i} V_{\epsilon,i} = \eta_i^\mathsf{T} \left(\Lambda_i^\mathsf{T} P_{\epsilon,i} + P_{\epsilon,i} \Lambda_i\right) \eta_i + 2\eta_i^\mathsf{T} P_i \Gamma_i b_i, \tag{3.20}$$

$$L_{\bar{g}_i} V_{\epsilon,i} = 2\eta_i^\mathsf{T} P_{\epsilon,i} \Gamma_i A_i. \tag{3.21}$$

The equality tasks encoded by RES-CLFs are prioritized by adjusting the elements of the diagonal penalty matrix W. The satisfaction of all equality tasks are therefore described by a single objective function through the value of the slack variables δ and the penalty parameters in W. Whenever equality tasks are incompatible, this fact invariably leads to trade-off configurations that do not satisfy any of the tasks. Hence, strict priority between tasks cannot be achieved in the sense that lower-priority tasks have no effect on the execution of higher-priority tasks. As a result, it is challenging to include lower-priority optimization-based tasks since they will interfere with more critical higher-priority tasks such as end-effector control whenever the tasks are incompatible.

3.2.2 Main Result: Enforcing Strict Priority Between a Selection of Tasks

In order to establish more than two strict priority levels, we propose to solve a quadratic program for every priority level as suggested for kinematic control in [7]. The idea is to begin by computing a control input according to (3.19) that only accounts for safety-related set-based tasks and equality tasks at the highest priority level. Subsequently, a new quadratic program is solved for each priority level, refining the previous solution in an attempt to satisfy lower-priority tasks without affecting the execution of higher-priority tasks.

Consider N equality tasks and M set-based tasks distributed to k priority levels, with $N = N_1 + \ldots + N_k$ and $M = M_1 + \ldots + M_k$, where N_i and M_i denotes the number of equality and set-based tasks at priority level i, respectively. A control input u_1^* that disregards all lower-priority tasks is obtained by solving (3.19) with $i = 1, \ldots, N_1$ and $k = 1, \ldots, M_1$. If the system is redundant with respect to these $N_1 + M_1$ tasks, the control input u_1^* can be refined without affecting how the N_1 higher-priority equality tasks are executed by enforcing

$$L_{\bar{f}_i} V_{\epsilon,i} + L_{\bar{g}_i} V_{\epsilon,i} u \leq L_{\bar{f}_i} V_{\epsilon,i} + L_{\bar{g}_i} V_{\epsilon,i} u_1^* \tag{3.22}$$

which implies that $L_{\bar{g}_i} V_{\epsilon,i} u \leq L_{\bar{g}_i} V_{\epsilon,i} u_1^*$ for all $i = 1, \ldots, N_1$. Similarly, the higher-priority set-based tasks are unaffected by enforcing

$$L_g L_f^{r_k - 1} h_k u \geq L_g L_f^{r_k - 1} h_k u_1^*, \tag{3.23}$$

for all $k = 1, \ldots, M_1$. Consider $\bar{N}_1$ additional equality-based tasks and $\bar{M}_1$ additional set-based tasks. The control input u_1^* can be modified to account for lower-priority tasks without affecting how the N_1 and M_1 equality- and set-based tasks are executed by solving:

$$\begin{aligned}
&\underset{(u,\delta,s)\in\mathbb{R}^{m+N_2+M_2}}{\text{minimize}} \quad && u^\mathsf{T} H(x) u + c^\mathsf{T}(x) u + \delta^\mathsf{T} W_2 \delta + s^\mathsf{T} K_2 s \\
&\text{subject to} \\
&L_{\bar{g}_i} V_{\epsilon,i} u \leq L_{\bar{g}_i} V_{\epsilon,i} u_1^*, && i{=}1,\ldots,N_1, \\
&L_{\bar{f}_j} V_{\epsilon,j} + L_{\bar{g}_j} V_{\epsilon,j} u \leq -\frac{\gamma_j}{\epsilon} V_{\epsilon,j} + \delta_j, && j{=}N_1{+}1,\ldots,N_1{+}\bar{N}_1, \\
&L_g L_f^{r_k - 1} h_k u \geq L_g L_f^{r_k - 1} h_k u_1^*, && k{=}1,\ldots,M_1, \\
&L_f^{r_l} h_l + L_g L_f^{r_l - 1} h_l u \geq -K_{\alpha,l} \eta_{b,l} - s_l, && l{=}M_1{+}1,\ldots,M_1{+}\bar{M}_1,
\end{aligned} \tag{3.24}$$

where slack variables s penalized by the elements in the diagonal matrix $K > 0$ have been added to the lower-priority set-based tasks enforced through ECBFs to ensure feasibility of the optimization problem.

By observing that the solution u_2^* to (3.24) enforces the constraints $L_{\bar{g}_i} V_{\epsilon,i} u_2^* \leq L_{\bar{g}_i} V_{\epsilon,i} u_1^*$ and $L_g L_f^{r_k - 1} h_k u_2^* \geq L_g L_f^{r_k - 1} h_k u_1^*$ for all i and k, it is straightforward to

generalize (3.24) to an arbitrary priority level n:

$$\begin{aligned}
&\underset{(u,\delta,s)\in\mathbb{R}^{m+N_n+M_n}}{\text{minimize}} \quad u^\mathsf{T}Hu + c^\mathsf{T}u + \delta^\mathsf{T}W_n\delta + s^\mathsf{T}K_n s \\
&\text{subject to} \\
&L_{\bar{g}_i}V_{\epsilon,i}u \leq L_{\bar{g}_i}V_{\epsilon,i}u^*_{n-1}, && i{=}\hat{N}_{n-1}{+}1,\ldots,\hat{N}_{n-1}{+}N_n, \\
&L_{\bar{f}_j}V_{\epsilon,j} + L_{\bar{g}_j}V_{\epsilon,j}u \leq -\frac{\gamma_j}{\epsilon}V_{\epsilon,j} + \delta_j, && j{=}\hat{N}_{n-1}{+}N_n{+}1,\ldots,\hat{N}_n, \\
&L_gL_f^{r_k-1}h_k u \geq L_gL_f^{r_k-1}h_k u^*_{n-1}, && k{=}\hat{M}_{n-1}{+}1,\ldots,\hat{M}_{n-1}{+}\bar{M}_n, \\
&L_f^{r_l}h_l + L_gL_f^{r_l-1}h_l u \geq -K_{\alpha,l}\eta_{b,l} - s_l, && l{=}\hat{M}_{n-1}{+}\bar{M}_n{+}1,\ldots,\hat{M}_n,
\end{aligned} \tag{3.25}$$

where $\hat{N}_n = \sum_{i=1}^{n}\left(N_i + \bar{N}_i\right)$ and $\hat{M}_n = \sum_{i=1}^{n}\left(M_i + \bar{M}_i\right)$. Note that the objective function is slightly different at every priority level, since the slack variables δ and s always correspond to tasks at the current priority level. This prevents trade-off configurations where none of the tasks are satisfied from occurring. The procedure is summarized in Algorithm 1.

Algorithm 1 Task priority CLF-ECBF QP controller

Input: $H(x)$, $c(x)$, $V_{\epsilon,i}(\eta_i)$, $i = 1,\ldots,N$, $h_j(x)$, $j = 1,\ldots,M$.
Output: u

1: Solve (3.19) to obtain u_1^* with $i = 1,\ldots,N_1$, $k = 1,\ldots,M_1$.
2: **for** $p = 2$ to k **do**
3: Solve (3.25) to obtain u_p^*.
4: **end for**
5: **return** $u = u_k^*$.

3.3 Simulations

In this section, the proposed hierarchical control scheme is validated in simulation on an AIAUV based on the Eelume robot [66, 67] depicted in Figure 3.1. The AIAUV is a floating base manipulator, with $n+1$ links interconnected by n joints, where link 1 is the tail, or base link and link $n+1$ is the head. The simulation model has $n = 8$ single DOF and revolute joints and $p = 7$ thrusters. The system configuration is described by $\xi = \left(p_{ib}^i, q, \theta\right) \in \mathbb{R}^{7+n}$, where $p_{ib}^i \in \mathbb{R}^3$ is the position of the base of the AIAUV in an inertial frame, $q = (\eta, \varepsilon) \in \mathbb{R}^4$ is a unit quaternion describing the orientation of the base and $\theta = (\theta_1,\ldots,\theta_n) \in \mathbb{R}^n$ are the joint angles. The joint velocities are given by $\dot{\theta}$ and the linear and angular velocities of the base frame with respect to an inertial frame are denoted v_{ib}^b and ω_{ib}^b, respectively. These velocities are collected in the velocity vector $\zeta = \left(v_{ib}^b, \omega_{ib}^b, \dot{\theta}\right) \in \mathbb{R}^{6+n}$. The equations of motion are given by [66]

$$\dot{\xi} = J_\xi(q)\zeta, \tag{3.26}$$

$$M(\theta)\dot{\zeta} + C(\theta,\zeta)\zeta + D(\theta,\zeta)\zeta + g(\xi) = B(\theta)u, \tag{3.27}$$

where $M(\theta)$ is the inertia matrix including hydrodynamic added mass, $C(\theta,\zeta)$ is the Coriolis-centripetal matrix including hydrodynamic added mass, $D(\theta,\zeta)$ is

Figure 3.1: The Eelume AIAUV (Courtesy of Eelume)

the damping matrix, $g(\xi)$ is the vector of gravitational and buoyancy forces and moments, $B(\theta)$ is the actuator configuration matrix and $u = (u_t, u_j) \in \mathbb{R}^{p+n}$ consists of the thruster inputs $u_t \in \mathbb{R}^p$ and joint torque inputs $u_j \in \mathbb{R}^n$. Moreover, the kinematic transformation matrix is given by

$$J_\xi(q) = \begin{pmatrix} R_b^i(q) & 0_{3\times 3} & 0_{3\times n} \\ 0_{4\times 3} & T_q(q) & 0_{4\times n} \\ 0_{n\times 3} & 0_{n\times 3} & I_n \end{pmatrix}, T_q(q) = \frac{1}{2}\begin{pmatrix} -\varepsilon^\mathsf{T} \\ \eta I_3 + [\varepsilon]_\times \end{pmatrix}, \tag{3.28}$$

where $R_b^i(q) \in \mathrm{SO}(3)$ is a rotation matrix describing the rotation between the base and inertial frame and $[\cdot]_\times : \mathbb{R}^3 \to \mathfrak{so}(3)$ denotes the skew symmetric map.

By defining $x = (x_1, x_2) = (\xi, \zeta)$, the equations of motion can be rewritten in state space form

$$\dot{x} = f(x) + g(x)u, \tag{3.29}$$

where

$$f(x) = \begin{pmatrix} J_\xi(x_1)x_2 \\ -M(x_1)^{-1}\left(C(x)x_2 + D(x)x_2 + g(x_1)\right) \end{pmatrix}, \tag{3.30}$$

$$g(x) = \begin{pmatrix} 0 \\ M(x_1)^{-1}B(x_1) \end{pmatrix}. \tag{3.31}$$

With $6 + n = 14$ DOFs and $p + n = 15$ control inputs, the system is overactuated, since the number of actuators is greater than the number of DOFs. Moreover, 14 DOFs imply that the system is redundant with respect to typical tasks such as end-effector configuration control.

We consider four equality-based tasks and three set-based tasks, at three different priority levels. The set-based tasks are safety-related and are thus placed at the highest priority level. The safety-related tasks consist of end-effector collision avoidance, actuator configuration matrix singularity avoidance and joint limit

avoidance. The purpose of the end-effector collision avoidance task is to avoid a spherical obstacle with radius $r_{\text{obs}} \in \mathbb{R}$. To this end, the scalar distance measure between the center of the obstacle and the end-effector is employed as a set-based task $\sigma_a \in \mathbb{R}$. In order to ensure that the distance from the end-effector to the center of the spherical obstacle is always greater than some lower limit, we enforce the positivity of the following ECBF

$$h_1(x) = \underbrace{\sqrt{\left(p^i_{\text{obs}} - p^i_{ie}\right)^{\mathsf{T}} \left(p^i_{\text{obs}} - p^i_{ie}\right)}}_{\sigma_a} - (r_{\text{obs}} + \epsilon), \tag{3.32}$$

where $\epsilon \in \mathbb{R}$ defines an inaccessible safety region around the spherical obstacle and p^i_{ie} and p^i_{obs} are the positions of the end-effector and the center of the spherical obstacle in an inertial frame, respectively.

Rank deficiency of the actuator configuration matrix $B(\theta)$ was pointed out in [68], and implies that no force or moment can be generated in certain directions in the vector space $\mathbb{R}^{6+n}$ belonging to τ. Inspired by the manipulability measure [69], the actuation measure $\sigma_b = \det\left(B(\theta)B^{\mathsf{T}}(\theta)\right)$ is introduced as a high-priority set-based task to prevent singular configurations. The actuation measure is kept above a minimum value $\sigma_{b,\min}$ through the following ECBF

$$h_2(x) = \det\left(B(\theta)B^{\mathsf{T}}(\theta)\right) - \sigma_{b,\min}. \tag{3.33}$$

The third safety-related task is the joint limit avoidance task $\sigma_c = \theta \in \mathbb{R}^n$, which has both lower and upper limits. Hence, $2n$ ECBFs are needed of the form

$$h_{j+2}(x) = \theta_j - \theta_{j,\min}, \tag{3.34}$$

$$h_{j+2+n}(x) = \theta_{j,\max} - \theta_j. \tag{3.35}$$

for $j = 1, \ldots, n$.

The second priority level contains the equality-based end-effector positioning and orientation tasks

$$y_1 = \vartheta_1(x) = p^i_{ie} - p^i_{d,e}, \tag{3.36}$$

$$y_2 = \vartheta_2(x) = \tilde{\varepsilon}, \tag{3.37}$$

where $p^i_{d,e}$ is the desired end-effector position and $\tilde{\varepsilon}$ is the imaginary part of the quaternion error vector $\tilde{q} = q_d \otimes q^*$, which is given by

$$\tilde{\varepsilon} = \eta\varepsilon_d - \eta_d\varepsilon + [\varepsilon]_\times \varepsilon_d, \tag{3.38}$$

where q_d and q are the quaternion representations of the desired and measured orientation of the end-effector, respectively.

In order to minimize movement of the base while repositioning the end-effector, a base positioning task is defined at the third priority level

$$y_3 = \vartheta_3(x) = p^i_{ib} - p^i_{d,b}, \tag{3.39}$$

where $p^i_{ib} \in \mathbb{R}^3$ and $p^i_{d,b} \in \mathbb{R}^3$ are the measured and desired positions of the AIAUV base in the inertial frame, respectively. Note that the end-effector positioning and

orientation and base positioning tasks only consume 9 DOFs, which entails that there are still 5 uncontrolled DOFs if all set-based tasks are inactive. Stability of the entire system can therefore only be guaranteed if the resulting zero dynamics is asymptotically stable. Instead of performing a complicated analysis of the zero dynamics, a joint velocity regulation task is designed to eliminate the residual DOFs of the system $y_4 = \dot{\theta}$, where $\dot{\theta} \in \mathbb{R}^n$ is the vector of joint velocities.

The input-output dynamics of the equality tasks are then obtained from (3.18) such that transverse dynamics states η_i and RES-CLFs $V_{\epsilon,i}$ can be defined analogously to (3.6a), (3.7) and (3.11), with $\rho_1 = \rho_2 = \rho_3 = 2$ and $\rho_4 = 1$, where ρ_i denotes the amount of times y_i has to be differentiated for the input to appear. Furthermore, the set-based tasks in (3.32)-(3.35) all have to be differentiated twice with respect to time for the input to show up, hence $r_1 = \cdots = r_{18} = 2$.

The design matrix $H(x)$ and design vector $c(x)$ in the objective functions are selected by minimizing the virtual control input $\mu = Au + b$ quadratically as done in [17, 18], where

$$A(x) = \begin{pmatrix} A_1(x) \\ A_2(x) \\ A_3(x) \\ A_4(x) \end{pmatrix}, \quad b(x) = \begin{pmatrix} b_1(x) \\ b_2(x) \\ b_3(x) \\ b_4(x) \end{pmatrix}. \tag{3.40}$$

In terms of u, this yields

$$\mu^\mathsf{T}\mu = u^\mathsf{T}A^\mathsf{T}Au + 2b^\mathsf{T}Au + b^\mathsf{T}b, \tag{3.41}$$

which implies that $H(x) = A^\mathsf{T}(x)A(x)$ and $c^\mathsf{T}(x) = 2b^\mathsf{T}(x)A(x)$.

According to Algorithm 1, we solve the following QP:

$$\begin{aligned} \underset{u\in\mathbb{R}^{15},(\delta_1,\delta_2)\in\mathbb{R}^2}{\text{minimize}} \quad & u^\mathsf{T}A^\mathsf{T}Au + 2b^\mathsf{T}Au + w_1\delta_1^2 + w_2\delta_2^2 \\ \text{subject to} \quad & \\ L_{\bar{f}_i}V_{\epsilon,i} + L_{\bar{g}_i}V_{\epsilon,i}u \leq -\frac{\gamma_1}{\epsilon_i}V_{\epsilon,i} + \delta_i, \quad & i = 1,2, \\ L_f^2 h_k + L_g L_f h_k u \geq -K_{\alpha,k}\eta_{b,k}, \quad & k = 1,\dots,18, \\ -u_{max} \leq u \leq u_{max}, & \\ -\Delta u_{max} \leq \Delta u \leq \Delta u_{max}, & \end{aligned} \tag{3.42}$$

where $\Delta u = u - u_{\text{prev}}$ is the change in control input, u_{prev} is the control input at the last sample, and $u_{max} = (50,\dots,50)$ and $\Delta u_{max} = (0.1,\dots,0.1)$ are thruster and joint torque limits and rate constraints, respectively. The QP in (3.42) yields a control input $u = u_1^*$ that only accounts for the safety-related tasks and the end-effector positioning and orientation tasks. The solution u_1^* is refined by utilizing the excess DOFs of the system in an attempt to keep the base stationary and minimize

Table 3.1: Equality task convergence rates ϵ and penalty parameters w

	y_1	y_2	y_3	y_4
ϵ	1.2	0.2	1.2	0.5
w	60	60	10	10

the joint velocities through the QP:

$$
\begin{aligned}
&\underset{u\in\mathbb{R}^{15},(\delta_3,\delta_4)\in\mathbb{R}^2}{\text{minimize}} \quad u^\mathsf{T}A^\mathsf{T}Au + 2b^\mathsf{T}Au + w_3\delta_3^2 + w_4\delta_4^2 \\
&\text{subject to} \\
&L_{\bar{g}_i}V_{\epsilon,i}u \leq L_{\bar{g}_i}V_{\epsilon,i}u_i^*, && i = 1, 2, \\
&L_{\bar{f}_j}V_{\epsilon,j} + L_{\bar{g}_j}V_{\epsilon,j}u \leq -\frac{\gamma_j}{\epsilon_j}V_{\epsilon,j} + \delta_j, && j = 3, 4, \\
&L_gL_fh_ku \geq L_gL_fh_ku_1^*, && k = 1, \ldots, 18, \\
&-u_{max} \leq u \leq u_{max}, \\
&-\Delta u_{max} \leq \Delta u \leq \Delta u_{max},
\end{aligned}
\tag{3.43}
$$

which yields the final control input $u = u_2^*$ that is applied to the AIAUV. The equality task control parameters are listed in Table 3.1, while $K_{\alpha,k} = (3, 4)$ for all $k = 1, \ldots, 18$.

We remark that the optimization problems are formulated in terms of the thruster and joint torque control inputs u, and not the commanded forces and torques $\tau = Bu$. Consequently, the proposed framework also solves the control allocation problem, which had to be solved separately in previous works [68, 70]. By unifying redundancy resolution, dynamic control and control allocation, strict priority among tasks can always be ensured. The same guarantee does not hold for redundancy resolution schemes that decouple dynamic control and control allocation, since the commanded forces and torques may not be exactly allocable, leading to a loss of priority among tasks.

Simulations were performed in Matlab/Simulink using the ode3 solver with a fixed step-size of 0.01. Simulation results are presented in Figures 3.2 to 3.5. From Figures 3.4 and 3.5 we observe that the high-priority set-based tasks are satisfied at all times. In general, the redundancy of the system is exploited such that the lower-priority equality tasks are satisfied even when higher-priority set-based tasks are at their limits and consuming DOFs. For instance, the actuation measure is kept above a minimum value of 0.1, which avoids singular configurations of the actuation configuration matrix from occurring and thereby reducing the magnitude and/or rates of change of the control inputs, at the cost of maneuverability [71]. However, the high-priority collision avoidance task results in a small deviation in the lower-priority end-effector positioning task. Specifically, we observe from Figure 3.2 and Figure 3.4 that the x-coordinate of the end-effector position deviates slightly from its reference and that the distance to the center of the spherical obstacle is at its minimum value between $t \simeq 268\,\text{s}$ and $t \simeq 281\,\text{s}$.

After $t \geq 350\,\text{s}$, the end-effector position is commanded outside of the manipulator workspace (when the base is kept at its current position), which implies that

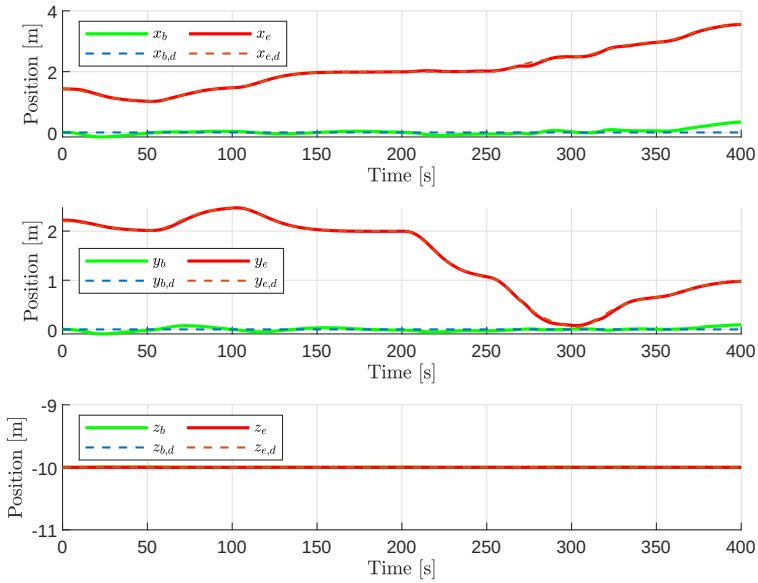

Figure 3.2: The position of the end-effector p_{ie}^i and base p_{ib}^i.

the lower-priority base positioning task is no longer compatible with the higher-priority end-effector positioning task. As desired, the strict priority between tasks is kept at all time, such that the end-effector position converges to its desired value at the expense of a greater error in the base position.

Finally, we note from Figure 3.3 that the thruster and joint torque control inputs are smooth and well within the physical limitations of the Eelume robot.

3.4 Conclusions and Future Work

This chapter has presented a novel task-priority framework for redundancy resolution, dynamic control and control allocation of redundant robotic systems based on a hierarchy of CLF- and CBF-based QPs. The framework provides strict priority, ensuring that lower-priority tasks have no effect on higher-priority tasks, by solving additional QPs to establish distinct priority levels. As a result, lower-priority control objectives can be safely included, without affecting the execution of higher-priority mission-related or safety-related tasks. Additionally, a soft priority measure in the form of slack variables can be utilized in order to prioritize tasks at the same priority level, resulting in considerable design freedom.

The proposed framework has been verified in simulations for an AIAUV, which is an overactuated and redundant robotic system. For these types of systems, the proposed task-priority framework also solves the control allocation problem, which is highly advantageous since control input bounds and rate constraints can be accounted for when resolving redundancy, effectively avoiding a situation in which commanded generalized forces and torques cannot be allocated explicitly, leading to a loss of priority among tasks.

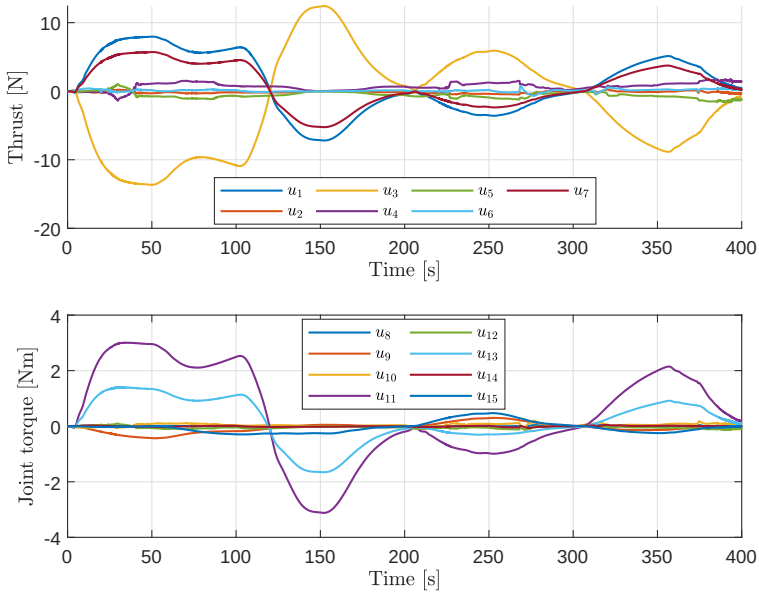

Figure 3.3: The thruster and joint torque control inputs.

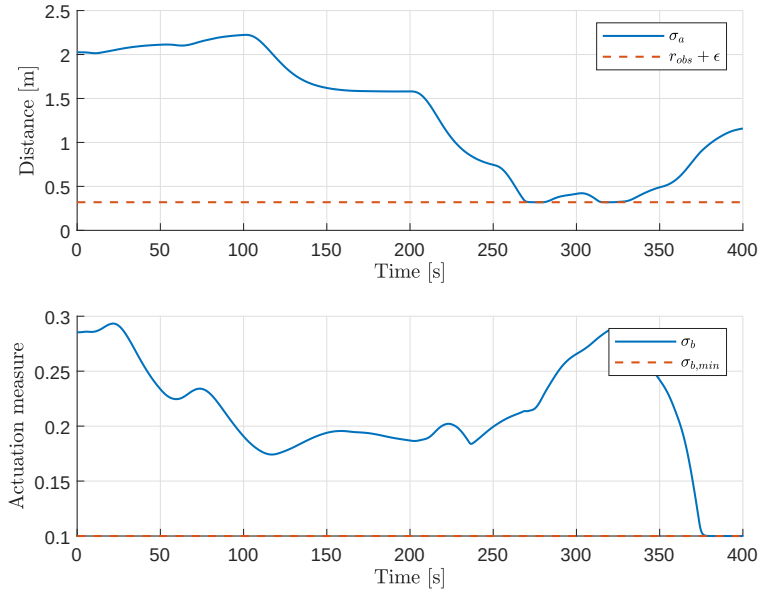

Figure 3.4: The distance to the center of the spherical obstacle σ_a and its minimum value $r_{\text{obs}} + \epsilon$, and the actuation measure σ_b and its minimum value $\sigma_{b,\text{min}}$.

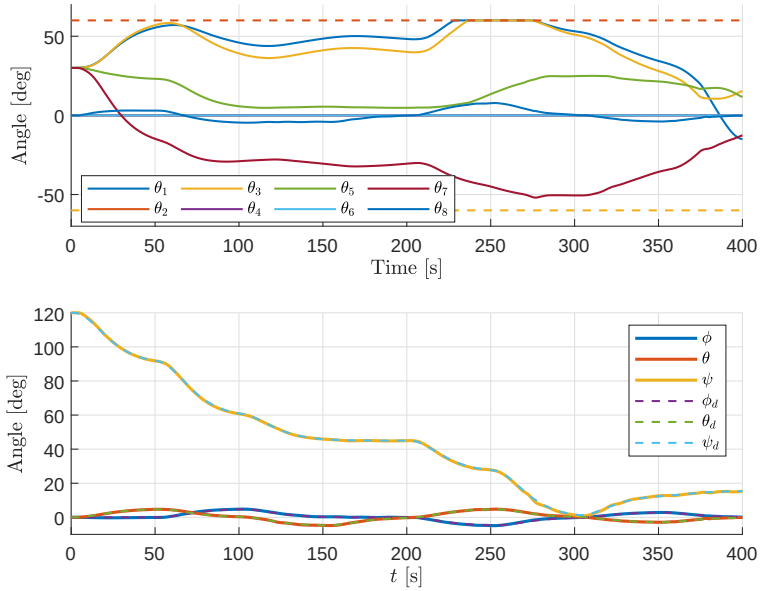

Figure 3.5: The joint angles θ, their maximum and minimum limits $\theta_{\max} = 60°$ and $\theta_{\min} = -60°$, and the orientation of the end-effector, represented by the roll-pitch-yaw Euler angles ϕ, θ and ψ.

Future work is aimed at investigating the robustness of the proposed framework with respect to modeling inaccuracies. This is especially relevant for an underwater vehicle application such as an AIAUV, where accurate identification of the dynamic model parameters is difficult [72]. An experimental implementation of the proposed control system on an AIAUV will further validate the framework.

Chapter 4

Safety-Critical Control of Autonomous Surface Vehicles in the Presence of Ocean Currents

In this chapter, we propose a CLF- and CBF-based convex quadratic optimization problem for robust safety-critical control of ASVs. The framework is motivated by Chapter 3, builds on [18, 28, 29, 73], and is applicable to a larger class of nonlinear affine control systems. Safety-related objectives are enforced through CBFs, while stabilization objectives are enforced through relaxed CLFs. Relaxation of the CLFs implies that the stabilization and safety-related objectives do not need to be simultaneously satisfiable. We propose CLFs endowed with integral action in order to mitigate the effects of unknown and slowly varying nonlinearities such as the effect of ocean currents. Moreover, we modify the results on robust CBFs in [73] for uncertain systems modeled by differential equations in order to provide analytical conditions guaranteeing safety in the presence of unknown nonlinearities. These conditions are subsequently utilized to obtain robust CBFs ensuring reactive collision avoidance for ASVs. Employing an optimization-based control law enables formulating the control problem in terms of the actuator control inputs and thereby unifying the control problem with the control allocation problem. This unification handles control input saturations more effectively than a decoupled approach and is less likely to lead to instability [17], which is especially relevant during emergency collision avoidance maneuvers. We consider ASVs with nonlinear actuator models and derive a partially linearized control design model by linearizing the actuator configuration matrix at every time step to avoid a non-convex optimization problem.

The material in this chapter is based on [50].

4.1 Introduction

In recent years, a significant research effort has been devoted to autonomous surface vehicles (ASVs). Fully autonomous surface vehicles will have a significant impact in a wide variety of areas such as commercial shipping [74], passenger transport [75],

scientific research [76], and military applications. ASVs are safety-critical systems with a tight coupling between the potentially conflicting maneuvering objectives (e.g. following a geometric path at a desired speed), and safety-related objectives such as collision avoidance. The control problem is further complicated by magnitude and rate constraints on the actuators, and nonlinear actuator models in the case of azimuth thrusters.

Control algorithms for marine vessels often decouple the control problem into two parts. First, a high-level motion control algorithm is developed for position and heading control by considering the forces and moments generated by the actuators as a virtual control input. After determining the virtual control input from the motion control algorithm, a control allocation problem must be solved in order to distribute the virtual control input into the physical control inputs of the actuators such that the total forces and moments generated by the actuators correspond to the virtual input. This decoupling is not very restrictive for systems where the actuator configuration is constant. However, for actuators such as azimuth thrusters, the azimuth angles are also control inputs, and a nonlinear control allocation problem must be solved, requiring sophisticated real-time optimization techniques [71, 77].

Decoupling the control problem makes it difficult to account for magnitude and rate constraints within the motion control algorithm, which can lead to virtual control inputs from the motion control algorithm that cannot be realized by the actuator control inputs. The actuator control inputs must then be found by minimizing the difference between the virtual control input and the total forces and moments generated by the actuators in some sense. A drawback of this approach is the fact that this minimization does not necessarily lead to minimizing the tracking error.

Control allocation algorithms for systems with linear and nonlinear actuator models were surveyed in [65]. In [78], a model predictive control algorithm combined position and heading control with control allocation for a dynamic positioning application. This approach requires a linear model and is less feasible for marine vessels operating at higher speeds, where centripetal forces and nonlinear damping effects dominate.

Control Lyapunov function (CLF)-based quadratic programs (QP) have been applied to a variety of systems including biped robots [14, 17, 18, 79], automotive systems [28], and hyper-redundant underwater manipulators as demonstrated in Chapter 3. CLF-based QP controllers are attractive due to their real-time feasibility on standard hardware [80] and natural inclusion of actuator magnitude and rate constraints. Gradual performance degradation of a CLF-based QP controller under strict input constraints was experimentally shown in [17]. While CLFs thus are attractive for achieving the maneuvering objectives of ASVs, control barrier functions (CBFs) are a powerful tool for ensuring forward invariance of sets in order to provide safety guarantees. CBFs were introduced in [25] and unified with CLFs in [26] and [28] using different formulations. This chapter builds on the approach taken in [28], which mediated safety and stabilization objectives by guaranteeing safety and achieving stabilization when the objectives are not in conflict. CBFs have been utilized for collision avoidance of miniature differential drive robots in [73, 81], underwater manipulators [49], and recently for ASVs in [82]. A method for robust

CLF-CBF-QP control was proposed in [79], which achieves robustness through constant scalar-valued upper bounds on the model uncertainty appearing in the CLF and CBF derivatives, often leading to overly conservative estimates. Robust CBFs for uncertain systems were also considered in [83] and [73]. The method in [83] results in a nonlinear optimization problem, making it less feasible for real-time applications, while [73] extended CBFs to a particular class of disturbed systems modeled by differential inclusions.

This rest of this chapter is organized as follows, Section 4.2 presents background theory on robust CBFs, specifically, conditions guaranteeing safety in the presence of unknown nonlinearities. These conditions are subsequently employed for safe CLF-CBF-QP controller synthesis for a general nonlinear affine control system. In Section 4.3, ASV models for simulation, and CLF and CBF design in the presence of unknown ocean currents are presented. For CBF design, an arbitrary number of ocean current approximations are generated and conditions guaranteeing safety are derived. Section 4.4 introduces the stabilization objective before we construct CLFs with integral action and robust CBFs for reactive collision avoidance. Moreover, a general CLF-CBF-QP controller for safety-critical control is presented. A simulation study for a double-ended passenger ferry implements the proposed framework in Section 4.5, before Section 4.6 concludes the chapter.

4.2 Safety-Critical Control of Nonlinear Affine Control Systems

This section presents the main theoretical result of this chapter. Specifically, Theorem 4.1 provides conditions for which an arbitrary number of nonlinear maps estimating some unknown system nonlinearity guarantees safety. Section 4.2.2 extends the CLF-CBF-QP controller from [28] by using Theorem 4.1 to guarantee safety in the presence of unknown nonlinearities and by incorporating CLFs with integral action to remove steady-state tracking errors.

4.2.1 Robust CBFs for a Class of Uncertain Nonlinear Systems

Assume that $f(\chi) = \tilde{f}(\chi) + \vartheta(\chi)$ and rewrite (2.15) as

$$\dot{\chi} = \tilde{f}(\chi) + \vartheta(\chi) + g(\chi)u, \tag{4.1}$$

where the unknown mapping $\vartheta : \mathbb{R}^n \to \mathbb{R}^n$ is continuous. We modify the robustness results for disturbed nonlinear affine control systems described by set-valued mappings in [73] to the system (4.1) as follows:

Theorem 4.1. *Consider $P > 0$ continuous mappings $\varphi_i : \mathbb{R}^n \to \mathbb{R}^n$, $i \in \mathcal{P} = \{1, \dots, P\}$, and let $h : \mathbb{R}^n \to \mathbb{R}$ be a continuously differentiable function defining K. Then, h is a CBF for (4.1) if there exists an open set $X \subset \mathbb{R}^n$ with $K \subset X$ such that for all $\chi \in X$*

1. *the mappings φ_i satisfy*

$$\min_{i \in \mathcal{P}} \nabla h(\chi)^\mathsf{T} \varphi_i(\chi) \leq \nabla h(\chi)^\mathsf{T} \vartheta(\chi); \tag{4.2}$$

2. *there exists a continuous control law* $\kappa : \mathbb{R}^n \to \mathbb{R}^p$ *and an extended class-*$\mathcal{K}_\infty$ *function* $\sigma : \mathbb{R} \to \mathbb{R}$ *such that*

$$\nabla h(\chi)^\mathsf{T} \tilde{f}(\chi) + \nabla h(\chi)^\mathsf{T} g(\chi)\kappa(\chi) \geq -\sigma(h(\chi)) - \min_{i \in \mathcal{P}} \nabla h(\chi)^\mathsf{T} \varphi_i(\chi), \tag{4.3}$$

then h *is a CBF for* (4.1) *and the control input* $u = \kappa(\chi)$ *renders the superzero level set* K *forward pre-invariant for* (4.1).

Proof. The proof follows from the fact that $\tilde{f}$ and g are continuous, the minimum of continuous mappings is in itself continuous, and by combining (4.2) with (4.3) to obtain

$$\nabla h(\chi)^\mathsf{T} \tilde{f}(\chi) + \nabla h(\chi)^\mathsf{T} g(\chi)\kappa(\chi) \geq -\sigma(h(\chi)) - \nabla h(\chi)^\mathsf{T} \vartheta(\chi), \quad \forall \chi \in X, \tag{4.4}$$

which is equivalent to

$$\nabla h(\chi)^\mathsf{T} f(\chi) + \nabla h(\chi)^\mathsf{T} g(\chi)\kappa(\chi) \geq -\sigma(h(\chi)), \tag{4.5}$$

for all $\chi \in X$. By Definition 2.22, h is a valid CBF for (4.1), which combined with the fact that κ is continuous and and $\kappa(\chi) \in U_h(\chi)$ for all $\chi \in X$, guarantees forward pre-invariance of the superzero level set K from Corollary 2.24. □

Theorem 4.1 can be used to synthesize safe controllers by generating P continuous mappings capturing the unknown nonlinearity with sufficient accuracy. By enforcing (4.3) as a constraint on the control input, the effect of the most conservative function estimate φ_i on the positivity of the function h can be accounted for. Moreover, by constructing state-dependent function estimates we can avoid excessively conservative scalar estimates on the norm of the uncertain term $\chi \mapsto \nabla h(\chi)^\mathsf{T} \vartheta(\chi)$ as in [79].

4.2.2 Controller Synthesis via Quadratic Programming

If the unknown mapping ϑ is slowly varying, it is reasonable to assume that an ES-CLF $V(\cdot)$ with integral action for the system (4.1) with $\vartheta = 0$ will stabilize (2.15). Moreover, consider a safety-related objective encoded by $h(\cdot)$. By relaxing the stabilization objective, a safe controller can be synthesized for the system (2.15) by solving the following QP

$$\begin{aligned}
&\underset{(u,\delta) \in \mathbb{R}^{p+1}}{\text{minimize}} \quad \frac{1}{2} u^\mathsf{T} H u + c^\mathsf{T} u + w\delta^2 && \text{(4.6a)}\\
&\text{subject to} \\
&\langle \nabla V(\chi), \tilde{f}(\chi) + g(\chi)u \rangle \leq -\gamma V(\chi) + \delta, && \text{(4.6b)}\\
&\langle \nabla h(\chi), \tilde{f}(\chi) + g(\chi)u \rangle \geq -\sigma(h(\chi)) - \min_{i \in \mathcal{P}} \langle \nabla h(\chi), \varphi_i(\chi) \rangle, && \text{(4.6c)}
\end{aligned}$$

where $H \in \mathbb{R}^{p \times p}$ is any positive definite matrix, $c \in \mathbb{R}^p$, and $\delta \in \mathbb{R}$ is a slack variable penalized by the weighting parameter $w > 0$. The slack variable is added to ensure feasibility of the optimization problem in case the stabilization objective

conflicts with the safety-related objective. Moreover, the addition of the slack variable ensures that the safety-related objective can always be satisfied. By choosing the weighting parameter appropriately, the solution to the QP will result in $\delta \approx 0$ when the stabilization and safety-related objectives are not conflicting.

4.3 Vessel Modeling for Safety and Stabilization

This section presents ASV models for stabilization and safety design. Specifically, in Sections 4.3.1 and 4.3.2 we describe the simulation model and the control allocation problem. The control design model, which does not include the effect of the unknown ocean currents, is presented in Section 4.3.3. Moreover, we formulate the model in terms of the azimuth angle and force magnitude control inputs of the actuators, and not the generalized forces produced by the actuators. This allows us to subsequently linearize the mapping from control inputs to generalized forces, avoiding a non-convex dynamic optimization problem. In Section 4.3.4 we consider the validity of the control design model and modify it accordingly for CBF design. Furthermore, we modify Theorem 4.1 to the case where the unknown map ϑ is known, but depends on an unknown vector of parameters, which enables safe controller synthesis in the presence of unknown ocean currents.

4.3.1 Vessel Model

The system configuration of a surface vessel can be described by $\eta = (p^n, \psi)$, where $p^n = (x^n, y^n) \in \mathbb{R}^2$ is the North and East coordinates of the body frame of the ship in the assumed inertial North-East-Down (NED) frame, and $\psi \in \mathbb{R}$ is the heading angle. Define the mapping $R : \mathbb{R} \to \mathrm{SO}(3)$ by

$$R(\varrho) := \begin{pmatrix} \cos\varrho & -\sin\varrho & 0 \\ \sin\varrho & \cos\varrho & 0 \\ 0 & 0 & 1 \end{pmatrix}. \tag{4.7}$$

Then, $R(\psi)$ denotes the rotation matrix around the z-axis describing the rotation between the body frame and NED frame. The velocity vector expressed in the body frame is defined by $\nu := (u, v, r) \in \mathbb{R}^3$.

Assumption 4.2. *The unknown ocean current V_c is defined in the NED frame, and is assumed to be constant and irrotational. Hence, $V_c = U_c\,(\cos(\beta_c), \sin(\beta_c), 0)$, where $\beta_c \in (-\pi, \pi]$ is the current direction and $U_c \geq 0$ is the current speed.*

Assumption 4.2 implies that the ocean current in the body frame is given by $\nu_c = (u_c, v_c, 0) = R(\psi)^\mathsf{T} V_c$, with $\dot{\nu}_c = (rv_c, -ru_c, 0) = \dot{R}(\psi, r)^\mathsf{T} V_c$. Defining the relative velocity by $\nu_r := \nu - \nu_c$, the equations of motion are given by [84]

$$\dot{\eta} = R(\psi)\nu, \tag{4.8a}$$

$$\dot{\nu} = \dot{R}(\psi, r)^\mathsf{T} V_c + M^{-1}\left(\tau - C(\nu_r)\nu_r - D(\nu_r)\nu_r\right), \tag{4.8b}$$

where M is the inertia matrix including hydrodynamic added mass, $C(\nu_r)$ is the Coriolis-centripetal matrix including hydrodynamic added mass, $D(\nu_r)$ is the

damping matrix, and $\tau \in \mathbb{R}^3$ are the generalized forces produced by the actuators. Moreover, the Coriolis and centripetal matrix can be expressed as $C(\nu_r) = C(\nu) + \bar{C}(\nu_c)$, while the damping matrix can be decomposed into a linear and nonlinear part $D(\nu_r) = D_l + D_n(\nu_r)$, where

$$D_n(\nu_r) = -\begin{pmatrix} d_1|u_r| & 0 & 0 \\ 0 & d_2|v_r| + d_3|r| & d_4|v_r| + d_5|r| \\ 0 & d_6|v_r| + d_7|r| & d_8|v_r| + d_9|r| \end{pmatrix}, \tag{4.9}$$

where $d_j \in \mathbb{R}$, $j \in \{1, \ldots, 9\}$. See [84] for further details.

4.3.2 Control Allocation

Consider a marine vessel equipped with m actuators, the mapping between the generalized forces τ and the control inputs $u = (\mu, \alpha) \in \mathbb{R}^{2m}$ is given by

$$\tau = B(\alpha)\mu, \tag{4.10}$$

where $B : \mathbb{R}^m \to \mathbb{R}^{3\times m}$ is the actuator configuration matrix, α are the azimuth angles of the actuators and μ is the vector of force magnitudes produced by the actuators. The ith column of the actuator configuration matrix is given by

$$B_i(\alpha_i) = \begin{pmatrix} \cos\alpha_i \\ \sin\alpha_i \\ -l_{y_i}\cos\alpha_i + l_{x_i}\sin\alpha_i \end{pmatrix}, \tag{4.11}$$

where the location of the ith actuator in a body-fixed coordinate system with origin at the center of rotation is at (l_{x_i}, l_{y_i}). Solving (4.10) for the actuator control inputs μ, α, given a desired generalized force τ, is known as the control allocation problem [71].

4.3.3 Vessel Model for CLF-based Control Design

For low-speed maneuvering up to 2 m/s, linear damping is the dominating dissipative force [84]. Moreover, from (4.9) it is apparent that approximating $D_n(\nu_r)$ by $D_n(\nu)$ is ill-advised when the vessel and current velocity are similar in magnitude and the current direction is unknown. Therefore, we simplify the model (4.8) for control design by by neglecting the effects of nonlinear damping and by assuming that $V_c = 0$

$$\dot{\eta} = R(\psi)\nu, \tag{4.12a}$$

$$M\dot{\nu} + C(\nu)\nu + D_l\nu = B(\alpha)\mu, \tag{4.12b}$$

where $u = (\mu, \alpha) \in \mathbb{R}^{2m}$ is the control input. Since the system (4.12) is not affine in the control input u, the design procedure in Section 4.2 will yield a non-convex dynamic optimization problem due to the resulting non-convexity of (4.6b) and (4.6c). Following [71], a control affine system is obtained by linearizing (4.10) about

the azimuth angles α_0 and force magnitudes μ_0 from the previous sample

$$\begin{aligned} B(\alpha)\mu &\approx B(\alpha_0)\Delta\mu + \frac{\partial}{\partial\alpha}\left(B(\alpha)\mu\right)\Big|_{\substack{\alpha=\alpha_0\\ \mu=\mu_0}} \Delta\alpha + B(\alpha_0)\mu_0 \\ &= \underbrace{\begin{pmatrix} B(\alpha_0) & \frac{\partial}{\partial\alpha}\left(B(\alpha)\mu\right)\big|_{\substack{\alpha=\alpha_0\\ \mu=\mu_0}} \end{pmatrix}}_{\bar{B}(\alpha_0,\mu_0)} \Delta u + B(\alpha_0)\mu_0, \end{aligned} \tag{4.13}$$

where $\Delta\mu = \mu - \mu_0$, $\Delta\alpha = \alpha - \alpha_0$ and $\Delta u = u - u_0 = (\Delta\mu, \Delta\alpha)$. Combining (4.13) and (4.12) yields the partially linearized control affine system

$$\dot{\eta} = R(\psi)\nu, \tag{4.14a}$$

$$M\dot{\nu} + C(\nu)\nu + D_l\nu = \bar{B}(u_0)\Delta u + B(\alpha_0)\mu_0. \tag{4.14b}$$

which admits the following state-space representation

$$\dot{x} = f(x) + g\Delta u, \tag{4.15}$$

where $x = (\eta, \nu)$ and

$$f(x) = \begin{pmatrix} R(\psi)\nu \\ M^{-1}\left(B(\alpha_0)\mu_0 - C(\nu)\nu - D_l\nu\right) \end{pmatrix}, \tag{4.16}$$

$$g = \begin{pmatrix} 0_{3\times 2m} \\ M^{-1}\bar{B}(\alpha_0, \mu_0) \end{pmatrix}. \tag{4.17}$$

4.3.4 Vessel Model for CBF Design

For CBF design, we assume low-speed maneuvering and modify the full model (4.8) by neglecting nonlinear damping

$$\dot{\eta} = R(\psi)\nu, \tag{4.18a}$$

$$\dot{\nu} = M^{-1}\left(\tau - C(\nu)\nu - D_l\nu\right) + \vartheta(\eta, \nu, \nu_c), \tag{4.18b}$$

where

$$\vartheta(\eta, \nu, \nu_c) = \dot{R}(\psi, r)^\mathsf{T} V_c + M^{-1}\left(C(\nu)\nu_c - \bar{C}(\nu_c)\nu_r + D_l\nu_c\right). \tag{4.19}$$

The system (4.18) admits the following state-space representation

$$\dot{x} = \breve{f}(x, \nu_c) + \breve{g}\tau, \tag{4.20}$$

where $x = (\eta, \nu) \in \mathbb{R}^3 \times \mathbb{R}^3$ and

$$\breve{f}(x, \nu_c) = f(x) + \begin{pmatrix} 0_{3\times 1} \\ \vartheta(\eta, \nu, \nu_c) \end{pmatrix}, \quad \breve{g} = \begin{pmatrix} 0_{3\times 3} \\ M^{-1} \end{pmatrix}, \tag{4.21}$$

where $\breve{f} : (\mathbb{R}^3 \times \mathbb{R}^3) \times \mathbb{R}^3 \to \mathbb{R}^6$ and $\breve{g} \in \mathbb{R}^{6\times 3}$ are continuous. We want to generate $P > 0$ continuous mappings approximating the dynamic effect of the ocean current. To this end, Theorem 4.1 is specialized for the case where the mapping ϑ is known, but instead depends on the unknown parameters ν_c.

Proposition 4.3. *Given $P > 0$ ocean current estimates $\hat{V}_{c,i}$, $i \in \mathcal{P} = \{1, \dots, P\}$, define P continuous mappings $\varphi_i : \mathbb{R} \times \mathbb{R} \times \mathbb{R}^3 \times \mathbb{R}^3 \to \mathbb{R}^3$ by*

$$\varphi_i(\psi, r, \nu, \hat{\nu}_{c,i}) := \dot{R}(\psi, r)^\mathsf{T} \hat{V}_{c,i} + M^{-1} \left(C(\nu)\hat{\nu}_{c,i} - \bar{C}(\hat{\nu}_{c,i})\hat{\nu}_{r,i} + D_l \hat{\nu}_{c,i} \right), \tag{4.22}$$

where $\hat{\nu}_{c,i} = R(\psi)^\mathsf{T} \hat{V}_{c,i}$ and $\hat{\nu}_{r,i} = \nu - \hat{\nu}_{c,i}$. Let $h : \mathbb{R}^3 \times \mathbb{R}^3 \to \mathbb{R}$ be a continuously differentiable function defining K. If there exists an open set $X \subset \mathbb{R}^3 \times \mathbb{R}^3$ with $K \subset X$ such that for all $(\eta, \nu, \nu_c) \in X \times \mathbb{R}^3$

- *the ocean current estimates $\hat{\nu}_{c,i}$ satisfy*

$$\min_{i \in \mathcal{P}} \nabla_2 h(\eta, \nu)^\mathsf{T} \varphi_i(\psi, r, \nu, \hat{\nu}_{c,i}) \leq \nabla_2 h(\eta, \nu)^\mathsf{T} \vartheta(\eta, \nu, \nu_c); \tag{4.23}$$

- *there exists a continuous control law $\kappa : \mathbb{R}^3 \times \mathbb{R}^3 \to \mathbb{R}^3$ and an extended class-$\mathcal{K}_\infty$ function $\sigma : \mathbb{R} \to \mathbb{R}$ such that*

$$\begin{aligned} &\nabla_1 h(\eta, \nu)^\mathsf{T} R(\psi)\nu + \nabla_2 h(\eta, \nu)^\mathsf{T} M^{-1} \left(\kappa(\eta, \nu) - C(\nu)\nu - D_l \nu \right) \\ &\geq -\sigma(h) - \min_{i \in \mathcal{P}} \nabla_2 h(\eta, \nu)^\mathsf{T} \varphi_i(\psi, r, \nu, \hat{\nu}_{c,i}), \end{aligned} \tag{4.24}$$

then h is a CBF for (4.18) and the control law $\tau = \kappa(\eta, \nu)$ renders the superzero level set K defined by h forward pre-invariant for (4.18).

Proof. The proof follows from noting that $\breve{f}$ and $\breve{g}$ are continuous, the minimum of continuous mappings is in itself continuous, and by combining (4.23) with (4.24)

$$\begin{aligned} &\nabla_1 h(\eta, \nu)^\mathsf{T} R(\psi)\nu + \nabla_2 h(\eta, \nu)^\mathsf{T} M^{-1} \left(\kappa(\eta, \nu) - C(\nu)\nu - D_l \nu \right) \\ &\geq -\sigma(h) - \nabla_2 h(\eta, \nu)^\mathsf{T} \vartheta(\eta, \nu, \nu_c), \end{aligned} \tag{4.25}$$

which is equivalent to

$$\nabla h(x)^\mathsf{T} \breve{f}(x, \nu_c) + \nabla h(x)^\mathsf{T} \breve{g} \kappa(\eta, \nu) \geq -\sigma(h(x)), \tag{4.26}$$

for all $(x, \nu_c) \in X \times \mathbb{R}^3$. By Definition 2.22, h is a valid CBF for (4.20), which combined with the fact that κ is continuous guarantees forward invariance of the superzero level set K from Corollary 2.24. □

To account for the unknown ocean current direction, Proposition 4.3 will be used to obtain safe controllers by specifying an upper limit on the current speed $\hat{U}_c \geq 0$ and constructing P ocean current approximations $\hat{V}_{c,i} = \hat{U}_c \big(\cos\left(\hat{\beta}_{c,i}\right), \sin\left(\hat{\beta}_{c,i}\right) \big)$, $i \in \mathcal{P} = \{1, 2, \dots, P\}$, with evenly spaced directions $\hat{\beta}_{c,i} \in \mathbb{R}$. Given an upper limit for the current speed $\hat{U}_c$, and a current direction $\hat{\beta}_c$ in the NED frame, we construct P ocean current approximations from

$$\hat{V}_{c,i} = \hat{U}_c R\left((i-1)\frac{2\pi}{P} \right) \begin{pmatrix} \cos\left(\hat{\beta}_c\right) \\ \sin\left(\hat{\beta}_c\right) \\ 0 \end{pmatrix}, \qquad i \in \mathcal{P}, \tag{4.27}$$

$$\hat{\nu}_{c,i} = R(\psi)^\mathsf{T} \hat{V}_{c,i}, \qquad i \in \mathcal{P}, \tag{4.28}$$

for any number of directions P divisible by 360.

Remark 4.4. *By specifying an upper bound on the current speed and constructing P evenly-spaced ocean current approximations, we are able to account for the dynamic effect that the worst possible ocean current approximation may have on some continuously differentiable function h encoding a safety-related objective. As long as the actual ocean current does not contribute to making h more negative than any of our estimates, i.e. as long as (4.23) holds, (4.24) can be enforced as a constraint on the control input and safety can be guaranteed from Proposition 4.3 when the linearization error from (4.13) is negligible and the control input is continuous.*

4.4 Safety-Critical Control of ASVs

In this section we apply the results from the previous sections for safety-critical control of ASVs in the presence of ocean currents. Section 4.4.1 defines the stabilization objectives, while Section 4.4.2 derives ES-CLFs for position and heading control. Section 4.4.3 describes CBF design for collision avoidance before the robust CLF-CBF-QP controller is presented in Section 4.4.4.

4.4.1 Stabilization Objectives

The stabilization objective is stated as a special case of the maneuvering problem [52]:

1. **Geometric Task:** For a given continuous path variable $\theta(t)$, force the configuration $\eta(t)$ to converge to the desired configuration $\eta_d(\theta(t))$, that is,
$$\lim_{t\to\infty} \left[\eta(t) - \eta_d(\theta(t))\right] = 0. \tag{4.29}$$
2. **Dynamic Task:** For a given continuous path speed $\dot{\theta}(t)$, force the configuration velocity $\dot{\eta}(t)$ to converge to a desired configuration velocity $\dot{\eta}_d(\theta(t), t)$, that is,
$$\lim_{t\to\infty} \left[\dot{\eta}(t) - \dot{\eta}_d\left(\theta(t), t\right)\right] = 0. \tag{4.30}$$

The primary benefit of this formulation is that design of the path and the desired motion along the path can be decoupled and approached individually in design. The desired path through K waypoints is denoted by $p_d(\theta) = (x_d(\theta), y_d(\theta))$. This is generated using a cubic spline interpolation method as outlined in [53]. Assigning the desired heading as the angle of the tangent vector along the path $\psi_d(\theta) = \text{atan2}\left(y_d'(\theta), x_d'(\theta)\right)$ results in the desired configuration

$$\eta_d(\theta) = \left(x_d(\theta), y_d(\theta), \psi_d(\theta)\right). \tag{4.31}$$

We transform the desired path into a time-varying trajectory by defining a desired path speed according to

$$\dot{\theta} = v_d(\theta, t) := \frac{u_d(t)}{\sqrt{\left(x_d'(\theta)\right)^2 + \left(y_d'(\theta)\right)^2}}, \tag{4.32}$$

where $u_d : \mathbb{R}_{\geq 0} \to \mathbb{R}$ is a commanded input speed. Given a piecewise constant reference speed assignment $U_r(t)$, continuous desired speed and acceleration references $u_d(t)$ and $\dot{u}_d(t)$ are obtained from the following second-order low-pass filter

$$\ddot{u}_d + 2\zeta\omega_n\dot{u}_d + \omega_n^2 u_d = \omega_n^2 U_r, \tag{4.33}$$

where $\zeta > 0$ is the damping ratio and $\omega_n > 0$ is the natural frequency of the filter. The desired configuration velocity and acceleration is found by differentiating (4.31) with respect to time

$$\dot{\eta}_d = \eta_d'(\theta)\dot{\theta} = \eta_d'(\theta)v_d(\theta, t), \tag{4.34}$$

$$\ddot{\eta}_d = \eta_d''(\theta)v_d(\theta, t)^2 + \eta_d'(\theta)\left(\frac{\partial v_d}{\partial \theta}(\theta, t)v_d(\theta, t) + \frac{\partial v_d}{\partial t}(\theta, t)\right). \tag{4.35}$$

4.4.2 Error Dynamics and Integral ES-CLFs for Stabilization

Consider the configuration error

$$y(\eta, \theta) = \eta - \eta_d(\theta). \tag{4.36}$$

The error dynamics is found by differentiating (4.36) with respect to time and substituting (4.8)

$$\dot{y} = R(\psi)^\mathsf{T}\nu - \dot{\eta}_d(\theta, t), \tag{4.37}$$

$$\begin{aligned}\ddot{y} &= R(\psi)^\mathsf{T}\dot{\nu} + \dot{R}(\psi, r)^\mathsf{T}\nu - \ddot{\eta}_d(\theta, t) \\ &= R(\psi)^\mathsf{T}M^{-1}\left(\bar{B}(u_0)\Delta u + B(\alpha_0)\mu_0\right) \\ &\quad - R(\psi)^\mathsf{T}M^{-1}\left(C(\nu)\nu + D(\nu)\nu\right) + \dot{R}(\psi, r)^\mathsf{T}\nu - \ddot{\eta}_d \\ &= A(\psi, u_0)\Delta u + b(\psi, \nu, u_0, \theta, t).\end{aligned} \tag{4.38}$$

In order to independently control the rate of convergence of the position and the heading angle, we let $y_1 \in \mathbb{R}^2$ and $y_2 \in \mathbb{R}$ denote the position and heading components of the configuration error y, respectively. As discussed in Section 4.3.4, the control model is sufficiently precise for control design provided that integral action is used in the controller to counteract the effect of the ocean currents. To this end, we define the integral states $\dot{z}_i := y_i \in \mathbb{R}^{k_i}$, where $k_i = \dim(y_i)$. The state-space representation of the error dynamics is found by defining $\xi_i := (z_i, \dot{z}_i, \ddot{z}_i) \in \mathbb{R}^{3k_i}$ and differentiating ξ_i with respect to time

$$\dot{\xi}_i = \Lambda_i\xi_i + \Gamma_i\left(A_i(\psi, u_0)\mu + b_i(\psi, \nu, u_0, \theta, t)\right) \tag{4.39}$$

$$= \bar{f}_i(\xi_i, \psi, \nu, u_0, \theta, t) + \bar{g}_i(\psi, u_0)\Delta u, \tag{4.40}$$

for $i \in \{1, 2\}$, where A_i and b_i are the rows and elements of A and b corresponding to y_i, respectively, and

$$\Lambda_1 = \begin{pmatrix} 0 & I & 0 \\ 0 & 0 & I \\ 0 & 0 & 0 \end{pmatrix}, \qquad \Lambda_2 = \begin{pmatrix} 0 & 1 & 0 \\ 0 & 0 & 1 \\ 0 & 0 & 0 \end{pmatrix}, \tag{4.41}$$

$$\Gamma_1 = \begin{pmatrix} 0 & 0 & I \end{pmatrix}^\mathsf{T}, \qquad \Gamma_2 = \begin{pmatrix} 0 & 0 & 1 \end{pmatrix}^\mathsf{T}. \tag{4.42}$$

As alluded to in Section 4.2, ES-CLFs will be used as they achieve fast convergence. Consider the following ES-CLF candidates for (4.40)

$$V_i(\xi_i) = \xi_i^\mathsf{T} P_i \xi_i, \quad i \in \{1, 2\}, \tag{4.43}$$

where $P_i = P_i^\mathsf{T}$ is positive-definite and solves the continuous-time algebraic Riccati equation

$$\Lambda_i^\mathsf{T} P_i + P_i \Lambda_i - P_i \Gamma_i \Gamma_i^\mathsf{T} P_i + Q_i = 0, \tag{4.44}$$

where Q_i is any positive definite matrix. Note that the symmetric and positive definite solution to (4.44) is guaranteed to exist since (Λ_i, Γ_i), $i \in \{1, 2\}$ is controllable [85]. The time derivative of (4.43) is given by

$$\dot{V}_i = \langle \nabla V_i(\xi_i), \bar{f}_i(\xi_i, \psi, \nu, u_0, \theta, t) + \bar{g}_i(\psi, u_0)\Delta u \rangle, \tag{4.45}$$

where

$$\nabla V_i(\xi_i)^\mathsf{T} \bar{f}_i = \xi_i^\mathsf{T} \left(\Lambda_i^\mathsf{T} P_i + P_i \Lambda_i \right) \xi_i + 2\xi_i^\mathsf{T} P_i \Gamma_i b_i, \tag{4.46}$$

$$\nabla V_i(\xi_i)^\mathsf{T} \bar{g}_i = 2\xi_i^\mathsf{T} P_i \Gamma_i A_i. \tag{4.47}$$

Inserting (4.44) results in

$$\dot{V}_i = \xi_i^\mathsf{T} \left(P_i \Gamma_i \Gamma_i^\mathsf{T} P_i - Q_i \right) \xi_i + 2\xi_i^\mathsf{T} P_i \Gamma_i \left(A_i \Delta u + b_i \right). \tag{4.48}$$

Define $\gamma_i := \frac{\lambda_{\min}(Q_i)}{\lambda_{\max}(P_i)} > 0$, where $\lambda_{\min}(\cdot)$ and $\lambda_{\max}(\cdot)$ are the minimum and maximum eigenvalues of the input matrix, respectively. It follows that $\gamma_i P_i \leq Q_i$, which yields

$$\begin{aligned} \dot{V}_i &\leq \xi_i^\mathsf{T} \left(P_i \Gamma_i \Gamma_i^\mathsf{T} P_i - \gamma_i P_i \right) \xi_i + 2\xi_i^\mathsf{T} P_i \Gamma_i \left(A_i \Delta u + b_i \right) \\ &= \xi_i^\mathsf{T} P_i \Gamma_i \left(\Gamma_i^\mathsf{T} P_i \xi_i + 2 \left(A_i \Delta u + b_i \right) \right) - \gamma_i \xi_i^\mathsf{T} P_i \xi_i. \end{aligned} \tag{4.49}$$

Assumption 4.5. *The rows of the decoupling matrix $A(\psi, u_0) = R(\psi)^\mathsf{T} M^{-1} \bar{B}(u_0)$ are linearly independent for all $(\psi, u_0) \in \mathbb{R} \times \mathbb{R}^{2m}$, which implies that the system is input-output feedback linearizable [86].*

Assumption 4.5 together with (4.49) implies that

$$\inf_{\Delta u \in \mathbb{R}^{2m}} \left[\langle \nabla V_i(\xi_i), \bar{f}_i + \bar{g}_i \Delta u \rangle + \gamma_i V_i(\xi_i) \right] \leq 0, \tag{4.50}$$

for all $(\xi_i, \psi, \nu, u_0, \theta, t) \in \mathbb{R}^{3k_i} \times D_\psi \times \mathbb{R}^3 \times \mathbb{R}^{2m} \times \mathbb{R}_{\geq 0} \times \mathbb{R}_{\geq 0}$. Consequently, V_i is an ES-CLF for (4.40) with $c_1 = \lambda_{\min}(P_i)$, $c_2 = \lambda_{\max}(P_i)$ and $c_3 = \gamma_i$. Note that the rate of exponential convergence γ_i can be controlled through the positive-definite matrix Q_i.

4.4.3 CBFs for Collision Avoidance with Static Obstacles

To achieve collision avoidance, we will employ Proposition 4.3, and the ocean current estimation procedure in Section 4.3.4 to obtain CBFs for the ASV model (4.8) without knowledge of the true ocean current. We only consider static obstacles, and refer to [82] for collision avoidance of dynamic obstacles using CBFs. The model (4.18) combined with (4.10) and (4.13) in state-space form is given by

$$\dot{x} = f(x) + g\Delta u + \begin{pmatrix} 0 \\ \vartheta(\eta, \nu, \nu_c) \end{pmatrix}, \tag{4.51}$$

where $x = (\eta, \nu)$ and the expressions for f and g are given in Section 4.3.3. Consider a spherical obstacle with radius $r_{\text{obs}} > 0$. A scalar distance measure between the obstacle and the body-fixed vessel frame is defined by

$$d(\eta) \coloneqq \sqrt{\left(p^n_{\text{obs}} - p^n\right)^\mathsf{T} \left(p^n_{\text{obs}} - p^n\right)} - r_{\text{obs}}. \tag{4.52}$$

where $p^n_{\text{obs}} \in \mathbb{R}^2$ is the position of the center of the obstacle in the NED frame. Enforcing the positivity of the following continuously differentiable function will avoid collisions [81]

$$h(\eta, \nu) = d(\eta) + kJ(\eta)\nu, \tag{4.53}$$

where $k > 0$ and $J(\eta) \coloneqq \nabla d(\eta)^\mathsf{T} R(\psi)$. Differentiating h with respect to time yields

$$\begin{aligned} \dot{h} &= \nabla h(\eta, \nu)^\mathsf{T} f(x) + \nabla h(\eta, \nu)^\mathsf{T} g\Delta u + \nabla_2 h(\eta, \nu)^\mathsf{T} \vartheta(\eta, \nu, \nu_c) && (4.54) \\ &= J(\eta)\left(\nu + k\vartheta(\eta, \nu, \nu_c)\right) + k\dot{J}(\eta, \nu)\nu \\ &\quad + kJ(\eta)M^{-1}\left(\bar{B}(u_0)\Delta u + B(\alpha_0)\mu_0 - C(\nu)\nu - D_l\nu\right). && (4.55) \end{aligned}$$

4.4.4 Safety-Critical Control via Quadratic Programming

In summary, the stabilization objectives consist of position and heading control encoded by the integral ES-CLFs V_1 and V_2, while the safety-related collision avoidance objective is encoded by the continuously differentiable function h. The CLF-CBF-QP from Section 4.2.2 is modified for an ASV with a nonlinear actuator model as follows

$$\underset{(\Delta u, \delta) \in \mathbb{R}^{2m+2}}{\text{minimize}} \; \Delta u^\mathsf{T}\left(H + \Omega\right)\Delta u + 2u_0^\mathsf{T} H\Delta u + \delta^\mathsf{T} W\delta \tag{4.56a}$$

subject to

$$\begin{aligned} &\langle \nabla V_1(\xi_1), \bar{f}_1 + \bar{g}_1\Delta u\rangle \leq -\gamma_1 V_1(\xi_1) + \delta_1, && (4.56b) \\ &\langle \nabla V_2(\xi_2), \bar{f}_2 + \bar{g}_2\Delta u\rangle \leq -\gamma_2 V_2(\xi_2) + \delta_2, && (4.56c) \\ &\langle \nabla h(x), f(x) + g\Delta u\rangle \geq -\sigma(h(x)) - \min_{i \in \mathcal{P}} kJ(\eta)\varphi_i(x), && (4.56d) \\ &\mu_{\min} - \mu_0 \leq \Delta\mu \leq \mu_{\max} - \mu_0, && (4.56e) \\ &T\Delta u_{\min} \leq \Delta u \leq T\Delta u_{\max}, && (4.56f) \end{aligned}$$

Table 4.1: Control Parameters

Param.	Value	**Param.**	Value	**Param.**	Value
P	12	r_{obs}	13 m	H_1	$0.5I_2$
β_c	$-60°$	$\sigma(h)$	ϕh	Ω_1	$0.0001I_2$
$\hat{\beta}_c$	$15°$	ϕ	0.1	Ω_2	$2500I_2$
U_c	1 m/s	k	$\frac{20}{3}$	W	$1.5 \cdot 10^4 I_2$
$\hat{U}_c$	1.1 m/s	$\mu_{\min}$	-293 N	$\mu_{\max}$	500 N
T	0.01 s	$\Delta\mu_{\max}$	160 N/s	$\Delta\mu_{\min}$	$-\Delta\mu_{\max}$
		$\Delta\alpha_{\max}$	30 deg/s	$\Delta\alpha_{\min}$	$-\Delta\alpha_{\max}$

where $H = \text{diag}(H_1, 0) \in \mathbb{R}^{2m\times 2m}$ penalizes the force magnitudes squared, while $\Omega \in \mathbb{R}^{2m\times 2m}$ is a diagonal matrix penalizing the squared rate of change of the force magnitude and azimuth angle control inputs, and $(\delta_1, \delta_2) \in \mathbb{R}^2$ are slack variables penalized by the diagonal weighting matrix $W \in \mathbb{R}^{2\times 2}$. Moreover, $\mu_{\min}$ and $\mu_{\max}$ are the negative and positive force magnitude constraints, T is the sampling time, and $\Delta u_{\min}$ and $\Delta u_{\max}$ are the negative and positive rate constraints, respectively.

4.5 Numerical Simulation

In this section we verify the theoretical developments from the previous sections through simulation of a double-ended autonomous passenger ferry [87]. In terms of actuators, the ferry is equipped with two azimuth thrusters and the simulation model consists of (4.8) with a realistic thruster model for (4.10) taking thruster force deadband, magnitude and rate constraints, and azimuth angle magnitude and rate constraints into account. Note that the simulation model includes nonlinear damping, which is not accounted for in the CLF or CBF design. The ES-CLF parameters are given by $Q_1 = \text{diag}\,(0.01I_2, 200I_2, 400I_2)$ and $Q_2 = \text{diag}\,(0.1, 400, 800)$, where I_2 is the 2×2 identity matrix. The remaining parameters are summarized in Table 4.1. Following the procedure outlined in Section 4.3.4, P evenly spaced ocean current approximations are constructed from (4.27)–(4.28). The dynamic effect of the worst-case ocean current is therefore approximated by the P continuous maps given by (4.22). Note that our choice of $\hat{\beta}_c$ is the worst possible guess, since each direction is separated by 30°, resulting in a 15° offset between the actual current direction and the best estimate(s).

Simulation results are shown in Figures 4.1 to 4.3 and 4.5, where simulations with and without the robustifying term in (4.56d), (i.e. assuming $\varphi = 0$, $i \in \mathcal{P}$) are depicted in Figures 4.1 and 4.5. From Figures 4.1 and 4.5, it is clear that the non-robust CBF candidate fails to achieve forward invariance of the superzero level set of (4.53), resulting in a collision. Observe from Figure 4.4 that both thrusters are in maximum positive saturation from $t \approx 170$ s to $t \approx 182$ s due to the strict penalty on non-zero slack variables and by using a linear $\mathcal{K}_\infty$ function in (4.56d). Moreover, the system exhibits excessively large tracking errors at $t \approx 190$ s because of the incompatibility between the collision avoidance and stabilization tasks, com-

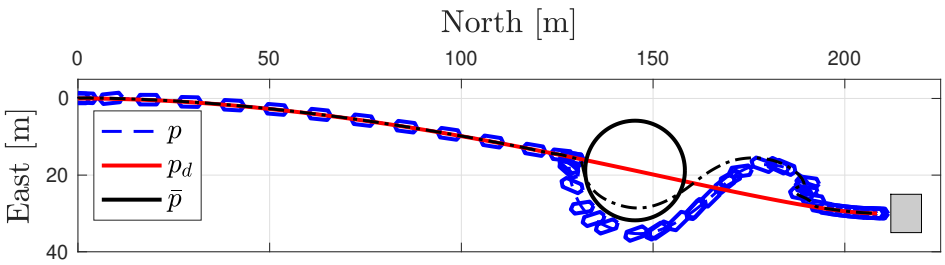

Figure 4.1: North-East plot showing the path p, the desired path p_d, the heading and the spherical obstacle. The black dash-dotted line $\bar{p}$ represents the path followed by the ASV when omitting the robustifying last term in (4.56d).

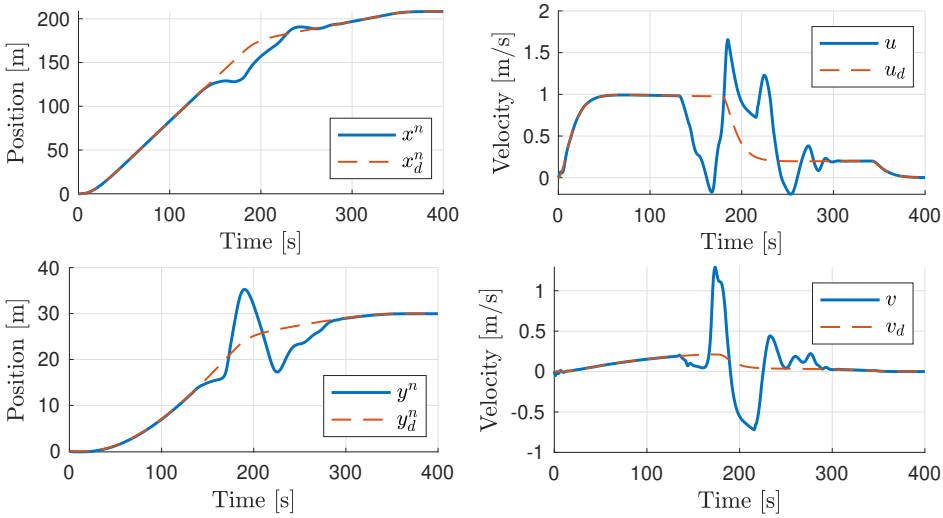

Figure 4.2: The actual and desired North and East positions x^n, y^n and x_d^n, y_d^n, and the actual and desired surge u, u_d and sway v, v_d velocities.

bined with the significant size of the spherical obstacle. Nevertheless, the system remains stable and successfully catches up with the reference trajectory. The overshoot in Figures 4.1 and 4.2 occurs due to the ocean current pushing the ship westward while the integral action saturates from attempting to recover from a significant tracking error. Improved transient behavior after avoiding a collision can be achieved by employing anti-wind up techniques and/or trajectory replanning if the positional tracking error exceeds some threshold. With the exception of poor transient performance due to successfully avoiding a collision, the integral ES-CLFs contribute to successful tracking of the configuration and velocity references as seen in Figures 4.2 and 4.3.

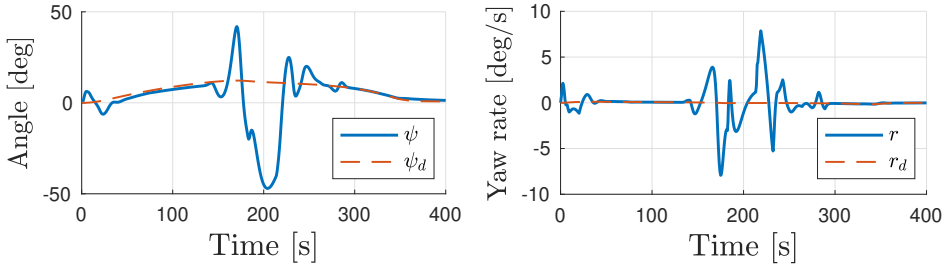

Figure 4.3: The actual and desired heading angle ψ and ψ_d and the actual and desired yaw rate r and r_d.

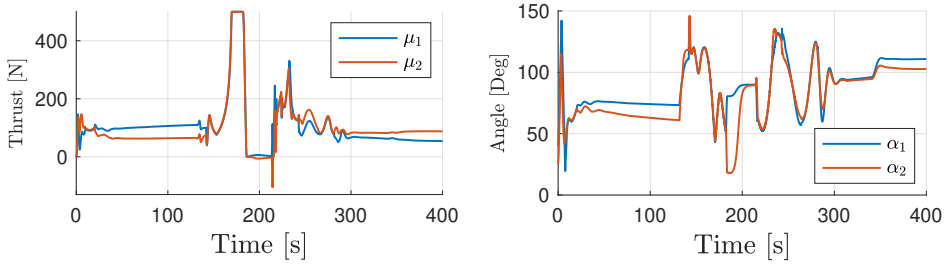

Figure 4.4: The thruster and azimuth angle control inputs, μ and α, respectively.

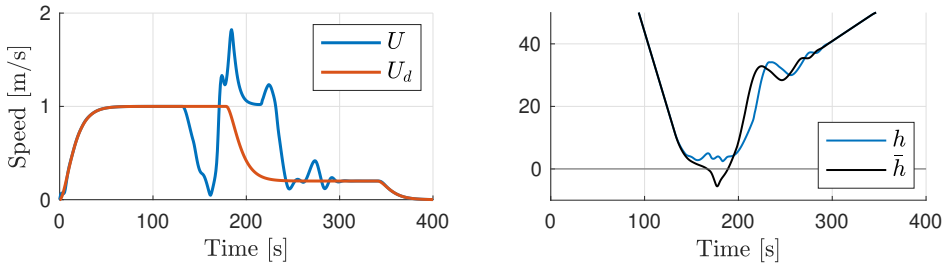

Figure 4.5: Actual and desired speed U and U_d, and the function h when the last term in (4.56d) is included, h, and omitted, $\bar{h}$, respectively.

4.6 Conclusions and Future Work

This chapter has presented an optimization-based framework for safety-critical control of ASVs with robustness guarantees in the presence of unknown ocean currents. The framework is holistic in the sense that it solves the problems of stabilization, reactive collision avoidance and control allocation in a unified manner. Conditions ensuring forward invariance of the superzero level set of continuously differentiable functions have been derived for a class of uncertain nonlinear systems. These conditions can be employed to ensure safety in the presence of unknown system nonlinearities. Moreover, we have specialized these conditions for an ASV subject to unknown ocean currents to obtain robust CBFs providing collision avoidance guarantees. Furthermore, the control allocation problem has been uni-

fied with the control problem by linearizing the actuator configuration matrix at every sampling instant to avoid a non-convex optimization problem, enabling constraints on the control input to be explicitly accounted for in the motion controller. This unification helps avoid instability due to actuator saturation. Additionally, we have incorporated integral action into CLFs encoding stabilization objectives. The framework has been verified in simulation for a double-ended passenger ferry, where successful tracking of a time-varying trajectory and reactive collision avoidance has been demonstrated. Future work is aimed at full-scale experiments of the proposed framework for a double-ended passenger ferry.

Part II

Hybrid Feedback Control of Marine and Aerial Vehicles

Chapter 5

Synergistic PID and Output Feedback Control on Matrix Lie Groups

In this chapter, we develop several synergistic hybrid feedback control laws for mechanical systems on matrix Lie groups with left-invariant Riemannian metrics. In particular, we propose hybrid PD and output feedback control laws ensuring global asymptotic tracking. To account for unknown and constant disturbances, we augment the hybrid PD control law with an integral state and derive two different hybrid PID-type control laws ensuring global asymptotic tracking in the presence of unknown disturbances in the system dynamics.

The material in this chapter is based on [51].

5.1 Introduction

A continuous intrinsic controller with integral action on compact Lie groups is presented in [88]. The integral action stems from integration of the P-action in the controller. The controller ensures bounded tracking error in the presence of uncertainty, and almost global asymptotic stability in the absence of uncertainty. Several similar controllers with integral action are presented in [89]. Here, the integral action stems from integrating the PD-action in the controller. This controller achieves almost global asymptotic stability in the presence of a constant disturbance.

This chapter is organized as follows. Section 5.2 introduces the equations of motion and the assumptions on the desired trajectories. In Section 5.3, we derive the error system and give the problem statement, before Section 5.4 defines the concept of a synergistic function. Then, we present a synergistic hybrid PD control law in Section 5.5 and an output feedback version which only utilizes configuration measurements in Section 5.6. Section 5.7 introduces two novel synergistic control laws with integral action, both of which globally asymptotically track a given bounded reference trajectory in the presence of a constant and unknown disturbance. Finally, Section 5.8 presents a case study with simulation results of both PID control laws, before Section 5.9 concludes the chapter.

5.2 Modeling

Consider a fully actuated control-affine mechanical system whose configuration space can be identified with a matrix Lie group $\mathcal{G} \subset \mathbb{R}^{n\times n}$ with dimension m. Let $g \in \mathcal{G}$ denote the configuration and $\nu \in \mathbb{R}^m$ the body velocity. The equations of motion are given by

$$\left.\begin{aligned} \dot{g} &= g\nu^{\wedge} \\ M\dot{\nu} - \operatorname{ad}_{\nu}^{\mathsf{T}} M\nu &= f(g,\nu) + \tau \end{aligned}\right\} \qquad (g,\nu,\tau) \in \mathcal{G}\times\mathbb{R}^m\times\mathbb{R}^m \tag{5.1}$$

where $M \in \mathbb{R}^{m\times m}$ is the inertia tensor and $\operatorname{ad}_{\nu}^{\mathsf{T}} M\nu$ describes inertial forces arising from curvature effects. Moreover, the continuous mapping $f : \mathcal{G}\times\mathbb{R}^m \to \mathbb{R}^m$ describes other external forces, and $\tau \in \mathbb{R}^m$ is an idealized control force.

Assumption 5.1. *The desired configuration $t \mapsto g_d(t)$ and its derivatives up to the second order are bounded and continuous, and $t \mapsto \det g_d(t)$ is bounded away from zero.*

For every desired configuration satisfying Assumption 5.1, there exist scalars $a \geq 0$ and $c \geq 0$ and a compact set $\Omega \subset \mathcal{G}$ such that the desired configuration and body velocity $t \mapsto (g_d(t), \nu_d(t))$ is a complete solution to the constrained differential inclusion

$$\left.\begin{aligned} \dot{g}_d &= g_d\nu_d^{\wedge} \\ \dot{\nu}_d &\in c\mathbb{B}^m \end{aligned}\right\} (g_d,\nu_d) \in \Omega\times a\mathbb{B}^m \tag{5.2}$$

5.3 Error System and Problem Statement

Define the left-invariant configuration and velocity errors by

$$g_e \coloneqq g_d^{-1} g, \tag{5.3}$$

$$\nu_e \coloneqq \nu - \nu_r = \nu - \operatorname{Ad}_{g_e}^{-1}\nu_d, \tag{5.4}$$

which results in the error system

$$\left.\begin{aligned} \dot{g}_e &= g_e\nu_e^{\wedge} \\ \dot{\nu}_e &= M^{-1}(\operatorname{ad}_{\nu}^{\mathsf{T}} M\nu + f(g,\nu) + \tau) - \dot{\nu}_r \\ \dot{g}_d &= g_d\nu_d^{\wedge} \\ \dot{\nu}_d &\in c\mathbb{B}^m \end{aligned}\right\} \quad x \in X \tag{5.5}$$

where $\dot{\nu}_r = \operatorname{Ad}_{g_e}^{-1}\dot{\nu}_d - \operatorname{ad}_{\nu_e}\nu_r$, $x \coloneqq (g_e,\nu_e,g_d,\nu_d) \in X$ and

$$X \coloneqq \mathcal{G}\times\mathbb{R}^m\times\Omega\times a\mathbb{B}^m. \tag{5.6}$$

Problem statement:

For a given compact set $\mathcal{A} \subset \mathcal{G}$, design a hybrid feedback control law with state $\xi \in \Xi$, input $x \in X$ and output $\tau \in \mathbb{R}^m$ such that the compact set

$$\mathcal{T} \coloneqq \mathcal{A} \times \{0\} \times \Omega \times a\mathbb{B}^m \times \mathcal{A}_c, \tag{5.7}$$

is globally pre-asymptotically stable for the resulting hybrid closed-loop system, where $\mathcal{A}_c \subset \Xi$ is the controller state attractor.

5.4 Synergistic Functions

The following definition of a synergistic function is similar to the ones found in [35] and [39].

Definition 5.2. *Let $Q \subset \mathbb{R}$ be a finite set and $\mathcal{A} \subset \mathcal{G}$ be a compact set. A continuously differentiable function $V : \mathcal{G} \times Q \to \mathbb{R}$ is synergistic with respect to the set $\mathcal{A}$ if*

- *V is proper and positive definite with respect to a set $\mathcal{B} \subset \mathcal{A} \times Q$ defined such that for every $g \in \mathcal{A}$, there exists $q \in Q$ such that $(g, q) \in \mathcal{B}$.*
- *there exists $\delta > 0$ such that the synergy gap*

$$\mu_V(g, q) \coloneqq V(g, q) - \min_{p \in Q} V(g, p), \tag{5.8}$$

satisfies $\mu_V(g, q) > \delta$ for each $(g, q) \in (\mathcal{E} \cup (\mathcal{A} \times Q)) \backslash \mathcal{B}$, where

$$\mathcal{E} \coloneqq \{(g, q) \in \mathcal{G} \times Q : \mathrm{d}V(g, q) = 0\}. \tag{5.9}$$

The function V from Definition 5.2 can also be thought of as a family of potential functions indexed by Q, $\{V_q\}_{q \in Q}$, such that $V(g, q) = V_q(g)$ for all $(g, q) \in \mathcal{G} \times Q$. Furthermore, there exists a family of compact sets indexed by Q, $\{\mathcal{B}_q\}_{q \in Q}$, such that $\mathcal{A} = \cup_{q \in Q} \mathcal{B}_q$ and $\mathcal{B} = \cup_{q \in Q} (\mathcal{B}_q \times \{q\})$. For each $q \in Q$, V_q is a proper and positive definite function with respect to $\mathcal{B}_q$. It must be remarked that there may exist $q \in Q$ such that $\mathcal{B}_q = \emptyset$, in which case the corresponding function V_q is proper and everywhere positive.

Definition 5.2 also requires that if $g \in (\mathcal{E}_q \cup \mathcal{A}) \setminus \mathcal{B}_q$, where $\mathcal{E}_q$ denotes the set of critical points of V_q, then there exists $\delta > 0$ such that $V_q(g) - \min_{p \in Q} V_p(g) > \delta$. Hence, if g is a critical point of V_q that is not in $\mathcal{B}_q$, or g lies in $\mathcal{B}_p$ with $p \in Q \setminus \{q\}$, then the minimal value of $s \mapsto V_s(g)$ is at least δ lower than $V_q(g)$. A consequence of this fact, continuity of the potential functions, and positive definiteness of the potential functions is that, for $(p, q) \in Q \times Q$, either $\mathcal{B}_p \cap \mathcal{B}_q = \emptyset$ or $\mathcal{B}_p = \mathcal{B}_q$.

A synergistic function induces the following kinematic hybrid control law [35]

$$\begin{cases} \dot{q} = 0 & (g, q) \in C_V \\ q^+ \in G_V(g) & (g, q) \in D_V \\ y = -\,\mathrm{d}V(g, q) \end{cases} \tag{5.10}$$

with state $q \in Q$, input $g \in \mathcal{G}$ and output y. Moreover, the flow set $C_V \subset \mathcal{G} \times Q$, jump set $D_V \subset \mathcal{G} \times Q$ and jump map $G_V : \mathcal{G} \rightrightarrows Q$ are defined according to

$$C_V \coloneqq \{(g, q) \in \mathcal{G} \times Q : \mu_V(g, q) \leq \delta\}, \tag{5.11}$$

$$D_V \coloneqq \{(g, q) \in \mathcal{G} \times Q : \mu_V(g, q) \geq \delta\}, \tag{5.12}$$

$$G_V(g) \coloneqq \{q \in Q : \mu_V(g, q) = 0\}. \tag{5.13}$$

Note that the sets C_V and D_V are closed in $\mathcal{G} \times Q$ due to the continuity of μ_V. It follows that C_V and D_V are closed in $\mathrm{GL}(n) \times \mathbb{R}$, but not necessarily in $\mathbb{R}^{n \times n} \times \mathbb{R}$. Furthermore, observe that G_V is outer semicontinuous relative to D_V since continuity of μ_V implies that $\operatorname{gph} G_V = \{(g, q) \in \mathcal{G} \times Q : \mu_V(g, q) = 0\}$ is closed in $\mathcal{G} \times Q$.

5.5 Synergistic PD Control

In this section, we employ a synergistic function to design a hybrid PD controller with state $q \in Q$ which renders the closed-loop system globally pre-asymptotically stable. Moreover, we employ a novel feedforward control which is independent of the system velocities.

Defining the following velocity independent feedforward control

$$\kappa_{ff}(g_e, g_d, \nu_d, \dot{\nu}_d) = M \operatorname{Ad}_{g_e}^{-1} \dot{\nu}_d - \operatorname{ad}_{\nu_r}^{\mathsf{T}} M \nu_r - f(g, \nu_r), \tag{5.14}$$

we propose the following synergistic PD control law

$$\begin{cases} \dot{q} = 0 & (g_e, q) \in C_V \\ q^+ \in G_V(g_e) & (g_e, q) \in D_V \\ \tau = \kappa_{ff}(g_e, g_d, \nu_d, \dot{\nu}_d) - \mathrm{d}V(g_e, q) - K_d \nu_e \end{cases} \tag{5.15}$$

where V is synergistic with respect to a compact set $\mathcal{A}$ and $K_d \in \mathbb{R}^{m \times m}$. Observe that the feedback control law (5.15) comprises a proportional action $\mathrm{d}V$ and a derivative action $K_d \nu_e$.

Lemma 5.1. *The feedforward control (5.14) results in the error dynamics*

$$\dot{\nu}_e = -\nabla^M_{\nu + \nu_r} \nu_e + M^{-1}(f(g, \nu) - f(g, \nu_r)). \tag{5.16}$$

Proof. With $\tau = \kappa_{ff}(g_e, g_d, \nu_d, \dot{\nu}_d)$, it follows from (5.5) that

$$M \dot{\nu}_e = M \operatorname{ad}_{\nu_e} \nu_r + \operatorname{ad}_{\nu}^{\mathsf{T}} M \nu - \operatorname{ad}_{\nu_r}^{\mathsf{T}} M \nu_r + f(g, \nu) - f(g, \nu_r).$$

Let $\varpi(\nu_e, \nu_r) = M \operatorname{ad}_{\nu_e} \nu_r + \operatorname{ad}_{\nu}^{\mathsf{T}} M \nu - \operatorname{ad}_{\nu_r}^{\mathsf{T}} M \nu_r$. Using the identities $\operatorname{ad}_\zeta \nu = \nabla^M_\zeta \nu - \nabla^M_\nu \zeta$, $\operatorname{ad}_\zeta \nu = -\operatorname{ad}_\nu \zeta$ and $\operatorname{ad}_\nu \nu = 0$, it holds that

$$\begin{aligned} \varpi(\nu_e, \nu_r) &= \operatorname{ad}_{\nu}^{\mathsf{T}} M \nu - \operatorname{ad}_{\nu_r}^{\mathsf{T}} M \nu_r + M \operatorname{ad}_{\nu_e} \nu_r \\ &= M \nabla^M_{\nu_r} \nu_r - M \nabla^M_\nu \nu + M \operatorname{ad}_{\nu_e} \nu_r \\ &= M(\nabla^M_{\nu_r} \nu_r - \nabla^M_\nu \nu + \nabla^M_{\nu_e} \nu_r - \nabla^M_{\nu_r} \nu_e) \\ &= M(-\nabla^M_\nu \nu_e - \nabla^M_{\nu_r} \nu_e) \\ &= -M \nabla^M_{\nu + \nu_r} \nu_e. \end{aligned}$$

□

Using Lemma 5.1, the interconnection between the control law (5.15) and the error system (5.5) leads to the following closed-loop system

$$\mathcal{H}_1 : \begin{cases} \left.\begin{aligned} \dot{g}_e &= g_e \nu_e^\wedge \\ \dot{\nu}_e &= -\nabla^M_{\nu+\nu_r}\nu_e \\ &\quad + M^{-1}(f(g,\nu) - f(g,\nu_r)) \\ &\quad - M^{-1}(\mathrm{d}V(g_e,q) + K_d\nu_e) \\ \dot{g}_d &= g_d \nu_d^\wedge \\ \dot{\nu}_d &\in c\mathbb{B}^m \end{aligned}\right\} & x_1 \in C_1 \\ q^+ \in G_V(g_e) & x_1 \in D_1 \end{cases}$$

where $x_1 \coloneqq (g_e, \nu_e, g_d, \nu_d, q) \in X_1$ and

$$\begin{aligned} X_1 &\coloneqq \mathcal{G} \times \mathbb{R}^m \times \Omega \times a\mathbb{B}^m \times Q, \\ C_1 &\coloneqq \{x_1 \in X_1 : (g_e, q) \in C_V\}, \\ D_1 &\coloneqq \{x_1 \in X_1 : (g_e, q) \in D_V\}. \end{aligned} \tag{5.17}$$

Theorem 5.3. *Let V be synergistic with synergy gap exceeding $\delta > 0$. If there exist $\varepsilon > 0$ and $K_d \in \mathbb{R}^{m\times m}$ such that $\nu \mapsto -f(g,\nu)$ is $(\varepsilon I - K_d)$-monotone for each $g \in \mathcal{G}$, then the hybrid control law (5.15) renders the compact set*

$$\mathcal{T}_1 \coloneqq \mathcal{A} \times \{0\} \times \Omega \times a\mathbb{B}^m \times Q, \tag{5.18}$$

globally pre-asymptotically stable for $\mathcal{H}_1$.

Proof. Define the flow and jump maps

$$F_1(x_1) \coloneqq \begin{pmatrix} g_e \nu_e^\wedge \\ -\nabla^M_{\nu+\nu_r}\nu_e + M^{-1}\left(f(g,\nu) - f(g,\nu_r) - \mathrm{d}V(g_e,q) - K_d\nu_e\right) \\ g_d \nu_d^\wedge \\ c\mathbb{B}^m \\ 0 \end{pmatrix}, \tag{5.19}$$

$$G_1(x_1) \coloneqq \begin{pmatrix} g_e \\ \nu_e \\ g_d \\ \nu_d \\ G_V(g_e)) \end{pmatrix}. \tag{5.20}$$

The hybrid closed-loop system is then defined by the data $\mathcal{H}_1 = (C_1, F_1, D_1, G_1)$. Consider the continuously differentiable function $W_1 : X_1 \to \mathbb{R}$ defined by

$$W_1(x_1) \coloneqq V(g_e, q) + \frac{1}{2}\langle \nu_e, M\nu_e \rangle. \tag{5.21}$$

Differentiating W_1 along the flows of $\mathcal{H}_1$ satisfies

$$\begin{aligned} \langle \nabla W_1(x_1), f_1 \rangle = \langle \mathrm{d}V(g_e,q), \nu_e \rangle &+ \langle \nu_e, -M\nabla^M_{\nu+\nu_r}\nu_e \rangle \\ &+ \langle \nu_e, f(g,\nu) - f(g,\nu_r) \rangle \\ &+ \langle \nu_e, -\mathrm{d}V(g_e,q) - K_d\nu_e \rangle, \end{aligned} \tag{5.22}$$

for all $x_1 \in C_1$ and $f_1 \in F_1(x_1)$. Using Lemma 2.4 and the fact that $\nu \mapsto -f(g,\nu)$ is $(\varepsilon I - K_d)$-monotone for each $g \in \mathcal{G}$, equation (5.22) can be rewritten as

$$\langle \nabla W_1(x_1), f_1 \rangle \leq -\varepsilon |\nu_e|^2, \quad \forall x_1 \in C_1, f_1 \in F_1(x_1). \tag{5.23}$$

The change of W_1 across jumps is

$$W_1(s_1) - W_1(x_1) \leq -\delta$$

for all $x_1 \in D_1$ and $s_1 \in G_1(x_1)$. Because W_1 is proper and positive definite with respect to the compact set

$$\mathcal{T}_1' \coloneqq \{x_1 \in X_1 : (g_e, q) \in \mathcal{B}, \nu_e = 0\}, \tag{5.24}$$

and non-increasing along flows and strictly decreasing across jumps, it follows that $\mathcal{T}_1'$ is stable and every solution to $\mathcal{H}_1$ is bounded. In fact, every sublevel set of W_1 is compact (since W_1 is proper) and forward pre-invariant, that is, given $r \geq 0$, every solution starting in the set $W_1^{-1}([0,r])$ remains in it. Consider the hybrid system $\mathcal{H}_{1,r}$, defined such that it is equal to $\mathcal{H}_1$ with the flow and jump sets replaced by $C_{1,r} \coloneqq C_1 \cap W_1^{-1}([0,r])$ and $D_{1,r} \coloneqq D_1 \cap W_1^{-1}([0,r])$, respectively. Then, for each $r \geq 0$, the hybrid system $\mathcal{H}_{1,r}$ satisfies the hybrid basic conditions (Assumption 2.17), because $C_{1,r}$ and $D_{1,r}$ are closed. Furthermore, every complete solution to $\mathcal{H}_1$ that starts in the set $W_1^{-1}([0,r])$ is a complete solution to $\mathcal{H}_{1,r}$. Since the time between jumps is lower bounded by a positive constant, it follows from Corollary 8.7 b) in [55] that, for each $r \geq 0$, complete solutions to $\mathcal{H}_{1,r}$ converge to the largest weakly invariant subset $\mathcal{W}_1$ contained in

$$W_1^{-1}(\gamma) \cap \{x_1 \in C_1 : \nu_e = 0\},$$

for some $\gamma \in [0,r]$. Each complete solution $\phi \in \mathcal{S}_{\mathcal{H}_{1,r}}(\mathcal{W}_1)$ satisfies $\nu_e(t,j) \equiv 0$, which implies that for each $j \in \mathbb{Z}_{\geq 0}$ such that $I^j = \{t : (t,j) \in \operatorname{dom}\phi\}$ has nonempty interior, it holds that

$$\frac{\mathrm{d}}{\mathrm{d}t}\nu_e(t,j) = 0,$$

for almost all $t \in I^j$, and the closed-loop system implies that $\mathrm{d}V(g_e(t,j), q(t,j)) \equiv 0$. By construction, the only points in C_1 where $\mathrm{d}V(g_e,q) = 0$ are those for which $(g_e,q) \in \mathcal{B}$. It follows that $\mathcal{W}_1 \subset \mathcal{T}_1'$ and hence that every complete solution to $\mathcal{H}_{1,r}$ converges to $\mathcal{T}_1'$. Since every complete solution to $\mathcal{H}_1$ is a complete solution to $\mathcal{H}_{1,r}$ for some $r \geq 0$, every complete solution to $\mathcal{H}_1$ converges to $\mathcal{T}_1'$. Consequently, $\mathcal{T}_1'$ is globally pre-asymptotically stable for $\mathcal{H}_1$ since it is stable, all solutions are bounded and every complete solution converges to $\mathcal{T}_1'$. Since $\mathcal{T}_1' \subset \mathcal{T}_1$, it follows that $\mathcal{T}_1$ is globally pre-attractive. Moreover, $\mathcal{T}_1$ is forward pre-invariant because $\mathcal{T}_1'$ is forward pre-invariant and

$$\mathcal{T}_1 \setminus \mathcal{T}_1' = \{x_1 \in X_1 : (g_e,q) \in (\mathcal{A} \times Q) \setminus \mathcal{B}\} \subset D_1 \setminus C_1$$

is such that any maximal solution reaching $\mathcal{T}_1 \setminus \mathcal{T}_1'$ is immediately mapped to $\mathcal{T}_1'$ via a single jump. It then follows from Proposition 7.5 of [55] that $\mathcal{T}_1$ is stable. Since $\mathcal{T}_1$ is stable and globally pre-attractive, it is globally pre-asymptotically stable. □

5.6 Synergistic Output Feedback Control

Due to the fact that the feedforward control in (5.14) is independent of the vehicle velocities, we can utilize it in the design of a Lyapunov-based output feedback tracking control law. To this end, let $U : \mathcal{G} \times H \to \mathbb{R}_{\geq 0}$ be synergistic with respect to $\mathcal{A}$, let $h \in H \subset \mathbb{R}$ be a logic variable, and consider the output feedback control law

$$\begin{cases} \dot{g}_f = g_f \left(\mathrm{Ad}_{g_o} K_f \, \mathrm{d}U(g_o, h)\right)^\wedge & (g_e, q, g_o, h) \in \widetilde{C}_2 \\ \left.\begin{aligned} q^+ &\in G_V(g_e) \\ h^+ &\in G_U(g_o) \end{aligned}\right\} & (g_e, q, g_o, h) \in \widetilde{D}_2 \\ \tau = \kappa_{ff}(g_e, g_d, \nu_d, \dot{\nu}_d) - \mathrm{d}V(g_e, q) - \mathrm{d}U(g_o, h). \end{cases} \tag{5.25}$$

where $g_o \coloneqq g_f^{-1} g_e$ is the filter error and

$$\widetilde{C}_2 \coloneqq \{(g_e, q, g_o, h) : (g_e, q) \in C_V \text{ and } (g_o, h) \in C_U\}, \tag{5.26}$$

$$\widetilde{D}_2 \coloneqq \{(g_e, q, g_o, h) : (g_e, q) \in D_V \text{ or } (g_o, h) \in D_U\}. \tag{5.27}$$

Defining $x_2 \coloneqq (g_e, \nu_e, g_d, \nu_d, q, g_o, h) \in X_2$ and

$$X_2 \coloneqq \mathcal{G} \times \mathbb{R}^m \times \Omega \times a\mathbb{B}^m \times Q \times \mathcal{G} \times H, \tag{5.28}$$

we arrive at the closed-loop system

$$\mathcal{H}_2 : \begin{cases} \left.\begin{aligned} \dot{g}_e &= g_e \nu_e^\wedge \\ \dot{\nu}_e &= -\nabla^M_{\nu+\nu_r} \nu_e \\ &\quad + M^{-1}(f(g, \nu) - f(g, \nu_r)) \\ &\quad - M^{-1}(\mathrm{d}V(g_e, q) + \mathrm{d}U(g_o, h)) \\ \dot{g}_d &= g_d \nu_d^\wedge \\ \dot{\nu}_d &\in c\mathbb{B}^m \\ \dot{g}_o &= g_o \left(\nu_e - K_f \, \mathrm{d}U(g_o, h)\right)^\wedge \end{aligned}\right\} & x_2 \in C_2 \\ \left.\begin{aligned} q^+ &\in G_V(g_e) \\ h^+ &\in G_U(g_o) \end{aligned}\right\} & x_2 \in D_2 \end{cases}$$

where

$$\begin{aligned} C_2 &\coloneqq \{x_2 \in X_2 : (g_e, q) \in C_V \text{ and } (g_o, h) \in C_U\}, \\ D_2 &\coloneqq \{x_2 \in X_2 : (g_e, q) \in D_V \text{ or } (g_o, h) \in D_U\}. \end{aligned} \tag{5.29}$$

Theorem 5.4. *Let V and U be synergistic with synergy gaps exceeding $\delta > 0$ and $\rho > 0$, respectively. If $\mathcal{A}$ is a finite set, K_f is positive definite and $\nu \mapsto -f(g, \nu)$ is monotone for every $g \in \mathcal{G}$, then the hybrid control law (5.25) renders the compact set*

$$\mathcal{T}_2 \coloneqq \mathcal{A} \times \{0\} \times \Omega \times a\mathbb{B}^m \times Q \times \mathcal{A} \times H, \tag{5.30}$$

globally pre-asymptotically stable for $\mathcal{H}_2$.

Proof. Define the flow and jump maps

$$F_2(x_2) \coloneqq \begin{pmatrix} g_e \nu_e^\wedge \\ -\nabla^M_{\nu+\nu_r} \nu_e + M^{-1}(f(g,\nu) - f(g,\nu_r) - \mathrm{d}V(g_e,q) - \mathrm{d}U(g_o,h)) \\ g_d \nu_d^\wedge \\ c\mathbb{B}^m \\ 0 \\ g_o \left(\nu_e - K_f \, \mathrm{d}U(g_o,h)\right)^\wedge \\ 0 \end{pmatrix}, \tag{5.31}$$

$$G_2(x_2) \coloneqq \begin{pmatrix} g_e \\ \nu_e \\ g_d \\ \nu_d \\ G_V(g_e)) \\ g_o \\ G_U(g_o) \end{pmatrix}. \tag{5.32}$$

The hybrid closed-loop system is then defined by the data $\mathcal{H}_2 = (C_2, F_2, D_2, G_2)$. Consider the continuously differentiable function $W_2 : X_2 \to \mathbb{R}$ defined by

$$W_2(x_2) \coloneqq V(g_e, q) + U(g_o, h) + \frac{1}{2}\langle \nu_e, M\nu_e \rangle. \tag{5.33}$$

W_2 is proper and positive definite with respect to the compact set

$$\mathcal{T}_2' \coloneqq \{x_2 \in X_2 : (g_e, q) \in \mathcal{B}, (g_o, h) \in \mathcal{B}, \nu_e = 0\}. \tag{5.34}$$

The derivative of W_2 along flows of the closed-loop system is

$$\begin{aligned} \langle W_2(x_2), f_2 \rangle &= \langle \mathrm{d}V(g_e, q), \nu_e \rangle + \langle \mathrm{d}U(g_o, h), \nu_e - K_f \, \mathrm{d}U(g_o, h) \rangle \\ &\quad - \langle \nu_e, M\nabla^M_{\nu+\nu_r} \nu_e \rangle + \langle \nu_e, f(g,\nu) - f(g,\nu_r) \rangle \\ &\quad + \langle \nu_e, -\mathrm{d}V(g_e, q) - \mathrm{d}U(g_o, h) \rangle \\ &\leq -\langle K_f \, \mathrm{d}U(g_o, h), \mathrm{d}U(g_o, h) \rangle \end{aligned}$$

for all $x_2 \in C_2$ and $f_2 \in F_2(x_2)$. The change of W_2 across jumps is given by

$$W_2(s_2) - W_2(x_2) \leq -\min\{\delta, \rho\}, \tag{5.35}$$

for all $x_2 \in D_2$ and $s_2 \in G_2(x_2)$. By a similar argument as in the proof of Theorem 5.3, it can be shown that $\mathcal{T}_2'$ is stable and that all solutions to $\mathcal{H}_2$ are bounded. Moreover, every complete solution to $\mathcal{H}_{2,r}$ converges to the largest weakly invariant subset $\mathcal{W}_2$ of $W_2^{-1}(\gamma) \cap \{x_2 \in C_2 : \mathrm{d}U(g_o, h) = 0\}$ for some $\gamma \in [0, r]$. Every complete solution $\phi \in \mathcal{S}_{\mathcal{H}_{2,r}}(\mathcal{W}_2)$ satisfies $g_o(t, j) \in \mathcal{A}$ for all $(t, j) \in \operatorname{dom} \phi$. Since $\mathcal{A}$ is finite, for each $j \in \mathbb{Z}_{\geq 0}$ such that $I^j = \{t : (t, j) \in \operatorname{dom} \phi\}$ has nonempty interior, it holds that

$$\frac{\mathrm{d}}{\mathrm{d}t} g_o(t, j) = 0,$$

for almost all $t \in I^j$, and (5.31) implies that $\nu_e(t,j) \equiv 0$. Thus, for each $j \in \mathbb{Z}_{\geq 0}$ such that I^j has nonempty interior, it holds that

$$\frac{\mathrm{d}}{\mathrm{d}t}\nu_e(t,j) = 0,$$

for almost all $t \in I^j$, and (5.31) implies that $\mathrm{d}V(g_e(t,j), q(t,j)) \equiv 0$. Hence, $(g_e(t,j), q(t,j)) \in \mathcal{B}$ for all $(t,j) \in \operatorname{dom}\phi$. It follows that $\mathcal{W}_2 \subset \mathcal{T}_2'$ and hence that every complete solution to $\mathcal{H}_{2,r}$ converges to $\mathcal{T}_2'$. Since every complete solution to $\mathcal{H}_2$ is a complete solution to $\mathcal{H}_{2,r}$ for some $r \geq 0$, every complete solution to $\mathcal{H}_2$ converges to $\mathcal{T}_2'$. The remainder of the proof is similar to Theorem 5.3. □

5.7 Synergistic Control with Integral Action

We now assume that $f(g,\nu) = \bar{f}(g,\nu) + b$, where $\bar{f} : \mathcal{G} \times \mathbb{R}^m \to \mathbb{R}^m$ describes a known external force and $b \in \mathbb{R}^m$ is an unknown constant disturbance. Consider the following synergistic PID control law

$$\begin{cases} \dot{\varphi} = \mathrm{d}V(g_e, q) & (g_e, q, \varphi) \in \widetilde{C}_3 \\ q^+ \in G_V(g_e) & (g_e, q, \varphi) \in \widetilde{D}_3 \\ \tau = M\dot{\nu}_r - \bar{f}(g,\nu) \\ \qquad - (I + MK_d^{-1}K_i)\,\mathrm{d}V(g_e, q) - K_d\nu_e - K_i\varphi \end{cases} \tag{5.36}$$

where K_d and K_i are diagonal matrices with positive entries and

$$\widetilde{C}_3 \coloneqq \{(g_e, q, \varphi) \in \mathcal{G} \times Q \times \mathbb{R}^m : (g_e, q) \in C_V\} \tag{5.37}$$

$$\widetilde{D}_3 \coloneqq \{(g_e, q, \varphi) \in \mathcal{G} \times Q \times \mathbb{R}^m : (g_e, q) \in D_V\} \tag{5.38}$$

Observe that the feedback control law comprises a proportional term $(I+MK_d^{-1}K_i)\,\mathrm{d}V$, an integral term $K_i b$ and a derivative term $K_d\nu_e$.

Let $\varphi_e \coloneqq \varphi - K_i^{-1}b$ denote the estimation error and define

$$x_3 \coloneqq (g_e, \nu_e, g_d, \nu_d, q, \varphi_e) \in X_3 \tag{5.39}$$

$$X_3 \coloneqq \mathcal{G} \times \mathbb{R}^m \times \Omega \times a\mathbb{B}^m \times Q \times \mathbb{R}^m. \tag{5.40}$$

The closed-loop system is then given by

$$\mathcal{H}_3 : \begin{cases} \left.\begin{aligned} \dot{g}_e &= g_e\nu_e^\wedge \\ \dot{\nu}_e &= -M^{-1}(I + MK_d^{-1}K_i)\,\mathrm{d}V(g_e, q) \\ &\quad - M^{-1}K_d\nu_e - M^{-1}K_i\varphi_e) \\ \dot{g}_d &= g_d\nu_d^\wedge \\ \dot{\nu}_d &\in c\mathbb{B}^m \\ \dot{\varphi}_e &= \mathrm{d}V(g_e, q) \end{aligned}\right\} & x_3 \in C_3 \\ q^+ \in G_V(g_e) & x_3 \in D_3 \end{cases}$$

where $C_3 \coloneqq \{x_3 \in X_3 : (g_e, q) \in C_V\}$ and $D_3 \coloneqq \{x_3 \in X_3 : (g_e, q) \in D_V\}$.

Theorem 5.5. *Let V be synergistic with synergy gap exceeding $\delta > 0$. If $\mathcal{A}$ is finite, K_d is diagonal and positive definite, and K_i is diagonal and positive definite, then the hybrid control law (5.36) renders the compact set*

$$\mathcal{T}_3 \coloneqq \mathcal{A} \times \{0\} \times \Omega \times a\mathbb{B}^m \times Q \times \{0\}, \tag{5.41}$$

globally pre-asymptotically stable for the closed-loop system $\mathcal{H}_3$.

Proof. Define the flow and jump maps of $\mathcal{H}_3$ by

$$F_3(x_3) \coloneqq \begin{pmatrix} g_e \nu_e^\wedge \\ -M^{-1}\left((I + MK_d^{-1}K_i)\,\mathrm{d}V(g_e, q) - K_d\nu_e - K_i\varphi_e\right) \\ g_d\nu_d^\wedge \\ c\mathbb{B}^m \\ 0 \\ \mathrm{d}V(g_e, q) \end{pmatrix}, \tag{5.42}$$

$$G_3(x_3) \coloneqq \begin{pmatrix} g_e \\ \nu_e \\ g_d \\ \nu_d \\ G_V(g_e)) \\ \varphi_e \end{pmatrix}. \tag{5.43}$$

The hybrid closed-loop system is then defined by the data $\mathcal{H}_3 = (C_3, F_3, D_3, G_3)$. Consider the continuously differentiable function $W_3 : X_3 \to \mathbb{R}$ defined by

$$W_3(x_3) \coloneqq V(g_e, q) + \frac{1}{2}\langle M(\nu_e + K_d^{-1}K_i\varphi_e), \nu_e + K_d^{-1}K_i\varphi_e\rangle + \frac{1}{2}\langle \varphi_e, K_d^{-1}K_i\varphi_e\rangle.$$

W_3 is proper and positive definite relative to the compact set

$$\mathcal{T}_3' \coloneqq \{x_3 \in X_3 : (g_e, q) \in \mathcal{B}, \nu_e = 0, \varphi_e = 0\}. \tag{5.44}$$

Differentiating W_3 along the flows of the closed-loop system yields

$$\begin{aligned} \langle W_3(x_3), f_3\rangle &= \langle \mathrm{d}V(g_e, q), \nu_e\rangle - |K_d^{1/2}(\nu_e + K_d^{-1}K_i\varphi_e)|^2 \\ &\quad - \langle \nu_e + K_d^{-1}K_i\varphi_e, \mathrm{d}V(g_e, q)\rangle + \langle \varphi_e, K_d^{-1}K_i\,\mathrm{d}V(g_e, q)\rangle \\ &= -|K_d^{1/2}(\nu_e + K_d^{-1}K_i\varphi_e)|^2, \end{aligned}$$

for all $x_3 \in C_3$ and $f_3 \in F_3(x_3)$. The analysis concerning the change in W_3 across the jumps of the closed-loop system is similar to the proof of Theorem 5.3 and leads to a strict decrease in W_3 upper bounded by $-\delta$ across jumps. By a similar argument as in the proof of Theorem 5.3, it can be shown that $\mathcal{T}_3'$ is stable and that all solutions to $\mathcal{H}_3$ are bounded. Moreover, every complete solution to $\mathcal{H}_{3,r}$ converges to the largest weakly invariant subset $\mathcal{W}_3$ of

$$W_3^{-1}(\gamma) \cap \{x_3 \in C_3 : \nu_e + K_d^{-1}K_i\varphi_e = 0\},$$

for some $\gamma \in [0, r]$. Every complete solution $\phi \in \mathcal{S}_{\mathcal{H}_{3,r}}(\mathcal{W}_3)$ satisfies $\nu_e(t,j) + K_d^{-1} K_i \varphi_e(t,j) \equiv 0$, which implies that for each $j \in \mathbb{Z}_{\geq 0}$ such that $I^j = \{t : (t,j) \in \operatorname{dom} \phi\}$ has nonempty interior, it holds that

$$\frac{\mathrm{d}}{\mathrm{d}t} \nu_e(t,j) + K_d^{-1} K_i \frac{\mathrm{d}}{\mathrm{d}t} \varphi_e(t,j) = 0,$$

for almost all $t \in I^j$, and (5.42) implies that $\mathrm{d}V(g_e(t,j), q(t,j)) \equiv 0$. Since the only points in C_2 where $\mathrm{d}V(g_e, q) = 0$ are those for which $(g_e, q) \in \mathcal{B}$, it follows that

$$\mathcal{W}_3 \subset W_3^{-1}(\gamma) \cap \left\{ x_3 \in C_3 : \nu_e + K_d^{-1} K_i \varphi_e = 0, (g_e, q) \in \mathcal{B} \right\}.$$

Therefore, from Definition 5.2 and the fact that $\mathcal{A}$ and hence $\mathcal{B}$ is finite, it follows that for each $j \in \mathbb{Z}_{\geq 0}$ such that I^j has nonempty interior

$$\frac{\mathrm{d}}{\mathrm{d}t} g_e(t,j) = 0,$$

for almost all $t \in I^j$, which implies that $\nu_e(t,j) \equiv 0$. Thus,

$$\frac{\mathrm{d}}{\mathrm{d}t} \nu_e(t,j) = 0,$$

for almost all $t \in I^j$. Hence (5.42) implies that $\varphi_e(t,j) \equiv 0$. It follows that $\mathcal{W}_3 \subset \mathcal{T}_3'$ and hence that every complete solution to $\mathcal{H}_{3,r}$ converges to $\mathcal{T}_3'$. Since every complete solution to $\mathcal{H}_3$ is a complete solution to $\mathcal{H}_{3,r}$ for some $r \geq 0$, every complete solution to $\mathcal{H}_3$ converges to $\mathcal{T}_3'$. The remainder of the proof is similar to Theorem 5.3. □

Although the cancellation term $M K_d^{-1} K_i \, \mathrm{d}V$ acts as a rescaling of the proportional action, it may often end up very small in practice because K_d is typically chosen considerably larger than K_i.

The cancellation term can be removed and the assumptions on $\mathcal{A}$ and K_d can be relaxed by modifying the dynamics of the integral state and only allowing the integral gain to be scalar-valued. To this end, consider the following synergistic controller with integral action

$$\begin{cases} \dot{\varphi} = \mathrm{d}V(g_e, q) + K_d \nu_e & (g_e, q, \varphi) \in \widetilde{C}_3 \\ q^+ \in G_V(g_e) & (g_e, q, \varphi) \in \widetilde{D}_3 \\ \tau = M \dot{\nu}_r - \mathrm{ad}_\nu^\mathsf{T} M \nu - \bar{f}(g, \nu) - \mathrm{d}V(g_e, q) - K_d \nu_e - k_i \varphi \end{cases} \tag{5.45}$$

which leads to the closed-loop system

$$\mathcal{H}_4 : \begin{cases} \left.\begin{aligned} \dot{g}_e &= g_e \nu_e^\wedge \\ \dot{\nu}_e &= -M^{-1}(\mathrm{d}V(g_e, q) + K_d \nu_e + k_i \varphi_e) \\ \dot{g}_d &= g_d \nu_d^\wedge \\ \dot{\nu}_d &\in c\mathbb{B}^m \\ \dot{\varphi}_e &= \mathrm{d}V(g_e, q) + K_d \nu_e \end{aligned}\right\} & x_3 \in C_3 \\ q^+ \in G_V(g_e) & x_3 \in D_3 \end{cases}$$

Theorem 5.6. *Let V be synergistic with synergy gap exceeding $\delta > 0$. If $k_i > 0$ and $K_d - k_i M$ is positive definite, then the hybrid control law (5.45) renders the compact set*

$$\mathcal{T}_4 \coloneqq \mathcal{A} \times \{0\} \times \Omega \times a\mathbb{B}^m \times Q \times \{0\}, \tag{5.46}$$

globally pre-asymptotically stable for the closed-loop system $\mathcal{H}_4$.

Proof. Define the flow map of $\mathcal{H}_4$ by

$$F_4(x_3) \coloneqq \begin{pmatrix} g_e \nu_e^\wedge \\ -M^{-1}(\mathrm{d}V(g_e, q) + K_d \nu_e + k_i \varphi_e) \\ g_d \nu_d^\wedge \\ c\mathbb{B}^m \\ 0 \\ \mathrm{d}V(g_e, q) + K_d \nu_e \end{pmatrix}, \tag{5.47}$$

The hybrid closed-loop system is then defined by the data $\mathcal{H}_4 = (C_3, F_4, D_3, G_3)$. Consider the continuously differentiable function $W_4 : X_3 \to \mathbb{R}$ defined by

$$W_4(x_3) \coloneqq V(g, q) + \tfrac{1}{2}\langle \nu_e, M\nu_e \rangle + \tfrac{1}{2}\langle M(\nu_e + M^{-1}\varphi_e), \nu_e + M^{-1}\varphi_e \rangle \tag{5.48}$$

W_4 is proper and positive definite with respect to the compact set $\mathcal{T}_3'$ defined in (5.44). Differentiating W_4 along the flows of the closed-loop system yields

$$\begin{aligned} \langle W_4(x_3), f_4 \rangle &= \langle \mathrm{d}V(g_e, q), \nu_e \rangle + \langle \nu_e, -K_d\nu_e - \mathrm{d}V(g_e, q) - k_i\varphi_e \rangle - \langle \nu_e + M^{-1}\varphi_e, k_i\varphi_e \rangle \\ &= -\langle K_d\nu_e, \nu_e \rangle - 2k_i\langle \nu_e, \varphi_e \rangle - k_i\langle M^{-1}\varphi_e, \varphi_e \rangle. \\ &= -\langle (K_d - k_i M)\nu_e, \nu_e \rangle - k_i\langle M^{-1}(\varphi_e + M\nu_e), \varphi_e + M\nu_e \rangle \\ &\leq -\varepsilon_1 |\nu_e|^2 - \varepsilon_2 |\varphi_e|^2 \end{aligned}$$

for all $x_3 \in C_3$ and $f_4 \in F_4(x_3)$, and where $\varepsilon_1 > 0$ and $\varepsilon_2 > 0$. The remainder of the proof is similar to the proof of Theorem 5.3. □

5.8 Case Study

This section presents simulation results of a small fully actuated underwater vehicle. The configuration of an underwater vehicle can be identified with the matrix Lie group $\mathrm{SE}(3) = \mathbb{R}^3 \rtimes \mathrm{SO}(3)$. An element $g = (p, R) \in \mathrm{SE}(3)$ contains the position $p \in \mathbb{R}^3$ and orientation $R \in \mathrm{SO}(3)$ of a vehicle-fixed frame with respect to an inertial frame. The equations of motion for an underwater vehicle are given by (5.1) with the inertia tensor $M = M_{rb} + M_a$ comprising rigid body and hydrodynamic inertia. Moreover, $f(g, \nu) = d(\nu) + \gamma(g) + b$ where $d : \mathbb{R}^6 \to \mathbb{R}^6$ is the damping wrench comprising linear and nonlinear contributions $d(\nu) \coloneqq -D_l\nu - D_n(\nu)\nu$, and $\gamma : \mathrm{SE}(3) \to \mathbb{R}^6$ denotes the net hydrostatic wrench including weight and buoyancy. More details are found in [84]. The center of gravity is $r_g = (0, 0, 0.02)\mathrm{m}$, the center of buoyancy is $r_b = 0\,\mathrm{m}$, the dry mass is $m = 13.69\,\mathrm{kg}$, and the buoyancy is 1%

larger than the weight. The hydrodynamic modeling is described by

$$\begin{aligned} M_a &\coloneqq \operatorname{diag}(5.5, 12.7, 14.6, 0.1, 0.1, 0.1) \\ D_l &\coloneqq \operatorname{diag}(4.0, 6.2, 5.2, 0.1, 0.1, 0.1) \\ D_n(\nu) &\coloneqq \operatorname{diag}(18.2|\nu_1|, 21.7|\nu_2|, 37.0|\nu_3|, 1.6|\nu_4|, 1.6|\nu_5|, 1.6|\nu_6|) \\ b &\coloneqq (2, 1, -1, -1, -1, 1) \end{aligned}$$

The control law (5.45) is developed by utilizing the universal covering group of $\mathrm{SE}(3)$, denoted $\widetilde{\mathrm{SE}}(3) \coloneqq \mathbb{R}^3 \rtimes \mathrm{SU}(2)$, where $\mathrm{SU}(2)$ is the special unitary group of dimension two, which is isomorphic to the group of unit quaternions. See Section 8.4.2 for more details. A unit quaternion is given by $z = (\eta, \epsilon) \in \mathbb{S}^3 \coloneqq \{x \in \mathbb{R}^4 : |x| = 1\}$, where $\eta \in \mathbb{R}$ and $\epsilon \in \mathbb{R}^3$ describe its real and imaginary components, respectively. Let $g_e = (p_e, z_e) \coloneqq (R(z_d)(p - p_d), z_d^{-1} \otimes z)$, where $\otimes$ denotes the quaternion product and $R : \mathbb{S}^3 \to \mathrm{SO}(3)$ is defined by $R(z) \coloneqq I + 2\eta\epsilon^\wedge + 2(\epsilon^\wedge)^2$, where $(\cdot)^\wedge : \mathbb{R}^3 \to \mathfrak{so}(3)$ is defined by $\alpha^\wedge\beta \coloneqq \alpha \times \beta$ with $\alpha, \beta \in \mathbb{R}^3$. It is easily verified that $V(g_e, q) = 2k(1 - q\eta_e) + \frac{1}{2}\langle K_p p_e, p_e\rangle$ satisfies Definition 5.2 with $k = 1$ and $K_p = 5I_3$. The other controller gains are set to $K_d = \operatorname{blkdiag}(10I_3, 2I_3)$ and $k_i = 0.1$. The controller has been implemented without the feedforward term that would cancel the acting hydrodynamic and hydrostatic wrenches to achieve a slightly more realistic picture of its performance. Simulation results are presented in Figures 5.1 to 5.3, from which we conclude that acceptable tracking performance is achieved despite this simplification of the control law.

5.9 Conclusion

In this chapter, we have introduced multiple synergistic control designs for mechanical systems described on matrix Lie groups. Specifically, we have proposed synergistic PD, output feedback, and PID type control laws ensuring global asymptotic tracking of a desired bounded reference trajectory. Additionally, the PID type control laws achieve global asymptotic tracking when the system dynamics are augmented with a constant and unknown disturbance.

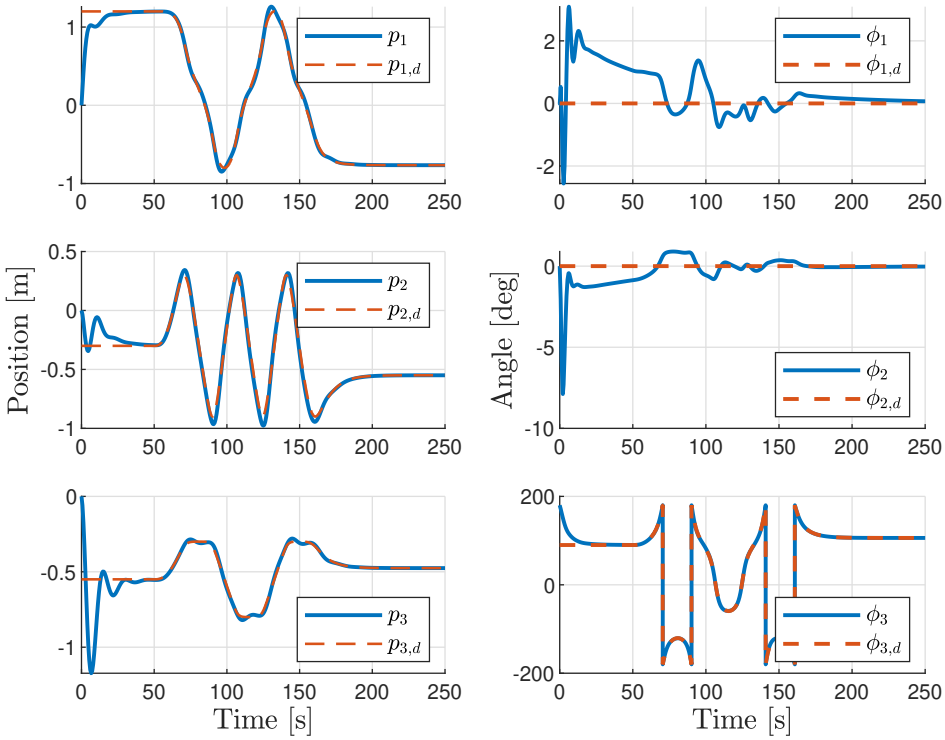

Figure 5.1: The position p, desired position p_d, roll-pitch-yaw angles ϕ and desired roll-pitch-yaw angles ϕ_d.

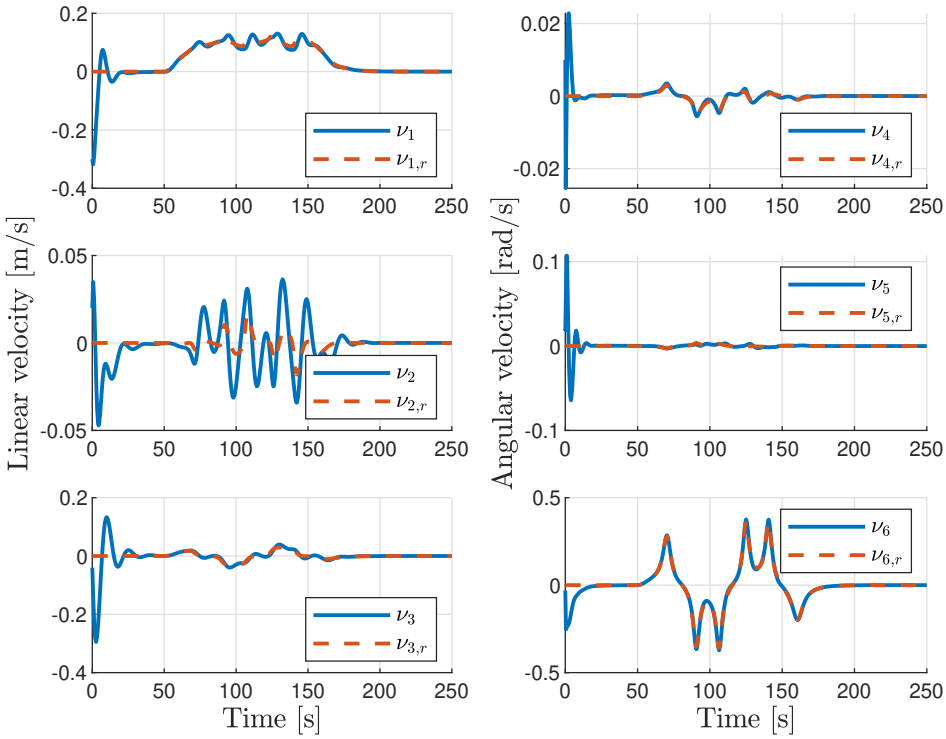

Figure 5.2: The velocity ν and the desired velocity ν_r.

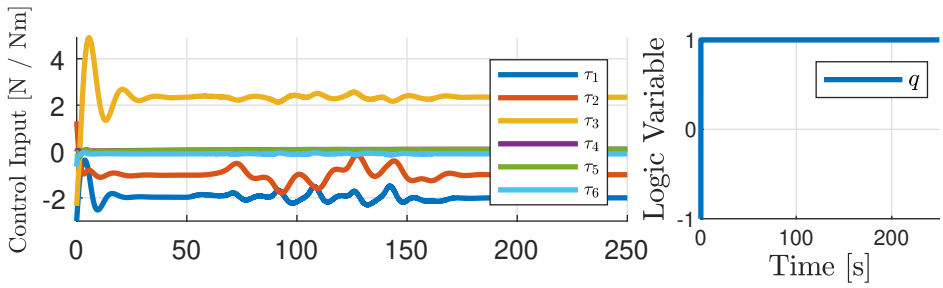

Figure 5.3: The control inputs τ and logic variable q.

Chapter 6

Synergistic Lyapunov Function and Feedback Triples

In this chapter, we extend the SLFF definition from [36]. The proposed generalization allows the logic variable, now referred to as the synergy variable, to be vector-valued and possess flow dynamics. Moreover, since the synergy variable is vector-valued, we define synergy gaps relative to components of product sets. These synergy gaps enable us to define flow and jump sets and jump conditions in the form of synergy gaps for different components of the synergy variable. As a result, we can show that the output feedback control method for rigid-body scheme outlined in [37] is synergistic. The proposed generalization encompasses the results for SO(3) and SE(3) in [43], in which the scalar logic variable is also allowed to change during flows. However, our proposed framework also includes path-following control scenarios in which the path variable exhibits jump dynamics, such as instantaneously moving the desired state closer to the actual state. As a result, ship maneuvering control as outlined in [52] and [53] can be augmented with discrete path dynamics and combined with a traditional synergistic control approach such as [44] to ensure global asymptotic stability within the proposed framework.

The material in this chapter is based on [54].

6.1 Introduction

Consider a continuous-time system

$$\dot{x} = f(x,u) \quad (x,v) \in X \times \mathbb{R}^k, \tag{6.1}$$

where $x \in X \subset \mathbb{R}^n$ is the state, $v \in \mathbb{R}^k$ is the input and $f : X \times \mathbb{R}^k \to \mathbb{R}^n$ is continuous. The following definition of an SLFF pair is the starting point of this chapter and is a slight modification of [1, Definition 7.3].

Definition 6.1 (Synergistic Lyapunov function and feedback pair)**.** *Given a system (6.1), a compact set $\mathcal{A} \subset X \times Q$, a continuously differentiable function $V : X \times Q \to \mathbb{R}_{\geq 0}$ and a continuous function $\kappa : X \to \mathbb{R}^k$ define*

$$\mu_V(x,q) \coloneqq V(x,q) - \min_{p \in Q} V(x,p). \tag{6.2}$$

The pair (V, κ) is a synergistic Lyapunov function and feedback pair relative to $\mathcal{A}$ with synergy gap exceeding $\rho > 0$ for (6.1) if

1. *V is proper and positive definite with respect to $\mathcal{A}$;*
2. *for all $(x, q) \in X \times Q$, it holds that*

$$\langle \nabla_1 V(x,q), f(x, \kappa(x,q)) \rangle \leq 0; \tag{6.3}$$

3. *$\mu_V(x,q) > \rho$ for each $(x,q) \in \mathcal{I} \setminus \mathcal{A}$, where $\mathcal{I}$ is the largest weakly invariant subset for the system*

$$\begin{aligned} \dot{x} &= f(x, \kappa(x,q)) \\ \dot{q} &= 0 \end{aligned} \qquad (x,q) \in \mathcal{E} \tag{6.4}$$

and

$$\mathcal{E} \coloneqq \{(x,q) \in X \times Q : \langle \nabla_1 V(x,q), f(x, \kappa(x,q)) \rangle = 0\}. \tag{6.5}$$

The remainder of this chapter is organized as follows. In Section 6.2, we extend the definition of SLFF pairs to SLFF triples, for which the synergy variables are allowed to have flow dynamics and be vector-valued. Moreover, we show how the hybrid feedback controller induced by an SLFF triple renders a given compact set globally pre-asymptotically stable. Section 6.3 introduces the notion of synergy gaps relative to components of product sets, which is a distinct feature of vector-valued synergy variables. Then, Section 6.4 introduces a weaker notion of SLFF triples, and we show that if an affine control system admits a weak SLFF triple, then the same system augmented with an integrator at the input admits a (non-weak) SLFF triple. Section 6.5 presents a case study which combines the classical synergistic control approach of [42] using the synergistic Lyapunov functions in [44] with the ship maneuvering control of [52]. Finally, Section 6.6 concludes the chapter.

6.2 Synergistic Lyapunov Function and Feedback

This section extends the definition of an SLFF pair in Definition 6.1 by augmenting the SLFF definition with a feedback representing the flow dynamics of the synergy variables. Moreover, we show that the hybrid feedback control law induced by an SLFF triple renders a given compact set globally pre-asymptotically stable.

Our goal is to design generalized synergistic controllers with state $\theta \in \Theta \subset \mathbb{R}^m$ of the form

$$\begin{aligned} \dot{\theta} &= \nu(x,\theta) \quad (x,\theta) \in C \\ \theta^+ &\in G(x,\theta) \quad (x,\theta) \in D \\ v &= \kappa(x,\theta) \end{aligned} \tag{6.6}$$

where $C \subset X \times \Theta$, $D \subset X \times \Theta$, $\nu : X \times \Theta \to \mathbb{R}^m$, and $G : X \times \Theta \rightrightarrows \Theta$ are the flow set, jump set, flow map and jump map of the controller, respectively. The controller state θ is also referred to as the synergy variable. We assume the following throughout the paper.

Assumptions.

1. $X \subset \mathbb{R}^n$ *is closed;*
2. $f : X \times \mathbb{R}^k \to \mathbb{R}^n$ *is continuous;*
3. $\Theta \subset \mathbb{R}^m$ *is closed.*

In the following, we generalize the notion of a synergy gap of a nonnegative and proper function V introduced in [36]. In particular, we evaluate the minimum of V over a set $\Psi \subset \Theta$ which need not be finite (or even compact).

Definition 6.2. *Let $V : X \times \Theta \to \mathbb{R}_{\geq 0}$ be continuous and proper, and let $\Psi \subset \Theta$ be closed and nonempty. The synergy gap of V with respect to Ψ is the function $\mu_{V,\Psi} : X \times \Theta \to \mathbb{R}$ defined by*

$$\mu_{V,\Psi}(x,\theta) \coloneqq V(x,\theta) - \min_{\psi \in \Psi} V(x,\psi). \tag{6.7}$$

The set-valued solution mapping associated with $\mu_{V,\Psi}$ is $G_{V,\Psi} : X \times \Theta \rightrightarrows \Theta$, defined as

$$G_{V,\Psi}(x,\theta) \coloneqq \{\psi \in \Psi : \mu_{V,\Psi}(x,\psi) = 0\}. \tag{6.8}$$

The fact that V is nonnegative, continuous, and proper is sufficient for its synergy gap relative to any nonempty and closed set $\Psi \subset \Theta$ to be continuous. Moreover, the associated solution mapping has the key properties it has in traditional synergistic control. Specifically, nonemptiness, outer semicontinuity, and local boundedness. Consequently, even when Ψ is not compact, the set of points where $\theta \mapsto V(x,\theta)$ attains its minimum on Ψ is compact for each $x \in X$.

Proposition 6.3. *The synergy gap $\mu_{V,\Psi}$ is continuous. The associated set-valued solution mapping $G_{V,\Psi}$ is nonempty-valued, outer semicontinuous, and locally bounded.*

Proof. The claims follow from [62, Corollary 7.42]. □

The following definition extends the notion of SLFF pairs from [36]. In addition to utilizing the generalized notion of synergy gap from Definition 6.2, we allow the synergy variable θ to flow.

Definition 6.4. *Let $\mathcal{A} \subset X \times \Theta$ be compact. A continuously differentiable function $V : X \times \Theta \mapsto \mathbb{R}_{\geq 0}$ and continuous functions $\kappa : X \times \Theta \to \mathbb{R}^k$ and $\nu : X \times \Theta \to \mathbb{R}^m$ define a synergistic Lyapunov function and feedback triple (V, κ, ν) relative to $\mathcal{A}$ with synergy gap relative to Ψ exceeding $\rho > 0$ for the system (6.1) if*

1. *V is proper and positive definite with respect to $\mathcal{A}$;*
2. *The closed loop system*

$$\begin{pmatrix} \dot{x} \\ \dot{\theta} \end{pmatrix} = \underbrace{\begin{pmatrix} f(x,\kappa(x,\theta)) \\ \nu(x,\theta) \end{pmatrix}}_{F_c(x,\theta)} \qquad (x,\theta) \in X \times \Theta \tag{6.9}$$

satisfies

$$\langle \nabla V(x,\theta), F_c(x,\theta) \rangle \leq 0, \quad \forall (x,\theta) \in X \times \Theta; \tag{6.10}$$

3. $\mu_{V,\Psi}(x,\theta) > \rho$ *for each* $(x,\theta) \in \mathcal{I} \setminus \mathcal{A}$, *where* $\mathcal{I}$ *is the largest weakly invariant subset for the system*

$$\begin{aligned} \dot{x} &= f(x,\theta,\kappa(x,\theta)) \\ \dot{\theta} &= \nu(x,\theta) \end{aligned} \qquad (x,\theta) \in \mathcal{E} \tag{6.11}$$

and

$$\mathcal{E} \coloneqq \{(x,\theta) \in X \times \Theta : \langle \nabla V(x,\theta), F_c(x,\theta) \rangle = 0\}. \tag{6.12}$$

We remark that if $\nu(x,\theta) = 0$ for all $(x,\theta) \in X \times \Theta$ and $\Theta = \Psi$ is finite, then Definition 6.4 reduces to the definition of an SLFF pair given in [36]. If $\Theta = \mathbb{R}$, and $\Psi \subset \mathbb{R}$ is finite, then Definition 6.4 encompasses the class of potential functions recently introduced in [43].

Analogous to SLFF pairs [36, Theorem 7], the existence of an SLFF triple relative to $\mathcal{A}$ with synergy gap relative to Ψ exceeding $\rho > 0$ guarantees global pre-asymptotic stability of $\mathcal{A}$ for a synergistic closed loop system resulting from (6.1).

Proposition 6.5. *Let* (V,κ,ν) *be an SLFF triple relative to* $\mathcal{A}$ *with synergy gap relative to* Ψ *exceeding* $\rho > 0$. *Then* $\mathcal{A}$ *is globally pre-asymptotically stable for the system*

$$\left.\begin{aligned} \dot{x} &= f(x,\kappa(x,\theta)) \\ \dot{\theta} &= \nu(x,\theta) \end{aligned}\right\} \quad (x,\theta) \in C$$
$$\theta^+ \in G(x,\theta) \qquad (x,\theta) \in D \tag{6.13}$$

where

$$\begin{aligned} C &\coloneqq \{(x,\theta) \in X \times \Theta : \mu_{V,\Psi}(x,\theta) \leq \rho\}, \\ D &\coloneqq \{(x,\theta) \in X \times \Theta : \mu_{V,\Psi}(x,\theta) \geq \rho\}, \\ G(x,\theta) &\coloneqq G_{V,\Psi}(x,\theta). \end{aligned} \tag{6.14}$$

Proof. The sets C and D are closed since $\mu_{V,\Psi}$ is continuous by Proposition 6.3. Moreover, the closed-loop flow map F_c is continuous, and G is nonempty-valued, outer semicontinuous, and locally bounded by Proposition 6.3. Consequently, the system (6.13) satisfies the hybrid basic conditions [55, Assumption 6.5] and is therefore well posed. From the definition of the jump set and jump map in (6.14), V decreases strictly across jumps by at least ρ. Since V is proper and positive definite with respect to $\mathcal{A}$ by 1) of Definition 6.4 and V does not grow along solutions to the system (6.13) by 2) of Definition 6.4 and the nonincrease of V across jumps, it follows that $\mathcal{A}$ is stable and that all solutions are bounded. Since V must vanish in $\mathcal{A}$ by 1) of Definition 6.4, it holds that $\mu_{V,\Psi}$ vanishes in $\mathcal{A}$ as well. Consequently, $\mathcal{A} \subset C$. From 3) of Definition 6.4, it then follows that $\mathcal{I} \cap C \subset \mathcal{A}$. The invariance principle [55, Corollary 8.4] then guarantees that complete solutions converge to $\mathcal{A}$. It follows that $\mathcal{A}$ is globally pre-asymptotically stable. □

Completeness of maximal solutions (and global asymptotic stability of $\mathcal{A}$ for (6.13)) is guaranteed if, in addition to the conditions of Proposition 6.5, it also holds that

$$F_c(x,\theta) \in T_{X\times\Theta}(x,\theta) \tag{6.15}$$

for all (x,θ) such that $\mu_{V,\Psi}(x,\theta) < \rho$, where $T_{X\times\Theta}(x,\theta)$ is the tangent cone to $X\times\Theta$ at (x,θ). Indeed, $T_{X\times\Theta}(x,\theta) = T_C(x,\theta)$ at these points, and the claim follows from [55, Proposition 6.10]. It should also be remarked that $T_{X\times\Theta} \neq T_X \times T_\Theta$ in general. See [62, Chapter 6], and in particular Proposition 6.41, for further results on this matter.

6.3 Synergy Gaps Relative to Components of Product Sets

The control approach covered in Proposition 6.5 updates the whole synergy variable θ when the instantaneous synergy gap is equal to or exceeds the threshold ρ. This approach offers relatively little flexibility in shaping the jump sets. When Θ is a product set, one can formulate the synergy gap and associated solution mapping relative to the components of Θ. For simplicity, it is assumed that Θ comprises two components, although the approach outlined in this section can be further generalized.

Assumptions (continued)**.**

4) $\Theta = \Theta_a \times \Theta_b$, where Θ_a and Θ_b are closed.

We now adapt Definition 6.2 to exploit the additional structure of Θ induced by this assumption.

Definition 6.6. *Let $V : X \times \Theta \to \mathbb{R}_{\geq 0}$ be continuous and proper, and let $\Psi = \Psi_a \times \Psi_b$ such that $\Psi_a \subset \Theta_a$ and $\Psi_b \subset \Theta_b$ are nonempty and closed. The synergy gap of V with respect to Ψ_a is defined as*

$$\mu_{V,\Psi_a}(x,\theta) := V(x,\theta) - \min_{\psi_a\in\Psi_a} V(x,(\psi_a,\theta_b)). \tag{6.16}$$

The synergy gap of V with respect to Ψ_b is defined as

$$\mu_{V,\Psi_b}(x,\theta) := V(x,\theta) - \min_{\psi_b\in\Psi_b} V(x,(\theta_a,\psi_b)). \tag{6.17}$$

The set-valued solution mapping associated with μ_{V,Ψ_a}, $G_{V,\Psi_a} : X \times \Theta \rightrightarrows \Theta$ is

$$G_{V,\Psi_a}(x,\theta) := \{\psi_a \in \Psi_a : \mu_{V,\Psi_a}(x,(\psi_a,\theta_b)) = 0\} \times \{\theta_b\}. \tag{6.18}$$

The objects introduced in Definition 6.6 have similar properties as the ones introduced in Definition 6.2.

Proposition 6.7. *The synergy gaps μ_{V,Ψ_a} and μ_{V,Ψ_b} are continuous. The set-valued solution mapping G_{V,Ψ_a} is nonempty-valued, outer semicontinuous, and locally bounded.*

Proof. Apply [62, Corollary 7.42] with (x, θ_b) as parameters and θ_a as optimization variable to show the claims for μ_{V,Ψ_a} and G_{V,Ψ_a}. Continuity of μ_{V,Ψ_b} is shown similarly. □

Consequently, we may specialize the notion of an SLFF triple to the case where Θ is product set.

Definition 6.8. *Let $\mathcal{A} \subset X \times \Theta$ be compact, and (V, κ, ν) satisfy 1) and 2) in Definition 6.4 for the system (6.1). We say that (V, κ, ν) is a synergistic Lyapunov function and feedback triple relative to $\mathcal{A}$ with synergy gap relative to Ψ_a exceeding $\rho_a > 0$ if*

3a) $\mu_{V,\Psi_a}(x, \theta) > \rho_a$ for each $(x, \theta) \in \mathcal{I} \setminus \mathcal{A}$.

We say that (V, κ, ν) is a synergistic Lyapunov function and feedback triple relative to $\mathcal{A}$ with synergy gap relative to (Ψ_a, Ψ_b) exceeding (ρ_a, ρ_b) with $\rho_a, \rho_b > 0$ if

3b) $\mu_{V,\Psi_a}(x, \theta) > \rho_a$ or $\mu_{V,\Psi_b}(x, \theta) > \rho_b$ for each $(x, \theta) \in \mathcal{I} \setminus \mathcal{A}$. Moreover, there exist $(x, \theta) \in \mathcal{I} \setminus \mathcal{A}$ such that $\mu_{V,\Psi_a}(x, \theta) \leq \rho_a$ and $(x, \theta) \in \mathcal{I} \setminus \mathcal{A}$ such that $\mu_{V,\Psi_b}(x, \theta) \leq \rho_b$.

In both cases, $\mathcal{I}$ is defined as in Definition 6.4.

It is clear that if (V, κ, ν) has synergy gap relative to Ψ_a exceeding $\rho_a > 0$, then it has synergy gap relative to Ψ exceeding ρ_a. If instead (V, κ, ν) has a synergy gap relative to to (Ψ_a, Ψ_b) exceeding (ρ_a, ρ_b), with $\rho_a, \rho_b > 0$, then it has a synergy gap relative to Ψ exceeding $\min(\rho_a, \rho_b) > 0$. The last part of item 3b) ensures that (V, κ, ν) is not an SLFF triple relative to $\mathcal{A}$ with synergy gap relative to Ψ_a or Ψ_b, and hence that ρ_a and ρ_b are well-defined.

6.3.1 Optional Jumps

When (V, κ, ν) is an SLFF triple relative to $\mathcal{A}$ with synergy gap relative to Ψ_a exceeding $\rho_a > 0$, it is not necessary to update θ_b to avoid the invariant sets where solutions may get stuck. Jumping θ_b may nonetheless increase the performance of the closed-loop system. We therefore define a closed-loop system in which jumps of θ_b are optional.

Proposition 6.9. *Let (V, κ, ν) be a synergistic Lyapunov function and feedback triple relative to $\mathcal{A}$ with synergy gap relative to Ψ_a exceeding $\rho_a > 0$. Then $\mathcal{A}$ is*

globally pre-asymptotically stable for the system (6.13) *with*

$$
\begin{aligned}
C &\coloneqq \{(x,\theta) \in X \times \Theta : \mu_{V,\Psi_a}(x,\theta) \leq \rho_a\},\\
D &\coloneqq \left\{(x,\theta) \in X \times \Theta : \begin{array}{l} \mu_{V,\Psi_a}(x,\theta) \geq \rho_a \\ \textit{or } \mu_{V,\Psi}(x,\theta) \geq \rho \end{array}\right\},\\
G(x,\theta) &\coloneqq \begin{cases} G_{V,\Psi_a}(x,\theta), & \begin{array}{l}\mu_{V,\Psi_a}(x,\theta) \geq \rho_a \\ \textit{and } \mu_{V,\Psi}(x,\theta) < \rho,\end{array}\\ (G_{V,\Psi_a} \cup G_{V,\Psi})(x,\theta), & \begin{array}{l}\mu_{V,\Psi_a}(x,\theta) \geq \rho_a \\ \textit{and } \mu_{V,\Psi}(x,\theta) \geq \rho,\end{array}\\ G_{V,\Psi}(x,\theta), & \begin{array}{l}\mu_{V,\Psi_a}(x,\theta) < \rho_a \\ \textit{and } \mu_{V,\Psi}(x,\theta) \geq \rho,\end{array}\\ \emptyset & \textit{otherwise,}\end{cases}
\end{aligned}
\tag{6.19}
$$

where $\rho \geq \rho_a$.

Proof. It is clear that C and the sets

$$D_{\Psi_a} \coloneqq \{(x,\theta) \in X \times \Theta : \mu_{V,\Psi_a}(x,\theta) \geq \rho_a\} \tag{6.20}$$

$$D_{\Psi} \coloneqq \{(x,\theta) \in X \times \Theta : \mu_{V,\Psi}(x,\theta) \geq \rho\} \tag{6.21}$$

are closed since μ_{V,Ψ_a} and $\mu_{V,\Psi}$ are continuous. Therefore, $D = D_{\Psi_a} \cup D_{\Psi}$ is closed. The closed-loop flow map is continuous on $X \times \Theta$. We know that G_{V,Ψ_a} and $G_{V,\Psi}$ are nonempty-valued, outer semicontinuous, and locally bounded. Denote then by $\widetilde{G}_{V,\Psi_a}$ and $\widetilde{G}_{V,\Psi}$ the restrictions of G_{V,Ψ_a} and $G_{V,\Psi}$ to D_{Ψ_a} and D_{Ψ}, respectively. These restrictions are also outer semicontinuous and locally bounded. Now, G is defined such that $\operatorname{gph} G = \operatorname{gph} \widetilde{G}_{V,\Psi_a} \cup \operatorname{gph} \widetilde{G}_{V,\Psi}$. Thus, G is nonempty-valued on D. Since outer semicontinuity of a set-valued mapping is equivalent to its graph being closed, it also follows that G is outer semicontinuous. Moreover, the union of two locally bounded set-valued mappings is locally bounded. Consequently, G is locally bounded. Hence, the closed loop system (6.13) with data defined by (6.19) satisfies the hybrid basic conditions. The rest of the proof proceeds as the proof of Proposition 6.5, with the strict decrease of V across jumps now being at least ρ_a. □

Completeness of maximal solutions to the closed-loop system with data (6.19) is guaranteed if the tangent cone condition (6.15) holds for all (x,θ) such that $\mu_{V,\Psi_a}(x,\theta) < \rho_a$. In this case, the system always admits complete solutions over the course of which θ_b does not jump.

6.3.2 Independently Triggered Jumps

The following proposition introduces the concept of independentely triggered jumps, where both components of θ jump when either of their jump conditions are met.

Proposition 6.10. *Let (V, κ, ν) be a synergistic Lyapunov function and feedback triple relative to $\mathcal{A}$ with synergy gap relative to (Ψ_a, Ψ_b) exceeding (ρ_a, ρ_b), with $\rho_a, \rho_b > 0$. Then $\mathcal{A}$ is globally pre-asymptotically stable for the system (6.13) with*

$$\begin{aligned} C &:= \left\{ (x,\theta) \in X \times \Theta : \begin{array}{l} \mu_{V,\Psi_a}(x,\theta) \leq \rho_a \\ \text{and } \mu_{V,\Psi_b}(x,\theta) \leq \rho_b \end{array} \right\}, \\ D &:= \left\{ (x,\theta) \in X \times \Theta : \begin{array}{l} \mu_{V,\Psi_a}(x,\theta) \geq \rho_a \\ \text{or } \mu_{V,\Psi_b}(x,\theta) \geq \rho_b \end{array} \right\}, \\ G(x,\theta) &:= G_{V,\Psi}(x,\theta). \end{aligned} \tag{6.22}$$

The proof of Proposition 6.10 is very similar to the proofs of Proposition 6.5 and Proposition 6.9 and is therefore omitted. An example where independently triggered switching is used is furnished by the quaternion output feedback control scheme for rigid-body orientation in [37, Section V-B]. In this work, θ_a corresponds to a traditional synergy variable for a feedback controller, and θ_b corresponds to a traditional synergy variable for an observer, while $\nu(x,\theta) = 0$ for all $(x,\theta) \in X \times \Theta$.

6.4 Backstepping

This section begins by introducing a weaker notion of SLFF triples for affine control systems. Then, given a system that admits a weak SLFF triple, we construct a (non-weak) SLFF triple for the same system augmented with an integrator at the input.

By assuming that (6.1) is affine in the control input v, we obtain the system

$$\dot{x} = f_0(x) + g_0(x)v \quad (x,v) \in X \times \mathbb{R}^k \tag{6.23}$$

Definition 6.11. *Let $\mathcal{A} \subset X \times \Theta$ be compact. A continuously differentiable function $V : X \times \Theta \mapsto \mathbb{R}_{\geq 0}$ and continuous functions $\kappa : X \times \Theta \to \mathbb{R}^k$ and $\nu : X \times \Theta \to \mathbb{R}^m$ define a weak synergistic Lyapunov function and feedback triple (V, κ, ν) relative to $\mathcal{A}$ with a weak synergy gap relative to Ψ exceeding $\rho > 0$ for (6.23) if*

1. *V is proper and positive definite with respect to $\mathcal{A}$;*
2. *The closed loop system*

$$\begin{pmatrix} \dot{x} \\ \dot{\theta} \end{pmatrix} = \underbrace{\begin{pmatrix} f_0(x) + g_0(x)\kappa(x,\theta) \\ \nu(x,\theta) \end{pmatrix}}_{F_0(x,\theta)} \qquad (x,\theta) \in X \times \Theta \tag{6.24}$$

satisfies

$$\langle \nabla V(x,\theta), F_0(x,\theta) \rangle \leq 0, \quad \forall (x,\theta) \in X \times \Theta; \tag{6.25}$$

3. *$\mu_{V,\Psi}(x,\theta) > \rho$ for each $(x,\theta) \in \mathcal{I} \setminus \mathcal{A}$, where $\mathcal{I}$ is the largest weakly invariant subset for the system*

$$\left.\begin{aligned} \dot{x} &= f_0(x) + g_0(x)\kappa(x,\theta) \\ \dot{\theta} &= \nu(x,\theta) \end{aligned}\right\} (x,\theta) \in \mathcal{E} \cap \mathcal{W} \tag{6.26}$$

where $\mathcal{E}$ is given in Definition 6.4, and

$$\mathcal{W} \coloneqq \{(x,q) \in X \times \Theta : g_0(x)^\mathsf{T} \nabla_1 V(x,\theta) = 0\}. \tag{6.27}$$

Augmenting the system (6.23) with an integrator at the input results in the control system

$$\dot{z} = f_1(z) + g_1(z)u \quad (z,u) \in Z \times \mathbb{R}^k \tag{6.28}$$

where $z = (x,v) \in Z \coloneqq X \times \mathbb{R}^k$, $u \in \mathbb{R}^k$ is the control input and

$$f_1(z) = \begin{pmatrix} f_0(x) + g_0(x)v \\ 0 \end{pmatrix}, g_1(z) = \begin{pmatrix} 0 \\ I \end{pmatrix}. \tag{6.29}$$

Now, let (V_0, κ_0, ν_0) be a weak SLFF triple relative to the compact set $\mathcal{A}_0 \subset X \times \Theta$, define the set

$$\mathcal{A}_1 = \{(z,\theta) \in Z \times \Theta : (x,\theta) \in \mathcal{A}_0, v = \kappa(x,\theta)\}, \tag{6.30}$$

and consider the following SLFF triple

$$V_1(z,\theta) = V_0(x,\theta) + \frac{1}{2}|v - \kappa_0(x,\theta)|_\Gamma^2, \tag{6.31a}$$

$$\begin{aligned} \kappa_1(z,\theta) = {} & \nabla_1 \kappa_0(x,\theta)\left(f_0(x) + g_0(x)v\right) \\ & + \nabla_2 \kappa_0(x,\theta)\nu_0(x,\theta) - \gamma_1(v - \kappa_0(x,\theta)) \\ & - \Gamma^{-1} g_0(x)^\mathsf{T} \nabla_1 V_0(x,\theta), \end{aligned} \tag{6.31b}$$

$$\nu_1(z,\theta) = \nu_0(x,\theta) - \vartheta_1(\nabla_2 V_1(z,\theta)), \tag{6.31c}$$

where $\Gamma \in \mathbb{R}^{k \times k}$ is positive definite, and $\gamma_1 : \mathbb{R}^k \to \mathbb{R}^k$ and $\vartheta_1 : \mathbb{R}^m \to \mathbb{R}^m$ are strongly passive and passive functions, respectively. The following proposition establishes that (V_1, κ_1, ν_1) is an SLFF triple for the system (6.28) with synergy gap exceeding $\rho > 0$ relative to Ψ.

Proposition 6.12. *If (V_0, κ_0, ν_0) is a weak synergistic Lyapunov function and feedback triple for the system (6.23) relative to $\mathcal{A}_0$, with a weak synergy gap relative to Ψ exceeding $\rho > 0$, then (V_1, κ_1, ν_1) is a (non-weak) synergistic Lyapunov function and feedback triple for the system (6.28) relative to $\mathcal{A}_1$ with a (non-weak) synergy gap relative to Ψ exceeding $\rho > 0$.*

Proof. The derivative of V_1 along the solutions of (6.23) is

$$\begin{aligned}
\dot{V}_1(z,\theta) &= \langle \nabla_1 V_1(z,\theta), f_1(z) + g_1(z)\kappa_1(z,\theta)\rangle \\
&\quad + \langle \nabla_2 V_1(z,\theta), \nu_1(z,\theta)\rangle \\
&= \langle \nabla_1 V_0(x,\theta), f_0(x) + g_0(x)\kappa_0(x,\theta)\rangle \\
&\quad - \langle v - \kappa_0(x,\theta), \Gamma\gamma_1(v - \kappa_0(x,\theta)\rangle \\
&\quad - \langle v - \kappa_0(x,\theta), \Gamma\nabla_2\kappa_0(x,\theta)(\nu_1(z,\theta) - \nu_0(x,\theta))\rangle \\
&\quad + \langle \nabla_2 V_0(x,\theta), \nu_1(z,\theta)\rangle \\
&= \langle \nabla_1 V_0(x,\theta), f_0(x) + g_0(x)\kappa_0(x,\theta)\rangle \\
&\quad - \langle v - \kappa_0(x,\theta), \Gamma\gamma_1(v - \kappa_0(x,\theta)\rangle \\
&\quad + \langle \nabla_2 V_0(x,\theta), \nu_0(x,\theta)\rangle \\
&\quad - \langle \nabla_2 V_1(z,\theta), \vartheta_1(\nabla_2 V_1(z,\theta))\rangle \\
&\leq 0.
\end{aligned} \tag{6.32}$$

Define $\mathcal{E}_0, \mathcal{W}_0$ and $\mathcal{E}_1, \mathcal{W}_1$ according to (6.12) and (6.27) for the systems (6.23) and (6.28), respectively. It follows from (6.32) that

$$\begin{aligned}
\mathcal{E}_1 &= \{(z,\theta) \in X \times \Theta : (x,\theta) \in \mathcal{E}_0, v = \kappa_0(x,\theta), \vartheta_1(\nabla_2 V_1(z,\theta)) = 0\} \\
&\subset \mathcal{W}_1.
\end{aligned} \tag{6.33}$$

Let $\mathcal{I}_1 \subset \mathcal{E}_1$ denote the largest weakly invariant subset for the system

$$\left.\begin{aligned}
\dot{z} &= f_1(z) + g_1(z)\kappa_1(z,\theta) \\
\dot{\theta} &= \nu_1(z,\theta)
\end{aligned}\right\} (z,\theta) \in \mathcal{E}_1 \tag{6.34}$$

It follows that

$$\mathcal{I}_1 = \big\{(z,\theta) \in Z \times \Theta : (x,\theta) \in \Omega_0, v = \kappa_0(x,\theta), \vartheta_1(\nabla_2 V_1(z,\theta)) = 0\big\}. \tag{6.35}$$

From Definition 6.2 and 3) in Definition 6.11 it holds that

$$\begin{aligned}
\mu_{V_1,\Psi} &\geq \mu_{V_0,\Psi}(x,\theta) + \frac{1}{2}|v - \kappa_0(x,\theta)|_\Gamma^2 - \min_{\psi\in\Psi} \frac{1}{2}|v - \kappa_0(x,\psi)|_\Gamma^2 \\
&\geq \mu_{V_0,\Psi}(x,\theta) && (6.36) \\
&> \rho. && (6.37)
\end{aligned}$$

Consequently, (V_1, κ_1, ν_1) is an SLFF triple with synergy gap relative to Ψ exceeding $\rho > 0$. □

6.5 Synergistic Maneuvering for Ships

In this section, the proposed theory is exemplified by combining the traditional synergistic control approach of [42], [44] with the ship maneuvering control of [52], [53], where we augment the path variable with jump dynamics. The configuration space of a ship can be reasonably described by $\mathrm{SE}(2) = \mathbb{R}^2 \rtimes \mathrm{SO}(2)$. Configurations

of the ship are then represented as $x = (p, R)$, where $p \in \mathbb{R}^2$ represents the ship position and $R \in \mathrm{SO}(2)$ represents the ship heading.

The desired position of the ship is described in terms of a sufficiently smooth planar path.

Definition 6.13. *A planar C^r-path is a C^r-mapping $\eta : [0,1] \to \mathbb{R}^2$. If $r \geq 1$, we say that a planar C^r-path is regular if $\eta'(s) \neq 0$ for all $s \in [0,1]$.*

Given a regular C^3-path η in $\mathbb{R}^2$, we synthesize a C^2-path in $\mathrm{SE}(2)$ by requiring that the heading of the ship is tangential to the path. Such a path has the form $s \mapsto (p_d(s), R_d(s))$, where

$$\begin{aligned} p_d(s) &\coloneqq \eta(s) \\ R_d(s) &\coloneqq \frac{1}{|\eta'(s)|} \begin{pmatrix} \eta'(s) & S\eta'(s) \end{pmatrix}. \end{aligned} \tag{6.38}$$

A desired speed assignment for $\dot{s}$ along the path, $u_d : [0,1] \to \mathbb{R}$, is chosen as

$$u_d(s) \coloneqq \frac{U_d(s)}{|p_d'(s)|}, \tag{6.39}$$

where $U_d : [0,1] \to \mathbb{R}$ is a continuously differentiable signed desired ship speed along the path. In particular, u_d is defined such that if $\dot{s} = u_d(s)$, then $\dot{p}_d(s) = \frac{p_d'(s)}{|p_d'(s)|} U_d(s)$. A two times continuously differentiable path in the configuration space $x_d : [0,1] \to \mathrm{SE}(2)$ can now be defined as $x_d(s) \coloneqq (p_d(s), R_d(s))$.

We denote by $v = (\zeta, \omega) \in \mathbb{R}^3$ the velocity of the ship, where $\zeta \in \mathbb{R}^2$ is its linear velocity and $\omega \in \mathbb{R}$ is its angular velocity. A model for the ship kinematics and dynamics is [84, Chapter 6.5]

$$\left.\begin{aligned} \dot{x} &= xv^\wedge \\ \dot{v} &= -\gamma(v) + M^{-1}(d(v) + u) \end{aligned}\right\} (x, v) \in \mathrm{SE}(2) \times \mathbb{R}^3, \tag{6.40}$$

where $M = M^\mathsf{T} > 0$ is the ship inertia tensor (including hydrodynamic inertia), $\gamma : \mathbb{R}^3 \to \mathbb{R}^3$ describes the Coriolis and centripetal accelerations associated with M, $d : \mathbb{R}^3 \to \mathbb{R}^3$ describes the hydrodynamic drag forces acting on the ship, and u are idealized input forces produced by the actuators.

The general ship maneuvering problem is then split into a geometric task that represents convergence to this path, and a dynamic task that represents the attainment of the speed assignment u_d on this path.

Problem Statement (Maneuvering Problem [53])**.**

- ***Geometric Task:*** *Force the position and heading of the ship to converge to the desired path,*

$$\lim_{(t+j)\to\infty} \|x_d(s(t,j))^{-1} x(t,j) - I\| = 0. \tag{6.41}$$

- ***Dynamic Task:*** *Force the path speed to converge to the desired speed assignment:*

$$\lim_{(t+j)\to\infty} |\dot{s}(t,j) - u_d(s(t,j))| = 0. \tag{6.42}$$

6.5.1 Backstepping Controller

We set $X = \mathrm{SE}(2)$ and $\Theta = \Theta_a \times \Theta_b$, where $\Theta_a = \{-1, 1\}$, $\Theta_b = [0, 1]$ and $\theta = (\theta_a, \theta_b) = (q, s)$. In particular, q is a classical synergistic logic variable and s is a path variable utilized in the ship maneuvering control problem. Then, the kinematics of the ship and the flow of q and s may be cast as a system of the form (6.23),

$$\dot{x} = xv^\wedge \quad (x, v) \in \mathrm{SE}(2) \times \mathbb{R}^3. \tag{6.43}$$

The set $\mathcal{A}_0 \subset X \times \Theta$ is now chosen as

$$\mathcal{A}_0 = \{(x, \theta) \in X \times \Theta : x = x_d(s)\}. \tag{6.44}$$

Compactness of $\mathcal{A}_0$ holds because the mapping $(q, s) \mapsto x_d(s)$ is continuous and Θ is compact.

We now introduce a synergistic potential function which is similar to [44] for the heading control of the ship. In particular, let $P : \mathrm{SO}(2) \times [0, 1] \to \mathbb{R}$ and, with $\rho_a > 0$, the mapping $T : \mathrm{SO}(2) \times \Theta \to \mathrm{SO}(2)$

$$P(R, s) \coloneqq (1 - \langle e_1, R_d(s)^\mathsf{T} R e_1 \rangle), \tag{6.45}$$
$$T(R, \theta) \coloneqq \exp(\rho_a q P(R, s) S) R_d(s)^\mathsf{T} R. \tag{6.46}$$

Let $k_0 > 0$ and let $K_0 = K_0^\mathsf{T}$ be a positive definite matrix. Then, (V_0, κ_0, ν_0) defined as

$$V_0(x, \theta) = \frac{1}{2} |R_d^\mathsf{T}(p - p_d(s))|^2_{K_0} + k_0 P(T(R, \theta), s) \tag{6.47a}$$
$$\kappa_0(x, \theta) = \mathrm{Ad}^{-1}_{x_d(s)^{-1}x}(x_d(s)^{-1} x_d'(s))^\vee u_d(s) - K \, \mathrm{d}_1 V_0(x, \theta) \tag{6.47b}$$
$$\nu_0(x, \theta) = \begin{pmatrix} 0 \\ u_d(s) \end{pmatrix}, \tag{6.47c}$$

where $K = K^\mathsf{T}$ is a positive definite matrix, is an SLFF triple for (6.43) with synergy gap relative to $\{-1, 1\}$ exceeding $\frac{1}{2}$.

We now augment (6.43) with the ship dynamics

$$\left.\begin{aligned} \dot{x} &= xv^\wedge \\ \dot{v} &= -\gamma(v) + M^{-1}(d(v) + u) \end{aligned}\right\} (z, u) \in (\mathrm{SE}(2) \times \mathbb{R}^3) \times \mathbb{R}^3, \tag{6.48}$$

and define

$$\mathcal{A}_1 = \{(x, v, \theta) : (x, \theta) \in \mathcal{A}_0, v = \kappa_0(x, \theta)\}. \tag{6.49}$$

It then follows directly from Proposition 6.12 that

$$V_1(z,\theta) = V_0(x,\theta) + \frac{1}{2}|v - \kappa_0(x,\theta)|_M^2, \tag{6.50a}$$

$$\begin{aligned}\kappa_1(z,\theta) = {} & M\,\mathrm{d}_1\kappa_0(x,\theta)v + M\nabla_2\kappa_0(x,\theta)\nu_0(x,\theta) \\ & + M\gamma(v) - d(v) \\ & - \gamma_1(v - \kappa_0(x,\theta)) \\ & - \mathrm{d}_1 V_0(x,\theta),\end{aligned} \tag{6.50b}$$

$$\nu_1(z,\theta) = \nu_0(x,\theta), \tag{6.50c}$$

is an SLFF triple for the system (6.48) relative to $\mathcal{A}_1$ with synergy gap relative to $\{-1,1\}$ exceeding $\frac{1}{2}$. Consequently, the synergistic controller

$$\dot{\theta} = \nu_1(z,\theta) \qquad (z,\theta) \in C, \tag{6.51}$$

$$\theta^+ \in G(z,\theta) \qquad (z,\theta) \in D, \tag{6.52}$$

$$u = \kappa_1(z,\theta), \tag{6.53}$$

where (C,D,G) are given by (6.19), renders $\mathcal{A}_1$ globally pre-asymptotically stable for the resulting closed-loop system by Proposition 6.9. Moreover, if $u_d(s) \in T_{\Theta_b}(s)$ for all $s \in \Theta_b$, then all maximal solutions are complete and $\mathcal{A}_1$ is globally asymptotically stable for the resulting closed-loop system, which implies that the problem statement is solved.

6.5.2 Simulations

Simulation results are presented in Figures 6.1 to 6.5. The model parameters can be found in [58]. In the simulations, we have chosen $\delta = 0.1$, $\rho_a = \delta k_0$, $\rho = 1.2\rho_a$, $k_0 = 5$, $K_0 = 5I_2$, $K = 0.05I_3$ and $\gamma_1 = \mathrm{diag}(10,10,7)$. The chosen path is given by $p_d(s) \coloneqq 5(\cos(\pi s), \sin(\pi s))$. The ship is initialized at $p = (5,2)$ with an initial heading of $\psi = -85°$, an initial velocity of $v = 0$ and a desired speed of $U_d = 0.3\,\mathrm{m/s}$.

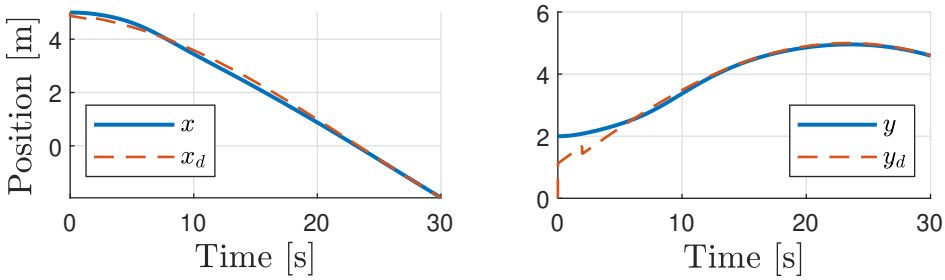

Figure 6.1: The position $p = (x,y)$ and desired position $p_d = (x_d, y_d)$.

From Figure 6.1 we observe that the position references are successfully tracked after an initial transient phase. An optional jump is immediately triggered such that q is mapped to -1 and s is mapped to approximately 0.08. An optional jump is

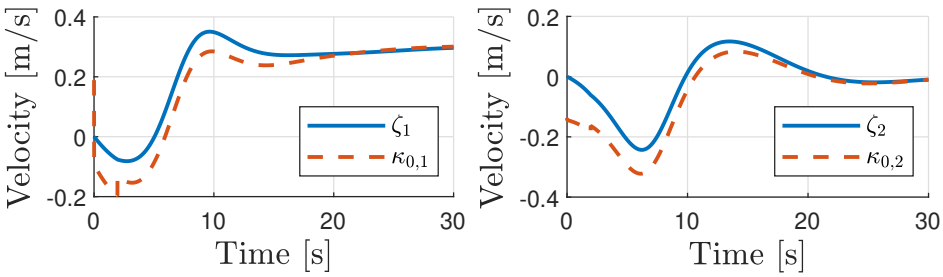

Figure 6.2: The body linear velocity ζ_1 and ζ_2 and the first and second component of κ_0.

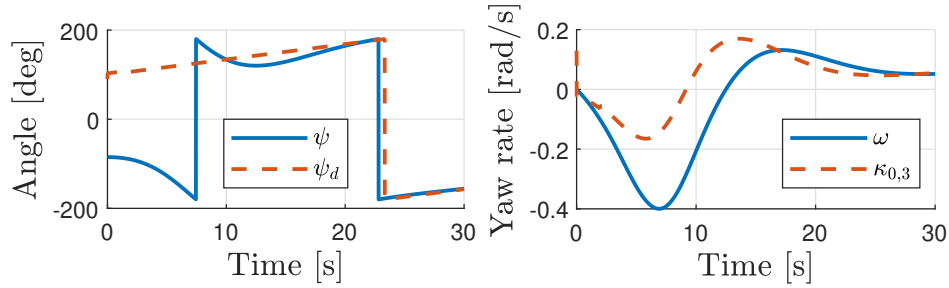

Figure 6.3: The heading angle $\psi = \text{atan2}(R_{21}, R_{11})$, desired heading angle $\psi_d = \text{atan2}(R_{d,21}, R_{d,11})$, angular velocity ω and the third component of κ_0.

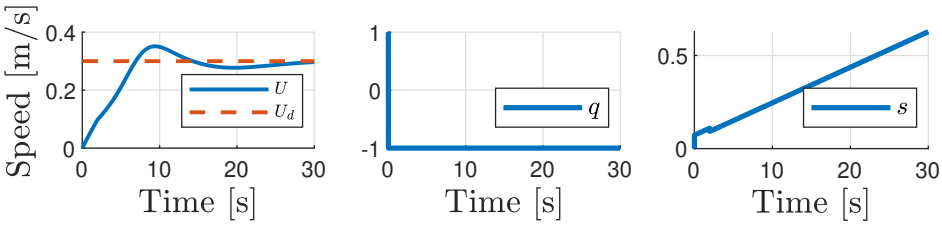

Figure 6.4: The speed $U = (\zeta_1^2 + \zeta_2^2)^{\frac{1}{2}}$, desired speed U_d and synergistic variables q and s.

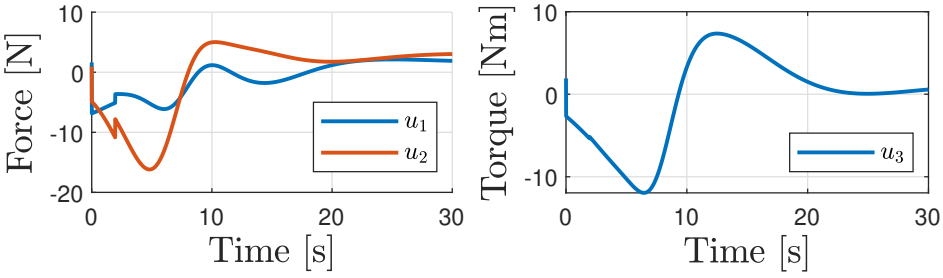

Figure 6.5: The control forces and moment u.

triggered around $t \approx 2\,\mathrm{s}$ as seen in Figure 6.1. The error in the x-direction is slightly decreased while the error in the y-direction is slightly increased. Moreover, from Figure 6.2 we note that the difference between ζ_1 and $\kappa_{0,1}$ decreases over the jump in s. In Figure 6.4, we observe that s is decreased over the jump, while q remains the same. Moreover, from Figure 6.5, we observe a discontinuity in u_2 at the time of the jump.

6.6 Conclusions

In this chapter, we have generalized the definition of synergistic Lyapunov functions and feedbacks to allow the traditional logic variable of synergistic control to be vector-valued and change during flows. Since the logic variable is allowed to be vector-valued, we have introduced the notion of synergy gaps relative to components of product sets, which enables existing hybrid output feedback control laws to be reformulated within the synergistic framework. Furthermore, we have shown that the properties of an SLFF triple are preserved through integrator backstepping. Finally, we have given an example in which a classical synergistic control approach is combined with a ship maneuvering control approach to enable discrete path dynamics and global asymptotic stability properties.

Chapter 7

Hysteretic Control Lyapunov Functions

In this chapter, we present a new class of control Lyapunov functions for hybrid feedback control of continuous-time systems, referred to as hysteretic control Lyapunov functions (HCLFs). HCLFs include a hysteresis-based switching mechanism and result in a hybrid control law, transforming the continuous-time system into a hybrid control system. We show that the existence of a family of HCLFs satisfying the small control property implies global stabilizability of a compact set. The hybrid feedback consists of a collection of continuous feedback laws and a hysteresis-based switching mechanism. Moreover, we prove that optimization-based hybrid feedback laws can be constructed under minor assumptions on the objective functions. The collection of optimization-based feedback laws are continuous along flows, implying that the hybrid basic conditions hold such that the stability is robust in the sense of [55].

The material in this chapter is based on [57].

7.1 Introduction

Control Lyapunov functions (CLFs) constitute a powerful tool for constructive nonlinear control design, since they can be utilized to determine a stabilizing control law from Lyapunov inequalities [11, 12]. General control laws for stabilization of nonlinear systems using CLFs were first introduced in [13] through Sontag's universal formula, and later in [15]. The control law in [15] is notable in the sense that it pointwise minimizes the norm of the control input with respect to the CLF. More recently, CLFs have been extended to hybrid systems with and without disturbances in [90] and [91], respectively. However, for global asymptotic stabilization of dynamical systems defined on non-contractible state-spaces, there does not exist a continuously differentiable CLF [92].

The remainder of this chapter is organized as follows. Section 7.2 defines a family of hysteretic CLFs, and proves that a family of continuous feedback laws derived from the feasible set-valued map of control inputs defined by the HCLFs results in global asymptotic stability of any compact set. Then, Section 7.3 presents suffi-

cient conditions for the existence of a family of continuous control selections from the feasible set-valued map. Given a collection of radially unbounded and strictly convex objective functions, we present an optimization-based hybrid feedback law that pointwise minimizes the objective functions subject to the stability constraints imposed by the HCLFs. Section 7.4 derives the quaternion tracking error dynamics for an underwater vehicle, before a family of HCLFs are constructed in Section 7.5. The HCLF family is subsequently employed for synthesis of a hybrid control law for global asymptotic configuration and velocity tracking. Then, Section 7.6 verifies the theoretical developments through simulations, before Section 7.7 presents our concluding remarks.

7.2 Hysteretic Control Lyapunov Functions

In this section, we define hysteretic control Lyapunov functions for the following class of continuous-time systems

$$\mathcal{N}: \begin{cases} \dot{x} = f(x, r, u) \\ \dot{r} \in c\mathbb{B} \end{cases} \qquad (x, r, u) \in \mathcal{X} \times \mathcal{R} \times \mathcal{U}, \tag{7.1}$$

where $c > 0$, $u \in \mathcal{U}$ describes the input, and $r \in \mathcal{R}$ describes a known exogenous reference signal. It is assumed that $\mathcal{N}$ satisfies

Assumptions.

(N1) the state space $\mathcal{X} \subset \mathbb{R}^n$ is closed;
(N2) the input space $\mathcal{U} \subset \mathbb{R}^m$ is closed and convex;
(N3) the exogenous reference space $\mathcal{R} \subset \mathbb{R}^k$ is compact;
(N4) the mapping $f : \mathcal{X} \times \mathcal{R} \times \mathcal{U} \to \mathbb{R}^n$ is continuous.

Systems of this form adequately describe a wide range of tracking problems for mechanical systems.

Definition 7.1 (HCLF Family)**.** *Let $\mathcal{A} \subset \mathcal{X}$ be compact and $\mathcal{Q} \subset \mathbb{Z}$ be finite. A collection of functions $\{V_q\}_{q\in\mathcal{Q}}$ is a family of hysteretic control Lyapunov functions for $(\mathcal{N}, \mathcal{A})$ with negativity margins $\{\gamma_q\}_{q\in\mathcal{Q}}$, if there exists collections of sets $\{\mathcal{I}_q\}_{q\in\mathcal{Q}}$, $\{\mathcal{O}_q\}_{q\in\mathcal{Q}}$, and $\{\mathcal{M}_q\}_{q\in\mathcal{Q}}$, class-$\mathcal{K}_\infty$ functions $\underline{\alpha}$ and $\overline{\alpha}$, and a class-$\mathcal{PD}$ function ρ, such that*

(H1) $\{\mathcal{I}_q\}_{q\in\mathcal{Q}}$ covers $\mathcal{X}$, and for each $q \in \mathcal{Q}$, $\mathcal{I}_q$ is closed in $\mathcal{X}$, $\mathcal{O}_q$ is open in $\mathcal{X}$, $\mathcal{M}_q$ is closed in $\mathcal{X}$, and $\mathcal{I}_q \subset \mathcal{O}_q \subset \mathcal{M}_q$;
(H2) for each $q \in \mathcal{Q}$, V_q is continuously differentiable on an open set containing $\mathcal{M}_q$, and for all $x \in \mathcal{M}_q$,

$$\underline{\alpha}(|x|_{\mathcal{A}}) \leq V_q(x) \leq \overline{\alpha}(|x|_{\mathcal{A}}); \tag{7.2}$$

(H3) for all $(q, s) \in \mathcal{Q} \times \mathcal{Q}$ and all $x \in (\mathcal{M}_q \setminus \mathcal{O}_q) \cap \mathcal{I}_s$,

$$V_s(x) \leq V_q(x); \tag{7.3}$$

(H4) for all $(r,q) \in \mathcal{R} \times \mathcal{Q}$ *and all* $x \in \mathcal{M}_q$, $\gamma_q : \mathcal{M}_q \times \mathcal{R} \to \mathbb{R}_{\geq 0}$ *is continuous,* $\gamma_q(x,r) \geq \rho(|x|_{\mathcal{A}})$, *and*

$$\inf_{u \in \mathcal{U}} \nabla V_q(x)^{\mathsf{T}} f(x,r,u) + \gamma_q(x,r) \leq -\rho(|x|_{\mathcal{A}}). \tag{7.4}$$

A family of HCLFs for $(\mathcal{N}, \mathcal{A})$ is a tool for the design of a hybrid controller of the form

$$\mathscr{C}\colon \begin{cases} u = \kappa_q(x,r) & (x,r) \in C_q \\ q^+ \in G_q(x) & (x,r) \in D_q, \end{cases} \tag{7.5}$$

where $\{\kappa_q\}_{q \in \mathcal{Q}}$ is a collection of feedback control laws, and the flow set, jump set, and jump map are defined as

$$C_q \coloneqq \mathcal{M}_q \times \mathcal{R}, \tag{7.6}$$
$$D_q \coloneqq \mathcal{X} \setminus \mathcal{O}_q \times \mathcal{R}, \tag{7.7}$$
$$G_q(x) \coloneqq \{s \in \mathcal{Q} : x \in \mathcal{I}_s \setminus \mathcal{O}_q\}, \tag{7.8}$$

respectively. Additionally, for a given $q \in \mathcal{Q}$, we also write

$$\mathcal{B}_q \coloneqq (\mathcal{A} \times \mathcal{R}) \cap C_q. \tag{7.9}$$

We remark that $\mathcal{M}_q$ can always be chosen as the closure of $\mathcal{O}_q$.

Applying the hybrid controller $\mathscr{C}$ to the system $\mathcal{N}$, results in the hybrid closed-loop system of the form

$$\mathcal{H}\colon \begin{cases} \left.\begin{aligned} \dot{x} &= f(x, \kappa_q(x,r), r) \\ \dot{r} &\in c\mathbb{B} \end{aligned}\right\} & (x,r) \in C_q \\ q^+ \in G_q(x) & (x,r) \in D_q. \end{cases} \tag{7.10}$$

For convenience of notation, the flow map (jump map) of a state in a hybrid system is omitted if it remains unchanged along flows (across jumps). When the the compact set $\mathcal{A} \times \mathcal{R} \times \mathcal{Q}$ is globally pre-asymptotically stable for the system $\mathcal{H}$, we shall say that $\mathscr{C}$ globally pre-asymptotically stabilizes $\mathcal{A}$ for $\mathcal{N}$.

The definition of an HCLF family naturally leads to a collection of feasible set-valued mappings for the input. These mappings can, for each $q \in \mathcal{Q}$, be defined as $\mathcal{F}_q : C_q \rightrightarrows \mathcal{U}$,

$$\mathcal{F}_q(x,r) \coloneqq \{u \in \mathcal{U} : \nabla V_q(x)^{\mathsf{T}} f(x,r,u) + \gamma_q(x,r) \leq 0\}. \tag{7.11}$$

The fact that the domain of $\mathcal{F}_q$ is C_q follows readily from (H4). Moreover, for each $q \in \mathcal{Q}$ and all $(x,r) \in C_q$, any input $u \in \mathcal{F}_q(x,r)$ results in a rate of change of V_q at (x,r) less than or equal to $-\gamma_q(x,r)$ while flowing. The negativity margins should therefore be viewed as design parameters.

The following theorem proves that a selection of continuous feedback laws from the feasible set-valued mapping $\mathcal{F}_q$ renders $\mathcal{A}$ globally pre-asymptotically stable for the system $\mathcal{N}$. This stability is robust to perturbations in the sense of [55, Definition 7.15], as seen from [55, Proposition 7.21].

Theorem 7.2. *Let $\{V_q\}_{q\in\mathcal{Q}}$ be an HCLF family for $(\mathcal{N},\mathcal{A})$ with negativity margins $\{\gamma_q\}_{q\in\mathcal{Q}}$. If there exists a collection of feedback control laws $\{\kappa_q\}_{q\in\mathcal{Q}}$ such that, for each $q\in\mathcal{Q}$, $\kappa_q : C_q \to \mathcal{U}$ is continuous, and for all $(x,r)\in C_q$, $\kappa_q(x,r)\in\mathcal{F}_q(x,r)$, then the controller $\mathscr{C}$ renders $\mathcal{A}$ globally pre-asymptotically stable for $\mathcal{N}$.*

Proof. Let $\widetilde{\mathcal{H}}$ denote the hybrid system $\mathcal{H}$ with each jump set D_q replaced by $\widetilde{D}_q = C_q \cap D_q$. Since $\mathcal{Q}$ is finite and each κ_q is continuous, it is straightforward to verify that $\mathcal{H}$ and $\widetilde{\mathcal{H}}$ satisfy the hybrid basic conditions [55, Assumption 6.5]. For each $q\in\mathcal{Q}$ and all $(x,r)\in\widetilde{D}_q$, we find that $s\in G_q(x)$ implies $(x,r)\in C_s\setminus\widetilde{D}_s$. It now follows from [93, Lemma 2.7] that, for each bounded solution to $\widetilde{\mathcal{H}}$, there exists a positive scalar that bounds the time of flow after each jump from below. We now define a Lyapunov function candidate $V:(x,q)\mapsto V_q(x)$. From (H2), (H3), and the non-increase along flows by definition of the feasible set-valued mapping (7.11), uniform global stability of $\mathcal{A}\times\mathcal{R}\times\mathcal{Q}$ for $\widetilde{\mathcal{H}}$, and hence boundedness of solutions, can be concluded. One may now apply [55, Proposition 3.27] to conclude global asymptotic stability of $\mathcal{A}\times\mathcal{R}\times\mathcal{Q}$ for $\widetilde{\mathcal{H}}$. Solutions to $\mathcal{H}$ that are not solutions to $\widetilde{\mathcal{H}}$ are those with initial values (x^*,r^*,q^*) such that $q^*\in\mathcal{Q}$ and $(x^*,r^*)\in D_{r^*}\setminus C_{r^*}$. Such solutions immediately jump from q^* to some $s\in G_{r^*}(x^*)$, after which they coincide with a solution to $\widetilde{\mathcal{H}}$ initiated in (x^*,r^*,s). It is therefore clear that $\mathcal{A}\times\mathcal{R}\times\mathcal{Q}$ is globally pre-asymptotically stable for $\mathcal{H}$. □

7.2.1 Connection with SLFF Pairs

HCLFs are closely related to the notions of synergistic functions and synergistic Lyapunov function and feeback pairs (SLFFs) from Chapters 5 and 6. Indeed, given a collection of continuously differentiable functions $V_q:\mathcal{X}\to\mathbb{R}_{\geq 0}$, we define

$$\mu_V(x,q) \coloneqq V_q(x) - \min_{p\in\mathcal{Q}} V_p(x), \tag{7.12}$$

the sets

$$\mathcal{M}_q = \{x\in\mathcal{X} : \mu_V(x,q)\leq\delta\}, \tag{7.13a}$$
$$\mathcal{O}_q = \{x\in\mathcal{X} : \mu_V(x,q)<\delta\}, \tag{7.13b}$$
$$\mathcal{I}_q = \{x\in\mathcal{X} : \mu_V(x,q)=0\}, \tag{7.13c}$$

and propose the following definition.

Definition 7.3 (SCLF Family)**.** *Let $\mathcal{A}\subset\mathcal{X}$ be compact and $\mathcal{Q}\subset\mathbb{Z}$ be finite. A collection of functions $\{V_q\}_{q\in\mathcal{Q}}$ is a family of synergistic control Lyapunov functions for $(\mathcal{N},\mathcal{A})$ with negativity margins $\{\gamma_q\}_{q\in\mathcal{Q}}$, if there exists class-$\mathcal{K}_\infty$ functions $\underline{\alpha}$ and $\overline{\alpha}$, and a class-$\mathcal{PD}$ function ρ, such that*

(S1) for each $q\in\mathcal{Q}$, $V_q:\mathcal{X}\to\mathbb{R}_{\geq 0}$ is continuously differentiable on an open set containing $\mathcal{X}$, and for all $x\in\mathcal{M}_q$,

$$\underline{\alpha}(|x|_{\mathcal{A}}) \leq V_q(x) \leq \overline{\alpha}(|x|_{\mathcal{A}}); \tag{7.14}$$

(S2) for all $(r,q) \in \mathcal{R} \times \mathcal{Q}$ *and all* $x \in \mathcal{M}_q$, $\gamma_q : \mathcal{M}_q \times \mathcal{R} \to \mathbb{R}_{\geq 0}$ *is continuous,* $\gamma_q(x,r) \geq \rho(|x|_{\mathcal{A}})$, *and*

$$\inf_{u \in \mathcal{U}} \langle \nabla V_q(x), f(x,r,u) \rangle + \gamma_q(x,r) \leq -\rho(|x|_{\mathcal{A}}). \tag{7.15}$$

From (7.13) and the fact that each V_q is defined globally, it is clear that an SCLF family is also an HCLF family. Furthermore, it is straightforward to show that (V,κ) is an SLFF pair according to [1, Definition 7.3] if for each $q \in \mathcal{Q}$, $\kappa_q : \mathcal{X} \times \mathcal{R} \to \mathcal{U}$ is continuous and satisfies

$$\nabla V_q(x)^{\mathsf{T}} f(x,r,\kappa_q(x,r)) + \gamma_q(x,r) \leq -\rho(|x|_{\mathcal{A}}), \quad \forall (x,r) \in \mathcal{M}_q \times \mathcal{R}. \tag{7.16}$$

7.3 Hysteretic Feedback Control Design

Let $\{V_q\}_{q\in\mathcal{Q}}$ be an HCLF family for $(\mathcal{N},\mathcal{A})$ with negativity margins $\{\gamma_q\}_{q\in\mathcal{Q}}$. The following theorem provides sufficient conditions for the existence of a hybrid control law for $\mathcal{N}$ with inherent robustness properties.

Theorem 7.4 (Continuous Selection)**.** *Let* $\{V_q\}_{q\in\mathcal{Q}}$ *be an HCLF family for* $(\mathcal{N},\mathcal{A})$ *with negativity margins* $\{\gamma_q\}_{q\in\mathcal{Q}}$. *If it holds that,*

(C1) for each $q \in \mathcal{Q}$ *and all* $(x,r) \in C_q$, *the mapping*

$$u \mapsto \nabla V_q(x)^{\mathsf{T}} f(x,r,u), \tag{7.17}$$

is convex on $\mathcal{U}$;

(C2) there exists a collection of control laws $\{\theta_q\}_{q\in\mathcal{Q}}$, *where for each* $q \in \mathcal{Q}$, $\theta_q \colon C_q \to \mathcal{U}$ *is continuous and the set-valued mapping* $\widetilde{\mathcal{F}}_q \colon C_q \rightrightarrows \mathcal{U}$ *defined by*

$$\widetilde{\mathcal{F}}_q(x,r) \coloneqq \begin{cases} \{\theta_q(x,r)\}, & \text{if } (x,r) \in \mathcal{B}_q \\ \mathcal{F}_q(x,r), & \text{if } (x,r) \in C_q \backslash \mathcal{B}_q, \end{cases} \tag{7.18}$$

is lower semicontinuous for all $(x,r) \in \mathcal{B}_q$,

then there exists a collection of feedback control laws $\{\kappa_q\}_{q\in\mathcal{Q}}$ *such that, for each* $q \in \mathcal{Q}$, $\kappa_q \colon C_q \to \mathcal{U}$ *is continuous, and the hybrid controller* $\mathscr{C}$ *renders the set* $\mathcal{A}$ *globally pre-asymptotically stable for the system* $\mathcal{N}$.

Proof. Since f is continuous, each ∇V_q and ρ_q are continuous, and each C_q is closed, it follows from [15, Corollary 2.13] that each $\mathcal{F}_q^{\circ} : C_q \backslash \mathcal{B}_q \rightrightarrows \mathcal{U}$ defined as

$$\mathcal{F}_q^{\circ}(x,r) = \big\{u \in \mathcal{U} : \nabla V_q(x)^{\mathsf{T}} f(x,r,u) + \gamma_q(x,r) < 0\big\},$$

is lower semicontinuous. From (C1), [94, Theorem 7.6], and the fact that taking closures preserves lower semicontinuity, it follows that for each $q \in \mathcal{Q}$ and all $(x,r) \in C_q \backslash \mathcal{B}_q$

$$\begin{aligned} \overline{\mathcal{F}_q^{\circ}(x,r)} &= \big\{u \in \mathcal{U} : \nabla V_q(x)^{\mathsf{T}} f(x,r,u) + \gamma_q(x,r) \leq 0\big\} \\ &= \mathcal{F}_q(x,r), \end{aligned}$$

is closed-convex-valued and lower semicontinuous. Now, it follows from (C2) that each $\widetilde{\mathcal{F}}_q$ is lower semicontinuous. Then, the Michael selection theorem [15, Theorem 2.18] implies the existence of a collection of functions $\{\kappa_q\}_{q\in\mathcal{Q}}$ such that $\kappa_q\colon C_q \to \mathcal{U}$ is continuous and $\kappa_q(x,r) \in \widetilde{\mathcal{F}}_q(x,r)$ for each $q \in \mathcal{Q}$ and all $(x,r) \in C_q$. The rest of the proof follows from Theorem 7.2 because $\widetilde{\mathcal{F}}_q(x,r) \subset \mathcal{F}_q(x,r)$ for each $q \in \mathcal{Q}$ and all $(x,r) \in C_q$. □

Condition (C1) always holds when the mapping $u \mapsto f(x,r,u)$ is affine for all $(x,r) \in \mathcal{X} \times \mathcal{R}$. Additionally, (C2) is recognized as the the small control property [15].

Theorem 7.4 implies the existence of a collection of continuous control laws rendering the compact set $\mathcal{A}$ globally pre-asymptotically stable for the system $\mathcal{N}$. However, it is neither constructive nor optimal. The following theorem enables us to take continuous selections from $\widetilde{\mathcal{F}}_q(x,r)$ minimizing a specified objective function.

Theorem 7.5 (Optimal Selection)**.** *Let $\{V_q\}_{q\in\mathcal{Q}}$ be an HCLF family for $(\mathcal{N},\mathcal{A})$ with negativity margins $\{\gamma_q\}_{q\in\mathcal{Q}}$ satisfying the assumptions of Theorem 7.4. If $\{h_q\}_{q\in\mathcal{Q}}$ is a collection of functions satisfying,*

(O1) for each $q \in \mathcal{Q}$, $h_q\colon \mathcal{X}\times\mathcal{R}\times\mathcal{U} \to \mathbb{R}_{\geq 0}$ is continuous and strictly convex in its third argument;

(O2) there exist class-$\mathcal{K}_\infty$ functions $\underline{\beta}$ and $\overline{\beta}$ such that, for each $q \in \mathcal{Q}$ and for all $(x,r) \in C_q$,

$$\underline{\beta}(|u-\theta_q(x,r)|) \leq h_q(x,r,u) \leq \overline{\beta}(|u-\theta_q(x,r)|), \tag{7.19}$$

where $\{\theta_q\}_{q\in\mathcal{Q}}$ is defined in (C2) in Theorem 7.4,

then there exists a family of feedback control laws $\{\kappa_q\}_{q\in\mathcal{Q}}$, such that for each $q \in \mathcal{Q}$, $\kappa_q\colon C_q \to \mathcal{U}$ is continuous and defined by

$$\kappa_q(x,r) = \underset{u\in\widetilde{\mathcal{F}}_q(x,r)}{\arg\min}\ h_q(x,r,u), \qquad (x,r) \in C_q, \tag{7.20}$$

such that the hybrid control law $\mathscr{C}$, renders the set $\mathcal{A}$ globally pre-asymptotically stable for the system $\mathcal{N}$.

Proof. Theorem 7.4 establishes that each $\mathcal{F}_q$ is nonempty, closed-convex-valued and lower semicontinuous for all $(x,r) \in C_q\backslash\mathcal{B}_q$. Additionally, $\mathcal{F}_q$ is upper semicontinuous for all $(x,r) \in C_q\backslash\mathcal{B}_q$ as it is closed-valued for all $(x,r) \in C_q\backslash\mathcal{B}_q$ and $\mathcal{U}$ is closed [62, Example 5.8]. Hence, by [55, Lemma 5.15] and [55, Lemma 5.10], for each $q \in \mathcal{Q}$, $\operatorname{gph}\mathcal{F}_q$ is closed relative to $C_q\backslash\mathcal{B}_q$. Then, (7.19) and continuity of each h_q on $\operatorname{gph}\mathcal{F}_q$, implies that for every compact set $\mathcal{K} \subset C_q\backslash\mathcal{B}_q$ and all $\lambda \in \mathbb{R}$, the sets

$$\{(x,r,u) : (x,r) \in \mathcal{K}, u \in \mathcal{F}_q(x,r), h_q(x,r,u) \leq \lambda\},$$

are compact. By [95, Theorem 1.4], each function

$$c_q(x,r) = \min_{u\in\mathcal{F}_q(x,r)} h_q(x,r,u), \quad (x,r) \in C_q\backslash\mathcal{B}_q,$$

is continuous, and each set-valued mapping $\mathcal{P}_q \colon C_q \backslash \mathcal{B}_q \rightrightarrows \mathcal{U}$ of minimal solutions, defined as

$$\mathcal{P}_q(x,r) \coloneqq \underset{u \in \mathcal{F}_q(x,r)}{\arg\min}\ h_q(x,r,u),$$

is upper semicontinuous and compact-valued for each $q \in \mathcal{Q}$. Now, $\mathcal{F}_q$ is nonempty and closed-convex-valued for each $q \in \mathcal{Q}$, for every $(x,r) \in C_q \backslash \mathcal{B}_q$, and each function h_q is strictly convex in u for all $u \in \mathcal{F}_q(x,r)$. It follows from [62, Theorem 2.6] that $\mathcal{P}_q$ is single-valued, such that it is possible to set $\kappa_q(x,r) \coloneqq \mathcal{P}_q(x,r)$ for each $q \in \mathcal{Q}$ and for all $(x,r) \in C_q \backslash \mathcal{B}_q$. Consequently, by [62, Corollary 5.20], κ_q is continuous for all $(x,r) \in C_q \backslash \mathcal{B}_q$ as it is upper semicontinuous in the sense of a set-valued mapping.

To show continuity of each κ_q in $\mathcal{B}_q$, rewrite (7.20) as

$$\kappa_q(x,r) \coloneqq \begin{cases} \theta_q(x,r) & \text{if } (x,r) \in \mathcal{B}_q \\ \underset{u \in \mathcal{F}_q(x,r)}{\arg\min}\ h_q(x,r,u) & \text{if } (x,r) \in C_q \backslash \mathcal{B}_q, \end{cases}$$

which follows from (7.19) and the fact that $\mathcal{F}_q(x,r) = \mathcal{U}$ when $(x,r) \in \mathcal{B}_q$. Now, $\widetilde{\mathcal{F}}_q(x,r)$ is lower semicontinuous for all $(x,r) \in C_q$ by (C2). Therefore, there exists a family of continuous selections $\mu_q(x,r) \in \widetilde{\mathcal{F}}_q(x,r)$ with $\mu_q(x,r) = \theta_q(x,r)$, for all $(x,r) \in \mathcal{B}_q$. It follows from (7.19) that for each $q \in \mathcal{Q}$, and for all $(x,r) \in C_q$,

$$0 \leq |\kappa_q(x,r) - \theta_q(x,r)| \leq \underline{\beta}^{-1} \circ \overline{\beta}(|\mu_q(x,r) - \theta_q(x,r)|). \tag{7.21}$$

From continuity of each θ_q and μ_q it follows that each κ_q is continuous. The rest of the proof follows from Theorem 7.2. □

The main difficulty in applying Theorem 7.5 appears to be how to verify that the HCLF family satisfies the small control property (C2) defined in Theorem 7.4. It turns out that if (C1) holds, then the existence of a family of continuous feasible control laws for the HCLF family implies that the small control property holds, as shown in the following result.

Lemma 7.1. *Let $\{V_q\}_{q \in \mathcal{Q}}$ be an HCLF family for $(\mathcal{N}, \mathcal{A})$ with negativity margins $\{\gamma_q\}_{q \in \mathcal{Q}}$ satisfying (C1) in Theorem 7.4. If there exists a collection of continuous mapping $\{\mu_q\}_{q \in \mathcal{Q}}$ such that for each $q \in \mathcal{Q}$, $\mu_q : C_q \to \mathcal{U}$ satisfies $\mu_q(x,r) \in \widetilde{\mathcal{F}}_q(x,r)$ for all $(x,r) \in C_q$, then $\widetilde{\mathcal{F}}_q$ is lower semicontinuous for all $(x,r) \in C_q$.*

Proof. We have already shown in the proof of Theorem 7.4 that $\widetilde{\mathcal{F}}_q$ is lower semicontinuous for all $(x,r) \in C_q \backslash \mathcal{B}_q$. Let $(\bar{x},\bar{r}) \in \mathcal{B}_q$. For every neighborhood W of $p = \mu_q(\bar{x},\bar{r})$, define $V \coloneqq \mu_q^{-1}(W)$. Then, V is a neighborhood of $(\bar{x},\bar{r})$ (relative to C_q) by continuity of μ_q. Moreover, since $\mu(x,r) \in \widetilde{\mathcal{F}}_q(x,r)$ for all $(x,r) \in C_q$, it holds that $V \subset \widetilde{F}_q^{-1}(W)$. Consequently, $\widetilde{F}_q$ is lower semicontinuous for all $(x,r) \in C_q$ by [62, Exercise 5.6]. □

7.4 Trajectory Tracking for Underwater Vehicles

In the remaining part of this chapter we will illustrate how the results of the previous sections can be applied. Specifically, we will construct a family of HCLFs and synthesize a hybrid control law ensuring global asymptotic tracking for an underwater vehicle. This section provides kinematic and dynamic models of an underwater vehicle, before the tracking error dynamics are derived.

7.4.1 Kinematics

The position and attitude of a rigid underwater vehicle are uniquely described by a vector $p \in \mathbb{R}^3$ specifying the position of the body frame origin with respect to the inertial frame origin, and a rotation matrix $R \in \mathrm{SO}(3)$ specifying the body frame axes projected onto the inertial frame axes. The rate of change of these quantities is related to the linear and angular body velocities, $v \in \mathbb{R}^3$ and $\omega \in \mathbb{R}^3$, respectively, by

$$\begin{aligned} \dot{p} &= Rv \\ \dot{R} &= R\omega^\wedge. \end{aligned} \tag{7.22}$$

It is well-known that no three-parameter parametrization of SO(3) is globally non-singular [96], which is why a four-parameter unit quaternion representation is often preferred for control design. A unit quaternion is written as a vector $z = (\eta, \epsilon) \in \mathbb{S}^3$, where $\eta \in \mathbb{R}$ and $\epsilon \in \mathbb{R}^3$, respectively describe the real and imaginary component of the quaternion. Any unit quaternion maps to a rotation matrix through the surjective map $R\colon \mathbb{S}^3 \to \mathrm{SO}(3)$ defined by

$$R(z) \coloneqq I_3 + 2\eta\epsilon^\wedge + 2\left(\epsilon^\wedge\right)^2. \tag{7.23}$$

The quaternion kinematic equation is given by

$$\dot{z} = \breve{T}(z)\omega, \tag{7.24}$$

where $\breve{T}\colon \mathbb{S}^3 \to \mathbb{R}^{4\times 3}$ is defined by

$$\breve{T}(z) \coloneqq \frac{1}{2}\begin{pmatrix} -\epsilon^\mathsf{T} \\ \eta I_3 + \epsilon^\wedge \end{pmatrix}. \tag{7.25}$$

Let $\bar{z} = (\bar{\eta}, \bar{\epsilon}) \in \mathbb{S}^3$ represent the desired quaternion. The error quaternion corresponding to $R(\tilde{z}) = \tilde{R} = \bar{R}^\mathsf{T} R$ is

$$\tilde{z} = \bar{z}^{-1} \otimes z = (\tilde{\eta}, \tilde{\epsilon}), \tag{7.26}$$

where $\otimes$ denotes the quaternion product. Note that the map defined in (7.23) is not injective, since it maps unit quaternions representing antipodal points in $\mathbb{S}^3$ to the same element in SO(3). Hence, the set of unit quaternions corresponding to $R(\tilde{z}) = I_3$ is $\tilde{z} = \pm e_1 = \pm(1, 0, 0, 0)$.

Defining $\varphi \coloneqq (p, z) \in \mathbb{R}^3 \times \mathbb{S}^3$, and collecting the linear and angular velocities in the vector $\nu = (v, \omega) \in \mathbb{R}^6$ results in the kinematic equation

$$\dot{\varphi} = \begin{pmatrix} R(z) & 0_{3\times 3} \\ 0_{4\times 3} & \breve{T}(z) \end{pmatrix} \nu \coloneqq T(z)\nu. \tag{7.27}$$

7.4.2 Dynamics

The dynamics of an underwater vehicle is modeled as [84]

$$M\dot{\nu} + F(\nu)\nu + g(R) = Bu, \tag{7.28}$$

where $M \in \mathbb{R}^{6\times6}$ is the inertia matrix, including hydrodynamic mass, $F\colon \mathbb{R}^6 \to \mathbb{R}^{6\times6}$ describes velocity dependent inertia and damping terms, $g\colon \mathrm{SO}(3) \to \mathbb{R}^6$ comprises the acting weight and buoyancy forces, $B \in \mathbb{R}^{6\times m}$ is the actuator configuration matrix and $u \in \mathcal{U} = \mathbb{R}^m$ is the vector of actuator control inputs. We make the following assumptions on these quantities

(A1) $M = M^\mathsf{T} = \begin{pmatrix} M_1 & M_2 \\ M_2^\mathsf{T} & M_3 \end{pmatrix} > 0$*;*
(A2) F *and* g *are continuous;*
(A3) the actuator configuration matrix B *has full rank;*

7.4.3 Tracking Error Dynamics using Quaternions

A bounded reference trajectory for the vehicle configuration, velocity and acceleration is generated from the exogenous system

$$\left.\begin{aligned} \dot{\bar{p}} &= \bar{R}\bar{v} \\ \dot{\bar{R}} &= \bar{R}\bar{\omega}^\wedge \\ \dot{\bar{\nu}} &= r \\ \dot{r} &\in c\mathbb{B} \end{aligned}\right\} \left(\bar{p}, \bar{R}, \bar{\nu}, r\right) \in \Omega_1 \times \mathrm{SO}(3) \times \Omega_2 \times \mathcal{R}, \tag{7.29}$$

where $c > 0$, and $\Omega_1 \subset \mathbb{R}^3$, $\Omega_2 \subset \mathbb{R}^6$ and $\mathcal{R} \subset \mathbb{R}^6$ are compact. Let $\bar{\varphi} = (\bar{p}, \bar{z}) \in \Omega_1 \times \mathbb{S}^3 \coloneqq \bar{\Phi}$ represent the desired position vector and unit quaternion, and define the configuration error by $\tilde{\varphi} \coloneqq (\tilde{p}, \tilde{z}) \in \mathbb{R}^3 \times \mathbb{S}^3 \coloneqq \widetilde{\Phi}$, where $\tilde{p} = R(\bar{z})^\mathsf{T}(p - \bar{p})$ is the natural position error. The error kinematics are given by

$$\dot{\tilde{\varphi}} = \begin{pmatrix} R(\tilde{z}) & 0_{3\times3} \\ 0_{4\times3} & \breve{T}(\tilde{z}) \end{pmatrix} \tilde{\nu} \coloneqq T(\tilde{z})\tilde{\nu}, \tag{7.30}$$

where $\tilde{\nu} = \nu - H(\tilde{\varphi})\bar{\nu}$ is the body velocity error, and $H\colon \widetilde{\Phi} \to \mathbb{R}^{6\times6}$ is defined by

$$H(\tilde{\varphi}) \coloneqq \begin{pmatrix} R(\tilde{z})^\mathsf{T} & -R(\tilde{z})^\mathsf{T}\tilde{p}^\wedge \\ 0_{3\times3} & R(\tilde{z})^\mathsf{T} \end{pmatrix}. \tag{7.31}$$

The error dynamics are then given by

$$\begin{aligned} \dot{\tilde{\nu}} &= M^{-1}\left(Bu - F(\nu)\nu - g(z)\right) - H(\tilde{\varphi})r - \dot{H}(\tilde{\varphi}, \tilde{\nu})\bar{\nu} \\ &= M^{-1}Bu + \breve{f}(\tilde{\varphi}, \tilde{\nu}, r). \end{aligned} \tag{7.32}$$

Defining the extended state-space

$$\mathcal{X} \coloneqq \widetilde{\Phi} \times \mathbb{R}^6 \times \bar{\Phi} \times \Omega_2, \tag{7.33}$$

with state vector $x = (\tilde{\varphi}, \tilde{\nu}, \bar{\varphi}, \bar{\nu}) \in \mathcal{X}$, results in the following quaternion representation of the kinematic and dynamic tracking error equations

$$\mathcal{N}\colon \begin{cases} \dot{x} = f(x, r, u) \\ \dot{r} \in c\mathbb{B} \end{cases} \qquad (x, r, u) \in \mathcal{X} \times \mathcal{R} \times \mathcal{U}, \tag{7.34}$$

where the continuous map $f\colon \mathcal{X} \times \mathcal{R} \times \mathcal{U} \to \mathbb{R}^{26}$ is given by

$$f(x, r, u) = \begin{pmatrix} T(\tilde{z})\tilde{\nu} \\ \breve{f}(\tilde{\varphi}, \tilde{\nu}, r) + M^{-1}Bu \\ T(\bar{z})\bar{\nu} \\ r \end{pmatrix}. \tag{7.35}$$

The tracking control objective is global asymptotic stabilization of the compact set

$$\mathcal{A}^\circ = \{x \in \mathcal{X}\colon \tilde{p} = 0, R(\tilde{z}) = I_3, \tilde{\nu} = 0\} \tag{7.36}$$

$$= \{x \in \mathcal{X}\colon \tilde{p} = 0, \tilde{z} = \pm e_1, \tilde{\nu} = 0\}. \tag{7.37}$$

7.5 HCLF-based Hybrid Control Design

This section constructs HCLFs for trajectory tracking of an underwater vehicle. The HCLFs are subsequently employed to synthesize an optimization-based hybrid feedback control law.

Consider the candidate family of kinematic HCLFs

$$V_{q,1}(\tilde{\varphi}) = \underbrace{2k_\epsilon\,(1 - q\tilde{\eta})}_{\breve{V}_q(\tilde{z})} + \frac{1}{2}\tilde{p}^\mathsf{T} K_p \tilde{p}, \tag{7.38}$$

Differentiating (7.38) along the error kinematics yields

$$\begin{aligned} \langle \nabla V_{q,1}(\tilde{\varphi}), T(\tilde{z})\tilde{\nu}\rangle &= k_\epsilon q \tilde{\epsilon}^\mathsf{T}\tilde{\omega} + \tilde{p}^\mathsf{T} K_p\,(R(\tilde{z})v - \bar{v} - \bar{\omega}^\wedge \tilde{p}) \\ &= \tilde{\vartheta}^\mathsf{T} K_{\tilde{\vartheta}} \Upsilon_q(\tilde{z})^\mathsf{T}\tilde{\nu}, \end{aligned} \tag{7.39}$$

where $\tilde{\vartheta} = (\tilde{p}, \tilde{\epsilon})$ and

$$K_{\tilde{\vartheta}} = \begin{pmatrix} K_p & 0_{3\times 3} \\ 0_{3\times 3} & k_\epsilon I_3 \end{pmatrix}, \qquad \Upsilon_q(\tilde{z})^\mathsf{T} = \begin{pmatrix} R(\tilde{z}) & 0_{3\times 3} \\ 0_{3\times 3} & qI_3 \end{pmatrix}. \tag{7.40}$$

Define the backstepping variable

$$\xi := \tilde{\nu} - \alpha_q(\tilde{\vartheta}), \tag{7.41}$$

and rewrite (7.39) as

$$\langle \nabla V_{q,1}(\tilde{\varphi}), T(\tilde{z})\tilde{\nu}\rangle = \tilde{\vartheta}^\mathsf{T} K_{\tilde{\vartheta}} \Upsilon_q(\tilde{z})^\mathsf{T} \alpha_q(\tilde{\vartheta}) + \tilde{\vartheta}^\mathsf{T} K_{\tilde{\vartheta}} \Upsilon_q(\tilde{z})^\mathsf{T}\xi.$$

The stabilizing function $\alpha_q(\tilde{\vartheta})$ for $\tilde{\nu}$ is chosen as

$$\alpha_q(\tilde{\vartheta}) = -\Upsilon_q(\tilde{z})\tilde{\vartheta}. \tag{7.42}$$

Since $q^2 = 1$ for all $q \in \mathcal{Q}$, it holds that $\Upsilon_q(\tilde{z})^\mathsf{T}\Upsilon_q(\tilde{z}) = I$, which results in

$$\langle \nabla V_{q,1}(\tilde{\varphi}), T(\tilde{z})\tilde{\nu}\rangle = -\tilde{\vartheta}^\mathsf{T} K_{\tilde{\vartheta}}\tilde{\vartheta} + \tilde{\vartheta}^\mathsf{T} K_{\tilde{\vartheta}}\Upsilon_q(\tilde{z})^\mathsf{T}\xi. \tag{7.43}$$

Augmenting $V_{q,1}$ with a positive definite term in ξ yields

$$V_q(x) = V_{q,1}(\tilde{\varphi}) + \frac{1}{2}\xi^\mathsf{T} M\xi, \tag{7.44}$$

which has compact sublevel sets and is positive definite with respect to the compact set

$$\mathcal{A} = \{(x,q) \in \mathcal{X}\times\mathcal{Q} \colon \tilde{p} = 0, \tilde{z} = qe_1, \xi = 0\}. \tag{7.45}$$

Differentiating V_q along flows yields

$$\begin{aligned}\langle \nabla V_q(x), f(x,r,u)\rangle &= -\tilde{\vartheta}^\mathsf{T} K_{\tilde{\vartheta}}\tilde{\vartheta}\\ &+ \xi^\mathsf{T}\Big(\Upsilon_q(\tilde{z})K_{\tilde{\vartheta}}\tilde{\vartheta} + M\dot{G}(\tilde{z},\tilde{\omega})\tilde{\vartheta} + M\Upsilon_q(\tilde{z})ST(\tilde{z})\tilde{\nu}\\ &+ Bu - F(\nu)\nu - g(z) - M\left[H(\tilde{\varphi})r + \dot{H}(\tilde{\varphi},\tilde{\nu})\bar{\nu}\right]\Big),\end{aligned} \tag{7.46}$$

where

$$\dot{G}(\tilde{z},\tilde{\omega}) = \begin{pmatrix} -\tilde{\omega}^\wedge R(\tilde{z})^\mathsf{T} & 0_{3\times 3}\\ 0_{3\times 3} & 0_{3\times 3}\end{pmatrix}, \tag{7.47}$$

$$\dot{\tilde{\vartheta}} = \begin{pmatrix} I_{3\times 3} & 0_{3\times 4}\\ 0_{3\times 4} & I_{3\times 3}\end{pmatrix} T(\tilde{z})\tilde{\nu} \coloneqq ST(\tilde{z})\tilde{\nu}. \tag{7.48}$$

Note that the set $\mathcal{Q}$ only consists of two elements. Thus, the only possible switching strategy for the logic variable is $q^+ = -q$. In order to derive the sets $\{\mathcal{I}_q\}_{q\in\mathcal{Q}}, \{\mathcal{O}_q\}_{q\in\mathcal{Q}}$ and $\{\mathcal{M}_q\}_{q\in\mathcal{Q}}$, defining the flow and jump sets, we calculate the change in V_q along jumps as

$$\begin{aligned}(V_{q^+} - V_q)(x) &= 4k_\epsilon r\tilde{\eta} + \tilde{\nu}^\mathsf{T} M\left(G_{q^+}(\tilde{z}) - \Upsilon_q(\tilde{z})\right)K_{\tilde{\vartheta}}\tilde{\vartheta}\\ &+ \frac{1}{2}\tilde{\vartheta}^\mathsf{T} K_{\tilde{\vartheta}}\left(G_{q^+}(\tilde{z})^\mathsf{T} M G_{q^+}(\tilde{z}) - \Upsilon_q^\mathsf{T}(\tilde{z})M\Upsilon_q(\tilde{z})\right)K_{\tilde{\vartheta}}\tilde{\vartheta},\end{aligned}$$

where

$$G_{q^+}(\tilde{z}) - \Upsilon_q(\tilde{z}) = -2q\bar{I} \tag{7.49}$$

$$G_{q^+}(\tilde{z})^\mathsf{T} M G_{q^+}(\tilde{z}) - \Upsilon_q(\tilde{z})^\mathsf{T} M\Upsilon_q(\tilde{z}) = -2q\Lambda(\tilde{z}), \tag{7.50}$$

and

$$\bar{I} = \begin{pmatrix} 0_{3\times 3} & 0_{3\times 3}\\ 0_{3\times 3} & I_3\end{pmatrix},\ \Lambda(\tilde{z}) = \begin{pmatrix} 0_{3\times 3} & R(\tilde{z})M_2\\ M_2^\mathsf{T} R(\tilde{z})^\mathsf{T} & 0_{3\times 3}\end{pmatrix}. \tag{7.51}$$

Let

$$\Psi(x) \coloneqq \tilde{\eta} - \frac{1}{2k_\epsilon}\tilde{\nu}^\mathsf{T} M\bar{I}K_{\tilde{\vartheta}}\tilde{\vartheta} - \frac{1}{4k_\epsilon}\tilde{\vartheta}^\mathsf{T} K_{\tilde{\vartheta}}\Lambda(\tilde{z})K_{\tilde{\vartheta}}\tilde{\vartheta}, \tag{7.52}$$

such that $V_{q^+}(x) - V_q(x) = 4k_\epsilon q\Psi(x)$. Define the sets

$$\begin{aligned} \mathcal{I}_q &\coloneqq \{x \in \mathcal{X} \colon q\Psi(x) \leq 0\}, \\ \mathcal{O}_q &\coloneqq \{x \in \mathcal{X} \colon q\Psi(x) < \delta\}, \\ \mathcal{M}_q &\coloneqq \{x \in \mathcal{X} \colon q\Psi(x) \leq \delta\}, \end{aligned} \tag{7.53}$$

where $\delta \in (0,1)$ is the hysteresis half-width. The flow and jump sets can now be constructed according to (7.6) and (7.7), respectively. Then, (H3) holds (strictly) by construction of $\mathcal{O}_q$ and $\mathcal{I}_q$ since $V_{q^+}(x) - V_q(x) = 4k_\epsilon q\Psi(x) < 0$ for all $q \in \mathcal{Q}$ and all $x \in (\mathcal{M}_q \backslash \mathcal{O}_q) \cap \mathcal{I}_{q^+}$. From (7.46), it is straightforward to verify that each V_q satisfies (H4) with $\gamma_q(x) = \tilde{\vartheta}^\mathsf{T} K_{\tilde{\vartheta}} \tilde{\vartheta} + \xi^\mathsf{T} K \xi$ for all $x \in \mathcal{M}_q$ and some $K = K^\mathsf{T} > 0$. Hence, by Definition 7.1, $\{V_q\}_{q \in \mathcal{Q}}$ is a family of HCLFs for $(\mathcal{N}, \mathcal{A})$.

In order to use Theorem 7.5 to synthesize an optimization-based hybrid control law, consider the set-valued map $\widetilde{\mathcal{F}}_q$, defined in (7.18). We choose θ_q such that it renders $\mathcal{A}$ forward invariant, i.e. that $\dot{\bar{\nu}} = 0$ when $(x, r) \in \mathcal{A}$. Inspection of (7.32) yields

$$\theta_q(x, r) = B^\dagger \left(F(\bar{\nu})\bar{\nu} + g(\bar{z}) + Mr \right), \tag{7.54}$$

where $B^\dagger \in \mathbb{R}^{m \times 6}$ is the Moore-Penrose inverse of B. In order to show lower semicontinuity of $\widetilde{\mathcal{F}}_q$, consider the continuous feedback control law

$$\begin{aligned} \mu_q(x, r) = B^\dagger \Big(& F(\nu)\nu + g(z) + M \left(H(\tilde{\varphi})r + \dot{H}(\tilde{\varphi}, \tilde{\nu})\bar{\nu} \right) \\ & - M\Upsilon_q(\tilde{z}) S T(\tilde{z}) \tilde{\nu} - M\dot{G}(\tilde{z}, \tilde{\omega})\tilde{\vartheta} - \Upsilon_q(\tilde{z}) K_{\tilde{\vartheta}} \tilde{\vartheta} - Kz \Big), \end{aligned} \tag{7.55}$$

which results in

$$\nabla V_q(x)^\mathsf{T} f(x, r, \mu_q(x, r)) + \gamma_q(x) = 0, \tag{7.56}$$

for all $(x, r) \in C_q$. Hence, $\mu_q(x, r) \in \mathcal{F}_q(x, r)$ for all $(x, r) \in C_q \backslash \mathcal{B}_q$. Moreover, for $(x, r) \in \mathcal{B}_q$ it holds that

$$\mu_q(x, r) = B^\dagger \left(F(\bar{\nu})\bar{\nu} + g(\bar{z}) + Me \right) = \theta_q(x, r). \tag{7.57}$$

Consequently, μ_q is a continuous single-valued selection of $\widetilde{\mathcal{F}}_q$ since $\mu_q(x, r) \in \widetilde{\mathcal{F}}_q(x, r)$ for all $(x, r) \in C_q$. By Lemma 7.1, $\widetilde{\mathcal{F}}_q$ is lower semicontinuous for all $(x, r) \in C_q$. Hence, by defining the objective function

$$h_q(x, r, u) \coloneqq |u - \theta_q(x, r)|^2, \tag{7.58}$$

all of the conditions in Theorem 7.5 are satisfied. Consequently, the set $\mathcal{A}$ can be rendered globally pre-asymptotically stable for the system $\mathcal{N}$ by the hybrid control law

$$\mathscr{C} \colon \begin{cases} u = \kappa_q(x, r) & (x, r) \in C_q \\ q^+ = -q & (x, r) \in D_q, \end{cases} \tag{7.59}$$

where $\kappa_q \colon C_q \to \mathcal{U}$ is obtained from the quadratic program

$$\begin{aligned} \kappa_q(x,r) = \underset{u\in\mathbb{R}^m}{\arg\min}\ & u^\mathsf{T}u - 2u^\mathsf{T}\theta_q(x,r) \\ \text{subject to} \\ & \xi^\mathsf{T}\Big(Bu + M\hat{f}_q(x) + \Upsilon_q(\tilde{z})K_{\tilde{\vartheta}}\tilde{\vartheta} + K\xi\Big) \leq 0, \end{aligned} \tag{7.60}$$

and where

$$\hat{f}_q(x) = \breve{f}(\tilde{\varphi},\tilde{\nu},r) + \dot{G}(\tilde{z},\tilde{\omega})\tilde{\vartheta} + \Upsilon_q(\tilde{z})ST(\tilde{z})\tilde{\nu}. \tag{7.61}$$

Proposition 7.6. *The hybrid control law* (7.59) *renders the compact set* $\mathcal{A}^\circ$ *defined in* (7.37) *globally pre-asymptotically stable for the system* (7.34).

Proof. We have shown that the HCLF family $\{V_q\}_{q\in\mathcal{Q}}$ defined in (7.44) together with the collection of objective functions $\{h_q\}_{q\in\mathcal{Q}}$ satisfy the conditions of Theorem 7.5. It follows that the hybrid control law (7.59)-(7.60) renders the compact set $\mathcal{A}$ defined in (7.45) globally pre-asymptotically stable. Observe from (7.41) and (7.42) that $\mathcal{A}$ is equivalent to $\mathcal{A}^\circ$, defined in (7.37), which implies that the control law (7.59) results in global asymptotic stability of $\mathcal{A}^\circ$. □

7.6 Numerical Simulation

In this section, we verify the theoretical results in simulation for the 6-DOF underwater vehicle ODIN, we refer to [72] for the model parameters. The system is initialized at the configuration $\varphi_0 = (0_{3\times1}, \epsilon_0)$, $\epsilon_0 = \frac{1}{\sqrt{50}}(3,4,5)$, with the initial velocity $\nu_0 = (0_{3\times1}, 1.2\epsilon_0)$. The desired position and orientation is obtained from the exogenous system in (7.29), initialized at $\bar{p} = 0$, $\bar{R} = I$. The desired acceleration r is generated from the low-pass filter

$$T\dot{r} + r = \Xi, \tag{7.62}$$

with time constant $T = 15\,\mathrm{s}$ and the reference acceleration

$$\Xi := \begin{cases} (0.1, 0.06, -0.07, 0, 0, 0), & 0 \leq t \leq 5 \\ 0_{6\times1}, & 5 < t \leq 10 \\ (0_{3\times1}, 0.05, -0.1, 0.02) & 10 < t \leq 15 \\ (0_{4\times1}, -0.1, 0.02) & t > 15. \end{cases} \tag{7.63}$$

The control gains are chosen as $k_\epsilon = 1, K_p = I_3$ and $K = \frac{1}{2}I_6$. The system is simulated with Simulink, using the ode15 solver with a maximum step-size of 0.01. Simulation results are presented in Figures 7.1 to 7.3. Observe that the only jump occurs at $t = 0$, which is due to the initial angular velocity. Moreover, note that the control input is continuous for all $t > 0$. To emphasize the necessity of (7.19) for continuity of the control law along flows, Figure 7.4 depicts the control inputs for the same control scenario with $h_q = |u|^2$, which clearly does not satisfy (7.19). From Figure 7.4, it is apparent that the control input exhibits significant discontinuities

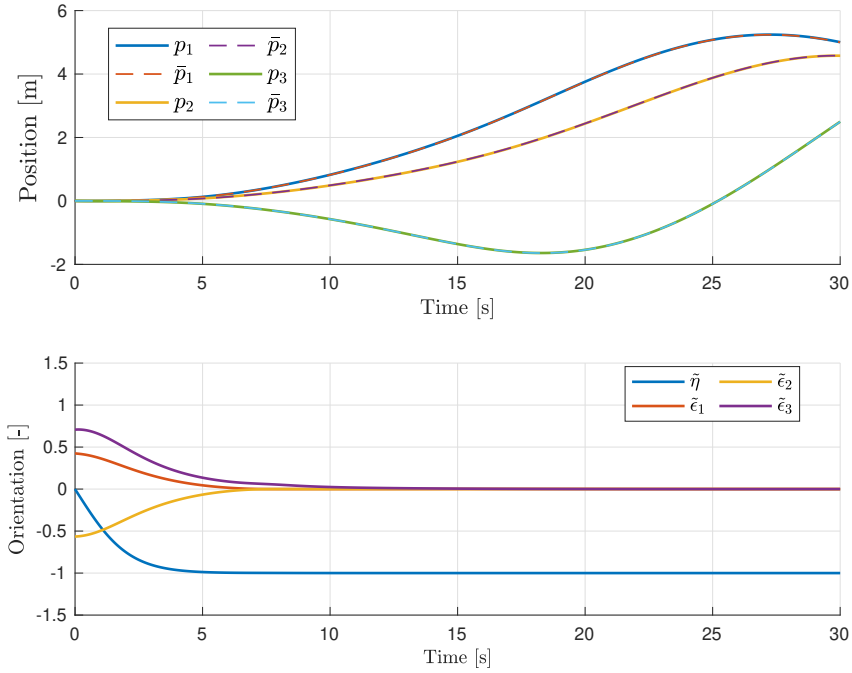

Figure 7.1: The position p, the desired position $\bar{p}$ and the unit quaternion orientation error $\tilde{z} = (\tilde{\eta}, \tilde{\epsilon})$.

for $t > 20\,\text{s}$, despite the fact that no jumps occur as observed from the logic variable q.

In order to highlight the benefits of the optimization-based control law obtained from (7.60), Figures 7.5 to 7.7 depict simulation results for the same control scenario using $u = \mu_q(x, r)$ given by (7.55). From Figures 7.1, 7.2, 7.5 and 7.6, it is clear that the optimization-based control law achieves faster convergence to the desired orientation with less control effort.

In Figure 7.8, we compare our HCLF approach with the local CLF $\breve{V}(z) = 2(1 - \tilde{\eta})$, corresponding to $q \equiv 1$. The system configuration is initialized at $\varphi_0 = (0_{3\times1}, z_0)$, $z_0 = (-0.95, 0, \sqrt{1 - 0.95^2}, 0)$ and the desired configuration is initialized at $\bar{p} = 0, \bar{R} = I$. Since $\breve{V}(z) = 0$ if and only if $\tilde{\eta} = 1$, the control law synthesized from $\breve{V}$ stabilizes $z = +e_1$ and leaves $z = -e_1$ unstable, despite the fact that both points correspond to the same physical rotation [97]. This can be observed in Figure 7.8, where the control law (unnecessarily) performs a full rotation of the rigid body. A naïve solution to this problem is to employ the CLF $\breve{V}(z) = 2(1-|\tilde{\eta}|)$ with the goal of rendering $z = \pm e_1$ asymptotically stable. However, this leads to a discontinuous control law with no robustness to measurement noise. In fact, it can be shown that arbitrarily small measurement noise can destroy any global attractivity property [37].

Another well-known CLF, albeit local, is $\breve{V}(z) = 2(1 - \tilde{\eta}^2)$, which achieves almost global asymptotic stability of the set $\{z \in \mathbb{S}^3 : z = \pm e_1\}$. However, since the

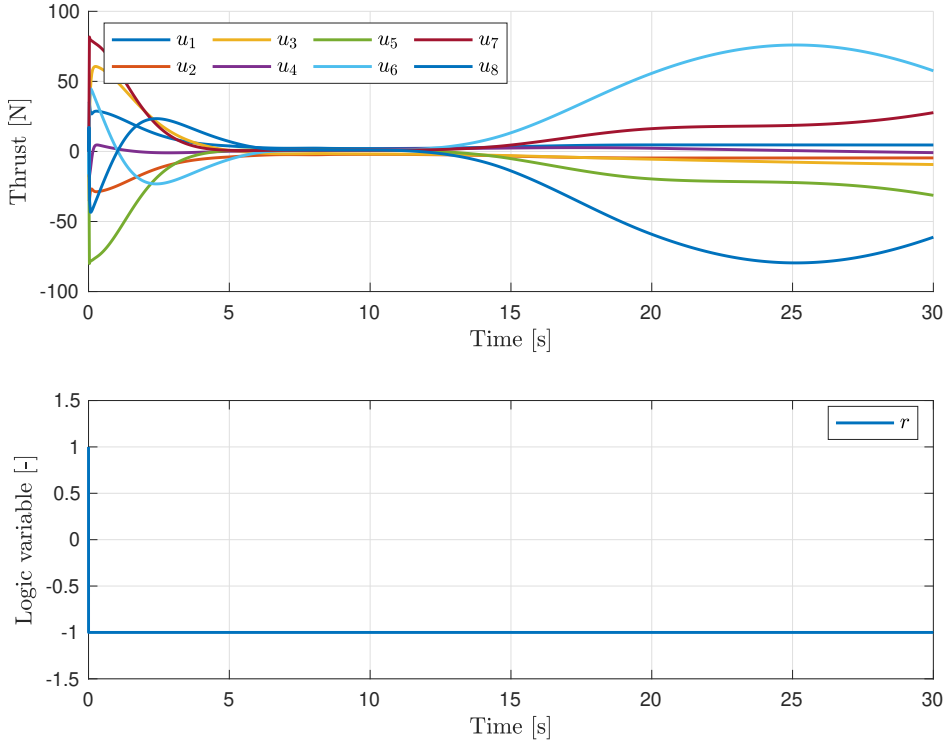

Figure 7.2: The thruster control inputs u, and the logic variable q.

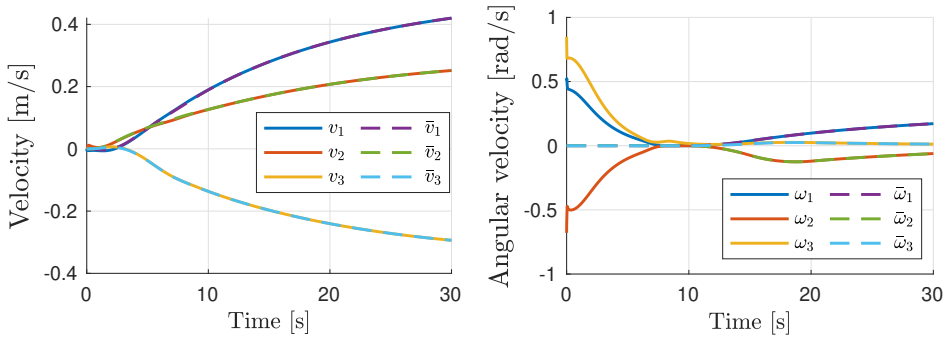

Figure 7.3: The linear and angular velocities v and ω, and their desired values $\bar{v}$ and $\bar{\omega}$, respectively.

gradient of $\breve{V}$ vanishes at $\tilde{\eta} = 0$, control laws synthesized from this CLF exhibit poor convergence properties around $\tilde{\eta} = 0$. This is demonstrated through simulation in Figure 7.9.

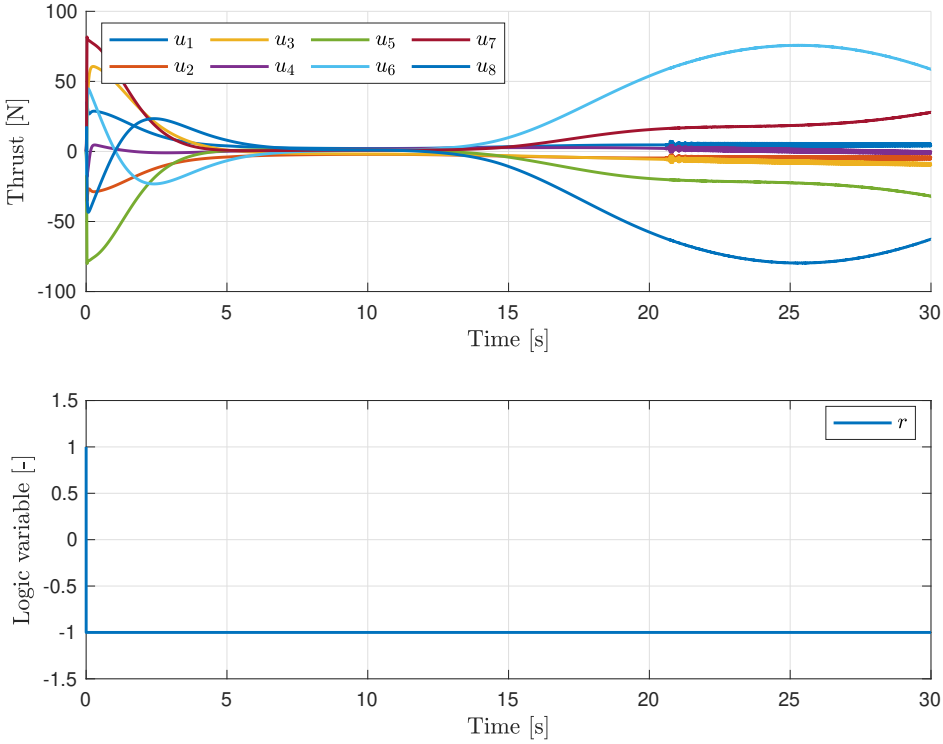

Figure 7.4: The thruster control inputs u with $h_q = |u|^2$.

7.7 Conclusions

This chapter has presented a new class of control Lyapunov functions, referred to as hysteretic control Lyapunov functions (HCLFs). We have stated sufficient conditions for the existence of a collection of continuous feedback laws, which together with the hysteresis-based switching mechanism defined by the HCLFs lead to a hybrid feedback law. This hybrid feedback law globally asymptotically stabilizes compact sets for a class of continuous-time systems defined on state-spaces that are not necessarily contractible. Moreover, we have shown how a collection of optimization-based feedback laws can be derived from a family of HCLFs under mild assumptions on the objective function. As a result, HCLFs can serve as a tool for synthesis of optimal feedback laws ensuring global asymptotic tracking of spatial rigid-bodies such as underwater vehicles and satellites. Finally, we have derived a family of HCLFs for configuration and velocity control of an underwater vehicle through backstepping, and synthesized a globally asymptotically stabilizing optimization-based control law from the derived HCLFs.

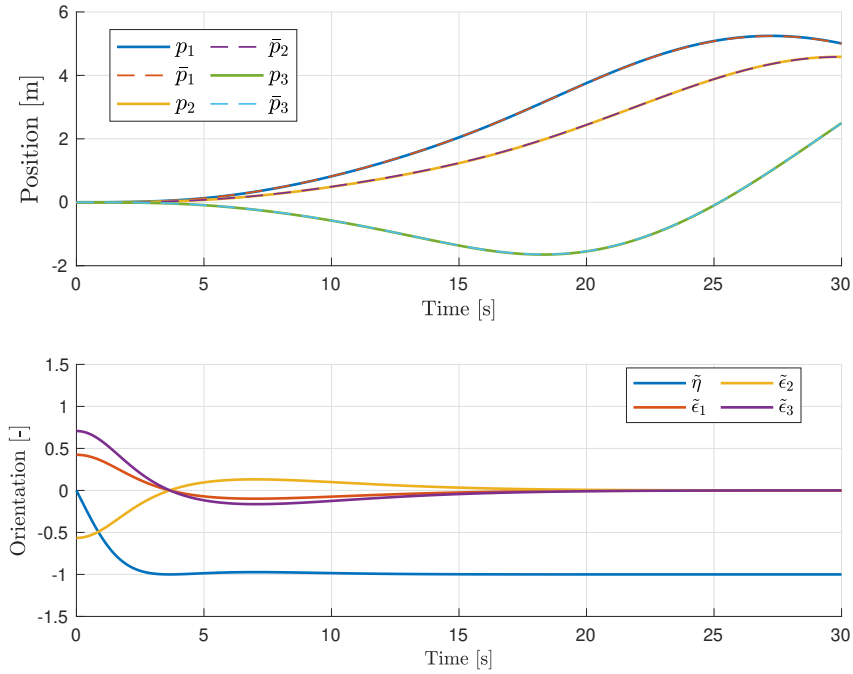

Figure 7.5: The position p, the desired position $\bar{p}$ and the unit quaternion orientation error $\tilde{z} = (\tilde{\eta}, \tilde{\epsilon})$ using (7.55).

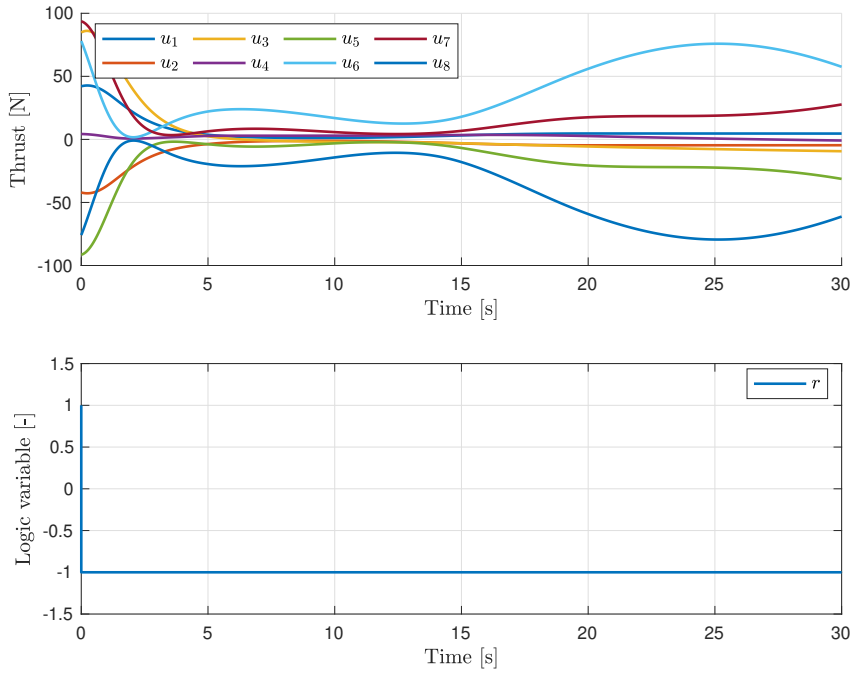

Figure 7.6: The thruster control inputs u, and the logic variable q using (7.55).

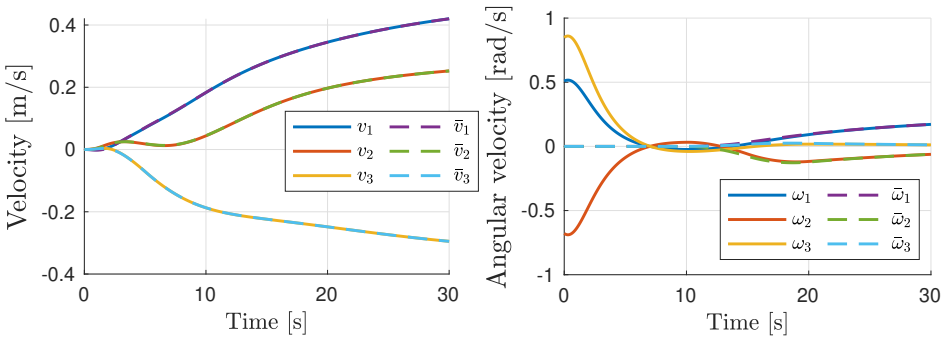

Figure 7.7: The linear and angular velocities v and ω, and their desired values $\bar{v}$ and $\bar{\omega}$, respectively, using (7.55).

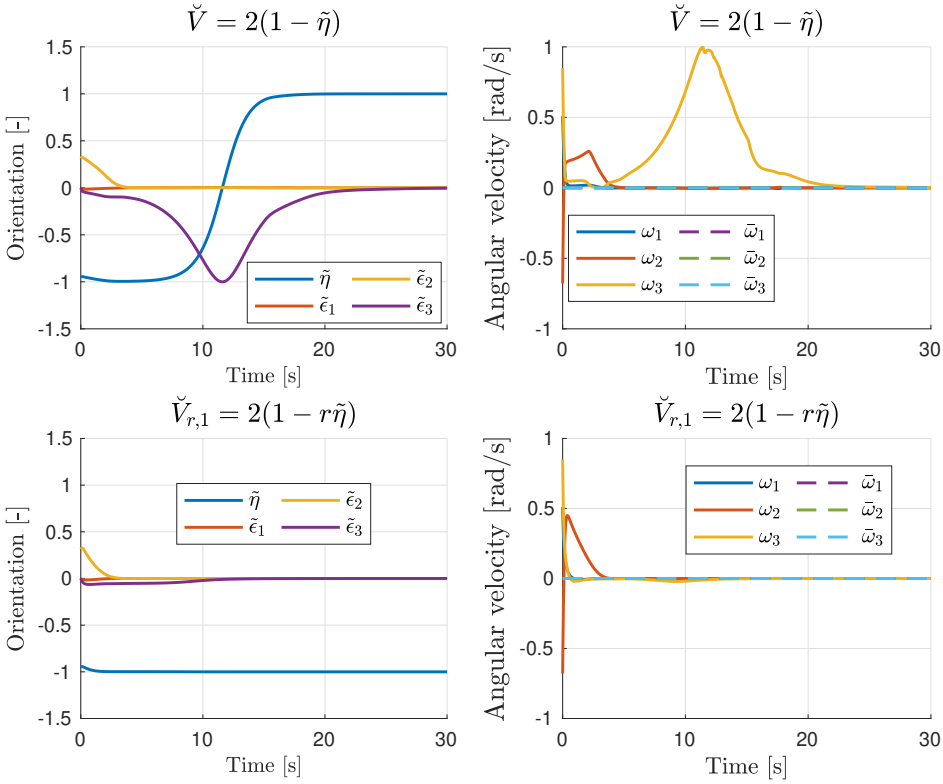

Figure 7.8: The unit quaternion orientation error $\tilde{z} = (\tilde{\eta}, \tilde{\epsilon})$ and the angular velocities ω and their desired values $\bar{\omega}$.

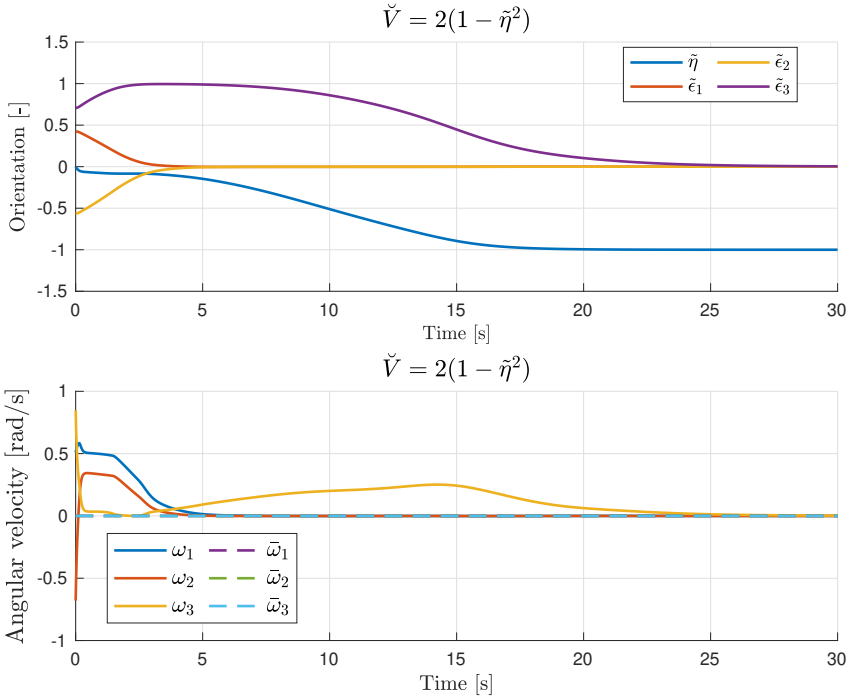

Figure 7.9: The unit quaternion orientation error $\tilde{z} = (\tilde{\eta}, \tilde{\epsilon})$ and the angular velocities ω and their desired values $\bar{\omega}$.

Chapter 8

Adaptive Hybrid Feedback Control for Marine Vehicles

This chapter develops an adaptive hybrid feedback controller for global asymptotic tracking of a hybrid reference system for marine vehicles subject to parametric uncertainties. In contrast to backstepping-based hybrid adaptive control [48], the proposed approach permits estimation of the inertia matrix, and the switching mechanism is independent of the system velocities. As our approach is based on traditional Euler-Lagrange system models, the adaptive hybrid control law is applicable to other mechanical systems as well. In particular, it can easily be extended to robot manipulators or, more generally, vehicle-manipulator systems. The hybrid reference system is constructed from a parametrized loop and a speed assignment for the motion along the loop. The main benefit of this formulation is that it decouples the design of the path from the motion along the path, allowing us to globally asymptotically track a given parametrized loop at a desired and time-varying speed. The proposed reference system can be considered an adaptation of the maneuvering problem [52, 53] to a hybrid dynamical systems setting. The theoretical developments are validated experimentally for surface and underwater vehicle applications.

The material in this chapter is based on [58, 59].

8.1 Introduction

Some of the first adaptive control laws proposed for underwater vehicles can be found in [98] and [99], where Euler angle representations were utilized for the vehicle orientation. The first quaternion-based control laws for underwater vehicles were introduced in [100], while adaptive and quaternion-based control approaches for underwater vehicles can be found in [101] and [102]. None of the aforementioned quaternion-based approaches achieve global asymptotic stability results, since they only stabilize one of the equilibrium points corresponding to the desired orientation. Adaptive backstepping designs for tracking control of ships were introduced in [103], [104], and [105]. However, none of these methods permit estimation of the inertia matrix parameters, and all of them lift the vehicle orientation from the circle to

the field of real numbers, which leads to unwinding problems.

To the best of our knowledge, experimental validations of globally stabilizing hybrid control laws for surface and underwater vehicles are virtually nonexistent in the existing literature. A combined hybrid observer/controller for dynamic positioning of a marine surface vehicle with global exponential stability properties was proposed in [106]. However, this result was achieved by a priori assuming that the angular velocity is bounded and by lifting the vehicle orientation from the circle to the field of real numbers, which leads to unwinding problems.

This rest of this chapter is organized as follows. Section 8.2 presents kinematic and dynamic models of marine vehicles, a hybrid reference system based on a parametrized loop and the problem statement. The hybrid control law developed in Section 8.3 is based on a set of potential functions and a hysteretic switching mechanism. In Section 8.4, we construct potential functions and switching mechanisms to overcome the topological obstructions of SE(2) and SE(3). Moreover, we show that the aforementioned potential functions and switching mechanisms satisfy the assumptions in Section 8.3. In Section 8.5, we present the results of three experiments conducted on marine surface and underwater vehicles, and then, Section 8.6 concludes the chapter.

8.2 Modeling and Problem Statement

This section begins by presenting kinematic and dynamic models of marine vehicles. Then, we derive a hybrid reference system generating continuous and bounded configuration, velocity and acceleration references from a parametrized loop. Moreover, the motion along the path can be independently controlled by specifying a desired speed, which takes values within a compact interval. Finally, we derive the error system and formulate the problem statement.

8.2.1 Models for Surface and Underwater Marine Vehicles

The configuration of a marine vehicle can be identified with a matrix Lie group $\mathcal{G} \subset \mathbb{R}^{n\times n}$ of dimension $k \leq 6$, which is typically either $\mathrm{SE}(2), \mathrm{SE}(3)$ or $\widetilde{\mathrm{SE}}(3)$. Let $g \in \mathcal{G}$ denote the configuration and $\nu = (v, \omega) \in \mathbb{R}^k$ denote the body velocity, where v and ω denote the linear and angular velocities of the vehicle. Using the Lie group structure of the configuration space, the equations of motion for fully actuated marine vehicles are given by

$$\dot{g} = g\nu^{\wedge}, \tag{8.1a}$$

$$M\dot{\nu} - \mathrm{ad}_{\nu}^{\intercal} M\nu = d(\nu) + f(g) + \tau, \tag{8.1b}$$

where $M \in \mathbb{R}^{k\times k}$ is the inertia matrix, including hydrodynamic added mass, $\mathrm{ad}_{\nu}^{\intercal} M\nu$ describes Coriolis and centrifugal forces, the function $d : \mathbb{R}^k \to \mathbb{R}^k$ describes dissipative forces, $f : \mathcal{G} \to \mathbb{R}^k$ contains potential forces and disturbances, and $\tau \in \mathbb{R}^k$ is the control force. Observe that the dynamic equation (8.1b) coincides with the dynamic equations of motion in [84, Ch. 7, 8] and [72, Ch. 2] by identifying $C(\nu)\bar{\nu} := -\mathrm{ad}_{\bar{\nu}}^{\intercal} M\nu$.

8.2.2 Hybrid Reference System

We construct a hybrid reference trajectory $g_d : \mathbb{R}_{\geq 0} \times \mathbb{Z}_{\geq 0} \to \mathcal{G}$ by composing a path $\gamma : [0,1] \to \mathcal{G}$ with a time scaling $s : \mathbb{R}_{\geq 0} \times \mathbb{Z}_{\geq 0} \to [0,1]$, i.e. $g_d(t,j) = \gamma(s(t,j))$. A key advantage of this formulation is that it decouples the geometric path from the desired motion along the path.

Definition 8.1. *Let $\mathcal{I} = [0,1]$, $\mathrm{H}_2 = \mathrm{SO}(2)$, $\mathrm{H}_3 = \mathrm{SU}(2)$ and $m \in \{2,3\}$. The parametric C^r-path $\gamma \colon \mathcal{I} \to \mathcal{G} \coloneqq \mathbb{R}^m \rtimes \mathrm{H}_m$ defined by*

$$\gamma(s) \coloneqq (\gamma_1(s), \gamma_2(s)), \quad \gamma_1(s) \in \mathbb{R}^m, \gamma_2(s) \in \mathrm{H}_m, \tag{8.2}$$

is a C^r-loop if it satisfies

$$\gamma^{(j)}(0) = \gamma^{(j)}(1), \tag{8.3}$$

for all $0 \leq j \leq r$.

Given a loop γ, the motion along the loop can be controlled through a speed assignment for $\dot{s}$. In particular, by assuming that $|\gamma_1'(s)| \neq 0$ for all $s \in \mathcal{I}$, the desired speed of the vehicle can be controlled through the following speed assignment [52]

$$\dot{s} = \varrho(s, u_d) \coloneqq \frac{u_d}{|\gamma_1'(s)|}, \tag{8.4}$$

where $u_d \in \mathbb{R}$ is a desired input speed. To ensure continuity of the velocity and acceleration references, the desired speed can be obtained from the following set-valued second-order low-pass filter with natural frequency $\omega_n > 0$ and damping factor $\zeta_f > 0$

$$\ddot{u}_d \in \mathcal{U}(u_d, \dot{u}_d) \coloneqq \omega_n^2 [0, c] - 2\zeta_f \omega_n \dot{u}_d - \omega_n^2 u_d, \tag{8.5}$$

where the interval $[0, c]$, with $c > 0$, contains the values of the commanded input speed μ.

Let $\Omega_1, \Omega_2 \subset \mathbb{R}$ be compact. The Lie group structure of the desired path γ leads to the following hybrid reference system:

$$\mathcal{R}: \begin{cases} \left.\begin{aligned} \dot{s} &= \varrho(s, u_d) \\ \dot{u}_d &= a_d \\ \dot{a}_d &\in \mathcal{U}(u_d, a_d) \end{aligned}\right\} & (s, u_d, a_d) \in \mathcal{I} \times \Omega_1 \times \Omega_2 \\ s^+ = 0 & (s, u_d, a_d) \in \{1\} \times \Omega_1 \times \Omega_2 \\ g_d = \gamma(s) \\ \nu_d = \kappa(s) \varrho(s, u_d) \\ \alpha_d = f_d(s, u_d, a_d) \end{cases}$$

where $\kappa(s) = (\gamma(s)^{-1} \gamma'(s))^\vee$ is the desired tangent vector expressed in the desired frame and the mapping $f_d \colon \mathcal{I} \times \Omega_1 \times \Omega_2 \to \mathbb{R}^k$ is given by

$$f_d(\cdot) = \kappa(s) \left(\frac{\partial \varrho}{\partial s} \varrho(s, u_d) + \frac{\partial \varrho}{\partial u_d} a_d \right) + \kappa'(s) \varrho(s, u_d)^2. \tag{8.6}$$

Conceptually, $\mathcal{R}$ can be considered as a hybrid system with the commanded speed $\mu \in [0, c]$ as the input, and

$$y := (g_d, \nu_d, \alpha_d) = (\gamma(s), \kappa(s)\varrho(s, u_d), f_d(s, u_d, a_d)), \tag{8.7}$$

as the output, where $g_d \in \operatorname{rge}\gamma, \nu_d \in \mathbb{R}^k$ and $\alpha_d \in \mathbb{R}^k$ are the desired configuration, velocity and acceleration references, respectively. We remark that the speed assignment for $\dot{s}$ in (8.4) ensures that the norm of the desired linear velocity v_d is equal to the desired speed u_d. Note that if γ is a C^2-loop, then it follows from $\gamma^{(j)}(0) = \gamma^{(j)}(1)$ for all $0 \leq j \leq 2$ and continuity of u_d, a_d that the output map $y = (g_d, \nu_d, \alpha_d)$ is continuous. We remark that for practical purposes, only a compact path is required. This, in turn, removes the switching component of the reference system. However, the loop assumption helps ensure that every maximal solution is complete.

8.2.3 Error System and Problem Statement

The error dynamics are obtained by considering the continuous and invertible transformation $(g, \nu, r) \mapsto (g_e, \nu_e, r)$, using the natural (and left-invariant) error defined by [64]

$$g_e := g_d^{-1} g, \tag{8.8}$$

$$\nu_e := \nu - \operatorname{Ad}_{g_e^{-1}} \nu_d. \tag{8.9}$$

We observe that g_e expresses the configuration of the vehicle-fixed frame with respect to the desired vehicle-fixed frame, while the term $\nu_r := \operatorname{Ad}_{g_e^{-1}} \nu_d$ can be interpreted as ν_d expressed in the vehicle-fixed frame. Moreover, the derivative of ν_r satisfies

$$\dot{\nu}_r = \operatorname{Ad}_{g_e^{-1}} \alpha_d - \operatorname{ad}_{\nu_e} \operatorname{Ad}_{g_e^{-1}} \nu_d. \tag{8.10}$$

The error dynamics can now be stated as

$$\mathcal{N}: \begin{cases} \left.\begin{aligned} \dot{g}_e &= g_e \nu_e^\wedge \\ \dot{\nu}_e &= f_e(g_e, \nu_e, s, u_d, a_d, \tau) \\ \dot{s} &= \varrho(s, u_d) \\ \dot{u}_d &= a_d \\ \dot{a}_d &\in \mathcal{U}(u_d, a_d) \end{aligned}\right\} & (g_e, \nu_e, s, u_d, a_d) \in \widehat{C} \\ s^+ = 0 & (g_e, \nu_e, s, u_d, a_d) \in \widehat{D} \end{cases}$$

where $\widehat{C} = \mathcal{G} \times \mathbb{R}^k \times \mathcal{I} \times \Omega_1 \times \Omega_2$, $\widehat{D} = \mathcal{G} \times \mathbb{R}^k \times \{1\} \times \Omega_1 \times \Omega_2$ and the mapping $f_e \colon \mathcal{G} \times \mathbb{R}^k \times \mathcal{I} \times \Omega_1 \times \Omega_2 \times \mathbb{R}^k \to \mathbb{R}^k$ is given by

$$\begin{aligned} f_e(\cdot) := M^{-1}(\tau - M\nabla_\nu^M \nu + d(\nu) + f(g)) \\ - \operatorname{Ad}_{g_e^{-1}} f_d(s, u_d, a_d) + \operatorname{ad}_{\nu_e} \operatorname{Ad}_{g_e^{-1}} \kappa(s)\varrho(s, u_d). \end{aligned} \tag{8.11}$$

We remark that the matrix representation of the adjoint maps Ad and ad are provided in Section 8.5 for the Lie groups SE(2) and SE(3) and their Lie algebras $\mathfrak{se}(2)$ and $\mathfrak{se}(3)$.

Lemma 8.1. *The hybrid system $\mathcal{N}$ satisfies the hybrid basic conditions [55, Assumption 6.5].*

Proof. The flow and jump sets $\widehat{C}$ and $\widehat{D}$ are closed since Ω_1 and Ω_2 are closed. Moreover, the jump map is single-valued and continuous. The flow map is single-valued and continuous for every state except a_d. However, since the set-valued mapping $\mathcal{U}$ is outer semicontinuous, convex and locally bounded, the flow map is outer semicontinuous, convex-valued and locally bounded. □

Problem Statement

For a given C^2-loop γ, the speed assignment ϱ defined in (8.4) for $\dot{s}$ and a compact set $\mathcal{A}^\circ \subset \mathcal{G}$, design a hybrid feedback control law with output $\tau \in \mathbb{R}^k$ such that every solution to $\mathcal{N}$ is bounded and converges to the compact set

$$\mathcal{B} = \{(g_e, \nu_e, s, u_d, a_d) : g_e \in \mathcal{A}^\circ, \nu_e = 0\}, \tag{8.12}$$

for the system $\mathcal{N}$ under parametric uncertainties.

8.3 Hybrid Control Design

In this section, we propose an adaptive hybrid feedback control law for the system $\mathcal{N}$. The control law is derived from a set of potential functions and a hysteretic switching mechanism encoded by the flow and jump sets and the jump map. The hybrid controller is based on the following assumption.

Assumption 8.2. *Given a 5-tuple $(\mathcal{A}, C, D, G, V)$, where $V : \mathcal{O} \to \mathbb{R}$ is defined by $(g, q) \mapsto V(g, q) = V_q(g)$, where $q \in Q$ is a logic variable, $Q \subset \mathbb{R}$ is a finite set and $\mathcal{O}$ is an open set containing $C \subset \mathcal{G} \times Q$.*

(A1) $\mathcal{A} \subset C$ is a compact set and $\pi_1(\mathcal{A}) = \mathcal{A}^\circ$;
(A2) C and D are closed subsets of $\mathcal{G} \times Q$ such that $C \cup D = \mathcal{G} \times Q$ and $\pi_1(C) = \mathcal{G}$;
(A3) The set-valued mapping $G : D \rightrightarrows Q$ is nonempty for all $(g, q) \in D$ and outer semicontinuous and locally bounded relative to D;
(A4) for every $(g, q) \in C \cap D$, it holds that $(g, w) \in C \setminus D$ for each $w \in G(g, q)$;
(A5) there exists $N \in \mathbb{Z}_{\geq 1}$ such that for every $(g, q) \in D$, it holds that $(g, w) \in C \setminus D$ for each $(g, w) \in \overline{G}^K(g, q)$, where $1 \leq K \leq N$, $\overline{G}(g, q) = \{g\} \times G(g, q)$ and $\overline{G}^K := \underbrace{\overline{G} \circ \overline{G} \circ \cdots \circ \overline{G}}_{K \text{ times}}$;
(A6) V is continuously differentiable on $\mathcal{O}$ and is proper and positive definite on C with respect to $\mathcal{A}$;
(A7) for all $(g, q) \in C \cap D$ and each $w \in G(g, q)$

$$V_w(g) - V_q(g) \leq 0; \tag{8.13}$$

(A8) for all $(g, q) \in C$, $\mathrm{d}V_q(g) = 0$ if and only if $(g, q) \in \mathcal{A}$.

Assumption 8.2 guarantees that the switching is hysteretic, the hybrid control law satisfies the hybrid basic conditions and is required to ensure that every solution to $\mathcal{N}$ converges to $\mathcal{B}$.

We remark that the conditions of Assumption 8.2 are different from the conditions for synergistic control [1, Definition 7.3]. First, they do not enforce a strict decrease in V across jumps. Second, they are not restricted to a switching mechanism based on the value of the potential functions V_q. Finally, they permit each potential function V_q to be defined locally, i.e., having a domain that is a strict subset of $\mathcal{G}$.

To establish convergence to the set $\mathcal{B}$ when the model parameters are unknown, we define the modified reference velocity $\nu_m \in \mathbb{R}^k$ and the corresponding reference velocity error $\zeta \coloneqq \nu_m - \nu_r$ through the differential equation

$$\Lambda[\dot{\zeta} + \nabla^{\Lambda}_{\nu}\zeta] = -\mathrm{d}V_q(g_e) - \vartheta_q(\zeta), \tag{8.14}$$

where $\vartheta_q : \mathbb{R}^k \to \mathbb{R}^k$ is strongly passive for each $q \in Q$. We remark that ϑ can be chosen independent of q and that the term $\Lambda\nabla^{\Lambda}_{\nu}\zeta$ is optional. The latter is because $\langle \zeta, \Lambda\nabla^{\Lambda}_{\xi}\zeta\rangle = 0$ for any $\xi \in \mathbb{R}^k$, which entails that any velocity can be used in place of ν in the bilinear map ∇^{Λ}. The velocity error is now redefined as

$$\xi \coloneqq \nu - \nu_m = \nu_e - \zeta. \tag{8.15}$$

Since $\zeta = 0$ implies $\xi = \nu_e$, the velocity tracking control objective $\nu_e = 0$ is accomplished when $(\xi, \zeta) = 0$. In practice, this type of velocity error may be advantageous when the configuration error encoded by $\mathrm{d}V$ is significant while the velocity error ν_e is zero.

Before delving into the proposed adaptive controller, we begin by presenting the non-adaptive version. Given a 5-tuple $(\mathcal{A}, C, D, G, V)$ satisfying Assumption 8.2 and if the model parameters in (8.1) are known, we propose the following hybrid control law

$$\begin{cases} \dot{\zeta} = -\nabla^{\Lambda}_{\nu}\zeta - \Lambda^{-1}\big(\mathrm{d}V_q(g_e) + \vartheta_q(\zeta)\big), & (g_e, q) \in C \\ q^+ \in G(g_e, q), & (g_e, q) \in D \\ \tau = M[\dot{\nu}_m + \nabla^{M}_{\nu}\nu_m] - d(\nu) \\ \qquad - f(g) - \mathrm{d}V_q(g_e) - \varphi_q(\xi). \end{cases} \tag{8.16}$$

Observe that the feedback control law (8.16) comprises a proportional action $\mathrm{d}V$ and a derivative action φ, where $\varphi_q \colon \mathbb{R}^k \to \mathbb{R}^k$ is strongly passive for each $q \in Q$. In other words, the control law (8.16) is essentially a PD+ control law [107] with desired velocity ν_m and hysteretic switching. We note that the derivative action can be chosen independently of the logic variable q. However, the proportional action can only be chosen independently of q provided that the configuration space is globally diffeomorphic to Euclidean space.

To make the control law (8.16) adaptive, we make the following assumption on the unknown model parameters.

Assumption 8.3. *There exists a known matrix-valued function of available data* $\Phi\colon \mathcal{G}\times\mathbb{R}^k\times\mathbb{R}^k\times\mathcal{I}\times\Omega_1\times\Omega_2\to\mathbb{R}^{k\times l}$ *and a vector of unknown model parameters* $\theta\in\mathbb{R}^l$ *with known lower and upper bounds* $\underline{\theta}$ *and* $\overline{\theta}$ *such that*

$$M[\dot{\nu}_m+\nabla_\nu^M\nu_m]-d(\nu)-f(g)=\Phi(g_e,\zeta,\xi,s,u_d,a_d)\theta, \tag{8.17}$$

for all $(g_e,\zeta,\xi,s,u_d,a_d)\in\mathcal{G}\times\mathbb{R}^k\times\mathbb{R}^k\times\mathcal{I}\times\Omega_1\times\Omega_2$.

The boundedness assumption on the parameters is justified by the fact that the parameters represent real physical quantities that we often have rough estimates of in practice. Assumption 8.3 implies that the parameters are contained in the convex set

$$\mathcal{P}\coloneqq\{\theta\in\mathbb{R}^l:\underline{\theta}\le\theta\le\overline{\theta}\}. \tag{8.18}$$

Define the extended tangent cone to $\mathcal{P}$ by

$$T_{\mathbb{R},\mathcal{P}}(\theta)\coloneqq T_{\mathbb{R},[\underline{\theta}_1,\overline{\theta}_1]}(\theta_1)\times T_{\mathbb{R},[\underline{\theta}_2,\overline{\theta}_2]}(\theta_2)\times\cdots\times T_{\mathbb{R},[\underline{\theta}_l,\overline{\theta}_l]}(\theta_l), \tag{8.19}$$

where the extended tangent cone to each interval is given by

$$T_{\mathbb{R},[\underline{\theta}_i,\overline{\theta}_i]}(\theta_i)\coloneqq\begin{cases}[0,\infty) & \text{if } \theta_i\le\underline{\theta}_i\\ (-\infty,\infty) & \text{if } \theta_i\in(\underline{\theta}_i,\overline{\theta}_i)\\ (-\infty,0] & \text{if } \theta_i\ge\overline{\theta}_i\end{cases} \tag{8.20}$$

Let $\theta_a\in\mathbb{R}^l$ denote the estimate of θ and define the convex set

$$\mathcal{P}_\epsilon\coloneqq\{\theta_a\in\mathbb{R}^l:\underline{\theta}-\epsilon\le\theta_a\le\overline{\theta}+\epsilon\}, \tag{8.21}$$

where $\epsilon=(\epsilon_1,\dots,\epsilon_l)\in\mathbb{R}^l$, defines boundary layers of length $\epsilon_i>0$ around each interval in (8.18). The goal is to enforce $\theta_a\in\mathcal{P}_\epsilon$ through the adaptive update law. To this end, we define the projection operator $\mathrm{Proj}\colon\mathbb{R}^l\times\mathcal{P}_\epsilon\to\mathbb{R}^l$ by [60]

$$\mathrm{Proj}(\chi,\theta_a)\coloneqq\begin{cases}\chi, & \text{if } \chi\in T_{\mathbb{R},\Omega}(\theta_a)\\ (1-h(\theta_a))\chi & \text{if } \chi\notin T_{\mathbb{R},\Omega}(\theta_a)\end{cases} \tag{8.22}$$

where the components of $h(\theta_a)$ are given by

$$h_i(\theta_{a,i})=\begin{cases}0, & \text{if } \theta_{a,i}\in(\underline{\theta}_i,\overline{\theta}_i)\\ \min\{1,\frac{\underline{\theta}_i-\theta_{a,i}}{\epsilon_i}\}, & \text{if } \theta_{a,i}\le\underline{\theta}_i\\ \min\{1,\frac{\theta_{a,i}-\overline{\theta}_i}{\epsilon_i}\}, & \text{if } \theta_{a,i}\ge\overline{\theta}_i\end{cases} \tag{8.23}$$

The following lemma can be found in [60, Lemma E.1].

Lemma 8.2. *The projection operator* (8.22) *satisfies*

(P1) The mapping $\mathrm{Proj}\colon\mathbb{R}^l\times\mathcal{P}_\epsilon\to\mathbb{R}^l$ *is Lipschitz continuous in* χ *and* θ_a.
(P2) The differential equation

$$\dot{\theta}_a=\mathrm{Proj}(\chi,\theta_a),\quad \theta_a(t_0)\in\mathcal{P}_\epsilon, \tag{8.24}$$

satisfies $\theta_a\in\mathcal{P}_\epsilon$ *for all* $t\ge t_0$.

(P3) Let $\theta_e = \theta - \theta_a$ denote the estimation error, then

$$-\langle \theta_e, \Gamma^{-1}\mathrm{Proj}(\chi, \theta_a)\rangle \leq -\langle \theta_e, \Gamma^{-1}\chi\rangle, \tag{8.25}$$

for all $\theta_a \in \mathcal{P}_\epsilon$ and $\theta \in \mathcal{P}$.

Using (8.17) and the projection operator defined in (8.22), we define an adaptive version of (8.16) by

$$\begin{cases} \left.\begin{aligned} \dot{\zeta} &= -\nabla_\nu^\Lambda \zeta - \Lambda^{-1}\big(\mathrm{d}V_q(g_e) + \vartheta_q(\zeta)\big) \\ \dot{\theta}_a &= \mathrm{Proj}(-\Gamma\Phi(g_e,\zeta,\xi,s,u_d,a_d)^\mathsf{T}\xi, \theta_a) \end{aligned}\right\} & (g_e,q)\in C \\ q^+ \in G(g_e,q) & (g_e,q)\in D \\ \tau = \Phi(g_e,\zeta,\xi,s,u_d,a_d)\theta_a - \mathrm{d}V_q(g_e) - \varphi_q(\xi). \end{cases} \tag{8.26}$$

By defining $x \coloneqq (g_e, \xi, s, u_d, a_d, \zeta, \theta_a, q) \in \mathcal{X}$ and the extended state space

$$\mathcal{X} \coloneqq \mathcal{G} \times \mathbb{R}^k \times \mathcal{I} \times \Omega_1 \times \Omega_2 \times \mathbb{R}^k \times \mathcal{P}_\epsilon \times Q, \tag{8.27}$$

the adaptive hybrid control law (8.26) applied to the hybrid system $\mathcal{N}$ leads to the hybrid closed-loop system

$$\mathcal{H}: \begin{cases} \left.\begin{aligned} \dot{g}_e &= g_e(\xi+\zeta)^\wedge \\ \dot{\xi} &= \tilde{f}(x) \\ \dot{s} &= \varrho(s,u_d) \\ \dot{u}_d &= a_d \\ \dot{a}_d &\in \mathcal{U}(u_d,a_d) \\ \dot{\zeta} &= -\nabla_\nu^\Lambda \zeta - \Lambda^{-1}\big(\mathrm{d}V_q(g_e) + \vartheta_q(\zeta)\big) \\ \dot{\theta}_a &= \mathrm{Proj}(-\Gamma\Phi(g_e,\zeta,\xi,s,u_d,a_d)^\mathsf{T}\xi, \theta_a) \end{aligned}\right\} & x \in \widetilde{C} \\ (q^+, s^+) \in \widetilde{G}(g_e,q,s) & x \in \widetilde{D}, \end{cases} \tag{8.28}$$

where

$$\tilde{f}(x) \coloneqq -M^{-1}\Phi(g_e,\zeta,\xi,s,u_d,a_d)\theta_e - \nabla_\nu^M \xi - M^{-1}(\mathrm{d}V_q(g_e) + \varphi_q(\xi)). \tag{8.29}$$

Moreover, the jump map $\widetilde{G} : \mathcal{G} \times Q \times \mathcal{I} \rightrightarrows Q \times \mathcal{I}$ is defined as

$$\widetilde{G}(g_e,q,s) \coloneqq \begin{cases} (G(g_e,q),s), & (g_e,q,s)\in D \times (\mathcal{I}\backslash\{1\}) \\ \{(G(g_e,q),s),(q,0)\} & (g_e,q,s)\in D\times\{1\} \\ (q,0), & (g_e,q,s)\in (C\backslash D)\times\{1\} \end{cases} \tag{8.30}$$

while the flow set $\widetilde{C}$ and jump set $\widetilde{D}$ are defined by

$$\widetilde{C} \coloneqq \{x \in \mathcal{X} : (g_e,q) \in C\}, \tag{8.31}$$

$$\widetilde{D} \coloneqq \{x \in \mathcal{X} : (g_e,q) \in D\} \cup \{x \in \mathcal{X} \colon s = 1\}. \tag{8.32}$$

Lemma 8.3. *The closed-loop system $\mathcal{H}$ satisfies the hybrid basic conditions.*

Proof. From Lemma 8.1, Assumption 8.2 and the definitions of the jump map, flow set and jump set, it follows that all of the assumptions in [1, Lemma 2.21] are satisfied. □

Theorem 8.4. *Let Assumption 8.3 hold. Given a 5-tuple $(\mathcal{A}, C, D, G, V)$ satisfying Assumption 8.2, the compact set*

$$\mathcal{A}_1 = \{x \in \mathcal{X} : (g_e, q) \in \mathcal{A}, \xi = 0, \zeta = 0, \theta_a = \theta\}, \tag{8.33}$$

is uniformly globally stable for the system $\mathcal{H}$ and every solution to $\mathcal{H}$ converges to

$$\mathcal{A}_2 = \{x \in \mathcal{X} : (g_e, q) \in \mathcal{A}, \xi = 0, \zeta = 0, \Phi(g_e, 0, 0, s, u_d, a_d)\theta_e = 0\}. \tag{8.34}$$

Proof. Let $\breve{\mathcal{H}}$ denote the hybrid system $\mathcal{H}$ with each jump set $\widetilde{D}$ replaced by $\breve{D} = \{x \in \mathcal{X} : (g_e, q) \in C \cap D\} \cup \{x \in \mathcal{X} \colon s = 1\}$ and consider the continuously differentiable function

$$W(g_e, q, \xi, \zeta, \theta_a) = V_q(g_e) + \frac{1}{2}\langle \xi, M\xi \rangle + \frac{1}{2}\langle \zeta, \Lambda\zeta \rangle + \frac{1}{2}\langle \theta_e, \Gamma^{-1}\theta_e \rangle. \tag{8.35}$$

For all $x \in \widetilde{C}$, the change in W along the solutions of $\breve{\mathcal{H}}$ is

$$\begin{aligned} &\langle \mathrm{d}V_q(g_e), \nu_e \rangle + \langle \zeta, -\mathrm{d}V_q(g_e) - \vartheta_q(\zeta) \rangle \\ &+ \langle \xi, -\Phi\theta_e - M\nabla_\nu^M \xi - \mathrm{d}V_q(g_e) - \varphi_q(\xi) \rangle \\ &- \langle \theta_e, \Gamma^{-1}\mathrm{Proj}(-\Gamma\Phi^\mathsf{T}\xi, \theta_a) \rangle, \end{aligned} \tag{8.36}$$

which simplifies to

$$\begin{aligned} &- \langle \xi, \varphi_q(\xi) \rangle - \langle \zeta, \vartheta_q(\zeta) \rangle - \langle \theta_e, \Gamma^{-1}\mathrm{Proj}(-\Gamma\Phi^\mathsf{T}\xi, \theta_a) + \Phi^\mathsf{T}\xi \rangle \\ &\leq -\langle \xi, \varphi_q(\xi) \rangle - \langle \zeta, \vartheta_q(\zeta) \rangle \\ &\leq 0, \end{aligned} \tag{8.37}$$

where the first inequality follows from (P3) in Lemma 8.2. For any $x \in \breve{D}$ and $(w, m) \in \widetilde{G}(g_e, q, s)$, the change in W across jumps is

$$W(g_e, w, \xi, \zeta, \theta_a) - W(g_e, q, \xi, \zeta, \theta_a) = V_w(g_e) - V_q(g_e),$$

which is clearly equal to zero when $(g_e, q, s) \in (C \backslash D) \times \{1\}$, i.e. when $w = q$. Otherwise, it follows from Assumption 8.2 that $V_w(g_e) - V_q(g_e) \leq 0$ for all $(q, w) \in Q \times \pi_1(\widetilde{G}(g_e, q, s))$. Consequently, the growth of W along solutions to $\breve{\mathcal{H}}$ is bounded by

$$u_c(x) = \begin{cases} -\langle \xi, \varphi_q(\xi) \rangle - \langle \zeta, \vartheta_q(\zeta) \rangle, & \text{if } x \in \widetilde{C} \\ -\infty, & \text{otherwise} \end{cases} \tag{8.38}$$

$$u_d(x) = \begin{cases} 0, & \text{if } x \in \breve{D} \\ -\infty, & \text{otherwise} \end{cases} \tag{8.39}$$

along flows and across jumps, respectively. It follows from Assumption 8.2 and (8.35) that W is proper and positive definite on $\widetilde{C} \cup \breve{D}$ with respect to the compact set $\mathcal{A}_1$. Hence, the proof of [55, Theorem 3.18] implies that $\mathcal{A}_1$ is uniformly globally stable for the hybrid system $\breve{\mathcal{H}}$. Observe that the system $\breve{\mathcal{H}}$ permits at most two consecutive jumps before a nonzero time of flow follows. Thus, since W is continuous, $\breve{\mathcal{H}}$ satisfies the hybrid basic conditions, and every maximal solution to $\breve{\mathcal{H}}$ is complete, it follows from [55, Corollary 8.7 (b)] that each solution to $\breve{\mathcal{H}}$ converges to the largest weakly invariant subset Ψ contained in

$$W^{-1}(r) \cap \overline{u_c^{-1}(0)}, \tag{8.40}$$

for some $r \in \mathbb{R}$, where

$$\overline{u_c^{-1}(0)} = \{x \in \mathcal{X} : \xi = 0, \zeta = 0, (g_e, q) \in C\}. \tag{8.41}$$

Moreover, the closed-loop system (8.28) is such that $\zeta \equiv 0$ implies $\mathrm{d}V_q(g_e) \equiv 0$, and it follows from Assumption 8.2 that $\mathrm{d}V_q(g_e) = 0$ implies $(g_e, q) \in \mathcal{A}$. Thus, $(\xi, \zeta) \equiv 0$ implies that $\Phi(g_e, 0, 0, s, u_d, a_d)\theta_e \equiv 0$, which results in

$$\Psi \subset W^{-1}(r) \cap \overline{u_c^{-1}(0)} \subset W^{-1}(r) \cap \mathcal{A}_2 \subset \mathcal{A}_2.$$

Consequently, since every solution is complete and bounded, every solution to $\breve{\mathcal{H}}$ converges to $\mathcal{A}_2$. Solutions to $\mathcal{H}$ that are not solutions to $\breve{\mathcal{H}}$ are those with initial values x^* such that $(g_e^*, q^*) \in D \backslash C$. However, it follows from (A5) that such solutions exhibit $1 \leq K \leq N$ immediate and consecutive jumps from q^* to some $w \in \overline{G}^K(g_e^*, q^*)$ satisfying $(g_e^*, w) \in C \backslash D$, after which the solutions coincide with a solution to $\breve{\mathcal{H}}$. Consequently, we conclude that $\mathcal{A}_1$ is uniformly globally stable for the hybrid system $\mathcal{H}$ and that every solution to the hybrid system $\mathcal{H}$ converges to $\mathcal{A}_2$. □

We remark that Theorem 8.4 implies that the problem statement is solved. Furthermore, note that uniform global asymptotic stability of the compact set

$$\widetilde{\mathcal{B}} = \{x \in \mathcal{X} : (g_e, q) \in \mathcal{A}, \zeta = 0, \xi = 0\}, \tag{8.42}$$

for the closed-loop system $\mathcal{H}$ implies that $\mathcal{B}$ is uniformly globally asymptotically stable for the error system $\mathcal{N}$. However, without further assumptions on the nature of the parametrized loop and commanded input speed, it is not possible to show that (8.26) uniformly globally asymptotically stabilizes the compact set $\widetilde{\mathcal{B}}$ for the closed-loop system $\mathcal{H}$. However, a trivial modification of the proof of Theorem 8.4 clearly shows that the non-adaptive hybrid control law (8.16) uniformly globally asymptotically stabilizes the compact set $\widetilde{\mathcal{B}}$ for the closed-loop system $\mathcal{H}$ with $\dot{\theta}_a = 0$ and $\theta_e = 0$, implying that $\mathcal{B}$ is uniformly globally asymptotically stable for the error system $\mathcal{N}$.

We remark that a trivial modification of the proof of Theorem 8.4 shows that the non-adaptive hybrid control law (8.16) uniformly globally asymptotically stabilizes the compact set $\widetilde{\mathcal{B}}$ for the closed loop system $\mathcal{H}$ with $\dot{\theta}_a = 0$ and $\theta_e = 0$, implying that $\mathcal{B}$ is uniformly globally asymptotically stable for the error system $\mathcal{N}$.

8.4 Potential Functions for Marine Vehicles

In this section we construct potential functions and derive 5-tuples $(\mathcal{A}, C, D, G, V)$ satisfying Assumption 8.2 for a surface vehicle and an underwater vehicle. This 5-tuple determines the proportional control action and the switching mechanism through the potential functions V and the flow set, jump set and jump map C, D, G, respectively.

8.4.1 Potential functions on SE(2)

The configuration of a surface vehicle can be identified with the matrix Lie group $\mathrm{SE}(2) = \mathbb{R}^2 \rtimes \mathrm{SO}(2)$. An element $g = (p, R) \in \mathrm{SE}(2)$ contains the position $p = (x, y) \in \mathbb{R}^2$ and orientation $R \in \mathrm{SO}(2)$ of a vehicle-fixed frame with respect to an inertial frame.

Using the linear action of $\mathrm{SO}(2)$ on $\mathbb{R}^2$ defined by $(p, R) \mapsto Rp$, the semidirect product $\mathrm{SE}(2) = \mathbb{R}^2 \rtimes \mathrm{SO}(2)$ yields the natural error on $\mathrm{SE}(2)$

$$g_e = g_d^{-1} g = (p_e, R_e) = (R_d^\mathsf{T}(p - p_d), R_d^\mathsf{T} R). \tag{8.43}$$

The goal is to construct potential functions and a switching mechanism for stabilization of the configuration corresponding to the compact set

$$\mathcal{A}^\circ = \{g_e \in \mathrm{SE}(2) : p_e = 0, R_e = e\}. \tag{8.44}$$

To this end, we let $\delta > 0$ and define the functions $\rho_1 : \mathcal{D}_1 \to \mathbb{R}$, $\rho_2 : \mathcal{D}_2 \to \mathbb{R}$ and $\rho_3 : \mathcal{D}_3 \to \mathbb{R}$, where $\mathcal{D}_1 = \mathcal{D}_2 := \{R \in \mathrm{SO}(2) : (\log R)^\vee \in [\delta, \pi] \cup (-\pi, -\delta]\}$ and $\mathcal{D}_3 := \mathrm{SO}(2)$ by

$$\rho_1(R) := \begin{cases} (\log R)^\vee, & \text{if } (\log R)^\vee \in [\delta, \pi] \\ (\log R)^\vee + 2\pi, & \text{if } (\log R)^\vee \in (-\pi, -\delta] \end{cases} \tag{8.45a}$$

$$\rho_2(R) := \begin{cases} (\log R)^\vee, & \text{if } (\log R)^\vee \in (-\pi, -\delta] \\ (\log R)^\vee - 2\pi, & \text{if } (\log R)^\vee \in [\delta, \pi] \end{cases} \tag{8.45b}$$

$$\rho_3(R) := (\log R)^\vee, \tag{8.45c}$$

where $(\log R)^\vee = \operatorname{atan2}(R_{21}, R_{11})$ is the principal logarithm of $R \in \mathrm{SO}(2)$, which corresponds to the heading angle $\psi \in (-\pi, \pi]$ in practice. Now, for each $q \in Q = \{1, 2, 3\}$, we define the potential functions $V_q : \mathcal{D}_q \times \mathbb{R}^2 \to \mathbb{R}_{\geq 0}$ by

$$V_q(g_e) := \tfrac{1}{2} k_q \rho_q(R_e)^2 + \tfrac{1}{2} p_e^\mathsf{T} K p_e + o_q, \tag{8.46}$$

where $K = K^\mathsf{T} > 0$, $k_1 = k_2 = k > 0$, $k_3 > 0$, $o_1 = o_2 = o$ and $o_3 = 0$. Due to the topology of $\mathrm{SO}(2)$, at least two potential functions are required to design a globally asymptotically stable hybrid control law. However, by using three potential functions we obtain improved transient performance by encoding smaller proportional gains into the global controllers ($q \in \{1, 2\}$) relative to the local controller ($q = 3$). To this end, the role of the offsets is to enable $k_3 > k$, i.e., a larger proportional gain locally around $R_e = e$. A visualization of the rotational part of the potential functions is shown in Figure 8.1.

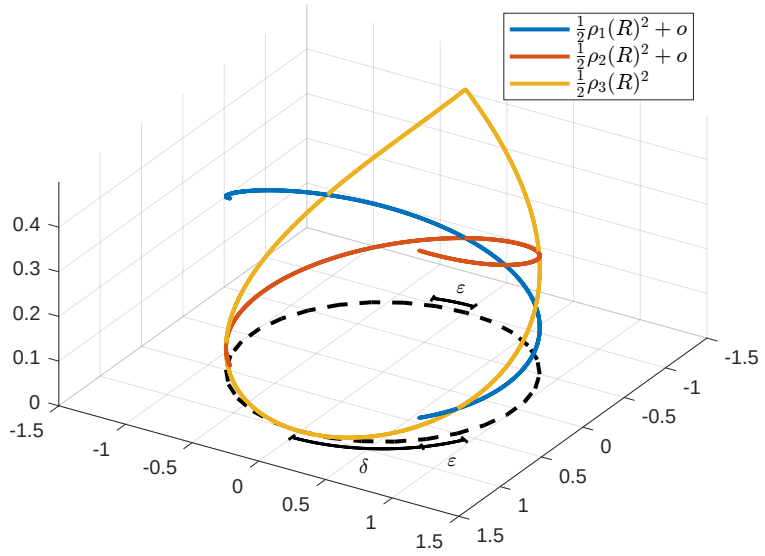

Figure 8.1: The rotational part of the potential functions $\{V_q\}_{q\in Q}$ with $k = \frac{1}{(2\pi)^2}$, $k_3 = \frac{4}{(2\pi)^2}$, $\delta = \frac{\pi}{4}$, $\varepsilon = \frac{\pi}{12}$, and $o = \frac{1}{2}(\delta+\varepsilon)^2(k_3 - k)$.

The switching mechanism is defined by the flow and jump sets $C, D \subset \mathrm{SE}(2)\times Q$ and the jump map $G\colon D \rightrightarrows Q$ associated with the potential functions $\{V_q\}_{q\in Q}$. We define the flow and jump sets by

$$C \coloneqq \bigcup_{q\in Q} C_q \times \{q\}, \tag{8.47a}$$

$$D \coloneqq \bigcup_{q\in Q} D_q \times \{q\}, \tag{8.47b}$$

where

$$C_1 \coloneqq \{g_e \in \mathrm{SE}(2) : \delta \le \rho_1(R_e) \le \pi + \varepsilon\}, \tag{8.48a}$$

$$C_2 \coloneqq \{g_e \in \mathrm{SE}(2) : \delta \le -\rho_2(R_e) \le \pi + \varepsilon\}, \tag{8.48b}$$

$$C_3 \coloneqq \{g_e \in \mathrm{SE}(2) : |\rho_3(R_e)| \le \delta + \varepsilon\}. \tag{8.48c}$$

and

$$\begin{aligned} D_1 \coloneqq &\{g_e \in \mathrm{SE}(2)\colon \pi + \varepsilon \le \rho_1(R_e) \le 2\pi - \delta\} \\ &\cup \{g_e \in \mathrm{SE}(2)\colon |\rho_3(R_e)| \le \delta\} \end{aligned} \tag{8.49a}$$

$$\begin{aligned} D_2 \coloneqq &\{g_e \in \mathrm{SE}(2)\colon \pi + \varepsilon \le -\rho_2(R_e) \le 2\pi - \delta\} \\ &\cup \{g_e \in \mathrm{SE}(2)\colon |\rho_3(R_e)| \le \delta\} \end{aligned} \tag{8.49b}$$

$$D_3 \coloneqq \{g_e \in \mathrm{SE}(2)\colon |\rho_3(R_e)| \ge \delta + \varepsilon\}. \tag{8.49c}$$

In (8.48) and (8.49), $\delta > 0$ determines the switching point between the local and global controllers while $\varepsilon > 0$ denotes the hysteresis half-width between the global

controllers. Finally, we define the set-valued jump map for all $(g_e, q) \in D$ by

$$G(g_e, q) \coloneqq \{w \in Q \setminus \{q\} : g_e \in C_w \cap D_q\}. \tag{8.50}$$

The following lemma provides conditions on the gains and offsets in (8.46), ensuring that V is nonincreasing across jumps.

Lemma 8.4. *Let $\mathcal{A} = \mathcal{A}^\circ \times \{3\}$. If $k_3 \geq k, \delta + 2\varepsilon < \pi$ and*

$$\tfrac{1}{2}\delta^2(k_3 - k) \leq o \leq \tfrac{1}{2}(\delta + \varepsilon)^2(k_3 - k), \tag{8.51}$$

then the 5-tuple $(\mathcal{A}, C, D, G, V)$ satisfies Assumption 8.2.

Proof. (A1-A2) $\mathcal{A}$ is compact since it is finite, while C and D are closed subsets of $\mathrm{SE}(2) \times Q$ since each ρ_q is continuous and the sublevel sets of a continuous function are closed. Moreover, $\bigcup_{q\in Q} C_q = \mathrm{SE}(2)$ and $C_q \cup D_q = \mathrm{SE}(2)$ for each $q \in Q$. Hence, (A1)-(A2) hold.

(A3) Observe that G is locally bounded since $\operatorname{rge} G = Q$ is compact. Moreover, it follows from (A2) that G nonempty for all $(g_e, q) \in D$. Since $G^{-1}(w) = \bigcup_{q\neq w} (C_w \cap D_q) \times \{q\}$ is closed, $\operatorname{gph} G^{-1} = \bigcup_{w\in Q} G^{-1}(w) \times \{w\}$ and the intersection of closed sets are closed, it follows from [62, Theorem 5.7 (a)] that G^{-1} is outer semicontinuous everywhere, and hence that G is outer semicontinuous everywhere.

(A4) Let $g_e \in C_q \cap D_q$ and $w \in G(g_e, q)$. Consider the case where $q \in \{1, 2\}$. If $w = 3$, then it follows that $|\rho_3(R_e)| = \delta$, and hence that $g_e \in C_3 \setminus D_3$. Otherwise, $w = 3 - q$ and it follows that $|\rho_q(R_e)| = \pi + \varepsilon$, which implies that $|\rho_w(R_e)| = \pi - \varepsilon$ and hence that $g_e \in C_{3-q} \setminus D_{3-q}$. Finally, consider that $q = 3$. Then, $g_e \in C_q \cap D_q$ implies that $|\rho_3(R_e)| = \delta + \varepsilon$, which further implies that $g_e \in C_w \setminus D_w$.

(A5) Let $(g_e, q) \in D \setminus C$. Then, $g_e \in C_w$ for some $w \in G(g_e, q)$. Consequently, $g_e \in C_w \setminus D_w$ or $g_e \in C_w \cap D_w$. It follows from (A4) that (A5) holds with $N = 2$.

(A6) V is clearly continuously differentiable on $\mathcal{O}$ and positive definite with respect to $\mathcal{A}$. Moreover, since the function $\tilde{V} : \mathcal{D} \to \mathbb{R}$, where $\mathcal{D} = \bigcup_{q\in Q} \mathcal{D}_q \times \{q\}$ defined by $(R, q) \mapsto \frac{1}{2} k_q \rho_q(R)^2$ is continuous, $\pi_1(\mathcal{D}) = \mathrm{SO}(2)$, and $\mathrm{SO}(2)$ is compact, it follows that $\tilde{V}_q$ is proper. Additionally, the function $\check{V}_q : \mathbb{R}^2 \to \mathbb{R}$ defined by $p \mapsto \frac{1}{2} p^\mathsf{T} K p$ is radially unbounded. Consequently, $V_q(g_e) = \tilde{V}_q(R_e) + \check{V}_q(p_e)$ is a proper map.

To prove (A7), consider $g_e \in C_q \cap D_q$, $q \in \{1, 2\}$, $w = 3 - q$, and $0 < \varepsilon < \pi$. It follows immediately from the definitions of ρ_1 and ρ_2 that $V_{3-q}(g_e) - V_q(g_e) < 0$. When $g_e \in C_q \cap D_q$, $q \in \{1, 2\}$, $w = 3$, $0 < \varepsilon < \pi$ and $0 < \delta < \pi$, it holds that $\rho_3(R_e)^2 \leq \rho_q(R_e)^2$, which implies that

$$V_3(g_e) - V_q(g_e) \leq \frac{1}{2}(k_3 - k)\rho_3(R_e)^2 - o.$$

Since $k_3 - k \geq 0$ and $\rho_3(R_e)^2 \leq \delta^2$, the lower bound $o \geq \frac{1}{2}(k_3 - k)\delta^2$ follows. Let $g_e \in C_3 \cap D_3$ and $w \in G(g_e, 3)$. Then $\delta + 2\varepsilon < \pi$ implies that $\rho_w(R_e)^2 = \rho_3(R_e)^2$, and hence

$$V_w(g_e) - V_3(g_e) \leq \frac{1}{2}(k - k_3)\rho_3(R_e)^2 + o.$$

Using $k - k_3 \leq 0$ and $\rho_3(R_e)^2 \geq \delta + \varepsilon > 0$, it holds that $o \leq \frac{1}{2}(k_3 - k)(\delta + \varepsilon)^2$.

(A8) For all $(g_e, q) \in C$, it is clear that $\mathrm{d}V_q(g_e) = (R_e^{\mathsf{T}} K p_e, k_q \rho_q(R_e)) = 0$ if and only if $(g_e, q) \in \mathcal{A}$. □

8.4.2 Potential functions on $\widetilde{\mathrm{SE}}(3)$

Analogous to the surface vehicle case, we can identify the configuration of an underwater vehicle with the matrix Lie group $\mathrm{SE}(3) = \mathbb{R}^3 \rtimes \mathrm{SO}(3)$. An element $g = (p, R) \in \mathrm{SE}(3)$ contains the position $p \in \mathbb{R}^3$ and orientation $R \in \mathrm{SO}(3)$ of a vehicle-fixed frame with respect to an inertial frame.

The goal is to construct potential functions and a switching mechanism for stabilization of the configuration corresponding to the compact set

$$\mathcal{A}_0 = \{g_e \in \mathrm{SE}(3) : p_e = 0, R_e = I\}, \tag{8.52}$$

However, working with 3×3 rotation matrices can be cumbersome in practice. Unfortunately, there does not exist any globally nonsingular three-parameter representation of $\mathrm{SO}(3)$. As a result, practical state estimation and control applications normally utilize a globally nonsingular four-parameter unit quaternion representation of the vehicle orientation.

Unit quaternions $z = (\eta, \epsilon) \in \mathbb{S}^3$, where $\eta \in \mathbb{R}$ and $\epsilon \in \mathbb{R}^3$, map to the Lie group $\mathrm{SU}(2)$ through the isomorphism $z \mapsto Z$ defined by

$$Z \coloneqq \begin{pmatrix} \eta + i\epsilon_3 & -\epsilon_2 + i\epsilon_1 \\ \epsilon_2 + i\epsilon_1 & \eta - i\epsilon_3 \end{pmatrix} \in \mathbb{C}^{2\times 2}, \tag{8.53}$$

and an element $\omega = (\omega_1, \omega_2, \omega_3) \in \mathbb{R}^3$ maps to $\mathfrak{su}(2)$ through the isomorphism $(\cdot)^\wedge_{\mathfrak{su}(2)} \colon \mathbb{R}^3 \to \mathfrak{su}(2)$ defined by

$$\omega^\wedge_{\mathfrak{su}(2)} \coloneqq \frac{1}{2} \begin{pmatrix} i\omega_3 & -\omega_2 + i\omega_1 \\ \omega_2 + i\omega_1 & -i\omega_3 \end{pmatrix}. \tag{8.54}$$

The Lie algebras of $\mathfrak{su}(2)$ and $\mathfrak{so}(3)$ are isomorphic. Hence, the surjective homomorphism $\mathrm{Ad} \colon \mathrm{SU}(2) \to \mathrm{SO}(3)$ given by

$$\mathrm{Ad}_Z \coloneqq I_3 + 2\eta\epsilon^\wedge + 2(\epsilon^\wedge)^2, \tag{8.55}$$

is a covering map, where $(\cdot)^\wedge \colon \mathbb{R}^3 \to \mathfrak{so}(3)$ is defined by

$$\epsilon^\wedge \coloneqq \begin{pmatrix} 0 & -\epsilon_3 & \epsilon_2 \\ \epsilon_3 & 0 & -\epsilon_1 \\ -\epsilon_2 & \epsilon_1 & 0 \end{pmatrix}. \tag{8.56}$$

Note that $\mathrm{Ad} : \mathrm{SU}(2) \to \mathrm{SO}(3)$ is globally two-to-one and satisfies $\mathrm{Ad}_Z = \mathrm{Ad}_{-Z}$ because $\mathrm{SU}(2)$ is the double cover of $\mathrm{SO}(3)$. In practice, this implies that $\pm Z$ corresponds to the same physical orientation.

Using the adjoint action of $\mathrm{SU}(2)$ on $\mathbb{R}^3$ given by $(p, Z) \mapsto \mathrm{Ad}_Z\, p$, the semidirect product $\mathbb{R}^3 \rtimes \mathrm{SU}(2)$ implies that the natural error on $\widetilde{\mathrm{SE}}(3) \coloneqq \mathbb{R}^3 \rtimes \mathrm{SU}(2)$ is [108]

$$g_e = g_d^{-1} g = (p_e, Z_e) = (\mathrm{Ad}_{Z_d^{-1}}(p - p_d), Z_d^{-1} Z). \tag{8.57}$$

We remark that $\widetilde{\mathrm{SE}}(3)$ is the universal covering group of $\mathrm{SE}(3)$. Due to the double cover property of $\mathrm{SU}(2)$, stabilizing the set $\{g_e \in \widetilde{\mathrm{SE}}(3) : p_e = 0, Z_e = e\}$ using the gradient of a potential function either leads to unwinding, where the control law unnecessarily performs a full rotation of the rigid body, or it may lead to very poor convergence properties around $\operatorname{tr}(Z_e) = 2\eta_e = 0$ [37, 57, 109]. Consequently, to prevent unwinding and obtain global convergence properties, we must stabilize the compact set of disconnected points

$$\mathcal{A}^\circ = \{g_e \in \widetilde{\mathrm{SE}}(3) : Z_e = \pm e\}. \tag{8.58}$$

To this end, we define the set $Q \coloneqq \{-1, 1\}$ and the potential functions $V_q \colon \widetilde{\mathrm{SE}}(3) \to \mathbb{R}_{\geq 0}$ as in [37] by

$$\begin{aligned} V_q(g_e) &\coloneqq k \operatorname{tr}(e - qZ_e) + \tfrac{1}{2} p_e^\mathsf{T} K p_e \\ &= 2k(1 - q\eta_e) + \tfrac{1}{2} p_e^\mathsf{T} K p_e, \end{aligned} \tag{8.59}$$

where $k > 0$ and $K = K^\mathsf{T} > 0$. Let $\varepsilon \in (0, 1)$ denote the hysteresis half-width and define the flow and jump sets by

$$C \coloneqq \{(g_e, q) \in \widetilde{\mathrm{SE}}(3) \times Q : q\eta_e \geq -\varepsilon\} \tag{8.60a}$$

$$D \coloneqq \{(g_e, q) \in \widetilde{\mathrm{SE}}(3) \times Q : q\eta_e \leq -\varepsilon\}. \tag{8.60b}$$

Finally, the jump map is defined as

$$G(q) \coloneqq -q. \tag{8.61}$$

Observe that the preceding definitions ensure that the switching is hysteretic since $q\eta_e \leq -\varepsilon$ implies that $G(q)\eta_e \geq \varepsilon$.

Lemma 8.5. *Let* $\mathcal{A} \coloneqq \left\{(g_e, q) \in \widetilde{\mathrm{SE}}(3) \times Q : \eta_e = q\right\}$. *The 5-tuple* $(\mathcal{A}, C, D, G, V)$ *satisfies Assumption 8.2.*

Proof. The proof is a straightforward extension of the results of [37, Lemma 5.1, Theorem 5.2]. It is clear that the function $\check{V}_q : \mathbb{R}^3 \to \mathbb{R}$ defined by $p \mapsto \frac{1}{2} p^\mathsf{T} K p$ is continuously differentiable, radially unbounded and positive definite with respect to $\pi_2(\mathcal{A})$, where $\mathcal{A}$ is regarded as a subset of $\mathrm{SU}(2) \times \mathbb{R}^3 \times Q$. Moreover, C and D are clearly closed subsets of $\widetilde{\mathrm{SE}}(3) \times Q$, $\mathcal{A}$ is compact, and for all $(g_e, q) \in C$, it holds that $\mathrm{d}V_q(g_e) = (R_e^\mathsf{T} K p_e, kq\epsilon_e) = 0$ if and only if $p_e = 0, \epsilon_e = 0$ which implies that $\eta = \pm 1$, i.e., $(g_e, q) \in \mathcal{A}$. □

8.5 Experimental results

In this section we report the results of three experiments conducted in the Marine Cybernetics Laboratory (MC Lab) [110] at the Norwegian University of Science and Technology (NTNU) in Trondheim. The main purpose of the experiments is to demonstrate the applicability of the devised controllers in realistic scenarios for surface and submerged marine vehicles. The first two experiments were conducted

using a scale model tug boat and the third experiment was conducted with a remotely operated underwater vehicle.

In the MC Lab, a local positioning system comprises sets of cameras mounted above and below the water surface and the Qualisys Track Manager (QTM) software. Light emitted by the cameras is reflected by a set of optical markers mounted on the vehicle to be tracked. These measurements are then processed with QTM, which outputs the position and orientation estimates at a rate of 100 Hz. A multiplicative extended Kalman filter (MEKF) [84, Section 14.4.3] is employed to reconstruct the velocities and filter the position and orientation. The MEKF is augmented with linear acceleration and angular velocity measurements for the underwater vehicle experiments.

Figure 8.2: The Marine Cybernetics Lab at NTNU

8.5.1 Cybership Enterprise

Cybership Enterprise (CSE) is a 1:50 scale model tug boat with a length of 1.105 m and beam of 0.248 m. CSE is equipped with two Voith Schneider propellers (VSPs) and one bow thruster. The configuration of CSE is described by $g = (p, R) \in \mathrm{SE}(2)$, where elements in $\mathrm{SE}(2)$ admit a homogeneous matrix representation through the injective homomorphism $\mathrm{SE}(2) \to \mathrm{GL}(3)$ defined by [108]

$$g \coloneqq \begin{pmatrix} R & p \\ 0 & 1 \end{pmatrix} \in \mathbb{R}^{3\times 3}. \tag{8.62}$$

Denoting the vehicle-fixed linear and angular velocities by $v \in \mathbb{R}^2$ and $\omega \in \mathbb{R}$, respectively, define the vehicle-fixed velocity as $\nu \coloneqq (v, \omega) \in \mathbb{R}^3$. An element $\nu \in \mathbb{R}^3$ maps to $\mathfrak{se}(2)$ through the isomorphism $(\cdot)^\wedge \colon \mathbb{R}^3 \to \mathfrak{se}(2)$ defined by

$$\nu^\wedge \coloneqq \begin{pmatrix} S\omega & v \\ 0 & 0 \end{pmatrix} \in \mathbb{R}^{3\times 3}, \quad S \coloneqq \begin{pmatrix} 0 & -1 \\ 1 & 0 \end{pmatrix}. \tag{8.63}$$

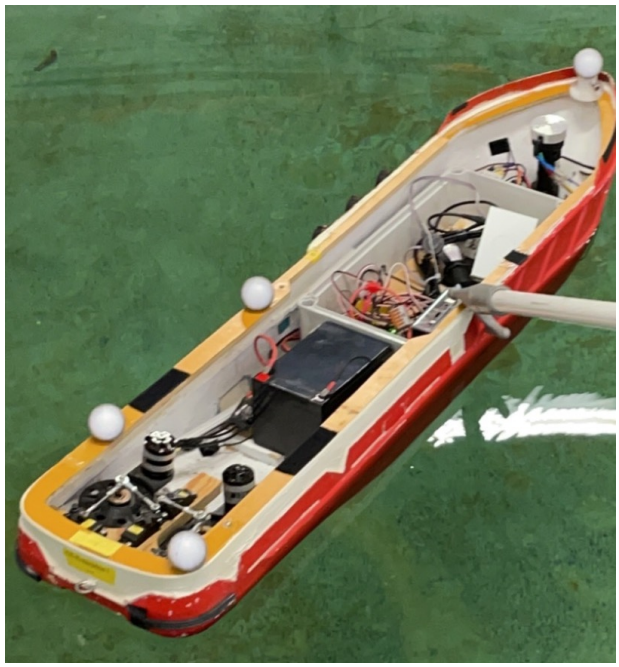

Figure 8.3: Cybership Enterprise in the MC-Lab

Let $\theta \in \mathbb{R}^{15}$ denote the model parameters. The equations of motion for a surface vehicle can be formulated by (8.1) with

$$M = \begin{pmatrix} \theta_1 & 0 & 0 \\ 0 & \theta_2 & \theta_3 \\ 0 & \theta_3 & \theta_4 \end{pmatrix}, \quad f(g) = b, \tag{8.64}$$

$$d(\nu) = \begin{pmatrix} -\theta_5 \nu_1 \\ -\theta_6 \nu_2 - \theta_8 \omega \\ -\theta_9 \nu_2 - \theta_7 \omega \end{pmatrix} + \begin{pmatrix} -\theta_{10} |\nu_1| \nu_1 \\ -\theta_{11} |\nu_2| \nu_2 \\ -\theta_{12} |\omega| \omega \end{pmatrix} \tag{8.65}$$

where $b = (\theta_{13}, \theta_{14}, \theta_{15}) \in \mathbb{R}^3$ is a constant bias. We remark that the expression for the regressor Φ follows from (8.17) together with (8.64) and (8.65).

The generalized forces are calculated using (8.26), where the adjoint actions of $\mathrm{SE}(2)$ and $\mathfrak{se}(2)$ on $\mathbb{R}^3$ for $g = (p, R) \in \mathrm{SE}(2)$ and $\nu = (v, \omega) \in \mathbb{R}^3$ are given by

$$\mathrm{Ad}_g = \begin{pmatrix} R & -Sp \\ 0 & 1 \end{pmatrix}, \quad \mathrm{ad}_\nu = \begin{pmatrix} S\omega & -Sv \\ 0 & 0 \end{pmatrix}. \tag{8.66}$$

The generalized forces $\tau \in \mathbb{R}^3$ map to the actuator inputs $(\alpha, u) \in \mathbb{R}^2 \times \mathbb{R}^3$ through

$$\tau = B(\alpha) K u, \tag{8.67}$$

where $\alpha = (\alpha_1, \alpha_2)$ are the VSP angles and $u = (u_1, u_2, u_3)$ are the thruster inputs. Specifically, (u_1, u_2) corresponds to the VSPs, and u_3 is the bow thruster.

Table 8.1: Control Parameters

Circle		**Lemniscate**	
δ	$\pi/6$	δ	$\pi/18$
ε	$\pi/18$	ε	$\pi/18$
K_p	$\mathrm{diag}(1.7, 1.7)$	K_p	$\mathrm{diag}(1.45, 1.45)$
k	0.5	k	0.5
k_3	1.2	k_3	1.5
K_d	$\mathrm{diag}(.7, .6, .6)$	K_d	$\mathrm{diag}(1.25, 1.25, 1)$
Λ	I_3	Λ	I_3

Using the transformation $(\alpha, u) \mapsto (\check{u}_1, \check{u}_2, \check{u}_3)$, where

$$\check{u}_1 = \begin{pmatrix} \cos(\alpha_1)u_1 \\ \sin(\alpha_1)u_1 \end{pmatrix}, \check{u}_2 = \begin{pmatrix} \cos(\alpha_2)u_2 \\ \sin(\alpha_2)u_2 \end{pmatrix}, \check{u}_3 = u_3. \tag{8.68}$$

we can rewrite (8.67) as $\tau = \check{B}\check{K}\check{u}$, which is solved using the Moore-Penrose pseudoinverse

$$\check{u}_* = (\check{B}\check{K})^\dagger \tau, \tag{8.69}$$

for a given $\tau \in \mathbb{R}^3$. The actuator control inputs (α, u) are then obtained by inverting the transformation (8.68). Note that the BT input is constrained to the interval $[-1, 1]$, while the VSP inputs are constrained to $[0, 1]$. The desired path is given by $\gamma(s) = (\gamma_1(s), \gamma_2(s)) \in \mathrm{SE}(2)$ where

$$\gamma_1(s) = \begin{pmatrix} x_d(s) \\ y_d(s) \end{pmatrix}, \gamma_2(s) = \exp(S\psi_d(s)), \tag{8.70}$$

where $\psi_d(s) = \mathrm{atan2}(y_d'(s), x_d'(s))$.

The hysteresis width and control gains are chosen according to Table 8.1 with $\vartheta_q(\zeta) = K_d\zeta$ and $\varphi_q(\xi) = K_d\xi$. Moreover, the adaptation gain and bounds on $\theta \in \mathbb{R}^{15}$ are given by

$$\begin{aligned} \Gamma &= \mathrm{blkdiag}(50, 40, 5, 20, 5I_{4\times 4}, 10I_{9\times 9}, 0.025, 0.1, 0.01), \\ \underline{\theta} &= (10, 15, 1, -3, 0_{7\times 1}, -1, -4, -4, -4), \\ \overline{\theta} &= (20, 30, 5, 3, 10_{7\times 1}, 10, 4, 4, 4), \end{aligned}$$

and the parameters are initialized as

$$\theta_0 = (10, 15, 1, 0_{12\times 1}). \tag{8.71}$$

Two two experiments are performed using different parametrized loops; the first loop is a circle, and the second is a lemniscate.

Circle

The circle is centered at $O = (1\,\text{m}, 0)$ with a radius of $R = 1.2\,\text{m}$ and is represented by the parametric equation

$$\gamma_1(s) = \begin{pmatrix} R\cos(s) \\ R\sin(s) \end{pmatrix} + O. \tag{8.72}$$

Experimental results are presented in Figures 8.4 to 8.10. The ship was ini-

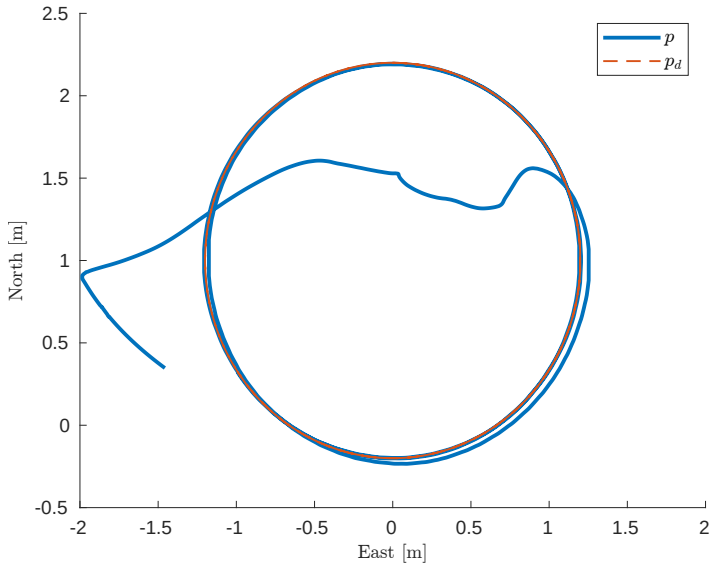

Figure 8.4: North-East plot showing the North-East position $p = (x, y)$ and the desired position $p_d = (x_d, y_d)$.

tialized at $p(0) = (0.35\,\text{m}, -1.46\,\text{m})$ with $\psi = -42°$. At this point in time, the orientation error was $\rho_3(R_e(t))|_{t=0} = -\pi\frac{106}{180} \geq \delta + \varepsilon$, and it follows from (8.46) that $\rho_2^2(R_e(t))|_{t=0} < \rho_1^2(R_e(t))|_{t=0}$. In other words, the orientation error was in the jump set corresponding to $q = 3$ and the jump map (8.50) implies that the global controller corresponding to $q^+ = 2$ was activated, which is what we observe in the lower plot in Figure 8.7. Then, at $t \approx 33\,\text{s}$, the commanded input speed μ was set to $0.08\,\text{m/s}$ as seen in Figure 8.7. Figures 8.4 and 8.5 shows that CSE accurately tracked the path after an initial transient due to the significant initial configuration error, even though the actuator inputs saturate until $t \approx 25\,\text{s}$ as seen in Figure 8.8. Figure 8.6 depicts the system velocities and desired velocities, while Figure 8.7 shows the commanded input speed $\mu(t)$, the desired speed $u_d(t)$ and the estimated speed $U(t) = \|v(t)\|$. Therefore, it is clear that the speed and velocities are tracked with sufficient accuracy.

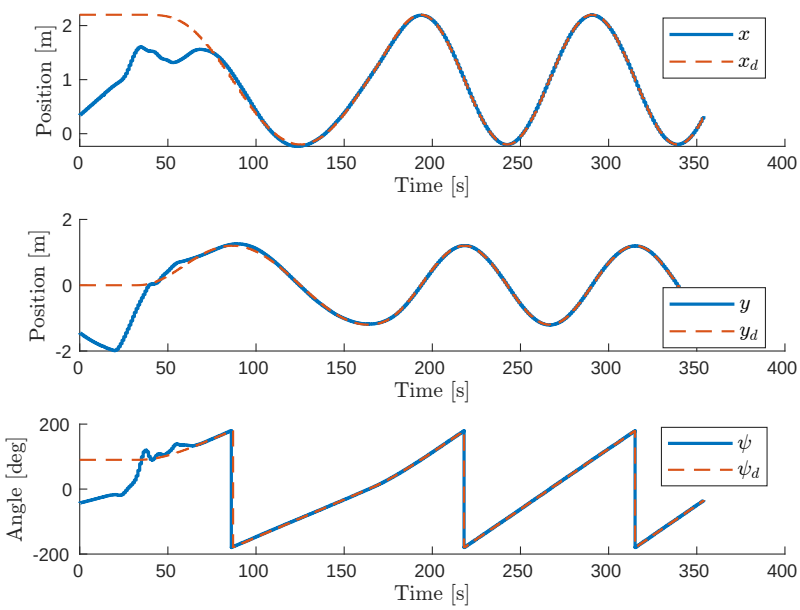

Figure 8.5: The configuration $p = (x, y), R = \exp(S\psi)$ and the desired configuration $p_d = (x_d, y_d), R_d = \exp(S\psi_d)$.

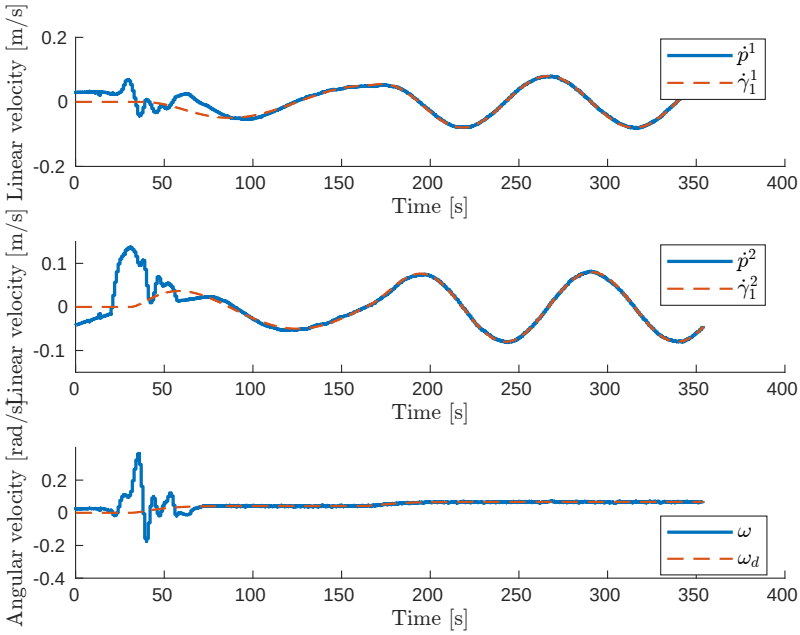

Figure 8.6: The velocity estimates $(\dot{p}, \omega)$ and the desired velocity references $(\dot{\gamma}_1, \omega_d)$.

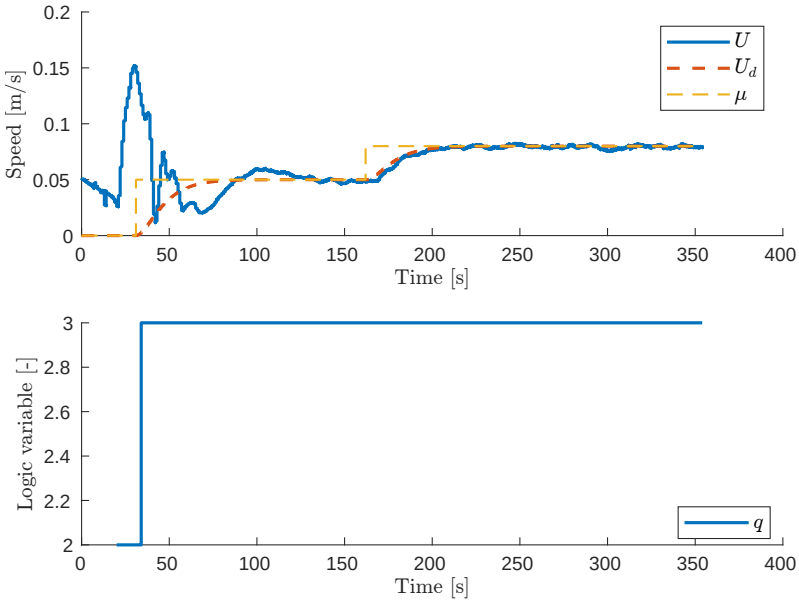

Figure 8.7: The speed U, desired speed u_d, commanded input speed μ and logic variable q.

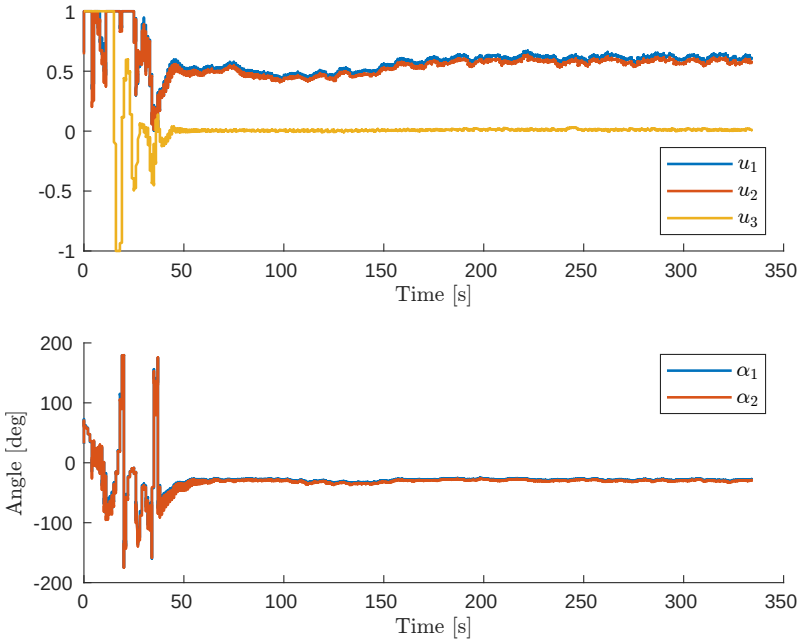

Figure 8.8: The VSP control inputs $u_1, u_2 \in [0, 1]$, the BT control input $u_3 \in [-1, 1]$ and VSP angle inputs α_1, α_2.

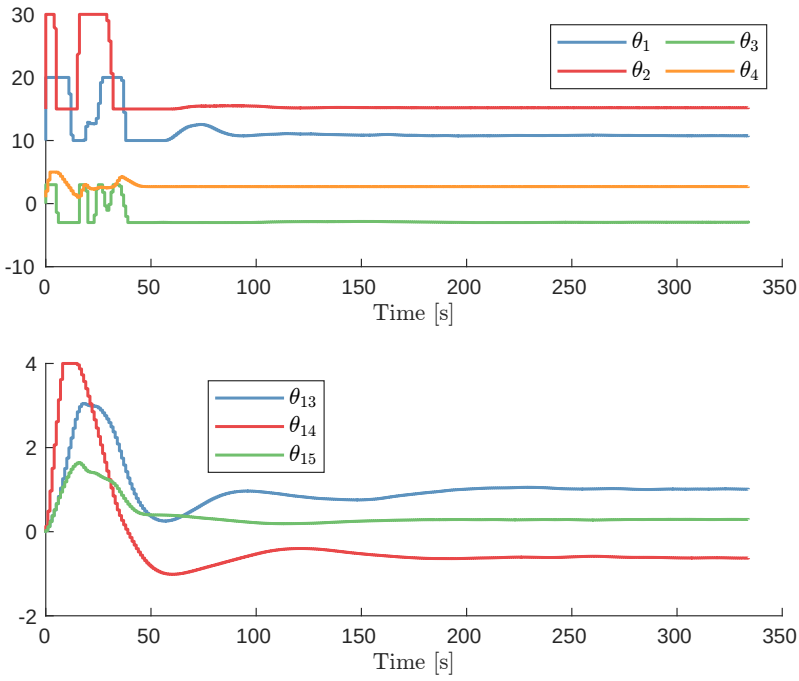

Figure 8.9: The inertia and bias parameters.

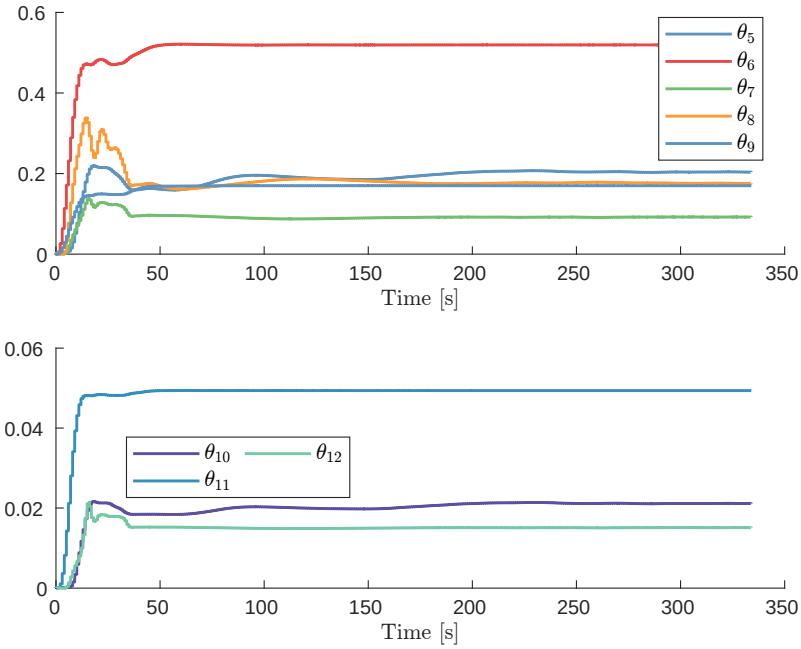

Figure 8.10: The damping parameters associated with the linear and nonlinear damping.

Lemniscate

The lemniscate is centered at $O = (2\,\mathrm{m}, 0)$ and is represented by the parametric equation

$$\gamma_1(s) = \begin{pmatrix} R_1 \dfrac{\cos s}{1 + \sin^2 s} \\ R_2 \dfrac{\sqrt{2} \sin 2s}{1 + \sin^2 s} \end{pmatrix} + O, \tag{8.73}$$

where $R_1 = 2\,\mathrm{m}$, $R_2 = 2.4\,\mathrm{m}$.

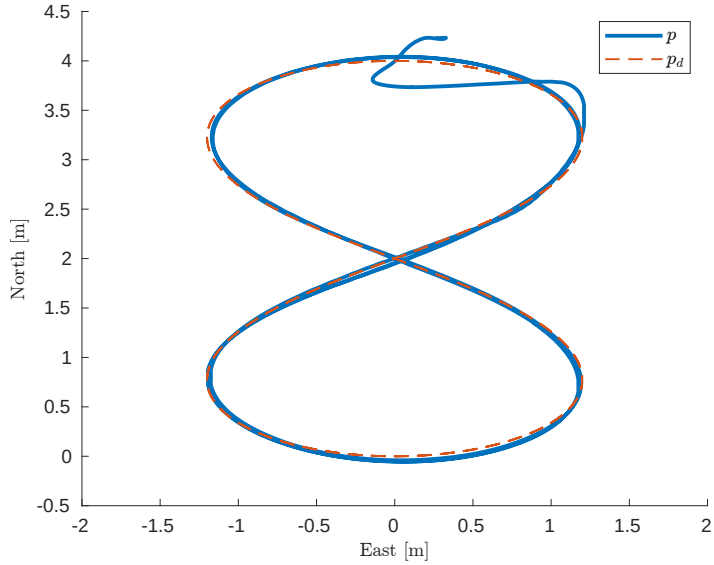

Figure 8.11: North-East plot showing the position p and the desired position p_d.

Experimental results are presented in Figures 8.11 to 8.17. The ship was initialized at $p(0) = (4.2\,\mathrm{m}, 0.3\,\mathrm{m})$ with a heading of $\psi = 130°$. Since the lemniscate loop given by (8.73) does not result in a constant acceleration with respect to the body-fixed frame for nonzero commanded input speeds, the control gains must be increased to compensate for the inaccuracies in the dynamic model and obtain similar performance to the circular trajectory.

By comparing Figures 8.9 and 8.10 with Figures 8.16 and 8.17, it is clear that the parameters do not converge to any 'true' value. This cannot be expected because we have not provided any persistency of excitation condition; that is, we have not given any conditions under which (8.26) uniformly globally asymptotically stabilizes the compact set $\widetilde{\mathcal{B}}$ for the closed-loop system $\mathcal{H}$. However, even if such conditions were provided, a constant bias in the vehicle-fixed frame will not fully capture the inaccuracies in the mapping between the forces produced by the actuators and their inputs. As a consequence, the desired forces and torque computed by the control law are significantly different from the actual forces and torque produced by the actuators. In turn, this leads to a tracking error, which induces parameter

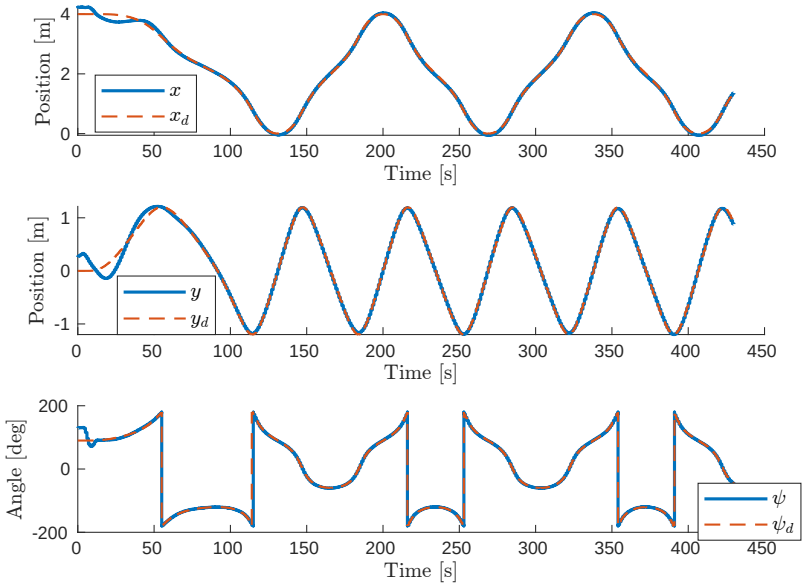

Figure 8.12: The configuration $p = (x, y), R = \exp(S\psi)$ and the desired configuration $p_d = (x_d, y_d), R_d = \exp(S\psi_d)$.

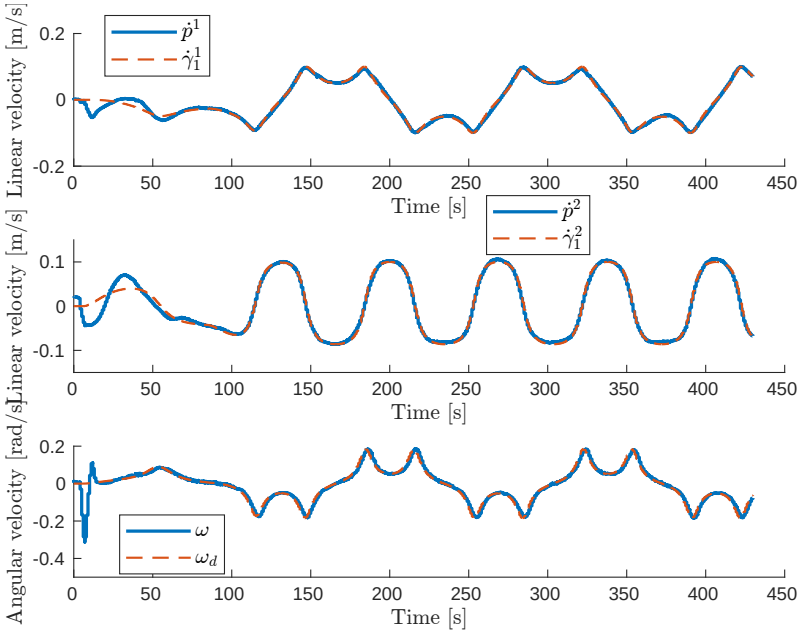

Figure 8.13: The velocity estimates $(\dot{p}, \omega)$ and the desired velocity references $(\dot{\gamma}_1, \omega_d)$.

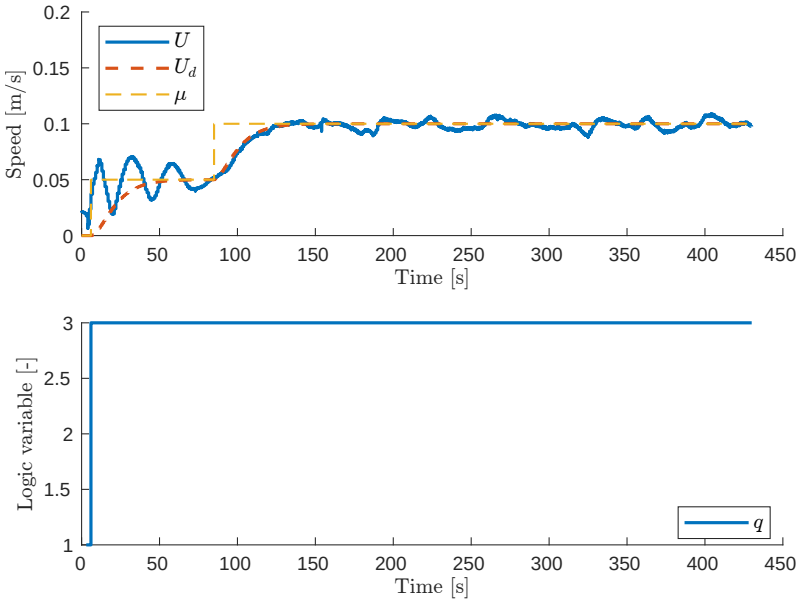

Figure 8.14: The speed U, desired speed u_d, commanded input speed μ and logic variable q.

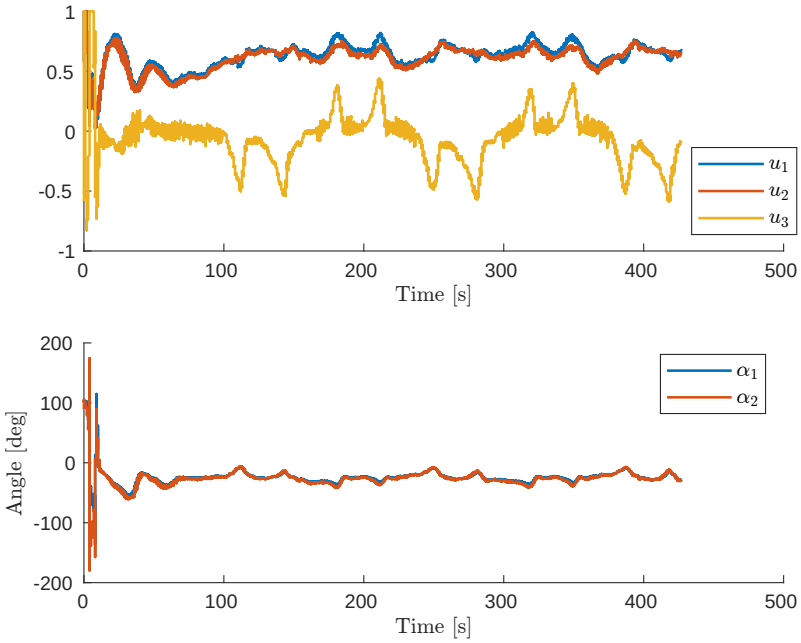

Figure 8.15: The VSP control inputs $u_1, u_2 \in [0, 1]$, the BT control input $u_3 \in [-1, 1]$ and VSP angle inputs α_1, α_2.

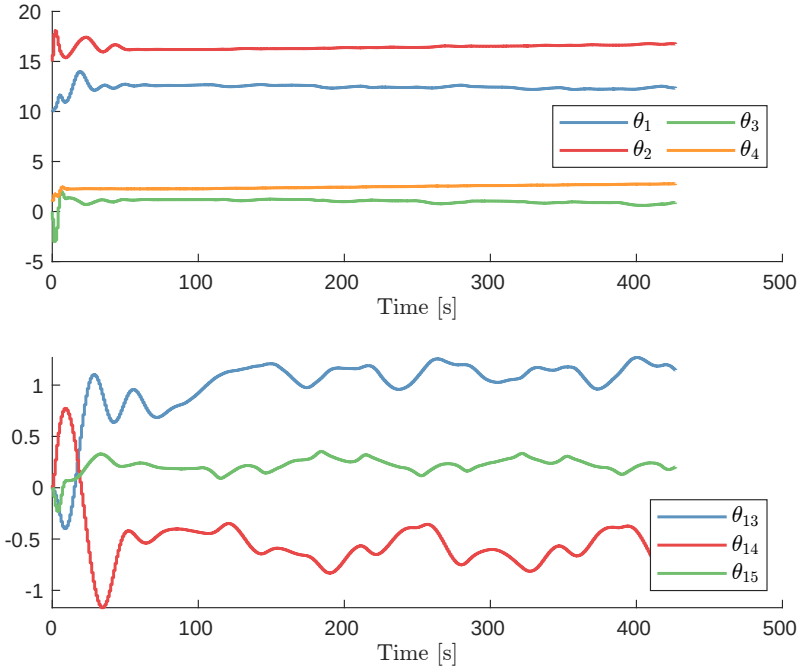

Figure 8.16: The inertia and bias parameters.

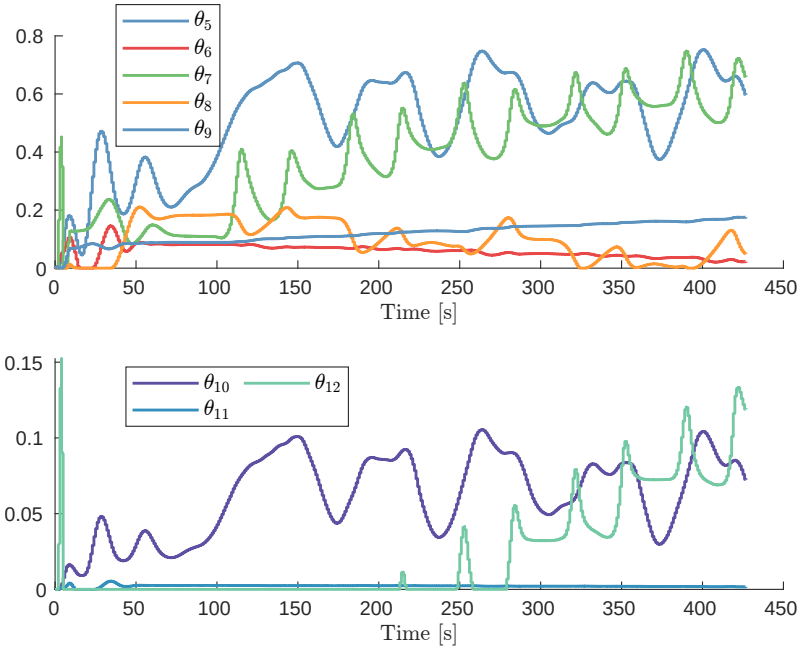

Figure 8.17: The damping parameters associated with the linear and nonlinear damping.

adaptation. Since this adaptation occurs due to unmodeled effects that are not correctly captured by our assumed model structure, we cannot expect to accurately identify the mass and damping model parameters for this system. Instead, due to the presence of a constant bias in our dynamic model, our control law is more reminiscent of a PID controller with adaptive feedforward. To see this, note that the bias feedforward term can be written as $-\int_0^t(\nu_e(\tau)-\zeta(\tau))\mathrm{d}\tau$, and that (8.14) can be interpreted as a multiple-input multiple-output low-pass filter with input $-\mathrm{d}V_q$ and output ζ. Thus, when the velocity error ν_e is zero, the bias feedforward term can be interpreted as the integral of the output of a low-pass filter whose input is the configuration error.

Finally, we observe that the parameters converge for the circular trajectory. This is a consequence of the steady-state nature of the circular trajectory, that is, constant desired velocities with respect to the desired frame when u_d has converged to the commanded input speed μ. For the lemniscate trajectory, however, the desired velocities are not constant even if the desired speed has converged to the commanded input speed. Hence, considering the inaccuracies in the mappings between the desired forces and torque and the produced forces and torque, it is not surprising that the parameters do not converge to any specific values and that the damping and bias parameters change more rapidly when the ship is in a turning maneuver, as seen in Figures 8.12, 8.16 and 8.17. Despite these structural modeling inaccuracies, the ship's position remains within 4 cm of the desired position after converging to the path, as seen in Figures 8.11 and 8.12. Moreover, from Figure 8.13 and Figure 8.14, we observe that the desired velocities and the desired speed are tracked with sufficient accuracies.

8.5.2 BlueROV2

The BlueROV2 is a remotely operated underwater vehicle developed by Blue Robotics. The experiments were conducted using the heavy configuration BlueROV2

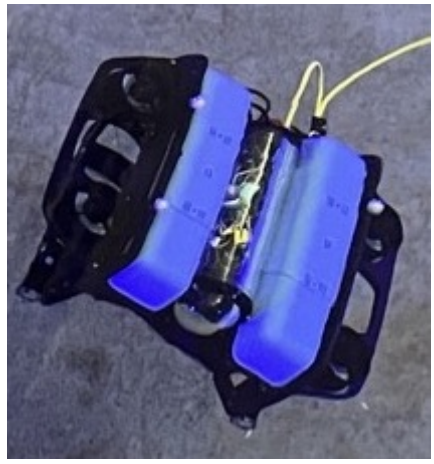

Figure 8.18: The BlueROV2 in the MC-Lab.

with eight thrusters, depicted in Fig. 8.18.

Elements $g = (p, Z) \in \widetilde{\mathrm{SE}}(3)$ admit a matrix representation using the injective homomorphism $\widetilde{\mathrm{SE}}(3) \to \mathrm{GL}(6, \mathbb{C})$ given by

$$g = \begin{pmatrix} \mathrm{Ad}_Z & p & 0 \\ 0 & 1 & 0 \\ 0 & 0 & Z \end{pmatrix} \in \mathbb{C}^{6\times 6} \tag{8.74}$$

Denoting the vehicle-fixed linear and angular velocities by $v \in \mathbb{R}^3$ and $\omega \in \mathbb{R}^3$, respectively, define the vehicle-fixed velocity as $\nu := (v, \omega) \in \mathbb{R}^6$. An element $\nu \in \mathbb{R}^6$ maps to $\widetilde{\mathfrak{se}}(3)$ through the isomorphism $(\cdot)^\wedge \colon \mathbb{R}^6 \to \widetilde{\mathfrak{se}}(3)$ defined by

$$\nu^\wedge = \begin{pmatrix} \omega^\wedge & v & 0 \\ 0 & 0 & 0 \\ 0 & 0 & \omega_{\mathfrak{su}}^\wedge \end{pmatrix} \in \mathbb{C}^{6\times 6}. \tag{8.75}$$

The equations of motion for an underwater vehicle can then be formulated by (8.1) with

$$f(g) = \beta(Z) + b, \tag{8.76}$$

where $\beta(Z) = (\theta_7 \,\mathrm{Ad}_Z^\mathsf{T} e_3, e_3^\wedge \,\mathrm{Ad}_Z^\mathsf{T} \theta_{8:10})$ contains gravitational and buoyancy forces and $b = (\theta_1, \ldots, \theta_6) \in \mathbb{R}^6$ is a constant bias. Moreover, by assuming port/starboard and fore/aft symmetry, the inertia matrix is parametrized by

$$M = \begin{pmatrix} \theta_{11} & 0 & 0 & 0 & \theta_{17} & 0 \\ 0 & \theta_{12} & 0 & \theta_{18} & 0 & 0 \\ 0 & 0 & \theta_{13} & 0 & 0 & 0 \\ 0 & \theta_{18} & 0 & \theta_{14} & 0 & 0 \\ \theta_{17} & 0 & 0 & 0 & \theta_{15} & 0 \\ 0 & 0 & 0 & 0 & 0 & \theta_{16} \end{pmatrix} \tag{8.77}$$

while the hydrodynamic drag forces are assumed to satisfy

$$d_i(\nu) = \theta_{18+i} + \theta_{24+i}|\nu_i|\nu_i, \tag{8.78}$$

for $i \in \{1, \ldots, 6\}$. We remark that the expression for the regressor Φ follows from (8.17) together with (8.76), (8.77) and (8.78). The generalized forces are calculated using the control law (8.26), where the adjoint actions of $\widetilde{\mathrm{SE}}(3)$ and $\widetilde{\mathfrak{se}}(3)$ on $\mathbb{R}^6$ for $g = (p, Z) \in \widetilde{\mathrm{SE}}(3)$ and $\nu = (v, \omega) \in \mathbb{R}^6$ are given by

$$\mathrm{Ad}_g = \begin{pmatrix} \mathrm{Ad}_Z & p^\wedge \,\mathrm{Ad}_Z \\ 0 & \mathrm{Ad}_Z \end{pmatrix}, \quad \mathrm{ad}_\nu = \begin{pmatrix} \omega^\wedge & v^\wedge \\ 0 & \omega^\wedge \end{pmatrix}. \tag{8.79}$$

The generalized forces $\tau \in \mathbb{R}^6$ map to the desired thrust $u \in \mathbb{R}^8$ through $\tau = Ku$, where each column of K is

$$K_i = \begin{pmatrix} r_i \\ L_i \times r_i \end{pmatrix}, \tag{8.80}$$

where $r_i \in \mathbb{R}^3$ is a unit vector pointing in the direction of thrust and $L_i \in \mathbb{R}^3$ is the position of the thruster relative to the body frame. Using (8.26), the actuator control inputs are then found from the expression $u = K^\dagger \tau$.

The desired path is given by $\gamma(s) = (p_d(s), Z_d(s)) \in \widetilde{\mathrm{SE}}(3)$, with

$$p_d(s) = \begin{pmatrix} L_1 \frac{\cos s}{1+\sin^2 s} \\ L_2 \frac{\sqrt{2}\sin 2s}{1+\sin^2 s} \\ L_3 \frac{2\sin s}{1+\sin^2 s} \end{pmatrix} + O, \; z_d(s) = \begin{pmatrix} \cos(\psi(s)/2) \\ 0 \\ 0 \\ \sin(\psi(s)/2) \end{pmatrix}$$

where z_d is a unit quaternion that maps to $\mathrm{SU}(2)$ through the isomorphism $z_d \mapsto Z_d$ defined in (8.53). Moreover, $O = (0.2\,\mathrm{m}, -0.3\,\mathrm{m}, -0.55\,\mathrm{m})$, $L_1 = 1\,\mathrm{m}$, $L_2 = 0.6\,\mathrm{m}$, $L_3 = 0.25\,\mathrm{m}$ and $\psi(s) = \mathrm{atan2}(y_d'(s), x_d'(s))$.

The desired speed reference is given by

$$\mu = \begin{cases} 0.1\,\mathrm{m/s}, & 5 \leq t < 125 \\ 0.2\,\mathrm{m/s}, & t \geq 125 \end{cases}, \tag{8.81}$$

while the hysteresis half-width is $\varepsilon = 0.1$. The control gains are chosen as $K_p = \mathrm{diag}(50, 50, 70), k = 16, \varphi_q(\xi) = K_d\xi, \vartheta_q(\zeta) = K_d\zeta$ and $\Lambda = I_6$ with $K_d = \mathrm{diag}(40, 40, 30, 7, 7, 7)$. Moreover, the adaptation gain and bounds on $\theta \in \mathbb{R}^{30}$ are given by

$$\begin{aligned} \Gamma &= \mathrm{blkdiag}(\Gamma_1, \Gamma_2, \Gamma_3), \\ \Gamma_1 &= \mathrm{diag}(1.5, 1.5, 1.5, 1.2, 1.2, 1.2), \\ \Gamma_2 &= \mathrm{diag}(2.5, 2, 2, 2), \\ \Gamma_3 &= \mathrm{diag}(7, 7, 7, 4, 4, 4, 5, 5, 20, 20, 20, 5, 5, 5, 20, 20, 20, 5, 5, 5), \\ \underline{\theta} &= (-40, -10_{9\times1}, 0_{7\times1}, -2, 0_{12\times1}), \\ \overline{\theta} &= (10_{10\times1}, 50_{6\times1}, 2, 0, 50_{12\times1}), \end{aligned}$$

and the parameters are initialized as

$$\begin{aligned} \theta_0 = (&0_{10\times1}, 19.17, 26.37, 28.24, 0.28, 0.28, \\ &0.28, 0.23, -0.23, 4.03, 6.22, 5.1, \\ &0.07, 0.07, 0.07, 18.18, 21.66, 36.99, \\ &1.55, 1.55, 1.55) \end{aligned} . \tag{8.82}$$

Experimental results are presented in Figures 8.19 to 8.27. Due to limitations in the hardware implementation, the controller activates a few seconds before the data logger and actuator driver do. As a result, the bias and gravitational parameters have already adapted for several seconds by the time the control signals are sent to the actuators. This can be observed in the upper plot in Figure 8.27, where θ_1 and θ_3, i.e., the x and z components of the bias, are already saturated at $t \approx 4\,\mathrm{s}$ when the actuator driver is activated and the control inputs are converted to pulse width modulated actuator signals. Remarkably, this has little effect on the transient performance, as observed in Figure 8.21. This occurs despite the fact that the BlueROV2 was initialized at the bottom of the pool at a distance $\|p_e\| \approx 1.36\,\mathrm{m}$

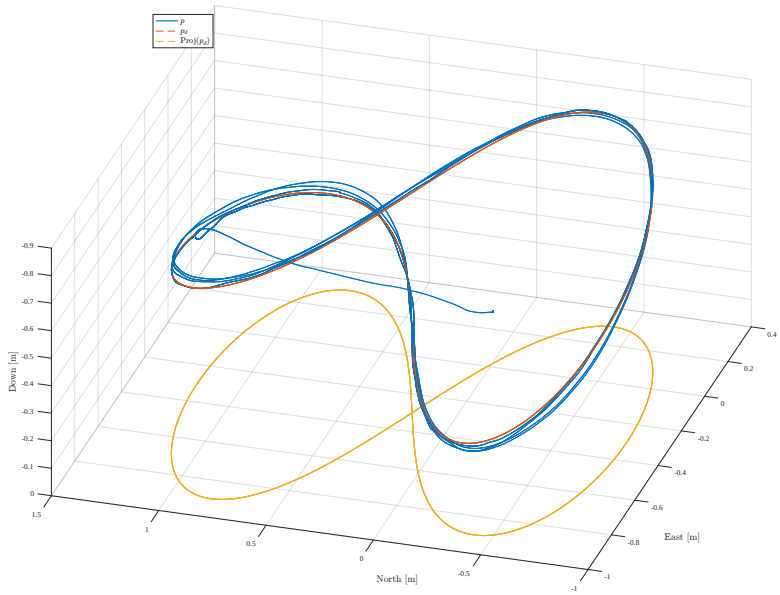

Figure 8.19: North-East-Down plot showing the position p, the desired position p_d and the projection of p_d onto the North-East plane.

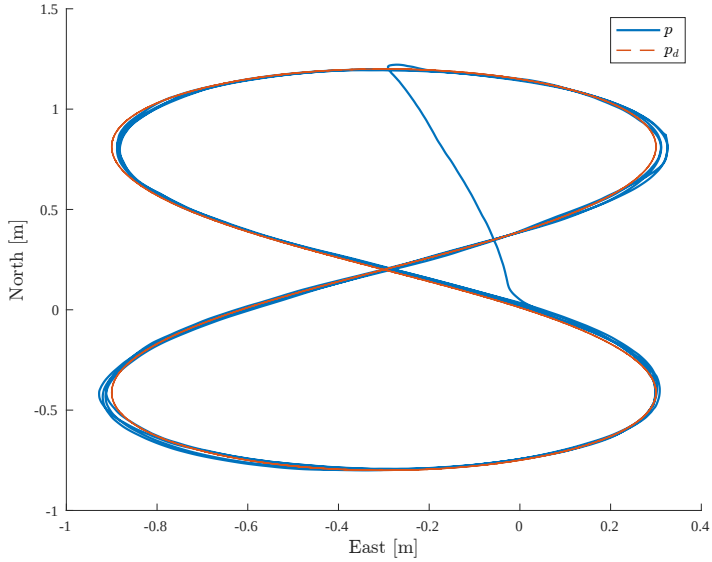

Figure 8.20: North-East plot of the position and desired position

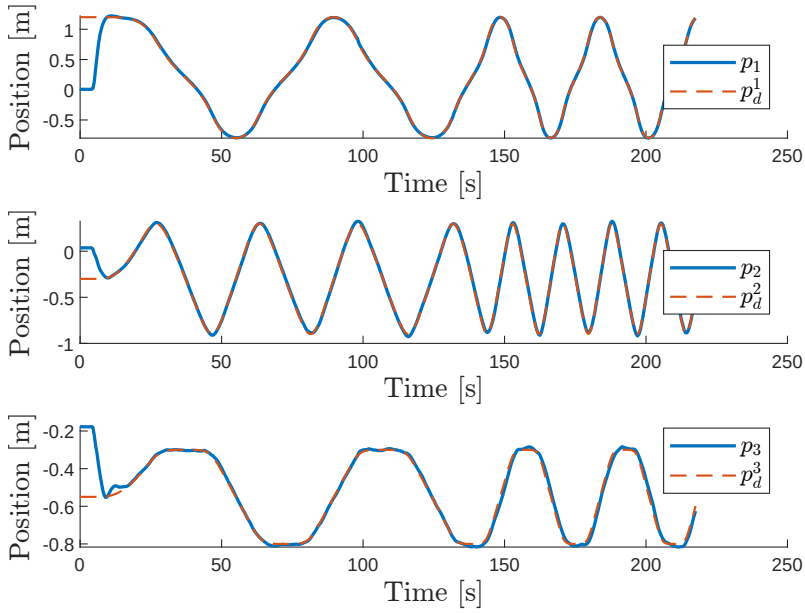

Figure 8.21: The position $p = (p_1, p_2, p_3)$ and desired position $p_d = (p_d^1, p_d^2, p_d^3)$.

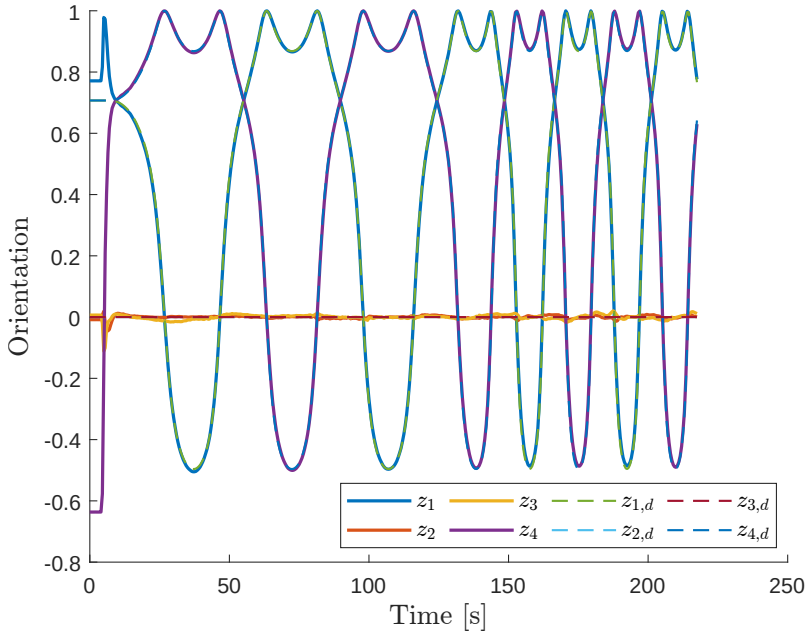

Figure 8.22: The orientation and desired orientation, represented by the unit quaternions z and z_d, respectively.

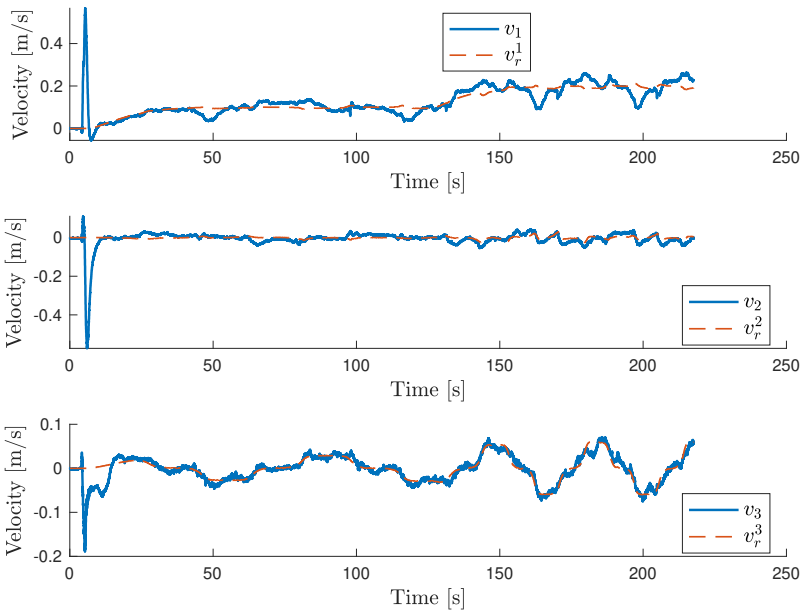

Figure 8.23: The linear velocities v and the desired linear velocities v_r, decomposed in the body frame.

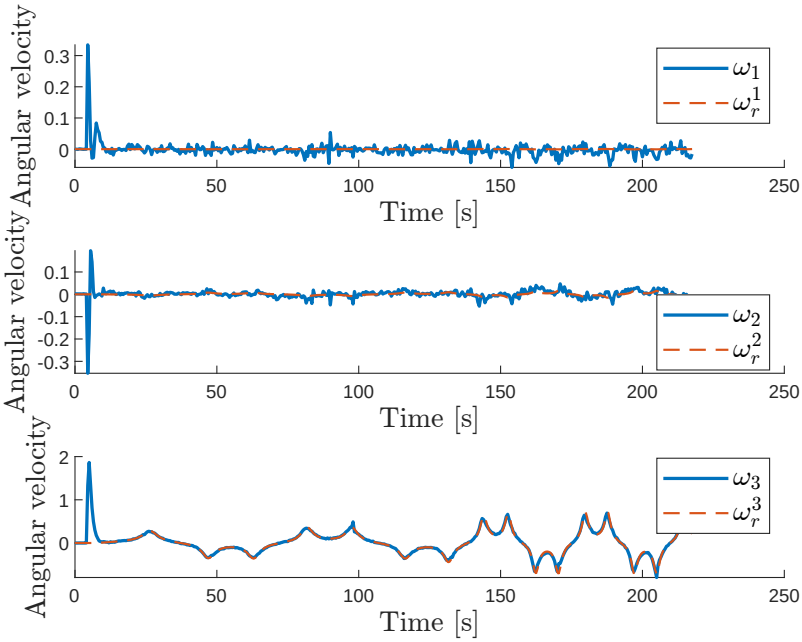

Figure 8.24: The angular velocities ω and the desired angular velocities ω_r decomposed in the body frame.

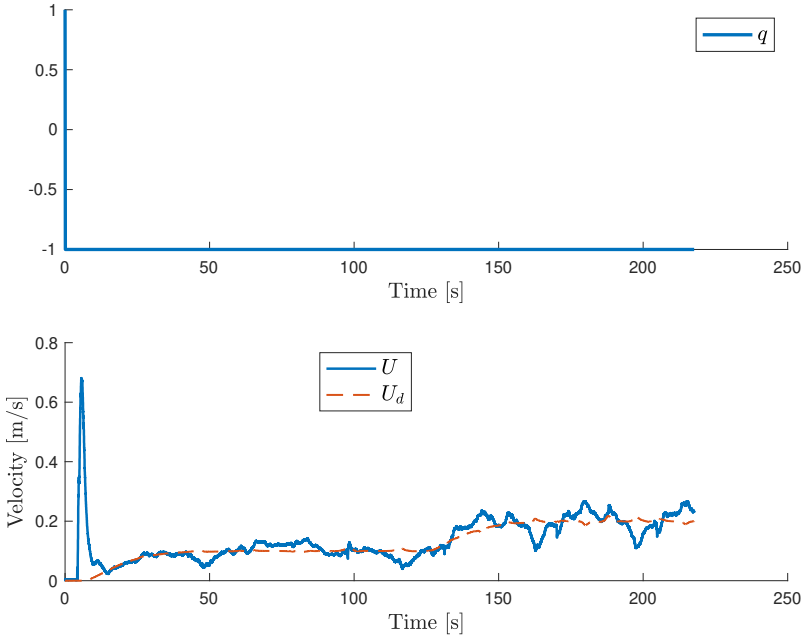

Figure 8.25: The logic variable q, the speed U, and the desired speed $U_d = |\dot{\gamma}_1|$

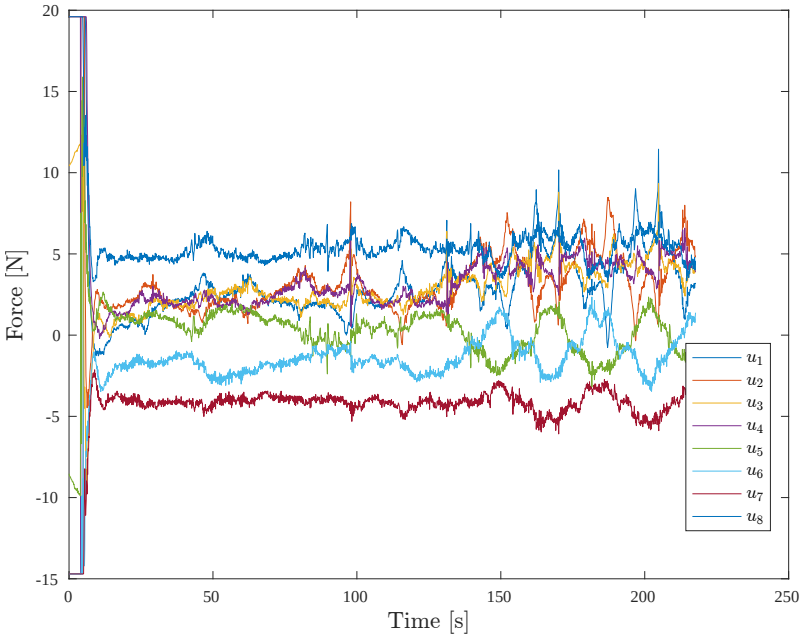

Figure 8.26: The control inputs u corresponding to the eight thrusters.

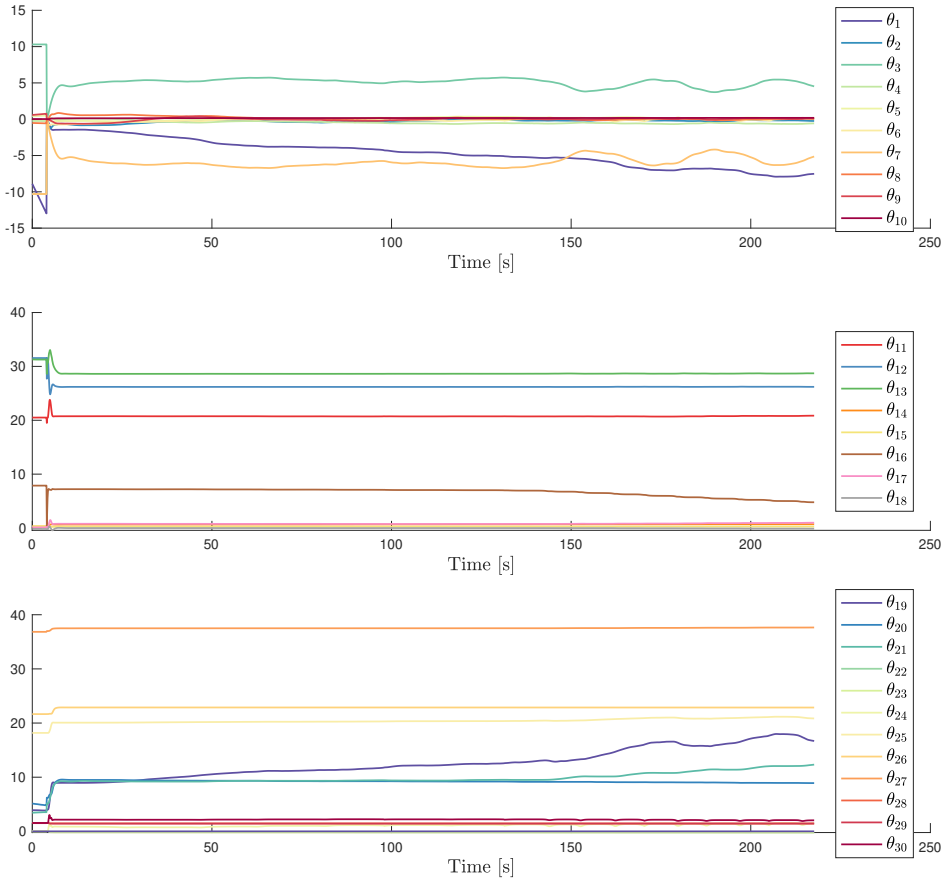

Figure 8.27: The bias and gravitational/buoyancy related parameters, the inertia matrix parameters and the damping parameters.

away from the desired position with no initial knowledge of the gravitational- and buoyancy-related parameters.

The initial quaternion error satisfies $\eta_e \leq -\varepsilon$, which entails that a switch from the initial value of $q = 1$ to $q = -1$ occurs at the first time step of the controller. Since the logger was initialized after the controller, although no control inputs were sent to the actuators, we have changed first logged value of the logic variable to $q = 1$ to highlight the fact that a switch has in fact occurred.

From Figures 8.19, 8.21 and 8.22, we observe that the ROV successfully tracks the position and orientation references with satisfactory accuracy. Moreover, from Figures 8.23 and 8.24, we see that the desired velocities $\nu_r = \mathrm{Ad}_{g_e^{-1}} \nu_d$ are tracked with satisfactory accuracy. However, we remark that v_3 contains significantly more noise compared to the other linear velocities. Moreover, the x-component of the linear velocity, v_1, exhibits spikes that coincide with the minima of p_3, i.e. the z-component of the position vector. This is due to poor tracking of the ROV from the camera-based underwater positioning system, which either loses track of the

ROV and/or outputs noisy and inaccurate position measurements (especially in the z-direction). This can be mitigated by further restricting the operating region of the ROV and/or lowering the weight of the camera-based position measurements relative to the accelerometer measurements in the Kalman filter.

8.6 Conclusion

In this chapter, we have proposed an adaptive hybrid feedback control law for marine vehicles. The control law tracks a hybrid reference system constructed from a parametrized loop and a speed assignment for the motion along the path and achieves global asymptotic tracking of the loop at a time-varying desired speed. The proposed hybrid feedback control law was implemented on a scale model tug boat and a remotely operated underwater vehicle, and laboratory experiments have demonstrated the effectiveness of the proposed control law.

Chapter 9

Adaptive Synergistic Feedback Control for Multirotors

In this chapter, we consider the problem of global asymptotic position and heading tracking for multirotors. To this end, we design an adaptive hybrid feedback control law by employing a tuning function-based backstepping procedure. In our proposed approach, we utilize some of the ideas from Chapter 8 in the design of the control law for the translational subsystem. Finally, we demonstrate the effectiveness of the hybrid control law in experiments on a quadrotor.

The material in this chapter is based on [61].

9.1 Introduction

Multirotor unmanned aerial vehicles (UAVs) have become increasingly popular in recent years. Their low-cost, vertical take-off and landing, and hovering abilities make them well suited to perform a wide variety of tasks, such as inspection [111], parcel delivery [112], surveillance, mapping and even autonomous recovery of fixed-wing UAVs [113].

Multirotors are typically designed with co-planar propellers. Although such systems have full torque actuation, forces can only be produced along a single vehicle-fixed axis, known as the thrust axis. Since the propulsion system cannot produce an arbitrary three-dimensional force vector, these systems are underactuated mechanical systems. Due to the underactuation of the system, position and orientation tasks cannot be fully decoupled. Instead, control algorithms for quadrotors often employ a cascaded structure consisting of an inner- and outer-loop control law for orientation and position control, respectively [114]. For such schemes, the outer position control loop often computes a desired three-dimensional force. The norm of this vector then serves as the thrust input, while the vehicle orientation is controlled such that the thrust direction of the vehicle is aligned with the desired force direction in the inertial frame. This is the approach we will take in this chapter.

There is an extensive amount of literature on the subject of trajectory tracking for multirotor UAVs, and the reader is referred to the surveys [115, 116] and the references therein. The following review is limited to earlier works on geometric

control of multirotors, that is, the development of control laws based on quaternion or rotation matrix feedback. The control law proposed in [117] guarantees local exponential tracking for multirotors that can produce both negative and positive thrust along the thrust axis. An adaptive position tracking control scheme for underactuated multirotors is proposed in [118]. However, the control law does not enable a desired heading to be tracked. Moreover, the adaptive control law is overparametrized.

The aforementioned approaches rely on continuous state-feedback. However, the non-contractibility of the configuration space of a rigid body implies that these control laws are at most almost globally stabilizing [32]. This is referred to as a topological obstruction to global asymptotic stability, and can be overcome by employing hybrid feedback with a properly defined switching logic[33]. The hybrid feedback approach in [119] achieves global asymptotic position tracking using the thrust and angular velocity as inputs. However, by using a reduced orientation control approach, the rotation angle around the thrust axis is left uncontrolled. A saturated tracking control law for a quadrotor in the presence of unknown constant disturbances is developed in [120]. The control law ensures that the position error is contained in an arbitrarily small neighborhood of the origin, but leaves the heading uncontrolled and does not ensure convergence of the position and linear velocity errors to zero. In [38], the hybrid quaternion feedback strategy from [37] is employed together with the results on backstepping of hybrid feedback laws from [42] to synthesize a hybrid feedback control law that achieves global asymptotic tracking of a smooth position reference trajectory while minimizing the rotation angle to a given orientation configuration. Moreover, the controller includes an integral/adaptive term and is shown to work in the presence of additive disturbances in the translational dynamics. However, stability of the translational subsystem is shown using a Lyapunov function with a cross term which results in a complicated expression for the gradient, and hence, the virtual backstepping control law. Moreover, due to the construction of the desired rotation matrix, a desired heading (specified by a basic rotation matrix around the z-axis) can only be tracked provided that the roll and pitch angles are zero. Furthermore, the control law is overparametrized, as the number of parameter estimates is three times larger than the number of unknown parameters. Consequently, if the control law in [38] were to be extended to the case of a constant disturbance in the rotational dynamics, parameter convergence would be impossible. Another hybrid feedback approach is introduced in [121]. This approach achieves robust global trajectory tracking for multirotors. However, due to a lack of integral action, the tracking errors do not converge to zero in the presence of disturbances.

The goal of this chapter is to achieve uniform global asymptotic tracking of both the position and heading of a multirotor in the presence of unknown constant disturbances in both the translational and rotational dynamics. To this end, we build on the work in [38], which we extend as follows. First, we propose a novel bounded adaptive control law for the translational subsystem, which leads to a simpler virtual control law when backstepping. Second, we propose a novel construction for the desired rotation matrix, which avoids the use of intermediary Euler angles, and is crucial in ensuring global asymptotic tracking of the desired heading reference. Third, we augment the rotational dynamics with a constant disturbance, and by

employing tuning functions [60], the number of parameter estimates becomes equal to the number of unknown parameters. As a consequence, we can show that the disturbance estimates in both the translational and rotational dynamics converge to their true values.

This chapter is organized as follows. In Section 9.2, we introduce the equations of motion and give the problem statement. Section 9.3 introduces a bounded adaptive control law for the translational subsystem, before extending this control law using a backstepping approach to account for the rotational dynamics. Finally, Section 9.4 presents experimental results verifying the theoretical developments, before Section 9.5 concludes the chapter.

9.2 Modeling and Problem Statement

Let $p \in \mathbb{R}^3$ denote the position of the vehicle in the inertial frame and let $R \in \mathrm{SO}(3)$ denote the orientation of the vehicle-fixed frame with respect to the inertial frame. Additionally, we define the heading relative to the inertial frame as $\nu \coloneqq \frac{1}{|(R_{11},R_{21})|}(R_{11},R_{21}) \in \mathbb{S}$ for $|(R_{11},R_{21})| \neq 0$. Furthermore, let $v \in \mathbb{R}^3$ and $\omega \in \mathbb{R}^3$ denote the linear and angular velocites of the vehicle in the inertial and vehicle-fixed frames, respectively. The equations of motion for a multirotor are given by [114]

$$\dot{p} = v \tag{9.1a}$$

$$\dot{R} = R\omega_\times \tag{9.1b}$$

$$m\dot{v} = -Re_3 f + mge_3 + b \tag{9.1c}$$

$$\mathcal{I}\dot{\omega} = -\omega_\times \mathcal{I}\omega + \mu + \theta, \tag{9.1d}$$

where $b, \theta \in \mathbb{R}^3$ are constant disturbances, $m > 0$ is the mass of the vehicle, $g > 0$ is the gravitational acceleration, $\mathcal{I} \in \mathbb{R}^{3\times 3}$ is the vehicle inertia matrix, $f \in \mathbb{R}$ is the total thrust generated by the rotors and $\mu \in \mathbb{R}^3$ is the total torque generated by the rotors in the vehicle-fixed frame.

Assumption 9.1. *The disturbances b, θ are upper and lower bounded by known constants $\overline{b}, \overline{\theta} \in \mathbb{R}^3$ and $\underline{b}, \underline{\theta} \in \mathbb{R}^3$, respectively.*

Clearly, Assumption 9.1 implies that the disturbances are contained in the convex sets

$$\mathcal{P} \coloneqq [\underline{b}_1, \overline{b}_1] \times [\underline{b}_2, \overline{b}_2] \times [\underline{b}_3, \overline{b}_3], \tag{9.2}$$

$$\Theta \coloneqq [\underline{\theta}_1, \overline{\theta}_1] \times [\underline{\theta}_2, \overline{\theta}_2] \times [\underline{\theta}_3, \overline{\theta}_3]. \tag{9.3}$$

Let $\overline{\mathrm{Proj}} : \mathbb{R}^3 \times \mathcal{S} \rightrightarrows \mathbb{R}^3$ be the outer semicontinuous, convex-valued and locally bounded set-valued mapping defined by

$$\overline{\mathrm{Proj}}(\sigma, s) \coloneqq (\overline{\mathrm{proj}}(\sigma_1, s_1), \overline{\mathrm{proj}}(\sigma_2, s_2), \overline{\mathrm{proj}}(\sigma_3, s_3)), \tag{9.4}$$

where $\underline{s}, \overline{s} \in \mathbb{R}^3$ and $\mathcal{S} \coloneqq [\underline{s}_1, \overline{s}_1] \times [\underline{s}_2, \overline{s}_2] \times [\underline{s}_3, \overline{s}_3] \subset \mathbb{R}^3$ and

$$\overline{\mathrm{proj}}(\sigma_i, s_i) \coloneqq \begin{cases} \sigma_i, & \text{if } \sigma_i \in \mathrm{T}_{[\underline{s}_i, \overline{s}_i]}(s_i) \\ [0,1]\sigma_i, & \text{if } \sigma_i \notin \mathrm{T}_{[\underline{s}_i, \overline{s}_i]}(s_i) \end{cases} \tag{9.5}$$

where the tangent cone $\mathrm{T}_{[\underline{a},\overline{a}]} : [\underline{a},\overline{a}] \rightrightarrows \mathbb{R}$ is defined by

$$\mathrm{T}_{[\underline{a},\overline{a}]}(\varphi) \coloneqq \begin{cases} [0,\infty), & \text{if } \varphi = \underline{a} \\ (-\infty,\infty), & \text{if } \varphi \in (\underline{a},\overline{a}) \\ (-\infty,0], & \text{if } \varphi = \overline{a} \end{cases} \tag{9.6}$$

for $\underline{a},\overline{a} \in \mathbb{R}$. Observe that the solutions to the constrained differential inclusion

$$\dot{s} \in \overline{\mathrm{Proj}}(\sigma, s), \quad s \in \mathcal{S}, \tag{9.7}$$

where σ is a hybrid input [122], include solutions arrived at if the discontinuous projection

$$\mathrm{proj}(\sigma_i, s_i) \coloneqq \begin{cases} \sigma_i, & \text{if } \sigma_i \in \mathrm{T}_{[\underline{s}_i,\overline{s}_i]}(s_i) \\ 0, & \text{if } \sigma_i \notin \mathrm{T}_{[\underline{s}_i,\overline{s}_i]}(s_i) \end{cases} \tag{9.8}$$

would have been used instead. As a result, there always exists a flow direction contained in $\overline{\mathrm{Proj}}(\sigma, s)$ that steers s within $\mathcal{S}$, i.e. $\overline{\mathrm{Proj}}(\sigma, s) \cap \mathrm{T}_{\mathcal{S}}(s) \neq \emptyset$ for all $s \in \mathcal{S}$, where $\mathrm{T}_{\mathcal{S}}(s) = \mathrm{T}_{[\underline{s}_1,\overline{s}_1]}(s_1) \times \mathrm{T}_{[\underline{s}_2,\overline{s}_2]}(s_2) \times \mathrm{T}_{[\underline{s}_3,\overline{s}_3]}(s_3)$. Therefore, since $\mathcal{S}$ is compact, every maximal solution to (9.7) is complete [55, Proposition 6.10].

Lemma 9.1. *Let $s, \hat{s} \in \mathcal{S}$, $\tilde{s} = s - \hat{s}$ denote the estimation error and $\Gamma \in \mathbb{R}^{3\times 3}$ be a positive definite and diagonal matrix. Then*

$$-\langle \tilde{s}, \Gamma^{-1}\overline{\mathrm{Proj}}(\sigma, \hat{s})\rangle \leq -\langle \tilde{s}, \Gamma^{-1}\sigma\rangle. \tag{9.9}$$

Proof. If $\underline{s} < \hat{s} < \overline{s}$, or if $\hat{s} \in \mathcal{S}$ and $\sigma \in \mathrm{T}_{\mathcal{S}}(s)$, it follows that $\overline{\mathrm{Proj}}(\sigma, \hat{s}) = \sigma$ and (9.9) is satisfied with equality. Since Γ is diagonal with positive entries, we only have to verify (9.9) componentwise for the case $\hat{s}_i \in \{\underline{s}_i, \overline{s}_i\}$ and $\sigma_i \notin \mathrm{T}_{[\underline{s}_i,\overline{s}_i]}(s_i)$. Observe that $\hat{s}_i = \overline{s}_i$ and $\sigma_i \notin \mathrm{T}_{[\underline{s}_i,\overline{s}_i]}(s_i)$ implies that $\sigma_i > 0$ and $\tilde{s} \leq 0$. Similarly, $\hat{s}_i = \underline{s}_i$ and $\sigma_i \notin \mathrm{T}_{[\underline{s}_i,\overline{s}_i]}(s_i)$ implies that $\sigma_i < 0$ and $\tilde{s}_i \geq 0$. In both cases it follows that

$$\begin{aligned} -\langle \tilde{s}_i, \Gamma_i^{-1}\sigma_i\rangle &\geq -\langle \tilde{s}_i, \Gamma_i^{-1}[0,1]\sigma_i\rangle \\ &= -\langle \tilde{s}_i, \Gamma_i^{-1}\overline{\mathrm{proj}}(\sigma_i, s_i)\rangle \geq 0. \end{aligned} \tag{9.10}$$

□

A desired trajectory for the multirotor consists of a desired position $p_d : \mathbb{R}_{\geq 0} \to \mathbb{R}^3$ of the multirotor relative to the inertial frame, and a desired heading $\nu_d : \mathbb{R}_{\geq 0} \to \mathbb{S}$ of the multirotor relative to the inertial frame. Given a continuously differentiable desired heading ν_d, the quantity $\dot{\nu}_d$ can always be expressed in terms of the scalar desired heading rate $\varpi_d(t) \coloneqq \langle S\nu_d(t), \dot{\nu}_d(t)\rangle$. Then, $\dot{\nu}_d(t) = S\nu_d(t)\varpi_d(t)$.

Assumption 9.2. *The desired position p_d and its derivatives up to the fourth order are bounded and continuous. The desired heading ν_d and its derivatives up to the second order are bounded and continuous. The bias b is lower and upper bounded by the constants $\underline{b}$ and $\overline{b}$, respectively. Finally, it holds that*

$$m(g - \sup_{t\geq 0} \ddot{p}_{d,3}(t)) + \underline{b}_3 \coloneqq c > 0. \tag{9.11}$$

Let $\chi = (p_d, \dot{p}_d, \ddot{p}_d, p_d^{(3)}, \nu_d, \varpi_d)$. For every desired trajectory satisfying Assumption 9.2, there exist scalars $c_1 \geq 0$, $c_2 \geq 0$ and a compact set $\Omega \subset \mathbb{R}^3 \times \mathbb{R}^3 \times \mathbb{R}^3 \times \mathbb{R}^3 \times \mathbb{S} \times \mathbb{R}$ such that the desired trajectory is a solution to the differential inclusion

$$\dot{\chi} \in F(\chi) \coloneqq (\dot{p}_d, \ddot{p}_d, p_d^{(3)}, c_1 \mathbb{B}^3, S\nu_d \varpi_d, c_2 \mathbb{B}^1), \chi \in \Omega. \tag{9.12}$$

Assumption 9.2 is relatively mild, seeing as the supremum of the desired acceleration in the z-direction is often small compared to the gravitational acceleration. When the z-component of the desired acceleration is zero and $\underline{b}_3$ is negative, we require that the absolute value of the lower bound of the z-component of the disturbance force is smaller than the gravitational force.

Let $R_d \in \mathrm{SO}(3)$ denote the desired orientation, which will be defined in Section 9.3. The desired angular velocity is given by $(\omega_d)^\wedge \coloneqq R_d^{-1} \dot{R}_d$, and by introducing the error coordinates $\tilde{p} \coloneqq p - p_d$, $\tilde{v} \coloneqq v - \dot{p}_d$, $\tilde{R} \coloneqq R R_d^\mathsf{T}$ and $\tilde{\omega} \coloneqq \omega - \omega_d$, we obtain the error system

$$\left.\begin{aligned} \dot{\tilde{p}} &= \tilde{v} \\ \dot{\tilde{R}} &= \tilde{R}(R_d \tilde{\omega})^\wedge \\ m\dot{\tilde{v}} &= mge_3 - Re_3 f - m\ddot{p}_d + b \\ \mathcal{I}\dot{\tilde{\omega}} &= \mu - \omega^\wedge \mathcal{I}\omega + \theta - \mathcal{I}\dot{\omega}_d \\ \dot{\chi} &\in F(\chi) \end{aligned}\right\} \quad \chi \in \Omega \tag{9.13}$$

Problem statement

Design a hybrid feedback control law with output $(f, \mu) \in \mathbb{R} \times \mathbb{R}^3$ such that the compact set

$$\mathcal{A}_0 = \left\{ (\tilde{p}, \tilde{R}, \tilde{v}, \tilde{\omega}, \chi) : \tilde{p} = 0, \tilde{R} = I, \tilde{v} = 0, \tilde{\omega} = 0 \right\}, \tag{9.14}$$

is globally pre-asymptotically stable for the system (9.13).

9.3 Control Design

As introduced in Chapter 8 for fully actuated marine vehicles, we define a modified velocity error $\xi \coloneqq \tilde{v} - \zeta$, where ζ is generated by the dynamical system

$$\Lambda \dot{\zeta} = -k_1 \vartheta(\tilde{p}) - \Xi \vartheta(\zeta), \tag{9.15}$$

where $\Xi, \Lambda \in \mathbb{R}^{3\times 3}$ are positive definite and diagonal, $k_1 > 0$ and $\vartheta : \mathbb{R}^n \to \mathbb{R}^n$ denotes the following saturation mapping

$$\vartheta(x) \coloneqq \frac{\tanh|x|}{|x|} x. \tag{9.16}$$

It is clear that $\zeta = 0$ implies $\xi = \tilde{v}$, which entails that the velocity tracking control objective $\tilde{v} = 0$ can be restated as $(\xi, \zeta) = 0$. We propose the following adaptive

control law for the translational subsystem

$$\left.\begin{aligned} \Lambda\dot{\zeta} &= -k_1\vartheta(\tilde{p}) - \Xi\vartheta(\zeta) \\ \dot{\hat{b}} &\in \overline{\mathrm{Proj}}(\Gamma\xi, \hat{b}) \\ u &= \hat{b} + mge_3 - m(\dot{\zeta} + \ddot{p}_d) + k_1\vartheta(\tilde{p}) + K\vartheta(\xi) \\ f &= |u| \end{aligned}\right\} \qquad \hat{b} \in \mathcal{P}$$

where $\hat{b}$ denotes the estimate of the disturbance b and $K \in \mathbb{R}^{3\times 3}$ is positive definite and diagonal.

Given a desired heading ν_d and a desired thrust direction $\rho := \frac{u}{|u|} \in \mathbb{S}^2$, we define the desired vehicle orientation by

$$R_d := \begin{pmatrix} r & \rho_\times r & \rho \end{pmatrix} \tag{9.17}$$

$$r := \frac{\operatorname{sgn}\rho_3}{\sqrt{\rho_3^2 + (\rho_1\nu_{d,1} + \rho_2\nu_{d,2})^2}} \begin{pmatrix} \rho_3\nu_d \\ -\rho_1\nu_{d,1} - \rho_2\nu_{d,2} \end{pmatrix}. \tag{9.18}$$

Moreover, by defining $w := (\rho, r)$, the desired angular velocity can be computed according to

$$\omega_d = \begin{pmatrix} r^\mathsf{T}\rho^\wedge\dot{\rho} \\ r^\mathsf{T}\dot{\rho} \\ -r^\mathsf{T}\rho^\wedge\dot{r} \end{pmatrix} = \begin{pmatrix} r^\mathsf{T}\rho^\wedge & 0 \\ r^\mathsf{T} & 0 \\ 0 & -r^\mathsf{T}\rho^\wedge \end{pmatrix} \begin{pmatrix} \dot{\rho} \\ \dot{r} \end{pmatrix} =: A(w)\dot{w}. \tag{9.19}$$

Observe that R_d is well-defined for any $\nu_d \in \mathbb{S}$ and $\rho \in \mathbb{S}^2$ provided $\rho_3 \neq 0$. The desired orientation aligns the thrust axis of the multirotor with the desired thrust direction ρ. The vector $r \in \mathbb{S}^2$ should be interpreted as the desired configuration of the vehicle-fixed x-axis of the multirotor expressed in the inertial frame. It is chosen such that its projection onto the horizontal plane is aligned with the desired heading. Note that R_d as defined in (9.17) can also be constructed using the approach in [123]. However, [123] employs an intermediary step in which the desired roll and pitch angles are computed as a function of ρ and the desired yaw angle. Although a direct computation of the desired roll-pitch-yaw angles are required for any control algorithm based on a three-parameter representation of SO(3), it is unnecessary for any control scheme based on rotation matrix or quaternion feedback. Also, note that the approach in [117] does not yield the same R_d as (9.17) and only guarantees that the vehicle-fixed x-axis converges to the projection of the desired body-fixed x-axis onto the plane orthogonal to ρ.

Let $z = (\eta, \epsilon) \in \mathbb{S}^3$ be a unit quaternion satisfying $\mathcal{R}(z) = \tilde{R}$. Since z is not measured, we employ the path-lifting mechanism proposed in [109] in order to lift the solution $t \mapsto \tilde{R}(t)$ of $\dot{\tilde{R}} = \tilde{R}(R_d\tilde{\omega})^\wedge$ to a continuous path $t \mapsto z(t)$ that satisfies the kinematic equation

$$\dot{z} = \frac{1}{2} \begin{pmatrix} \epsilon^\mathsf{T} \\ \eta I_3 + \epsilon^\wedge \end{pmatrix} R_d\tilde{\omega} =: T(z)R_d\tilde{\omega}. \tag{9.20}$$

If ω_d were entirely known, it would be straightforward to design a backstepping control law using the angular velocity error as the virtual control input. However,

due to the presence of the constant disturbance b in the translational dynamics, the following part of ω_d is problematic

$$A(w)\Big(\frac{\partial w}{\partial u}\dot{\hat{b}} + \frac{1}{m}\frac{\partial w}{\partial u}\frac{\partial u}{\partial \xi}\tilde{b}\Big). \tag{9.21}$$

Although the first term is known, it cannot be canceled without increasing the dynamic order of the system. In other words, we would need two additional estimators for the same bias due to its appearance in ω_d and $\dot{\omega}_d$. Note that this is the approach taken in [38]. To circumvent this, we will follow a tuning function based design procedure. For $i \in \{2, 3\}$, we define β_i as the known part of ω_d with $\dot{\hat{b}}$ replaced by $\Gamma\tau_i$

$$\beta_i \coloneqq \omega_d - A(w)\left(\frac{\partial w}{\partial u}\dot{\hat{b}} + \frac{1}{m}\frac{\partial w}{\partial u}\frac{\partial u}{\partial \xi}\tilde{b}\right) + A(w)\frac{\partial w}{\partial u}\Gamma\tau_i, \tag{9.22}$$

which can be rewritten as

$$\begin{aligned}\beta_i = A(w)\frac{\partial w}{\partial u}\Big(&\Gamma\tau_i - m(\ddot{\zeta} + p_d^{(3)}) + k_1 J(\tilde{p})\tilde{v} \\ &+ KJ(\xi)\big(ge_3 - \ddot{p}_d - \dot{\zeta} + \frac{1}{m}(\hat{b} - \mathcal{R}(z)u)\big)\Big) + A(w)\frac{\partial w}{\partial \nu_d}\dot{\nu}_d\end{aligned} \tag{9.23}$$

where τ_i is the ith tuning function and $J(\varepsilon) \coloneqq \frac{\partial \vartheta(\varepsilon)}{\partial \varepsilon}$. Let $q \in \mathcal{Q} \coloneqq \{-1, 1\}$ be a logic variable, let $k_2, k_z > 0$ and define the virtual control input α by

$$\alpha_q \coloneqq \beta_2 + qR_d^{\mathsf{T}}h, \tag{9.24}$$

$$h = -k_2 k_z \epsilon + \frac{2}{k_z}((\eta I + \epsilon^\wedge)u)^\wedge \xi. \tag{9.25}$$

Furthermore, following the tuning function-based backstepping approach in [60], we define the tuning functions

$$\tau_1 \coloneqq \xi \tag{9.26}$$

$$\tau_2 \coloneqq \tau_1 - \frac{k_z q}{m}\left(\frac{\partial u}{\partial \xi}\right)^{\mathsf{T}}\left(\frac{\partial w}{\partial u}\right)^{\mathsf{T}} A(w)^{\mathsf{T}} R_d^{\mathsf{T}}\epsilon \tag{9.27}$$

$$\tau_3 \coloneqq \tau_2 - W(x)\mathcal{I}(\omega - \alpha_q), \tag{9.28}$$

$$\begin{aligned}W(x) \coloneqq \frac{1}{m}\Bigg(&\left(\frac{\partial u}{\partial \xi}\right)^{\mathsf{T}}\left(\frac{\partial w}{\partial u}\right)^{\mathsf{T}}\left(\frac{\partial \beta_2}{\partial w}\right)^{\mathsf{T}} + \left(\frac{\partial u}{\partial \xi}\right)^{\mathsf{T}}\left(\frac{\partial \beta_2}{\partial u}\right)^{\mathsf{T}} + \left(\frac{\partial \beta_2}{\partial \tilde{v}}\right)^{\mathsf{T}} \\ &+ \left(\frac{\partial \beta_2}{\partial \xi}\right)^{\mathsf{T}} - \left(\frac{\partial u}{\partial \xi}\right)^{\mathsf{T}}\left(\frac{\partial w}{\partial u}\right)^{\mathsf{T}} A(w)^{\mathsf{T}} R_d^{\mathsf{T}} T(z)^{\mathsf{T}}\left(\frac{\partial \beta_2}{\partial z}\right)^{\mathsf{T}} \\ &+ \frac{k_z q}{m}\left(\frac{\partial u}{\partial \xi}\right)^{\mathsf{T}}\left(\frac{\partial w}{\partial u}\right)^{\mathsf{T}} A(w)^{\mathsf{T}}(R_d^{\mathsf{T}}\epsilon)^\wedge A(w)\frac{\partial w}{\partial u}\frac{\partial u}{\partial \xi}\Gamma\left(\frac{\partial w}{\partial u}\right)^{\mathsf{T}} A(w)^{\mathsf{T}} \\ &+ q\left(\frac{\partial u}{\partial \xi}\right)^{\mathsf{T}}\left(\frac{\partial h}{\partial u}\right)^{\mathsf{T}} R_d - q\left(\frac{\partial u}{\partial \xi}\right)^{\mathsf{T}}\left(\frac{\partial w}{\partial u}\right)^{\mathsf{T}} A(w)^{\mathsf{T}}(R_d^{\mathsf{T}}h)^\wedge \\ &+ q\left(\frac{\partial h}{\partial \xi}\right)^{\mathsf{T}} R_d - q\left(\frac{\partial u}{\partial \xi}\right)^{\mathsf{T}}\left(\frac{\partial w}{\partial u}\right)^{\mathsf{T}} A(w)^{\mathsf{T}} R_d^{\mathsf{T}} T(z)^{\mathsf{T}}\left(\frac{\partial h}{\partial z}\right)^{\mathsf{T}} R_d\Bigg).\end{aligned}$$

Define the state space $\mathcal{X} \coloneqq \mathbb{R}^3 \times \mathbb{S}^3 \times \mathbb{R}^3 \times \mathbb{R}^3 \times \mathbb{R}^3 \times \mathcal{P} \times \Theta \times \Omega$, the state vector $x \coloneqq (\tilde{p}, z, \xi, \zeta, \tilde{\omega}, \tilde{b}, \hat{\theta}, \chi)$, where $\hat{\theta}$ denotes the estimate of θ, and the flow and jump sets

$$C \coloneqq \{(x, q) \in \mathcal{X} \times \mathcal{Q} : q\Psi(x) \geq -\delta\}, \tag{9.29}$$
$$D \coloneqq \{(x, q) \in \mathcal{X} \times \mathcal{Q} : q\Psi(x) \leq -\delta\}, \tag{9.30}$$

where $\delta \in (0, 1)$ is the hysteresis half-width, and

$$\Psi(x) \coloneqq \eta + \frac{1}{2k_z}(\omega - \beta_2 + A(w)\frac{\partial w}{\partial u}\Gamma(\tau_2 - \tau_1))^{\mathsf{T}}\mathcal{I}o(x) \tag{9.31}$$
$$o(x) \coloneqq R_d^{\mathsf{T}}h - \frac{k_z}{m}A(w)\frac{\partial w}{\partial u}\Gamma\left(\frac{\partial u}{\partial \xi}\right)^{\mathsf{T}}\left(\frac{\partial w}{\partial u}\right)^{\mathsf{T}}A(w)^{\mathsf{T}}R_d^{\mathsf{T}}\epsilon. \tag{9.32}$$

Consider the following hybrid control law

$$\begin{cases} \left.\begin{aligned} \dot{\zeta} &= -\Lambda^{-1}\left(k_1\vartheta(\tilde{p}) + \Xi\vartheta(\zeta)\right) \\ \dot{\tilde{b}} &\in \overline{\mathrm{Proj}}(\Gamma\tau_3, \hat{b}) \\ \dot{\hat{\theta}} &\in \overline{\mathrm{Proj}}(\Gamma_2(\omega - \alpha_q), \hat{\theta}) \end{aligned}\right\} & (x, q) \in C \\ q^+ = -q & (x, q) \in D \\ u = \hat{b} + mge_3 - m(\dot{\zeta} + \ddot{p}_d) + k_1\vartheta(\tilde{p}) + K\vartheta(\xi) \\ f = |u| \\ \mu = -\hat{\theta} + \omega^\wedge\mathcal{I}\omega - K_2(\omega - \alpha_q) - qk_zR_d^{\mathsf{T}}\epsilon \\ \quad + \mathcal{I}\gamma_q - qk_z\mathcal{I}W(x)^{\mathsf{T}}\Gamma\left(\frac{\partial w}{\partial u}\right)^{\mathsf{T}}A(w)^{\mathsf{T}}R_d^{\mathsf{T}}\epsilon \end{cases} \tag{9.33}$$

where $K_2 = K_2^{\mathsf{T}} \in \mathbb{R}^{3\times3}$ is positive definite and

$$\begin{aligned} \gamma_q \coloneqq &\left(\frac{\partial\beta_2}{\partial w}\frac{\partial w}{\partial u} + \frac{\partial\beta_2}{\partial u}\right)(\dot{u} - \frac{1}{m}KJ(\xi)\tilde{b}) + \frac{\partial\beta_2}{\partial z}T(z)R_d(\omega - \beta_3) \\ &+ \frac{\partial\beta_2}{\partial\tilde{v}}(\dot{\tilde{v}} - \frac{1}{m}\tilde{b}) + \frac{\partial\beta_2}{\partial\xi}(\dot{\xi} - \frac{1}{m}\tilde{b}) + \frac{\partial\beta_2}{\partial y}\dot{y} + \frac{\partial\beta_2}{\partial\hat{b}}\dot{\hat{b}} \\ &- \frac{k_zq}{m}A(w)\frac{\partial w}{\partial u}\Gamma\left(\frac{\partial u}{\partial\xi}\right)^{\mathsf{T}}\left(\frac{\partial w}{\partial u}\right)^{\mathsf{T}}A(w)^{\mathsf{T}}(R_d^{\mathsf{T}}\epsilon)^\wedge\beta_3 + q(R_d^{\mathsf{T}}h)^\wedge\beta_3 \\ &+ qR_d^{\mathsf{T}}\frac{\partial h}{\partial z}T(z)R_d(\omega - \beta_3) + \frac{1}{m}A(w)\frac{\partial w}{\partial u}KJ(\xi)\mathcal{R}(z)u^\wedge(\omega - \beta_3), \end{aligned} \tag{9.34}$$

where $y \coloneqq (\tilde{p}, \zeta, p_d^{(3)}, \nu_d, \varpi_d)$. The hybrid control law (9.33) leads to the following

hybrid closed-loop system

$$\mathcal{H}:\begin{cases}\left.\begin{aligned}\dot{\tilde{p}} &= \mathcal{R}(z)\tilde{v}\\ \dot{z} &= T(z)\tilde{\omega}\\ \dot{\xi} &= ge_3 - \ddot{p}_d - \dot{\zeta} + \frac{1}{m}\Big(b - \mathcal{R}(z)u\Big)\\ \dot{\zeta} &= -\Lambda^{-1}(k_1\vartheta(\tilde{p}) + \Xi\vartheta(\zeta))\\ \dot{\tilde{\omega}} &= \kappa(x)\\ \dot{\hat{b}} &\in \overline{\mathrm{Proj}}(\Gamma\tau_3, \hat{b})\\ \dot{\hat{\theta}} &\in \overline{\mathrm{Proj}}(\Gamma_2(\omega - \alpha_q), \hat{\theta})\\ \dot{\chi} &\in F(\chi)\end{aligned}\right\} & (x,q) \in C\\ q^+ = -q & (x,q) \in D\end{cases} \tag{9.35}$$

where

$$\kappa(x) = \tilde{\theta} + \gamma_q - \dot{\omega}_d - \mathcal{I}^{-1}K_2(\omega - \alpha_q) - qk_z\mathcal{I}^{-1}\Big(I + \mathcal{I}W^\mathsf{T}\Gamma\left(\frac{\partial w}{\partial u}\right)^\mathsf{T}A^\mathsf{T}\Big)R_d^\mathsf{T}\epsilon. \tag{9.36}$$

Theorem 9.3. *If Assumptions 9.1 and 9.2 hold and the gains satisfy*

$$k_1 + K_{33} + mk_1\frac{1}{\Lambda_{33}} + m\frac{\Xi_{33}}{\Lambda_{33}} < c, \tag{9.37}$$

with c defined as in Assumption 9.2, then there exists $\varsigma > 0$ such that $\rho_3 \geq \varsigma$ for all solutions to $\mathcal{H}$, and the compact set

$$\mathcal{A} = \{(x,q) \in \mathcal{X} \times \mathcal{Q} : \tilde{p} = 0, z = qe_1, \xi = 0, \zeta = 0, \hat{b} = b, \tilde{\omega} = 0, \hat{\theta} = \theta\}, \tag{9.38}$$

is globally pre-asymptotically stable for $\mathcal{H}$.

Proof. It follows from Assumption 9.2, equations (9.37) and (9.33) that $u_3(t,j) \geq \inf_{(t,j)} u_3(t,j) > 0$. Therefore, there exists $\varsigma' > 0$ such that $u_3(t,j) \geq \varsigma'$ for all (t,j) in the hybrid time domain of the solution. Since u is bounded, it follows that there exists $\varsigma > 0$ such that $\rho_3(t,j) = \frac{u_3(t,j)}{|u(t,j)|} \geq \varsigma$. Let $\mathcal{U}$ be an open set containing $\mathcal{X}$ and consider the continuously differentiable function $V : \mathcal{U} \times \mathcal{Q} \to \mathbb{R}$ defined by

$$\begin{aligned}V(x,q) \coloneqq\ & k_1 \ln\cosh|\tilde{p}| + \frac{m}{2}\xi^\mathsf{T}\xi + \frac{1}{2}\zeta^\mathsf{T}\Lambda\zeta + \frac{1}{2}\tilde{b}^\mathsf{T}\Gamma^{-1}\tilde{b}\\ &+ \frac{1}{2}\tilde{\theta}^\mathsf{T}\Gamma_2^{-1}\tilde{\theta} + 2k_z(1 - q\eta) + \frac{1}{2}(\omega - \alpha_q)^\mathsf{T}\mathcal{I}(\omega - \alpha_q).\end{aligned}$$

For all $(x,q) \in C$, the change in V along the solutions of $\mathcal{H}$ can be shown to be

$$\begin{aligned}\dot{V}(x,q) \leq\ & -\xi^\mathsf{T}K\vartheta(\xi) - \zeta^\mathsf{T}\Xi\vartheta(\zeta) - k_zk_2\epsilon^\mathsf{T}\epsilon\\ & - (\omega - \alpha_q)^\mathsf{T}K_2(\omega - \alpha_q) \leq 0.\end{aligned}$$

Figure 9.1: ModalAI Qualcomm Flight RB5

Consequently, the growth of V along the flow solutions of $\mathcal{H}$ is bounded by

$$u_c(x) = \begin{cases} -\xi^{\mathsf{T}} K \vartheta(\xi) - \zeta^{\mathsf{T}} \Xi \vartheta(\zeta) - k_z k_2 \epsilon^{\mathsf{T}} \epsilon \\ \quad - (\omega - \alpha_q)^{\mathsf{T}} K_2 (\omega - \alpha_q) & x \in C \\ -\infty, & \text{otherwise} \end{cases}$$

For all $(x, q) \in D$, the change in V across jumps is

$$V(x, -q) - V(x, q) = 2k_z q \Psi(x) < 0,$$

where the last inequality follows from the definition of the jump set D. Since the continuously differentiable function V has compact sublevel sets and is positive definite with respect to the compact set $\mathcal{A}$, it follows that $\mathcal{A}$ is uniformly globally stable. Furthermore, $\mathcal{H}$ satisfies the hybrid basic conditions, and the time between jumps is lower bounded by a positive constant. Thus, it follows from [55, Corollary 8.7 (b)] that each solution to $\mathcal{H}$ converges to the largest weakly invariant subset Φ contained in $V^{-1}(\bar{r}) \cap \overline{u_c^{-1}(0)}$, for some $\bar{r} \in \mathbb{R}$, where

$$\overline{u_c^{-1}(0)} = \{(x, q) \in C : \xi = 0, \zeta = 0, \epsilon = 0, \omega = \alpha_q\}.$$

Note that for every $z \in \mathbb{S}^2$, $\epsilon = 0$, implies $\eta = \pm 1$. The closed-loop system $\mathcal{H}$ is such that $\zeta \equiv 0$ implies $\tilde{p} \equiv 0$. Thus, $\xi \equiv 0$ implies that $\tilde{b} \equiv 0$, since $\epsilon = 0$ implies $\mathcal{R}(z) = I$. Finally, $\epsilon \equiv 0$ and $\xi \equiv 0$ imply that $\alpha_q = \beta_2$ and that $\tau_2 \equiv 0$, from which we can conclude that $\omega = \alpha_q = \omega_d$. It follows that $\dot{\tilde{\omega}} \equiv 0$ and hence that $\hat{\theta} = \theta$. Consequently, no solution ϕ makes $V(\phi(t, j))$ equal to a non-zero constant, and it follows from [55, Theorem 8.8] that $\mathcal{A}$ is globally pre-asymptotically stable. □

We remark that Theorem 9.3 implies that the problem statement is solved. Indeed, by employing the path-lifiting mechanism from [109], it follows from [109, Thm. 9] and Theorem 9.3 that $\mathcal{A}_0$ is globally pre-asymptotically stable for the interconnection between (9.13) and (9.33).

9.4 Experimental results

The experimental platform is the ModalAI Qualcomm Flight RB5 depicted in Figure 9.1. The mass of the quadrotor is $m = 1.4\,\text{kg}$, the inertia matrix is $\mathcal{I} =$

$\mathrm{diag}(0.029\,\mathrm{kgm}^2, 0.029\,\mathrm{kgm}^2, 0.052\,\mathrm{kgm}^2)$, the lower and upper bounds for the parameters are given by $\underline{\theta} = (-0.3, -0.12, -0.3)$, $\overline{\theta} = (0.2, 0.2, 0.2)$, $\underline{b} = (-1, -1, -0.3)$, and $\overline{b} = (1, 1, 3)$. Moreover, the reference trajectory is given by

$$p_d(t) = \begin{cases} (0, 0, -0.75) & t < 30 \\ \begin{pmatrix} \sin(0.5(t-30)) \\ 1 - \cos(0.5(t-30)) \\ -0.8 + 0.5(\cos(0.5(t-30)) - 1) \end{pmatrix} & t \geq 30 \end{cases} \tag{9.39}$$

$$\nu_d(t) = (\cos\psi_d(t), \sin\psi_d(t)), \tag{9.40}$$

$$\psi_d(t) = \begin{cases} \frac{\pi}{2} & t < 30 \\ \frac{\pi}{2} - \frac{25\pi}{180}\sin(0.3(t-30)) & t \geq 30 \end{cases} \tag{9.41}$$

and the control parameters are chosen as $k_1 = 2.2$, $K = \mathrm{diag}(2.9, 2.9, 3.3)$, $\Xi = K$, $K_2 = \mathrm{diag}(0.08, 0.08, 0.05)$, $k_z = 3.1$, $k_2 = 1$, $\Lambda = I$, $\Gamma = \mathrm{diag}(0.25, 0.25, 0.52)$ and $\Gamma_2 = 0.05I$. It is straightforward to verify that (9.37) is satisfied. In the implementation, we apply the approximation $\vartheta(x) \approx x$ when $|x| \leq 10^{-6}$. Moreover, we implement the maximal solution to (9.7), which employs the discontinuous projection (9.8), i.e. a componentwise saturation.

The experimental results are presented in Figures 9.2 to 9.5. From Figures 9.2 and 9.3 we observe that the quadrotor successfully tracks the position and velocity references. Figure 9.4 shows that the estimate $\hat{b}_3$ approaches a value of approximately 1.7 N. This suggests that there are minor modelling errors in the mass of the quadrotor and the thrust produced by the propellers. Indeed, as $\hat{b}_3$ approaches its

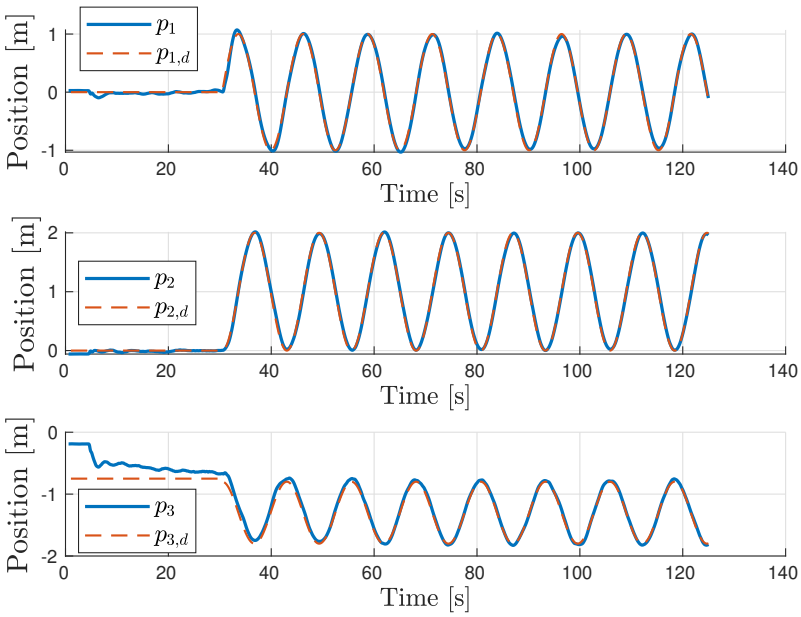

Figure 9.2: The position $p \in \mathbb{R}^3$ and the desired position $p_d \in \mathbb{R}^3$.

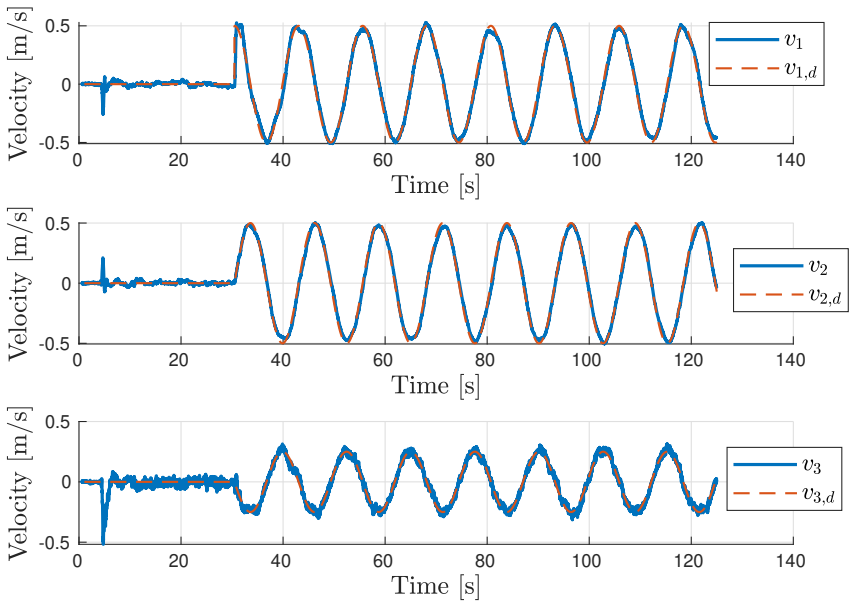

Figure 9.3: The linear velocity v and the desired linear velocity v_d.

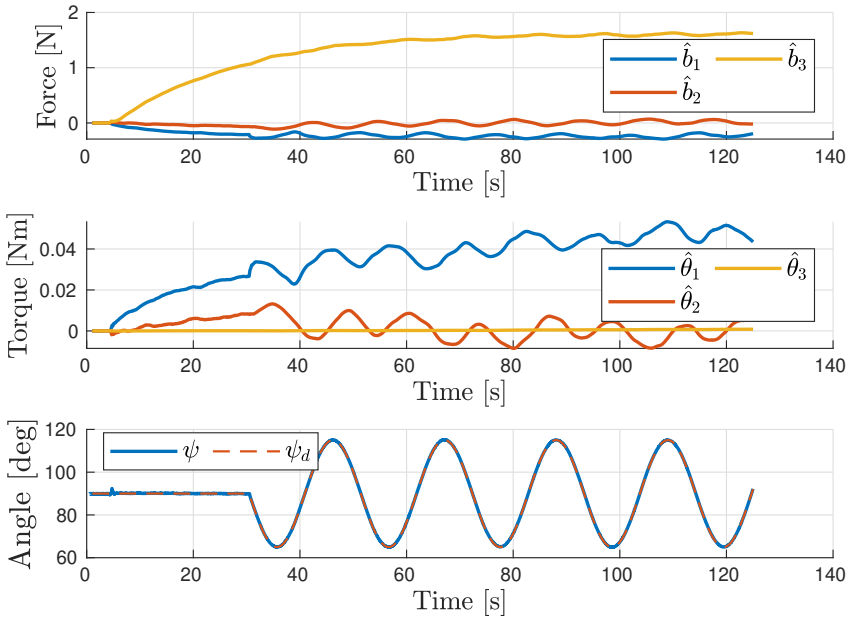

Figure 9.4: The estimates $\hat{b}$ and $\hat{\theta}$ and the yaw angle and desired yaw angle ψ and ψ_d.

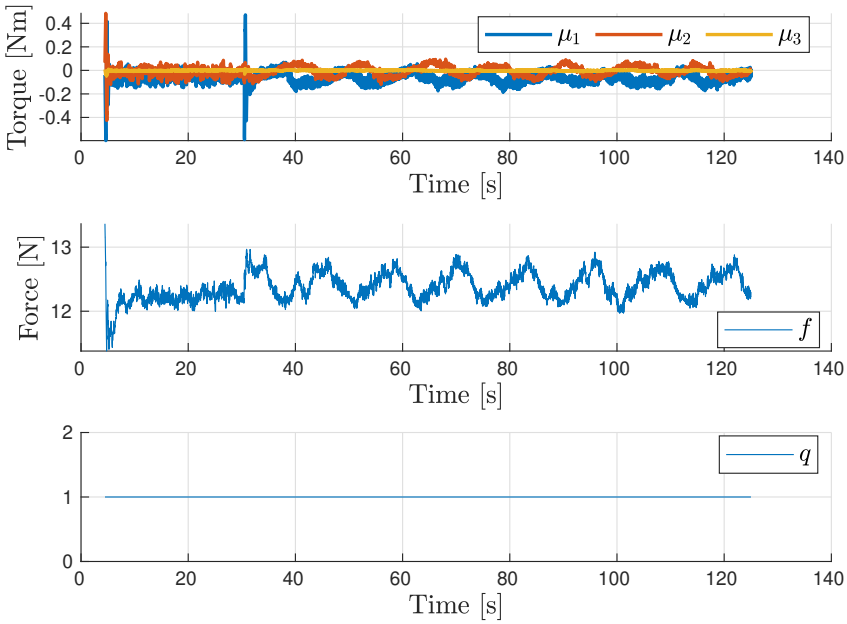

Figure 9.5: The control torque μ, control thrust f and the logic variable q.

steady-state value, we see that p_3 approaches $p_{3,d}$. The estimates $\hat{b}_1$ and $\hat{b}_2$ remain very close to zero. The orientation disturbance $\hat{\theta}_1$ increases to a value of approximately 0.05 Nm. This suggests that there are minor modeling errors in the roll-loop of the quadrotor, most likely in the position of the center of mass and the moments produced by the propellers. The two other orientation disturbances remain small. Moreover, we observe that the yaw angle of the quadrotor $\psi := \text{atan2}(\nu_2, \nu_1)$, successfully tracks the desired yaw angle ψ_d. The desired propeller torque, total propeller thrust, and logic variable q, are plotted in Figure 9.5. The two spikes in the desired torque correspond to lift off and the abrupt change in the desired trajectory at $t = 30$ s, respectively. The logic variable q does not change sign during the motion.

9.5 Conclusions

This chapter has addressed the global position and heading tracking control problem for multirotor aerial vehicles. The proposed control law achieves uniform global asymptotic position and heading tracking. Global asymptotic heading tracking is achieved by utilizing a novel construction of the desired rotation matrix. Moreover, the use of tuning functions ensures that the number of parameter estimates is equal to the number of unknown parameters. In turn, this guarantees that the parameter estimates in both the translational and rotational dynamics converge to their actual values. The effectiveness of the control law has been demonstrated through experiments.

Chapter 10

Conclusions and Future Work

In this thesis, we have proposed new methods for prioritized control of robotic systems and hybrid feedback control of marine and aerial vehicles. A general set-based task-priority framework for redundant robotic systems was introduced in Chapter 3. The framework utilizes a hierarchy of CLF- and CBF-based quadratic programs and provides strict priority between tasks, ensuring that lower-priority tasks have no effect on the execution of higher-priority tasks.

CLF- and CBF-based quadratic programs were employed once more in Chapter 3. By utilizing robustness results for CBFs we obtain safety guarantees for affine nonlinear control systems in the presence of unknown system nonlinearities. We apply this to an ASV to obtain a unified framework for stabilization, reactive collision avoidance and control allocation. Simulation results have demonstrated the effectiveness of the proposed framework.

In Chapter 5, we have proposed multiple synergistic control designs for fully actuated mechanical systems described on matrix Lie groups with left-invariant Riemannian metrics. Specifically, we have proposed synergistic PD, output feedback and PID type control laws ensuring global asymptotic tracking of some desired bounded reference trajectory. Moreover, we have shown that the PID type control laws achieve global asymptotic tracking when the system dynamics are augmented with a constant and unknown disturbance.

The synergistic control laws in Chapter 5 were based on the notion of a synergistic function, also known in the literature as a synergistic potential function. In Chapter 6, our starting point was the notion of a synergistic Lyapunov function and feedback pair, which we have generalized to a synergistic Lyapunov function and feedback triple. This generalization allows the logic variable, which we refer to as a synergy variable in this generalized setting, to possess flow dynamics. By introducing synergy gaps relative to components of product sets, we have shown that it is possible to define jump conditions in the form of synergy gaps for different components of the synergy variable. Finally, we have shown that this generalized definition is amenable to backstepping, and given an example for how traditional synergistic control can be combined with ship maneuvering control with discrete path dynamics.

Hysteretic control Lyapunov functions were introduced in Chapter 7 as a tool

for synthesizing hybrid control laws for continuous-time nonlinear systems with global stability properties. We have shown that HCLFs represent a generalization of the natural concept of a synergistic control Lyapunov function. Moreover, we have provided sufficient conditions for the existence of a collection of continuous feedback laws, which together with the hysteresis-based switching mechanism defined by the HCLFs lead to a hybrid feedback control law. We have shown that this hybrid feedback control law globally asymptotically stabilizes compact sets for a class of continuous-time systems defined on state-spaces that may be subject to topological constraints. Moreover, we shown how a collection of optimization-based feedback laws can be derived from a family of HCLFs under mild assumptions on the objective function. Consequently, HCLFs may serve as a tool for synthesis of optimal feedback laws ensuring global asymptotic tracking of spatial rigid-bodies such as underwater vehicles and satellites. Indeed, the chapter ended with a case study where we derived a HCLF family for configuration and velocity control of an underwater vehicle.

Chapter 8 introduced an adaptive hybrid feedback control law for marine vehicles. The proposed control law ensures global asymptotic tracking of a hybrid reference system for marine vehicles subject to parametric modeling uncertainties. The control law was derived from a set of potential functions and a hysteretic switching mechanism, which are required to satisfy a set of assumptions. These assumptions are less restrictive than the synergistic conditions presented in Chapters 5 and 6. However, the switching mechanism is not directly encoded through the potential functions, as is the case with synergistic functions. This chapter included experimental validations of the proposed hybrid control law for both surface and underwater vehicle applications.

In Chapter 9, we have addressed the problem of global asymptotic position and heading tracking for multirotor aerial vehicles. We have proposed an adaptive hybrid feedback control law which globally asymptotically tracks a position and heading reference in the presence of a unknown and constant disturbances in both the translational and rotational dynamics. By employing a tuning function-based backstepping approach, the number of parameter estimates, and hence the dynamic order of the control law, is kept to a minimum. We have employed some of the ideas from Chapter 8 to design a novel bounded adaptive control law for the translational subsystem, which resulted in a simpler virtual control law when backstepping. A crucial element to achieving global asymptotic tracking of a desired heading reference is our proposed construction of the desired rotation matrix, which also avoids the use of Euler angles as an intermediary step. Finally, we have demonstrated the effectiveness of the proposed control scheme in experiments.

Future directions from this work includes merging Part I and II of this thesis by employing tools from hybrid feedback control in the design of task-priority methods for redundant robotic systems. In turn, this could lead to global asymptotic stability guarantees for tasks whose configuration space is not necessarily contractible. Another direction for future work is to prove the same stability properties for the integral control laws in Chapter 5 using the velocity-independent feedforward control defined in (5.14), which would make the feedforward control less sensitive to noisy velocity measurements. Another direction for future work is the development of hybrid feedback control algorithms for interaction control of underwater vehi-

cles. Finally, it might be possible to simplify the control law for the rotational subsystem in Chapter 9 considerably by employing interconnection results for hybrid systems. Either in the form of the reduction principle [55, Corollary 7.24], or by developing new and specialized interconnection results for this particular system. This would remove the need for a backstepping controller which cancels the undesirable coupling terms from the translational control law that appear in the Lyapunov analysis.

References

[1] R. G. Sanfelice, *Hybrid Feedback Control*. Princeton University Press, Princeton, NJ, 2021.

[2] H. Hanafusa, T. Yoshikawa, and Y. Nakamura, "Analysis and control of articulated robot arms with redundancy," in *Proc. 8th IFAC World Congress*, Kyoto, Japan, Aug. 1981.

[3] Y. Nakamura, H. Hanafusa, and T. Yoshikawa, "Task-priority based redundancy control of robot manipulators," *The International Journal of Robotics Research*, vol. 6, no. 2, pp. 3–15, Jul. 1987, ISSN: 0278-3649.

[4] B. Siciliano and J.-. E. Slotine, "A general framework for managing multiple tasks in highly redundant robotic systems," in *Proc. 5th Int. Conf. Advanced Robotics*, Pisa, Italy, Jun. 1991.

[5] S. Moe, G. Antonelli, A. R. Teel, K. Y. Pettersen, and J. Schrimpf, "Set-based tasks within the singularity-robust multiple task-priority inverse kinematics framework: General formulation, stability analysis, and experimental results," *Frontiers in Robotics and AI*, vol. 3, p. 16, 2016.

[6] E. Simetti and G. Casalino, "A novel practical technique to integrate inequality control objectives and task transitions in priority based control," *Journal of Intelligent & Robotic Systems*, vol. 84, no. 1, pp. 877–902, Dec. 2016.

[7] O. Kanoun, F. Lamiraux, and P. Wieber, "Kinematic control of redundant manipulators: Generalizing the task-priority framework to inequality task," *IEEE Transactions on Robotics*, vol. 27, no. 4, pp. 785–792, Aug. 2011, ISSN: 1552-3098.

[8] O. Khatib, "A unified approach for motion and force control of robot manipulators: The operational space formulation," *IEEE Journal on Robotics and Automation*, vol. 3, no. 1, pp. 43–53, Feb. 1987, ISSN: 0882-4967.

[9] L. Sentis and O. Khatib, "Prioritized multi-objective dynamics and control of robots in human environments," in *Proc. 4th IEEE/RAS International Conference on Humanoid Robots, 2004.*, Santa Monica, CA, USA, Nov. 2004.

[10] N. Mansard, O. Khatib, and A. Kheddar, "A unified approach to integrate unilateral constraints in the stack of tasks," *IEEE Transactions on Robotics*, vol. 25, no. 3, pp. 670–685, Jun. 2009, ISSN: 1552-3098.

[11] Z. Artstein, "Stabilization with relaxed controls," *Nonlinear Analysis: Theory, Methods & Applications*, vol. 7, no. 11, pp. 1163–1173, 1983.

[12] E. D. Sontag, "A Lyapunov-like characterization of asymptotic controllability," *SIAM Journal on Control and Optimization*, vol. 21, no. 3, pp. 462–471, 1983.

[13] E. D. Sontag, "A universal construction of Artstein's theorem on nonlinear stabilization," *Systems & Control Letters*, vol. 13, no. 2, 1989.

[14] A. D. Ames, K. Galloway, K. Sreenath, and J. W. Grizzle, "Rapidly exponentially stabilizing control Lyapunov functions and hybrid zero dynamics," vol. 59, no. 4, pp. 876–891, Apr. 2014.

[15] R. A. Freeman and P. Kokotović, *Robust Nonlinear Control Design*. Birkhäuser Boston, 1996.

[16] I. R. Petersen and B. R. Barmish, "Control effort considerations in the stabilization of uncertain dynamical systems," *Systems & Control Letters*, vol. 9, no. 5, pp. 417–422, Nov. 1987.

[17] K. Galloway, K. Sreenath, A. D. Ames, and J. W. Grizzle, "Torque saturation in bipedal robotic walking through control Lyapunov function-based quadratic programs," *IEEE Access*, vol. 3, pp. 323–332, 2015, ISSN: 2169-3536.

[18] A. Ames and M. Powell, "Towards the unification of locomotion and manipulation through control Lyapunov functions and quadratic programs," *Control of Cyber-Physical Systems*, pp. 219–240, 2013.

[19] A. Forsgren, P. E. Gill, and M. H. Wright, "Interior methods for nonlinear optimization," *SIAM Review*, vol. 44, no. 4, pp. 525–597, 2002.

[20] S. Boyd and L. Vandenberghe, *Convex Optimization*. Cambridge University Press, 2004, 732 pp., ISBN: 0521833787.

[21] S. Prajna and A. Jadbabaie, "Safety verification of hybrid systems using barrier certificates," in *Hybrid Systems: Computation and Control*, Springer, 2004, pp. 477–492.

[22] S. Prajna, "Barrier certificates for nonlinear model validation," *Automatica*, vol. 42, no. 1, pp. 117–126, Jan. 2006.

[23] K. P. Tee, S. S. Ge, and E. H. Tay, "Barrier Lyapunov functions for the control of output-constrained nonlinear systems," *Automatica*, vol. 45, no. 4, pp. 918–927, Apr. 2009.

[24] M. Maghenem and R. G. Sanfelice, "Sufficient conditions for forward invariance and contractivity in hybrid inclusions using barrier functions," *Automatica*, vol. 124, p. 109 328, Feb. 2021, ISSN: 00051098. DOI: 10.1016/j.automatica.2020.109328. [Online]. Available: https://linkinghub.elsevier.com/retrieve/pii/S0005109820305288 (visited on 11/03/2022).

[25] P. Wieland and F. Allgöwer, "Constructive safety using control barrier functions," *IFAC Proc. Volumes*, vol. 40, no. 12, pp. 462–467, 2007.

[26] M. Z. Romdlony and B. Jayawardhana, "Uniting control Lyapunov and control barrier functions," in *Proc. 53rd IEEE Conf. Decision and Control*, Los Angeles, CA, USA, Dec. 2014.

[27] M. Z. Romdlony and B. Jayawardhana, "Stabilization with guaranteed safety using control Lyapunov –barrier function," *Automatica*, vol. 66, pp. 39–47, Apr. 2016.

[28] A. D. Ames, J. W. Grizzle, and P. Tabuada, "Control barrier function based quadratic programs with application to adaptive cruise control," in *Proc. 53rd IEEE Conf. Decision and Control*, Los Angeles, CA, USA, Dec. 2014.

[29] A. D. Ames, X. Xu, J. W. Grizzle, and P. Tabuada, "Control barrier function based quadratic programs for safety critical systems," vol. 62, no. 8, pp. 3861–3876, Aug. 2017, ISSN: 0018-9286.

[30] A. D. Ames, S. Coogan, M. Egerstedt, G. Notomista, K. Sreenath, and P. Tabuada, "Control barrier functions: Theory and applications," in *Proc. 2019 European Control Conference*, Naples, Italy, Jun. 2019.

[31] Q. Nguyen and K. Sreenath, "Exponential control barrier functions for enforcing high relative-degree safety-critical constraints," in *Proc. 2016 American Control Conf.*, Boston, MA, USA, Jul. 2016.

[32] S. P. Bhat and D. S. Bernstein, "A topological obstruction to continuous global stabilization of rotational motion and the unwinding phenomenon," *Systems & Control Letters*, vol. 39, no. 1, pp. 63–70, 2000, ISSN: 0167-6911.

[33] A. R. Teel, "Robust hybrid control systems: An overview of some recent results," in *Advances in Control Theory and Applications*, C. Bonivento, A. Isidori, L. Marconi, and C. Rossi, Eds., Springer, 2007, pp. 279–302, ISBN: 978-3-540-70701-1. DOI: 10.1007/978-3-540-70701-1_15.

[34] R. Goebel, C. Prieur, and A. R. Teel, "Smooth patchy control Lyapunov functions," *Automatica*, vol. 45, no. 3, pp. 675–683, 2009.

[35] C. G. Mayhew, "Hybrid control for topologically constrained systems," Ph.D. dissertation, University of California, Santa Barbara, 2010.

[36] C. G. Mayhew, R. G. Sanfelice, and A. R. Teel, "Synergistic Lyapunov functions and backstepping hybrid feedbacks," in *Proc. 2011 American Control Conf.*, San Francisco, CA, USA, Jun. 2011, pp. 3203–3208.

[37] C. G. Mayhew, R. G. Sanfelice, and A. R. Teel, "Quaternion-based hybrid control for robust global attitude tracking," *IEEE Transactions on Automatic Control*, vol. 56, no. 11, 2011.

[38] P. Casau, R. G. Sanfelice, R. Cunha, D. Cabecinhas, and C. Silvestre, "Robust global trajectory tracking for a class of underactuated vehicles," *Automatica*, vol. 58, pp. 90–98, 2015, ISSN: 0005-1098.

[39] C. G. Mayhew and A. R. Teel, "Synergistic hybrid feedback for global rigid-body attitude tracking on SO(3)," *IEEE Transactions on Automatic Control*, vol. 58, no. 11, pp. 2730–2742, Nov. 2013, ISSN: 2334-3303. DOI: 10.1109/TAC.2013.2266852.

[40] D. E. Koditschek, "The application of total energy as a Lyapunov function for mechanical control systems," *Contemporary Mathematics*, vol. 97, p. 131, 1989.

[41] S. Berkane and A. Tayebi, "Construction of synergistic potential functions on SO(3) with application to velocity-free hybrid attitude stabilization," *IEEE Transactions on Automatic Control*, vol. 62, no. 1, pp. 495–501, 2017.

[42] C. G. Mayhew and A. R. Teel, "Synergistic potential functions for hybrid control of rigid-body attitude," in *Proc. 2011 American Control Conf.*, San Francisco, CA, USA, Jun. 2011, pp. 875–880. DOI: 10.1109/ACC.2011.5990826.

[43] M. Wang and A. Tayebi, "Hybrid feedback for global tracking on matrix lie groups SO(3) and SE(3)," *IEEE Transactions on Automatic Control*, 2021. DOI: 10.1109/TAC.2021.3097704.

[44] C. G. Mayhew and A. R. Teel, "Hybrid control of planar rotations," in *Proc. 2010 American Control Conf.*, Baltimore, MD, USA, 2010.

[45] C. G. Mayhew and A. R. Teel, "Global stabilization of spherical orientation by synergistic hybrid feedback with application to reduced-attitude tracking for rigid bodies," *Automatica*, vol. 49, no. 7, pp. 1945–1957, 2013.

[46] M. Marley, R. Skjetne, E. A. Basso, and A. R. Teel, "Maneuvering with safety guarantees using control barrier functions," *IFAC-PapersOnLine*, vol. 54, no. 16, pp. 370–377, 2021, 13th IFAC Conference on Control Applications in Marine Systems, Robotics, and Vehicles CAMS 2021, ISSN: 2405-8963. DOI: https://doi.org/10.1016/j.ifacol.2021.10.118.

[47] T. Lee, "Global exponential attitude tracking controls on $\mathsf{SO}(3)$," *IEEE Transactions on Automatic Control*, vol. 60, no. 10, 2015.

[48] P. Casau, R. G. Sanfelice, and C. Silvestre, "Adaptive backstepping of synergistic hybrid feedbacks with application to obstacle avoidance," in *Proc. 2019 American Control Conf.*, Philadelphia, PA, USA, 2019, pp. 1730–1735.

[49] E. A. Basso and K. Y. Pettersen, "Task-priority control of redundant robotic systems using control Lyapunov and control barrier function based quadratic programs," in *Proc. 21st IFAC World Congress*, Berlin, Germany, Jul. 2020.

[50] E. A. Basso, E. H. Thyri, K. Y. Pettersen, M. Breivik, and R. Skjetne, "Safety-critical control of autonomous surface vehicles in the presence of ocean currents," in *Proc. 2020 IEEE Conference on Control Technology and Applications (CCTA)*, 2020, pp. 396–403. DOI: 10.1109/CCTA41146.2020.9206276.

[51] E. A. Basso, H. M. Schmidt-Didlaukies, K. Y. Pettersen, and J. T. Gravdahl, "Synergistic PID and output feedback control on matrix Lie groups," in *Proc. 12th IFAC Symposium on Nonlinear Control Systems*, Canberra, Australia, Jan. 2022.

[52] R. Skjetne, T. I. Fossen, and P. V. Kokotović, "Robust output maneuvering for a class of nonlinear systems," *Automatica*, 2004, ISSN: 0005-1098. DOI: https://doi.org/10.1016/j.automatica.2003.10.010.

[53] R. Skjetne, "The maneuvering problem," Ph.D. dissertation, Norwegian University of Science and Technology, 2005.

[54] H. M. Schmidt-Didlaukies, E. A. Basso, and K. Y. Pettersen, "A generalization of synergistic hybrid feedback control with application to maneuvering control of ships," in *Proc. 61st IEEE Conference on Decision and Control*, Cancún, Mexico, Dec. 2022. [Online]. Available: https://bit.ly/3AvhAoA.

[55] R. Goebel, R. G. Sanfelice, and A. R. Teel, *Hybrid Dynamical Systems: Modeling Stability, and Robustness*. Princeton University Press, Princeton, NJ, 2012.

[56] C. G. Mayhew, R. G. Sanfelice, and A. R. Teel, "Robust global asymptotic stabilization of a 6-DOF rigid body by quaternion-based hybrid feedback," in *Proc. 48h IEEE Conf. on Decision and Control*, Shanghai, China, Dec. 2009. DOI: 10.1109/CDC.2009.5400338.

[57] E. A. Basso, H. M. Schmidt-Didlaukies, and K. Y. Pettersen, "Hysteretic control Lyapunov functions with application to global asymptotic tracking for underwater vehicles," in *Proc. 59th Conf. on Decision and Control*, Jeju Island, Republic of Korea, 2020.

[58] E. A. Basso, H. M. Schmidt-Didlaukies, K. Y. Pettersen, and A. J. Sørensen, "Global asymptotic tracking for marine surface vehicles using hybrid feedback in the presence of parametric uncertainties," in *Proc. 2021 American Control Conf.*, New Orleans, LA, USA, 2021, pp. 1432–1437. DOI: 10.23919/ACC50511.2021.9483419.

[59] E. A. Basso, H. M. Schmidt-Didlaukies, K. Y. Pettersen, and A. J. Sorensen, "Global asymptotic tracking for marine vehicles using adaptive hybrid feedback," *IEEE Transactions on Automatic Control*, 2022. DOI: 10.1109/TAC.2022.3161372.

[60] M. Krstic, P. V. Kokotovic, and I. Kanellakopoulos, *Nonlinear and Adaptive Control Design*. John Wiley & Sons, 1995, ISBN: 0471127329.

[61] E. A. Basso, H. M. Schmidt-Didlaukies, and K. Y. Pettersen, "Global asymptotic position and heading tracking for multirotors using tuning function-based adaptive hybrid feedback," *IEEE Control Systems Letters*, vol. 7, pp. 295–300, 2023. DOI: 10.1109/LCSYS.2022.3187505.

[62] R. T. Rockafellar and R. J.-B. Wets, *Variational Analysis*. Springer, 2009.

[63] J. P. Aubin and H. Frankowska, *Set-Valued Analysis* (Systems & control). Birkhäuser Boston, 1990. DOI: 10.1007/978-0-8176-4848-0.

[64] F. Bullo and A. D. Lewis, *Geometric Control of Mechanical Systems*. Springer, 2005.

[65] T. A. Johansen and T. I. Fossen, "Control allocation – a survey," *Automatica*, vol. 49, pp. 1087–1103, May 2013.

[66] H. M. Schmidt-Didlaukies, A. J. Sørensen, and K. Y. Pettersen, "Modeling of articulated underwater robots for simulation and control," in *Proc. 2018 IEEE OES AUV Symposium*, Porto, Portugal, Nov. 2018.

[67] P. Liljebäck and R. Mills, "Eelume: A flexible and subsea resident IMR vehicle," in *OCEANS 2017*, Aberdeen, Scotland, Jun. 2017.

[68] J. Sverdrup-Thygeson, E. Kelasidi, K. Y. Pettersen, and J. T. Gravdahl, "The Underwater Swimming Manipulator – A Bioinspired Solution for Subsea Operations," *IEEE Journal of Oceanic Engineering*, vol. 43, no. 2, pp. 402–417, 2018.

[69] T. Yoshikawa, "Manipulability of robotic mechanisms," *The International Journal of Robotics Research*, vol. 4, no. 2, pp. 3–9, 1985. eprint: https://doix.org/10.1177/027836498500400201.

[70] I.-L. G. Borlaug, K. Y. Pettersen, and J. T. Gravdahl, "Tracking control of an articulated intervention-auv in 6 DOF using the generalized super-twisting algorithm," in *Proc. 2019 American Control Conf.*, Philadelphia, PA, USA, Jul. 2019.

[71] T. A. Johansen, T. I. Fossen, and S. P. Berge, "Constrained nonlinear control allocation with singularity avoidance using sequential quadratic programming," vol. 12, no. 1, pp. 211–216, Jan. 2004, ISSN: 1063-6536.

[72] G. Antonelli, *Underwater Robots*, 4th. Springer, 2018, ISBN: 9783319778990.

[73] Y. Emam, P. Glotfelter, and M. Egerstedt, "Robust barrier functions for a fully autonomous, remotely accessible swarm-robotics testbed," in *Proc. 58th IEEE Conf. Decision and Control*, Nice, France, Dec. 2019.

[74] Autonomous Shipping Initiative for European Waters (AUTOSHIP). (2020), [Online]. Available: https://cordis.europa.eu/project/id/815012.

[75] Norwegian SciTech News. "Driverless ferries to replace footbridges." (2018), [Online]. Available: https://norwegianscitechnews.com/2018/06/driverless-ferries-to-replace-footbridges/.

[76] A. Orthmann and A. Ziegwied, "The force multiplier effect using autonomous surface vessels for hydrographic survey in the arctic," in *OCEANS 2017*, Anchorage, AK, USA, Sep. 2017, pp. 1–4.

[77] A. Veksler, T. A. Johansen, F. Borrelli, and B. Realfsen, "Cartesian thrust allocation algorithm with variable direction thrusters, turn rate limits and singularity avoidance," in *Proc. 2014 IEEE Conf. Control Applications*, Antibes, France, Oct. 2014, pp. 917–922. DOI: 10.1109/CCA.2014.6981453.

[78] A. Veksler, T. A. Johansen, F. Borrelli, and B. Realfsen, "Dynamic positioning with model predictive control," vol. 24, no. 4, pp. 1340–1353, Jul. 2016, ISSN: 2374-0159. DOI: 10.1109/TCST.2015.2497280.

[79] Q. Nguyen and K. Sreenath, "Optimal robust control for constrained nonlinear hybrid systems with application to bipedal locomotion," in *Proc. 2016 American Control Conf.*, Boston, MA, USA, Jul. 2016.

[80] Y. Wang and S. Boyd, "Fast evaluation of quadratic control-Lyapunov policy," vol. 19, no. 4, pp. 939–946, 2010.

[81] U. Borrmann, L. Wang, A. D. Ames, and M. Egerstedt, "Control barrier certificates for safe swarm behavior," *IFAC-PapersOnLine*, vol. 48, no. 27, pp. 68–73, 2015, ISSN: 2405-8963.

[82] E. H. Thyri, E. A. Basso, M. Breivik, K. Y. Pettersen, R. Skjetne, and A. M. Lekkas, "Reactive collision avoidance for ASVs based on control barrier functions," in *Proc. 4th IEEE Conf. Control Technol. and Applications*, Montreal, Canada, Aug. 2020.

[83] T. Gurriet, A. Singletary, J. Reher, L. Ciarletta, E. Feron, and A. Ames, "Towards a framework for realizable safety critical control through active set invariance," in *Proc. 2018 ACM/IEEE 9th International Conference on Cyber-Physical Systems*, Porto, Portugal, Apr. 2018, pp. 98–106. DOI: 10.1109/ICCPS.2018.00018.

[84] T. I. Fossen, *Handbook of Marine Craft Hydrodynamics and Motion Control*, 2nd. Wiley, 2020.

[85] J. Willems, "Least squares stationary optimal control and the algebraic riccati equation," vol. 16, no. 6, pp. 621–634, Dec. 1971, ISSN: 2334-3303. DOI: 10.1109/TAC.1971.1099831.

[86] A. Isidori, *Nonlinear Control Systems*, 3rd ed. Springer, 1995, ISBN: 3540199160.

[87] A. A. Pedersen, "Optimization based system identification for the milliAmpere ferry," M.S. thesis, Norwegian University of Science and Technology (NTNU), Trondheim, Norway, 2019.

[88] D. Maithripala and J. M. Berg, "An intrinsic pid controller for mechanical systems on Lie groups," *Automatica*, vol. 54, pp. 189–200, 2015, ISSN: 0005-1098.

[89] Z. Zhang, A. Sarlette, and Z. Ling, "Integral control on Lie groups," *Systems & Control Letters*, 2015.

[90] R. G. Sanfelice, "On the existence of control Lyapunov functions and state-feedback laws for hybrid systems," *IEEE Transactions on Automatic Control*, vol. 58, no. 12, pp. 3242–3248, 2013.

[91] R. G. Sanfelice, "Robust asymptotic stabilization of hybrid systems using control Lyapunov functions," in *Proc. 19th International Conference on Hybrid Systems: Computation and Control*, Vienna, Austria, 2016, pp. 235–244.

[92] H. Nakamura and Y. Satoh, "Étale backstepping for control Lyapunov function design on manifold," *Automatica*, vol. 83, pp. 100–107, 2017, ISSN: 0005-1098. DOI: https://doi.org/10.1016/j.automatica.2017.05.010.

[93] R. G. Sanfelice, R. Goebel, and A. R. Teel, "Invariance principles for hybrid systems with connections to detectability and asymptotic stability," *IEEE Transactions on Automatic Control*, vol. 52, no. 12, pp. 2282–2297, Dec. 2007.

[94] R. T. Rockafellar, *Convex Analysis*. Princeton University Press, 1970.

[95] E. A. Feinberg, P. O. Kasyanov, and M. Voorneveld, "Berge's maximum theorem for noncompact image sets," *Journal of Mathematical Analysis and Applications*, vol. 413, no. 2, pp. 1040–1046, 2014.

[96] J. Stuelpnagel, "On the parametrization of the three-dimensional rotation group," *SIAM review*, vol. 6, no. 4, pp. 422–430, 1964.

[97] C. G. Mayhew, R. G. Sanfelice, and A. R. Teel, "On quaternion-based attitude control and the unwinding phenomenon," in *Proc. 2011 American Control Conf.*, San Francisco, CA, USA, 2011.

[98] T. I. Fossen and S. I. Sagatun, "Adaptive control of nonlinear underwater robotic systems," in *Proc. 1991 IEEE International Conference on Robotics and Automation*, Sacramento, CA, USA, 1991.

[99] T. I. Fossen and O.-E. Fjellstad, "Robust adaptive control of underwater vehicles: A comparative study," in *Proc. 3rd IFAC Workshop on Control Applications in Marine Systems*, Trondheim, Norway, 1995.

[100] O.-E. Fjellstad and T. I. Fossen, "Position and attitude tracking of AUV's: A quaternion feedback approach," *IEEE Journal of Oceanic Engineering*, vol. 19, no. 4, pp. 512–518, 1994. DOI: 10.1109/48.338387.

[101] G. Antonelli, F. Caccavale, S. Chiaverini, and G. Fusco, "A novel adaptive control law for underwater vehicles," *IEEE Transactions on control systems technology*, vol. 11, no. 2, pp. 221–232, 2003.

[102] G. Antonelli, S. Chiaverini, N. Sarkar, and M. West, "Adaptive control of an autonomous underwater vehicle: Experimental results on ODIN," *IEEE Transactions on Control Systems Technology*, vol. 9, no. 5, pp. 756–765, 2001. DOI: 10.1109/87.944470.

[103] J.-M. Godhavn, T. I. Fossen, and S. P. Berge, "Non-linear and adaptive backstepping designs for tracking control of ships," *International Journal of Adaptive Control and Signal Processing*, 1998.

[104] R. Skjetne, O. Smogeli, and T. Fossen, "A nonlinear ship manoeuvering model: Identification and adaptive control with experiments for a model ship," *Modeling, Identification and Control*, vol. 25, pp. 3–27, 2004. DOI: 10.4173/mic.2004.1.1.

[105] R. Skjetne, T. I. Fossen, and P. V. Kokotović, "Adaptive maneuvering, with experiments, for a model ship in a marine control laboratory," *Automatica*, vol. 41, no. 2, pp. 289–298, 2005, ISSN: 0005-1098.

[106] A. H. Brodtkorb, S. A. Værnø, A. R. Teel, A. J. Sørensen, and R. Skjetne, "Hybrid controller concept for dynamic positioning of marine vessels with experimental results," *Automatica*, 2018, ISSN: 0005-1098. DOI: https://doi.org/10.1016/j.automatica.2018.03.047.

[107] B. Paden and R. Panja, "Globally asymptotically stable PD+ controller for robot manipulators," *International Journal of Control*, 1988.

[108] J. M. Selig, *Geometric Fundamentals of Robotics*. Springer, 2004.

[109] C. G. Mayhew, R. G. Sanfelice, and A. R. Teel, "On path-lifting mechanisms and unwinding in quaternion-based attitude control," *IEEE Transactions on Automatic Control*, vol. 58, no. 5, pp. 1179–1191, 2013. DOI: 10.1109/TAC.2012.2235731.

[110] Marine Cybernetics Lab, (Accessed Oct. 14th, 2021). [Online]. Available: https://www.ntnu.edu/imt/lab/cybernetics (visited on 10/14/2021).

[111] B. J. Guerreiro, C. Silvestre, R. Cunha, and D. Cabecinhas, "Lidar-based control of autonomous rotorcraft for the inspection of pierlike structures," *IEEE Transactions on Control Systems Technology*, 2018.

[112] P. M. Kornatowski, A. Bhaskaran, G. M. Heitz, S. Mintchev, and D. Floreano, "Last-centimeter personal drone delivery: Field deployment and user interaction," *IEEE Robotics and Automation Letters*, 2018. DOI: 10.1109/LRA.2018.2856282.

[113] K. Klausen, T. I. Fossen, and T. A. Johansen, "Autonomous recovery of a fixed-wing UAV using a net suspended by two multirotor UAVs," *Journal of Field Robotics*, 2018. DOI: https://doi.org/10.1002/rob.21772.

[114] R. Mahony, V. Kumar, and P. Corke, "Multirotor aerial vehicles: Modeling, estimation, and control of quadrotor," *IEEE Robotics Automation Magazine*, vol. 19, no. 3, pp. 20–32, 2012. DOI: 10.1109/MRA.2012.2206474.

[115] M.-D. Hua, T. Hamel, P. Morin, and C. Samson, "Introduction to feedback control of underactuated VTOL vehicles: A review of basic control design ideas and principles," *IEEE Control Systems Magazine*, 2013.

[116] F. Ruggiero, V. Lippiello, and A. Ollero, "Aerial manipulation: A literature review," *IEEE Robotics and Automation Letters*, 2018. DOI: 10.1109/LRA.2018.2808541.

[117] T. Lee, M. Leok, and N. H. McClamroch, "Geometric tracking control of a quadrotor UAV on SE(3)," in *49th IEEE Conference on Decision and Control (CDC)*, 2010, pp. 5420–5425. DOI: 10.1109/CDC.2010.5717652.

[118] A. Roberts and A. Tayebi, "Adaptive position tracking of VTOL UAVs," *IEEE Transactions on Robotics*, vol. 27, no. 1, pp. 129–142, 2011. DOI: 10.1109/TRO.2010.2092870.

[119] P. Casau, R. Cunha, and C. Silvestre, "Improved maneuverability for multirotor aerial vehicles using globally stabilizing feedbacks," in *Proc. 2020 American Control Conference*, 2020.

[120] W. Xie, G. Yu, D. Cabecinhas, R. Cunha, and C. Silvestre, "Global saturated tracking control of a quadcopter with experimental validation," *IEEE Control Systems Letters*, vol. 5, no. 1, pp. 169–174, 2021. DOI: 10.1109/LCSYS.2020.3000561.

[121] R. Naldi, M. Furci, R. G. Sanfelice, and L. Marconi, "Robust global trajectory tracking for underactuated vtol aerial vehicles using inner-outer loop control paradigms," *IEEE Transactions on Automatic Control*, 2017. DOI: 10.1109/TAC.2016.2557967.

[122] C. Cai and A. R. Teel, "Characterizations of input-to-state stability for hybrid systems," *Systems & Control Letters*, 2009, ISSN: 0167-6911.

[123] Z. Zuo, "Trajectory tracking control design with command-filtered compensation for a quadrotor," *IET Control Theory & Applications*, vol. 4, no. 11, 2010.

ISBN 978-82-326-5429-1 (printed ver.)
ISBN 978-82-326-6967-7 (electronic ver.)
ISSN 1503-8181 (printed ver.)
ISSN 2703-8084 (online ver.)

NTNU

Norwegian University of
Science and Technology